Templated Carbons for Hydrogen Storage Application

RUHIT JYOTI KONWAR

Department of Chemical Engineering
Indian Institute of Technology Guwahati
March 2015

Templated Carbons for Hydrogen Storage Application

RUHIT JYOTI KONWAR

Templated Carbons for Hydrogen Storage Application

Submitted in partial fulfillment of the requirements for the degree of

Doctor of Philosophy

By

Ruhit Jyoti Konwar

(Roll No. 09610728)

Department of Chemical Engineering
Indian Institute of Technology Guwahati

March 2015

Dedicated to my parents and family

You are the reason I have become what I am today…….

Department of Chemical Engineering
Indian Institute of Technology Guwahati
Guwahati - 781039, India

CERTIFICATE

This is to certify that the work contained in the thesis entitled **"Templated Carbons for Hydrogen Storage Application"** submitted by ***Ruhit Jyoti Konwar*** for award of degree of Doctor of Philosophy, has been carried out under my supervision and this work has not been submitted elsewhere for award of any degree.

(Dr. Mahuya De)
Associate Professor
Department of Chemical Engineering,
Indian Institute of Technology Guwahati
Guwahati - 781039, India.

Acknowledgements

It's a pleasure to finally express my appreciation to all those who made it possible for my successful completion of thesis. First and foremost, I would like to express my gratitude to my thesis supervisor Dr. Mahuya De, for her invaluable support and encouragement throughout the research work. I appreciate her moral support and guidance since the early stage of my research study, to develop an understanding in this area. It has been an amazing experience working with her; especially I enjoyed her style of mentoring students from which I have been benefited greatly in my professional and personal growth.

My heartiest gratitude goes to all doctoral committee members Dr. G. Pugazhenthi, Dr. Ashok Kumar Dasmahapatra and Prof. P. K. Iyer, for their valuable advices and suggestions throughout my research work. I must also thanks to the faculty members of the Department of Chemical Engineering for their kind inspiration and suggestions during my entire research period.

My sincere thanks goes to all the staff members of Chemical Engineering department of IITG especially Mr. Jayanta Mout, Mr. Harsaraj Biswanath, Mr. Kaustavmoni Deka, Dr. Lukumoni Borah, and Bhagya Boro for their help and support in different aspects of my work.

I would like to acknowledge the Central Instruments Facility of IIT Guwahati for allowing me to carry out SEM, FESEM, EDX, TEM and high pressure adsorption analysis of my samples and in this regard my sincere thanks goes to Mr. Madhurjya Borah and Dr. Kula Kamal Senapati.

My special thanks goes to my friends Dr. Amrita Agarwal, Mr. Rupak Kishor and Mr. Ratan Baruah (Tezpur University) for their moral support, encouragements and kind help in different aspects.

Moreover, I am lucky enough to work with Ms. Priyanka Hajare, Mr. Sohanbir Singh, Dr. N. Vinothkumar, Mr. Yashwant, Mr. Rishabh Saxena, Ms. Shiva Sukla, Chirag Patel,

Amit, Prakram Sehgal, Paran and many more as lab-mate and would like to acknowledge their help and encouragement throughout this research period.

I am fortunate enough to get excellent friends as Ms. Richa Sharma, Ms. Chitrita Kundu, Dr. Leela Monohar, Dr Akshaya Kumar Verma, Himadri Saikia, Dr. Jutika Boro, Dr. Avijit Ghosh, Dr Rahul Singh Chutia, Bikiron Borpujari, Dr. Bhaskar Nath, Bhaskar Jyoti Medhi, Reeta Saikia, Atanu Kumar Pal and Dr. Dharamashibhai V. Rabari for their friendly support, encouragement and timely assistance whenever needed.

I must thank Mr. Shayamal Mitra Baruah, Dr. Himanshu Sonowal, Mr. Jayanta Kumar Mout, Mr. Partha Pratim Dey, Mr. Sanjib Barma and Dr. Avijit Das who made my stay most enjoyable and unforgettable here in IIT Guwahati.

Most of all, I would like to express my deepest sense of gratitude to all my family members and my parents. Their love, care, sacrifices and encouragement have made it possible for me to come so far. I appreciate the courage, understanding and dedicated support shown by all of them despite many testing times at their end. My sincere apology goes to all of those to whom I forget to mention but helped me at any part of the research work.

Ruhit Jyoti Konwar

Abstract

Hydrogen has gained considerable attention as an alternate energy source due to its high energy content as well as renewable and non polluting nature. However, storage of hydrogen for on–board applications is still a challenge. The conventional compressed or liquefied hydrogen storage methods are associated with significant safety hazards. Hence, efforts have been directed towards the development of alternate solid hydrogen storage systems. Solid state hydrogen storage systems are mainly based on hydride or porous materials. The hydride based materials mainly include metal, chemical and complex hydrides. The hydrides have high gravimetric hydrogen storage capacity. But slow kinetics and high hydrogen desorption temperature have reduced their efficiency and applicability in vehicular applications. The porous adsorbents, such as zeolite, metal organic framework, porous polymer or carbon based materials, have been investigated due to their fast adsorption–desorption kinetics and higher surface area. However, lower hydrogen uptake capacity of zeolites and relatively low thermal stability of metal organic frameworks and porous polymers have limited their applicability as hydrogen storage materials. Amongst the porous adsorbents, carbon based materials have attracted interest for hydrogen storage due to their stability, low weight and lower cost. Recently, templated carbons have emerged as potential hydrogen storage material due to high surface area and defined pore structure. The surface properties and pores of the templated carbons can be tailored by controlling the synthesis parameters.

The objective of the present work was to develop templated carbons for hydrogen storage applications. In this study a simple carbonization method with optimized process conditions was developed for synthesis of templated carbon. The effects of process parameters such as carbonization temperature, dwelling time, heating ramp and flow rate of carrier gas on the development of porous structure and surface area of templated carbons were studied in details. The role of templates and carbon precursors on the physicochemical properties of undoped templated carbons were studied. The templated carbons were further chemically modified by incorporation of dopants. The nitrogen and nickel were incorporated in templated carbons using different precursors and effects on

physicochemical properties were determined. The incorporated dopants were expected to act as additional centers for hydrogen activation and further enhance the hydrogen uptake capacity of carbon.

The effects of loading of dopants, template type as well as precursor type on surface area and pore size distributions of the doped carbons were studied. The hydrogen uptake capacities of undoped and doped carbons were determined at different temperatures and pressures. To understand the correlation between physicochemical properties and the hydrogen storage capacity, detailed characterization studies of templates, templated carbons and doped carbons were done. Finally, heat of adsorption, desorption kinetics, and cycle life stability were determined for selected samples.

The templated carbons were synthesized by carbonization method using ammonium zeolite Y and silica gel as inorganic templates. The furfuryl alcohol and sucrose were used as carbon precursors. The template was initially filled with required amount of carbon precursor followed by carbonization at predetermined conditions. After carbonization, the template was removed from template–carbon composite by treatment with aqueous hydrofluoric acid. The doped templated carbons were synthesized using acetonitrile and aniline as nitrogen precursors and nickel acetate tetrahydrate as nickel precursor. The nitrogen and nickel precursors were incorporated along with the carbon precursor. The physicochemical properties of the templates, and carbons were studied by different characterizations techniques such as thermogravimetric analysis, surface area and pore analysis, X-ray diffraction, scanning electron microscopy, field emission scanning electron microscopy, energy dispersive X-ray spectroscopy, temperature programmed reduction, carbon monoxide chemisorption and transmission electron microscopy. The atmospheric and high pressure hydrogen uptakes at different temperatures were measured by temperature programmed desorption and volumetric sorption techniques.

The thermal stability of zeolite and silica gel templates was confirmed by thermogravimetric study in nitrogen environment. The degradation was negligible upto 750 ^{o}C and small at higher temperature. The nitrogen adsorption-desorption isotherms as

well as X-ray diffraction profiles of zeolite and silica gel samples before and after calcination at various temperatures also showed negligible variation, confirming their potential as template.

The effect of carbonization temperature, dwelling time, heating profile and flow rate of carrier gas on the development of surface area and pore volume of the templated carbons were studied for zeolite and silica gel templated carbons using furfuryl alcohol and sucrose as carbon precursors. For zeolite template and furfuryl alcohol precursor, the BET surface area and micropore area of templated carbon increased with temperature from 650 to 750 ^{o}C and thereafter decreased at higher carbonization temperatures of 850 ^{o}C, for all dwelling times. At all carbonization temperature, with increasing dwelling time the BET surface area and micropore area increased upto 3h and then decreased at higher dwelling time of 4h. Thus carbonization temperature of 750 ^{o}C and dwelling time of 3h were observed to be the optimum conditions for obtaining highest surface area for zeolite templated carbons from furfuryl alcohol under conditions studied. The lower carbonization temperature and dwelling time resulted in lower surface area and pore volume of templated carbons, due to incomplete carbonization of the precursor materials. On the other hand, longer dwelling time at higher carbonization temperature caused severe sintering of zeolite or carbon structure resulting in lower surface area and pore volume. The higher flow rate of nitrogen carrier gas during carbonization resulted in higher surface area. It was also observed that use of stepwise heating profile resulted in higher BET and micropore surface areas compared to continuous heating profile was used. Maximum hydrogen uptake of 0.29 wt. % was obtained at -100 ^{o}C and atmospheric pressure for the sample with highest BET surface area (1886 m^2/g) and micropore area (1136 m^2/g). On using sucrose as the carbon precursor the highest surface area was again observed at carbonization temperature of 750 ^{o}C and 3h dwelling time. However, the surface area was significantly lower (1033 m^2/g) compared to that obtained using furfuryl alcohol. The major advantage of using sucrose precursor was generation of significant amount of micropores. A maximum micropore area of 80% was observed for the templated carbon carbonized at 650 ^{o}C with 2h dwelling time.

Abstract

For silica gel as inorganic template and furfuryl alcohol as carbon precursor, the effect of dwelling time on the development of surface properties was similar to zeolite template and 3h was observed to be optimum. However, the effect of carbonization temperature on surface area and pore volume was different. The carbonization temperature of 650 ^{o}C was observed to be most favorable in this case. The highest surface area of 1975 m^2/g and pore volume of 3.07 ml/g was obtained at 650 ^{o}C and 3h dwelling time. For all silica gel templated carbons no micropores were observed and 90–95% of the pores were in the range of 2–20 nm. Highest hydrogen uptake of 0.16 wt.% was observed at atmospheric pressure and adsorption temperature of –100 ^{o}C for the optimized sample having surface area of 1975 m^2/g. The use of sucrose as carbon precursor significantly lowered BET surface area but favored generation of micropores. These phenomena were similar to that observed in case of zeolite templated carbons synthesized using sucrose.

The templated carbons were chemically modified by nonmetal (nitrogen) and metal (nickel) to study the effect on hydrogen storage capacity. The roles of template and nitrogen precursors on the physicochemical properties and hydrogen uptake capacities were also studied. For silica gel templated doped carbons, significant pore rearrangement was observed due to nitrogen. The surface area and pore volume dropped on incorporation of dopant. The effect was more significant for aniline precursor compared to that of acetonitrile precursor. For acetonitrile and aniline derived carbons, the surface areas dropped to 1744 and 1295 m^2/g respectively, compared to 1975 m^2/g for undoped silica gel templated carbon. For aniline derived carbon micropore area of 123 m^2/g was observed. The nitrogen content depended on type of precursors; 4 and 6.7 wt.% nitrogen respectively, were observed for acetonitrile and aniline derived carbons. Pore distribution analysis of undoped and doped templated carbons suggested that nitrogen mainly resided in the pores of 10-20 nm size. On incorporation of nitrogen hydrogen uptake capacity increased for silica gel templated doped carbons in spite of lower surface area compared to undoped carbon. The hydrogen uptake capacities for doped carbons were 0.30 and 0.20 wt.% respectively for acetonitrile and aniline precursors at atmospheric pressure and -100 ^{o}C. The incorporation of nitrogen in carbon networks facilitated the activation of the hydrogen molecules increasing their adsorption. With zeolite as template, surface area of

doped carbon was quite low irrespective of nitrogen precursor used. The observed BET surface areas were 573 and 624 m^2/g respectively for doped carbon prepared using acetonitrile and aniline. This decrease was about 50% of the BET surface area of undoped templated carbons. About 8.5 and 7.8 wt.% nitrogen loadings were observed, respectively, for carbon obtained from acetonitrile and aniline precursors. For zeolite templated carbon significant amount of micropores were observed, whereas mainly mesoporous carbon was obtained for silica gel template. For nitrogen doped zeolite templated carbons, significant decrease in hydrogen uptake capacity was observed which may be attributed to severe decrease in BET surface area and micropore area. The decrease in surface area may have resulted from higher nitrogen loadings and blocking of pore mouths. Pore blocking was more severe for microporous zeolite compared to mesoporous silica gel.

The nickel doped carbons were developed using both activated carbon and templated carbon as the base material. The effect of nickel loadings (5-30 wt.%) and adsorption temperature on hydrogen uptake were studied using nickel doped activated carbon. On increasing the nickel content, the BET surface area and pore volume decreased significantly due to the partial pore blockage by nickel oxide. The 15wt.% NiO loading was observed to be optimum loading for hydrogen uptake. At subzero temperatures (-100 and -50 ^oC) both physisorption and chemisorption contributed to hydrogen uptake but at higher adsorption temperatures, (150 and 200 ^oC) only chemisorption was responsible for hydrogen uptake. The maximum uptake of 0.24 wt.% was observed at –100 ^oC and atmospheric pressure for 15 wt.% NiO doped activated carbon. Nickel enhanced the hydrogen uptake by providing additional active sites for chemisorption and facilitating hydrogen spillover phenomenon. The role of template and carbon precursors on the development of surface area and porous structure of nickel doped templated carbons was also studied. The highest BET surface area of 2008 m^2/g was observed for the nickel doped carbon synthesized from furfuryl alcohol using silica gel as template. Significant pore rearrangement due to nickel was observed when silica gel was used as template. The highest hydrogen uptake of 0.21 wt.% was observed at -100 ^oC and atmospheric pressure. This capacity was comparatively higher than that for undoped templated carbon prepared

under similar conditions. The use of sucrose as carbon precursor and zeolite as inorganic template decreased the surface area and hydrogen uptake capacity.

At subzero temperature the hydrogen uptake capacity mainly depended on three factors such as BET surface area, micropore area and the nature of dopant. No hydrogen uptake was observed for doped and undoped carbons at room temperature. For undoped carbons the hydrogen uptake capacity was higher for the samples having more micropore and mesopores of lower diameters. For doped carbon hydrogen uptake was significant in spite of lower BET or micropore area. For doped carbon presence of dopant contributed to additional hydrogen uptake and compensated the drop in surface area. For both undoped and doped carbons the highest hydrogen uptake was 0.29 wt.% under atmospheric conditions and -100 ^{o}C. The hydrogen uptake capacities at high pressure were determined for selected samples. The higher adsorption pressure resulted in higher hydrogen uptakes at all temperatures. At liquid nitrogen temperature, ~1wt.% of hydrogen uptake at 1 bar increased to 2.45 wt.% at pressure of 8 bar. Hydrogen adsorption cycles were carried out for the same sample and uptake capacity was observed to be repeatable. The heat of adsorption increased for nitrogen doped carbon compared to that of undoped carbon. The heat of adsorption was 6.1 kJ/mol for undoped silica gel templated carbon and 9.5 kJ/mol for nitrogen doped silica gel templated carbon. Desorption kinetics was observed to be faster for all silica gel and zeolite templated carbons. The hydrogen desorption for the studied samples was completed within 15 minute.

Publications

1. **Ruhit Jyoti Konwar** and Mahuya De, Effects of synthesis parameters on zeolite templated carbon for hydrogen storage application, ***Microporous and Mesoporous Materials*** **(2013),** 175, 16-24.
2. **Ruhit Jyoti Konwar** and Mahuya De, Synthesis of high surface area silica gel templated carbon for hydrogen storage application, ***Journal of Analytical and Applied Pyrolysis***, **(2014)** 107, 224–232 .
3. **Ruhit Jyoti Konwar** and Mahuya De, Development of templated carbon by carbonization of sucrose–zeolite composite for hydrogen storage, ***International Journal of Energy Research*** **(2015)** 39, 223–233.
4. **Ruhit Jyoti Konwar** and Mahuya De, Nickel modified activated carbon for low pressure hydrogen storage: Effect of nickel loading and adsorption temperature. **(To be submitted).**
5. **Ruhit Jyoti Konwar** and Mahuya De, Nitrogen doped templated carbon for hydrogen storage: Effect of templates and nitrogen precursors (**To be submitted**).
6. **Ruhit Jyoti Konwar** and Mahuya De, Templated carbons with dispersed nickel for hydrogen storage: Effect of templates and precursors **(To be submitted).**

Conference publication

7. **Ruhit Jyoti Konwar** and Mahuya De, "High surface area silica gel templated carbon: synthesis, characterization and hydrogen adsorption studies", Proceedings of 65th Annual Session of Indian Institute of Chemical Engineers, **CHEMCON–2012**.

Contents

List of Figures

List of Tables

Chapter 1

Introduction

1.1 Hydrogen as energy carrier

Energy and environment are two major concerns for our modern society. Energy demand is increasing at very rapid rate with increase in world population. At present, most of the required energy is derived from fossil fuel based sources such as coal, petroleum and natural gas. However, rapid consumption along with limited availability of fossil fuels have forced development of alternative energy sources. The consumption of the fossil fuels also releases significant amount of carbon dioxide into the atmosphere causing global warming and adverse climatic effect. Hence, utilization of energies from renewable sources that have carbon neutral characteristics is considered as the plausible solution of present energy and environment crisis. The major renewable energy sources are solar, wind, ocean, geothermal, bio-based materials etc.

Hydrogen is emerging as a potential alternative to fossil fuels due to its high energy content, non-toxicity, versatility, ease of transportation and environmental compatibility (Grimes et al. 2008 and Vasiliev et al. 2010). Wide range of applications as stationary and mobile sources of energy is an added advantage (Jain et. al. 2010) . Hydrogen is the most abundant element on the earth. The hydrogen has carbon neutral characteristics and can be generated from renewable energy sources. As compared to other liquid hydrocarbons or natural gas, hydrogen stores higher chemical energy per unit mass. A comparison of specific energy content of hydrogen with different fuels is shown in Figure 1.1. It can be observed that specific energy of hydrogen is more than 7 times that of coal, 3 times that of diesel or gasoline and 2.5 times that of methane. However, hydrogen occupies about 4 times of the volume of gasoline that have equal amount of energy. This is one of the major disadvantages for hydrogen. The International Centre for Hydrogen Energy Technologies of the United Nations Industrial Development Organization has projected hydrogen as the dominating fuel by 2074 (Figure 1.2).

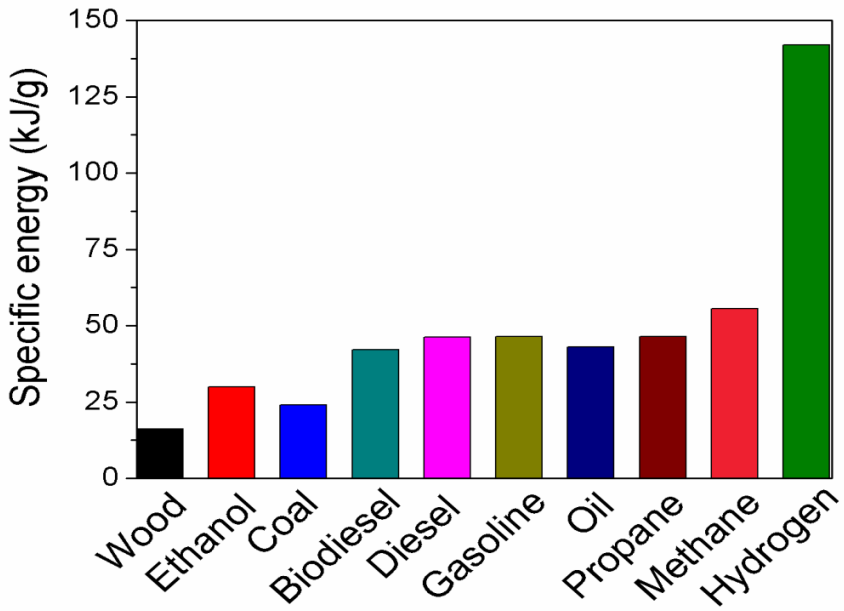

Figure 1.1. Comparison of specific energies of different fuels (Green econometrics information 2007).

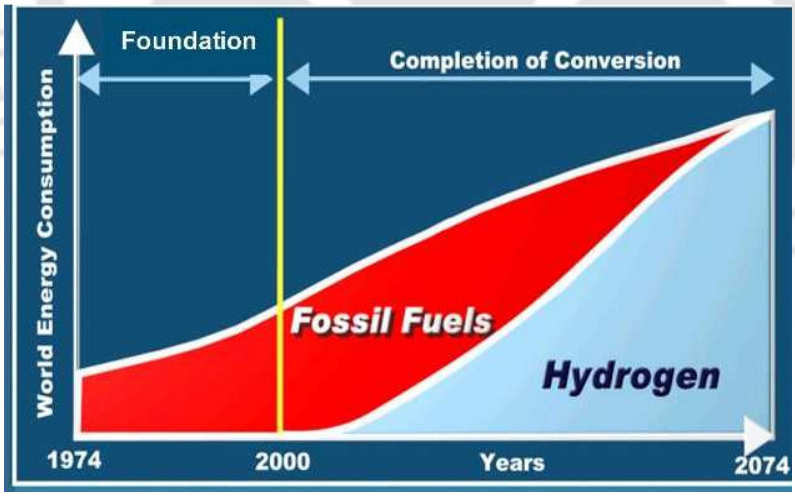

Figure 1.2. Projection of global hydrogen energy consumption (UNIDO-ICHET).

It has been technically demonstrated that hydrogen can be used for transportation, heating or power generation and could replace current fuels in all their present applications

(Gupta 2009). It releases energy through chemical reactions with oxygen in heat engines or fuel cells and produces only water as byproduct. Hence, from environmental perspective it is a clean energy. Similar to all energy sources, hydrogen requires process of generation, storage and conversion. Hydrogen can be produced from various renewable and non-renewable sources. The conventional fossil fuel based technologies used for hydrogen production includes steam reforming of natural gas, partial oxidation of natural gas, autothermal reforming and coal gasification. Water electrolysis, photo-electrolysis, photo catalysis, thermo-chemical, biological, photo-biological, etc. are process based on renewable energy sources. These hydrogen production technologies based on renewable sources are in different stages of development and have their own advantages and disadvantages. The hydrogen will truly become a clean usable fuel when it can be produced economically from renewable sources. The next most important aspect for using hydrogen as fuel is its storage. Efficient and safe storage of hydrogen for various applications is one area of intensive research.

1.2 Hydrogen storage specifications

The hydrogen as a fuel can be used in stationary and mobile applications. The requirements of the hydrogen storage system are different depending upon their applications. Stationary applications do not have weight and space limitations and storage can be done at high pressure and temperature. However for mobile applications, weight, space as well as safety, all are major issues that have to be resolved to generate an effective storage facility. Thus, for the development of feasible hydrogen storage systems for mobile applications, several scientific and technological challenges have to be overcome. For utilization as transportation fuel, hydrogen storage system is required to satisfy certain specifications. The specifications, given by the United States Department of Energy and accepted globally are as follows (Anton et al. 2013):

* High gravimetric (0.055 kg H_2/kg system) and volumetric (0.04 kg H_2/L system) hydrogen storage capacity
* Low operating pressure for safety reasons

* Operating temperature in the range of -40 to 60 °C
* Minimum and maximum delivery pressures of 5 and 12 bar respectively
* Faster kinetics, reversibility and high cycle life (1500cycles)
* System filling time of 3.3 minute
* Fuel purity (hydrogen from storage system) should be 99.97%
* Reasonable cost and leak proof.

The above specifications have been targeted to be achieved by the year 2017. Till date, no hydrogen storage system has been able to satisfy all the conditions simultaneously. For realization of hydrogen as transportation fuel, worldwide research is directed towards the development of safe, cost-effective as well as efficient storage materials and technologies.

1.3 Hydrogen storage technology

The storage of hydrogen unlike liquid hydrocarbons is a major technical and economic challenge due to its low density (Zuttel 2003). Hydrogen can be stored by means of physical and chemical methods. Conventionally hydrogen is stored under compressed or cryogenic conditions. The chemical method of hydrogen storage involves solid state hydrogen storage.

1.3.1 Pressurized storage

Hydrogen can be compressed to high pressure (> 200 bar) at near ambient temperature. Pressurized storage is one of the most common hydrogen storage technologies and pressurized hydrogen is commercially available. Typically in hydrogen vehicles the working storage pressure is 350 bar. Composite cylinders are also available for hydrogen storage pressure up to 700 bar. At this pressure the gravimetric storage capacity is about 4.5 wt.%. However, the volumetric capacity is only 0.025 kg of hydrogen per liter (Takeichia et al. 2003). Though, at present, the compressed hydrogen storage technology is the best option for on-board applications, but still is unable to meet all the required specifications. For mobile applications where space and weight are major issues,

compressed gas storage becomes bulky. On using light weight materials for storage tank that can withstand the high pressure, though the weight problem is reduced, but cost increases as this kind of materials are usually expensive. In summary, compressed storage requires higher capital and operating costs and also vulnerable in terms of safety (Leon 2008).

1.3.2 Cryogenic storage

Cryogenic storage is another commercially available method for hydrogen storage. In cryogenic tanks liquefied hydrogen can be stored at atmospheric pressure and -253 ^{o}C temperature. At this temperature the density of hydrogen (70.8 g/l) is nearly twice that of compressed hydrogen at 700 bar. However, the liquefaction of hydrogen is a high energy consumption process. The energy required to liquefy hydrogen is about 30-40% of the energy content of the gas. Continuous 'boil-off' during storage is one of the main disadvantages of this method. From the viewpoint of safety, cryogenic storage is therefore highly undesirable in automotive applications. Further, in this storage process refueling of hydrogen is also difficult. Though the density of liquefied hydrogen is considerably higher than that of compressed hydrogen, but the expenses involved in liquefaction, storage, handling, complex infrastructure and continuous 'boil-off', minimize the applicability and overall efficiency of this system (Walker 2008, Leon 2008 and Gupta 2009).

The above discussions suggest that the conventional compressed and liquefied hydrogen storage technologies are unable to satisfy all the requirements for transportation applications and also have major safety issues. Hence, alternate storage technologies for hydrogen are extensively investigated and solid state hydrogen storage is one of such potential methods (Zuttel 2003, Sakintuna et al. 2007, Wang et al. 2008 and Jain et al. 2010).

1.3.3 Solid state storage

Solid state storage of hydrogen has attracted attention as it has the potential to be a safe and efficient method to store energy for both stationary and mobile applications (Jana

2011). Some solid surfaces have strong affinity towards hydrogen molecules. When hydrogen comes in contact with the surface a fraction of gas is trapped physically or chemically on the surface.

For mobile applications the solid state storage materials should satisfy the requirements in terms of volumetric and gravimetric energy density, realistic kinetics for hydrogen adsorption-desorption and high cycle life (Thomas 2007 and Anton et al. 2013). The solid state hydrogen storage technology has been reported to have advantages compared to compressed or liquid hydrogen storage in terms of volumetric density (Schlapbach et al. 2001 and Sakintuna et al. 2007). Few metal hydride based materials have higher volumetric energy density compared to liquid or pressurized hydrogen storage (Hoffman et al.1976). The hydrogen storage capacities of 7.6 wt.% for magnesium hydride and 18 wt.% for lithium borohydride satisfy the target capacity and are among promising storage materials (Sakintuna et al. 2007 and Zuttel et al. 2003). In terms of cycle life, the Cr_2O_3 catalyzed MgH_2 was stable upto 1000 cycles without decrease in storage capacity (Dehouche et al. 2002). However, lower gravimetric density is one of the major disadvantages for hydride based materials. Fast adsorption-desorption kinetics, reversibility, longer cycle life, high durability and low temperature desorption are important requirements for solid state hydrogen storage system. The porous adsorbents, especially carbon based materials, possess these criteria and are observed to be among promising materials (Nishihara et al. 2009, Yang et al. 2010). However, low storage capacity is one of the main disadvantages for carbon based materials.

The solid state hydrogen storage materials are categorized mainly into two categories; (a) hydride based materials (Hagstrom et al. 1995, Imamura et al. 1998, Ross et al. 2004, Pinkerton et al. 2005, Sakintuna et al. 2007, Berube et al. 2007, Biniwale et al. 2008, Aardahl et al 2009, Milanese et al. 2010, Graetz et al. 2010, Moussa et al. 2013) and (b) porous adsorbents (Cheng et al. 2001, Takagi et al 2004, Strobel et al. 2006, Thomas 2007, Jin et al. 2007, Attia et al. 2013, He et al. 2013, Rallapalli et al. 2013 and Yuan et al. 2013). The hydride based materials include metal, chemical and complex hydrides, whereas the porous adsorbents include carbons, polymers, metal organic frameworks, and zeolites. All these materials have their own advantages and disadvantages. Research is

dovetailed to meet the pressure and temperature requirements for hydrogen storage systems and to understand the fundamental mechanism of processes. The conventional high pressure and liquefied hydrogen storage methods have reached the engineering prototype stage, while for solid state hydrogen storage system, extensive research is still required to achieve the commercial stage. Various solid state hydrogen storage materials are discussed in following sections.

1.4 Hydrogen storage materials

1.4.1 Hydride based

Hydrogen can be stored in the form of hydrides under moderate temperature and pressure. The hydrides are chemically bounded hydrogen storage materials. The hydrogen stored in form of hydride is relatively compact in size. For efficient on-board applications, the metal hydride should possess high hydrogen capacity per unit mass and volume, low desorption temperature, low heat dissipation during hydride formation, fast kinetics, cycle stability, and cost effectiveness (Gupta et al. 2009). Hydrides have gained special interest due to their higher volumetric energy density compared to cryogenic and pressurized storage (Hoffman et al. 1976). The hydride based materials such as metal hydrides, complex hydrides, hydrides of some intermetallic compounds have been extensively studied for hydrogen storage applications (Sandrock et al. 1999, Zuttel et al. 2003, Sakintuna et al. 2007 and Moussa et al. 2013). The metal hydrides are composed of metal and hydrogen atoms and are formed at certain temperature and pressure. The hydrogen storage density for magnesium based hydrides is about 6.5 hydrogen atoms/cm^3 and observed as significantly higher compared to that of gaseous hydrogen (0.99 hydrogen atoms/cm^3) or liquefied hydrogen (4.2 hydrogen atoms/cm^3) (West et al. 1982). The regeneration of the metal can be accomplished either by increasing the temperature or by reducing the pressure. For magnesium based hydrides though the reversible hydrogen storage capacity is high, upto 7.6 wt.%, however, slow kinetics and high hydrogen desorption temperature of about 300 ^oC reduce their efficiency and applicability in vehicular applications (Sakintuna et al. 2007). The hydrides of Li, Be, Na, Mg, B, and Al are also investigated due to their high gravimetric hydrogen storage

capacity (Lu et al. 2006 and Fakioglu et al. 2004). However, increased weight, instability and poisoning are some of the major issues that need attention. Extensive work has been done on metal hydride based materials in order to decrease their decomposition temperature and enhance the kinetics and cycle life by using appropriate catalysts (Berube et al. 2007 and Klebanoff 2013).

The complex hydrides are light weight storage materials which include alanates, nitrides, amides and borohydrides. The alanates of sodium, lithium and potassium were mostly studied materials for the applications in hydrogen storage (Sakintuna et al. 2007). The lithium borohydride, sodium borohydride, and ammonia borane are the borohydride compounds extensively studied for hydrogen storage (Moussa et al. 2013). Borohydrides have the highest gravimetric hydrogen storage capacity among the different complex hydrides. For $LiBH_4$ the storage capacity of about 18 wt.% was reported (Zuttel et al. 2003). However, slow kinetics and thermodynamic limitations are the major challenges of complex hydrides. The intermetallic compounds are ordered stoichiometric compounds and classified on the basis of their crystal structures. The intermetallic hydrides are available in the form of AB_5, A_2B_7, AB_3, AB_2, AB and A_2B, where A and B are two metallic components (Sandrock et al. 1999, Züttel et al. 2003 and Sakintuna et al. 2007). The hydrogen storage capacities of the intermettalic compounds are not satisfactory as compared to other hydride based solid storage materials (Sakintuna et al. 2007).

1.4.2 Porous adsorbents

The porous adsorbents store hydrogen by physical adsorption mechanism. The main advantage of porous adsorbents is its faster adsorption desorption kinetics. Hydrogen storage on different porous materials such as zeolites (Langmi et al. 2005), metal organic frameworks (Lin et al. 2006), porous polymers (Budd et al. 2007) and porous carbons (Poirier et al. 2004) have received considerable attention in recent years.

Zeolites are crystalline microporous alumino-silicate compounds with well defined porous structure (Kulprathipanja 2010 and Fraenkel et al. 1977). High specific surface

area and ordered pore structure have made zeolites potential for hydrogen storage application. Different types of zeolites, such as A, X, Y covering a range of different pore geometries and compositions, were investigated as hydrogen storage materials (Langmi et al. 2003). Zeolites exhibit diverse behavior with respect to hydrogen adsorption depending on the structure of framework and the nature of the compensating cations. The cages and the channel diameters of the zeolites can be tailored by ion exchange. The cations may also act as binding sites for hydrogen molecules (Chung et al. 2010). The microporous zeolites have number of advantages compared to other microporous adsorbents. Zeolites have relatively rigid frameworks and possess higher thermal stability as compared to metal organic frameworks and organic polymers. They have defined microporous structure in comparison with activated carbons. However, the lower hydrogen uptake capacity as compared to other adsorbents such as metal hydride, metal organic frameworks and activated carbons, has limited its applicability as hydrogen storage materials (Cejka et al. 2010).

The metal organic frameworks have gained considerable interest as potential hydrogen storage materials because of high specific surface area, high microporosity, structural flexibility and exposed metal sites (Rosi et al. 2003, Mulder et al. 2005, and Zhao et al. 2008). Metal organic frameworks are crystalline inorganic-organic hybrid porous compounds, containing metal ions or clusters linked by organic ligands (Rowsell et al. 2004). By combination of different organic ligands and metal ions, large number of geometrical and chemical variations can be achieved. The metals linking the organic clusters create additional adsorption sites for hydrogen. The major disadvantage of metal organic frameworks is lower thermal stability as compared to other porous adsorbents such as zeolites or activated carbons (Rowsell et al. 2004). The weak interaction between the metal organic frameworks and hydrogen, which results in very low capacity, is another major bottleneck for storage application (Zhao et al. 2008).

The non-crystalline highly porous organic materials are also studied for hydrogen storage applications. The polymers with intrinsic microporosity as well as hyper-crosslinked polymers are presently investigated as hydrogen storage materials (Makowski et al. 2009). The high specific surface areas with controlled porosity make the porous polymers

advantageous for hydrogen storage. The porous organic polymers have narrower pore size distributions than activated carbons and better chemical stability compared to that of metal organic frameworks. The pore structures of the organic porous polymers closely resemble activated carbon (Broom 2011). The possibility of large scale production of the porous polymers is additional advantage (Lee et al. 2006 and Ibrahim 2013). However, the thermal stability of the porous polymer is lower compared to zeolites or activated carbons.

The carbon based materials have received special attention for hydrogen storage among the solid state materials due to lower weight, faster adsorption-desorption kinetics, good recyclability and better chemical and thermal stability (Liang et al. 2008). The hydrogen can be adsorbed on a carbon surface by means of physical adsorption. The physical adsorption is usually associated with multilayered adsorption. Wide range of carbon based materials, that may be amorphous or structured, can be used for hydrogen storage. Activated carbons (Noh et al. 1987 and Kojima et al. 2006), graphite (Hirscher et al. 2003), carbon nanofibers (Hwang et al. 2002), carbon nanotubes (Dillon et al. 1997, Cheng et al. 2001 and Zuttel et al. 2002), graphene (Dimitrakakis 2008), fullerenes (Pupysheva 2008) and templated carbons (Chen et al. 2007) are classes of carbon materials that have been investigated for hydrogen storage applications. For all these carbon based materials the hydrogen adsorption capacity may be enhanced by addition of small amount of metals or non metals to the carbon network. These heteroatoms mainly contribute to hydrogen uptake by facilitating chemisorption on these sites. Among the carbon based materials, the activated carbons and templated carbons have the advantage of high surface area and ease of productions. However, the major disadvantage of carbon based materials is lower hydrogen storage capacity. Details on carbon materials are discussed in second chapter. At present, all the conventional storage technologies and solid state hydrogen storage materials are not in condition to satisfy all the criteria for transportation applications (Zhou 2005). This study investigated and developed porous carbons based materials for hydrogen storage applications due the above stated advantages associated with the carbon based materials.

.

1.5 Objectives

The objective of the present work was to develop templated carbons for hydrogen storage applications by simple carbonization method. The main objectives are summarized as below:

1. Preparation of templated carbons using furfuryl alcohol and sucrose as carbon precursors with zeolite and silica gel as inorganic templates. The role of templates and carbon precursors on the physicochemical properties of undoped templated carbons was investigated.
2. Study the effects of process parameters such as carbonization temperature, dwelling time, heating ramp and flow rate of carrier gas on the development of porous structure. The optimum conditions required for maximizing the surface area and micropore area were determined.
3. Study the effect of chemical modification of templated carbon by incorporation of metal and nonmetal heteroatoms. The nickel and nitrogen were used as metal and nonmetal heteroatoms respectively.
4. The effects of dopant precursor, carbon precursors, loading of dopants and template type on physical and chemical properties of the doped carbons were studied.
5. Hydrogen uptake capacities of undoped and doped templated carbons were determined at different temperatures and pressures using temperature programmed desorption and volumetric adsorption methods.
6. Characterizations of templates, templated carbons and doped carbons were carried out by various techniques such as thermogravimetric analysis (TGA), X-ray diffraction (XRD), surface area and pore analysis, scanning electron microscopy (SEM), field emission scanning electron microscopy (FESEM), energy dispersive X-ray (EDX), transmission electron microscope (TEM), Raman spectroscopy, Fourier transform infrared spectroscopy (FTIR), temperature programmed reduction (TPR) and carbon monoxide pulse chemisorption to determine the physicochemical properties and understand their role in hydrogen storage.

7. Heat of adsorption, desorption kinetics, and cycle life were determined for selected samples.

Chapter 2

Literature review

2. 1 Mechanism of hydrogen storage for porous adsorbents

Hydrogen adsorption is a process of trapping or binding of hydrogen by solid surfaces. Adsorbent surfaces show affinity towards hydrogen molecules, the extent of which depends on nature of solid surface. The adsorption is the consequence of interactions between the solid surface and the hydrogen molecules. Depending on the interactive forces, the adsorption may be physical adsorption (physisorption) or chemical adsorption (chemisorption) (Rouquerol et al.1999). The classification is based on the way hydrogen gets attached to the solid adsorbents. Hydrogen can be adsorbed either in molecular form without being dissociated or in atomic form after dissociation. The dissociated form favors stronger chemical interactions of hydrogen with the host material. Both physisorption and chemisorption mechanisms may contribute to hydrogen storage on porous adsorbent depending on nature and structure of adsorbent surface as well as adsorbate.

(a) Physical adsorption

Physical adsorption is the mechanism by which hydrogen is stored in the molecular form on the surface of a solid material. The potential energy curves for hydrogen adsorption are shown in Figure 2.1. The potential energy curve is a representation of variation of the energy as the adsorbate approaches the solid adsorbent. In physical adsorption process, the forces of attraction between the hydrogen molecules and solid adsorbent surfaces mainly originate from van der Waals interactions (Darkrim et al. 2002 and Nishihara et al 2012). These forces give rise to a shallow minimum in the potential energy curve before the strong repulsive forces arises due to electronic interaction. No change in the electronic orbital patterns of the involved species occurs in physisorption. The strength of this interaction is very weak. For molecular hydrogen adsorption, the binding energy is about 0.1eV and heat of adsorption is in the range of 1-10 kJ/mol depending on the nature of solid surface (Hirscher 2010). Physically adsorbed molecules may diffuse along the surface of the adsorbent and typically are not bounded to a specific location on the surface. Physical adsorption can take place on all surfaces under favorable conditions of

temperature and pressure (Hirscher 2010). The adsorption processes are generally exothermic in nature, accompanied by release of energy. The adsorption is a spontaneous process. Consequently, the change in Gibbs free energy should be negative ($\Delta G=\Delta H-T\Delta S<0$). However, the entropy change associated with adsorption is usually negative because the adsorbate molecules lose their translation freedom when they are attached to the surface of the adsorbent. Therefore, in order to keep total change in Gibbs free energy less than zero, the enthalpy change (ΔH) must be sufficiently negative. Hence the physisorption processes are usually associated with release of heat and favored with decrease in temperature. Higher storage capacities are achieved at lower adsorption temperature. At a given temperature, the amount of gas adsorbed is a function of pressure. Desorption of gases occurs when temperature increases or pressure decreases (Darkrim et al. 2002).

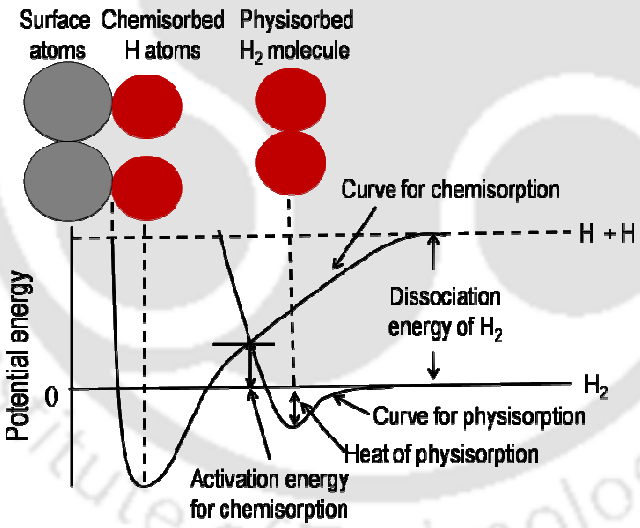

Figure 2.1. Typical potential energy curves for physical and chemical adsorptions of hydrogen (Thomas et al. 1997).

For hydrogen storage by physical adsorption lower pore size has been observed to favor the process. Hence microporous materials with high specific surface area are reported to give high storage capacity (Benard et al. 2007). In physical adsorption process saturation of the surface is achieved quite fast. Being only weakly bounded, physical adsorption is

also easily reversed. Consequently, hydrogen storage by physical adsorption has very fast adsorption and desorption kinetics with very low change of enthalpy making the process very attractive for on-board refueling. Since the physical adsorption is a surface phenomenon, the research interest has been focused on to develop porous materials with high surface area for high capacity.

(b) Chemical adsorption

Chemical adsorption or chemisorption is the other type of adsorption mechanism responsible for hydrogen storage by solid adsorbents. The chemisorption of hydrogen on a solid adsorbent occurs when the hydrogen atoms or molecules are bounded to the solid surface by overlapping of their electronic orbitals. The chemical interaction between hydrogen and solid surface may result in transfer or sharing of electrons (Taylor 1932 and Orinakova et al. 2011). In this case the potential energy curve is dominated by deeper chemisorption minimum as shown in Figure 2.1. The depth of the chemisorption well is a measure of binding energy of hydrogen to the surface and represent the energy of adsorption. As shown in the figure the chemisorption process may be activated one requiring certain activation energy for initiation. Chemisorption is a site specific process. These active sites can be incorporated on the adsorbent surface in form of heteroatoms. The chemisorption takes place very rapidly on these active sites under favorable adsorption conditions (Leon 2008). After formation of monolayer of adsorbate on the surface, unavailability of the active site prevent further adsorption. Thus chemisorption follows a monolayer adsorption mechanism. Hydrogen chemisorption may be either dissociative or non dissociative. Various theoretical and experimental studies have showed that few metals and non-metals can activate or dissociate hydrogen on carbon based materials and facilitate hydrogen chemisorption (Zhong et al. 2002, Giasafaki et al. 2012 and Sankaran et al. 2006). The hydrogen spillover mechanism has been reported for metal active sites involving dissociative chemisorption of hydrogen. The molecular hydrogen splits into atomic hydrogen in presence of metal particles followed by migration of atomic hydrogen to the surface of the adsorbent (Beebe et al. 1924 and Jimenez et al. 2012).

Chemisorption is also an exothermic process associated with release of energy. As discussed in section 2.2.1 (a), the exothermic nature of the process is associated with negative entropy change. However few cases of endothermic chemisorption have been observed such as dissociative chemisorption of molecular hydrogen on glass (Thomas 1961). In these cases, due to structural change of adsorbent the overall entropy change of the process was found to be positive and thereby facilitating occurrence of endothermic chemisorption. Since the interaction during chemisorption is usually much stronger compared to physical adsorption, heat of adsorption is in higher range of 10-50 kJ/mol. Hence, higher temperature is required for desorption of chemisorbed hydrogen (Strobel et al. 2006). Chemisorption is usually an activated process. Molecules possessing certain amount of activation energy can therefore undergo the process. High gravimetric hydrogen storage capacity can be expected by chemical adsorption of hydrogen.

2.2 Carbon based hydrogen storage materials

The carbon based materials have high potential as solid state hydrogen storage systems for mobile applications. These materials are attractive because of its high specific surface area, faster adsorption-desorption kinetics and lower weight. However, the major disadvantage of carbon based materials is lower hydrogen storage capacity. For better feasibility as solid state hydrogen storage materials, this limitation has to be overcome. The feasibility of different amorphous and structured carbons has been extensively discussed in the following subsections.

2.2.1 Amorphous carbon

The amorphous activated carbons have received consideration as hydrogen storage material due to their high surface area and larger pore volume (Liang et al. 2008). Activated carbons are commercially available in large quantities for diverse applications such as catalysis, adsorption and gas storage (Liang et al. 2008 and Yurum et al. 2009). Possibility of large scale production at lower cost is the additional advantage of activated carbons for storage application compared to that of nano-crystalline carbons (Jin et al.

2007). Activated carbons are synthesized from coal and bio-based materials such as wood, sawdust, cellulose, straw, etc. via chemical or physical activation techniques (Marsh et al. 2006). The porosity and the surface area of activated carbons can be controlled by regulating the activation process conditions and raw material composition. In general, the activated carbon tends to have slit-shaped pores. Regular grade activated carbons have specific surface areas in the range of 700-1800 m^2/g. However, super activated carbons like Maxsorb and AX-21 have surface area up to 3000 m^2/g (Chahine et al. 1994). The hydrogen uptake capacity by activated carbons mainly depends on their total surface area and microporosity. Though because of high surface area the activated carbons are attractive for gas storage application however, their wide pore size distribution limits the interaction of carbon surface with hydrogen molecules and thereby, affects the hydrogen storage capacity adversely (Dillon et al. 2001). A range of hydrogen uptake capacities have been reported in the literature depending on pore size distribution and surface area. Kojima et al. (2006) reported 0.7 wt.% hydrogen uptake at room temperature and 90 bar for activated carbon with surface area of 3220 m^2/g. The hydrogen uptake capacity of the same activated carbon increased to about 5 wt.% at liquid nitrogen temperature and 30 bar pressure. Functional groups present on the surface of activated carbon have also been reported to affect the hydrogen storage uptake. Huang et al. (2010) studied the influence of surface oxides of activated carbons on hydrogen adsorption and reported a hydrogen capacity of 0.7 – 2.6 wt.% at –196 ^oC and 1bar. However, Jin et al (2007) reported capacity of less than 1 wt.% on activated carbons at a pressure of 100 bar and room temperature.

2.2.2 Structured carbon

The nanostructured carbons such as carbon nanotubes (Dillon et al. 1997, Cheng et al. 2001, Barghi et al. 2014 and Dundar et al. 2014), carbon nanofibres (Hwang 2002) and fullerene (Kuc et al. 2007 and Pupysheva et al. 2008) have also been investigated in recent years to explore their potential as hydrogen storage materials. Dillon and his co-worker (1997) was the pioneer who reported carbon nanotubes as a material for hydrogen

storage applications and stimulated worldwide research in the area. As a hydrogen storage material, carbon nanotubes have attracted considerable research interest because of its extraordinary chemical stability, hollowness and regular microstructure with high surface area (Shaijumon et al. 2005). Carbon nanotubes were reported to be mainly microporous (Zuttel et al. 2002). Both single and multi walled carbon nanotubes have been used for hydrogen storage (Darkrim et al. 2000 and Liu et al. 2003). The hydrogen is suggested to be adsorbed on the interior surface of the nanotubes forming a cylindrical monolayer as well as on external surfaces (Ioannatos et al. 2010). However, the complexity associated in the bulk synthesis of carbon nanotubes and inadequate reproducibility of reported data have limited the application of carbon nanotubes as an effective medium for hydrogen storage (Orinakova et al. 2011). The carbon nanofibres, consisting of graphene layers stacked together in various directions with respect to the axis of the fibers, have also been investigated (Strobel et al. 2006). Fullerenes and carbon nanohorns are also investigated for their hydrogen storage properties (Pubysheva et al. 2008 and Xu et al. 2007). A wide range of hydrogen storage capacities (0.005 – 20 wt.%) for different nanostructured carbons have been reported at different adsorption pressures (0.4-1000 bar) and temperatures (-196 to 400 ^{o}C) (Strobel et al. 2006 and Yurum et al. 2009).

Porous carbons with controlled pore structure have received significant attention for hydrogen storage applications. Researchers have used different techniques to synthesize carbons with controlled pore structure and recently synthesis method using inorganic templates has been reported for same. Porous carbons prepared by template method are reported to have a more defined pore structure as compared to conventionally prepared activated carbons (Kyotani 2000 Yang et al. 2007 and Hu et al. 2008). The surface properties of the templated carbons can be controlled by the process conditions during synthesis. In this method appropriate carbon precursor is deposited on an ordered inorganic porous template followed by heat treatment at elevated temperature. Deposition of carbon precursor can be done in vapor or liquid phase. The removal of the template is expected to result in formation of porous carbon having pore size comparable to the wall thickness of the template framework (Kyotani et al. 1997). The final structure, however,

was reported to be affected by shrinkage during carbonization process (Su et al. 2004). In another study, Kruk et al. (2000) observed that the pore size of the templated carbons can be tailored by controlling the pore wall thickness of the template. The pore size distribution of templated carbon was observed to be dependent on selection of template and carbon precursors (Kamegawa et al. 1997, Kyotani et al. 2003 and Fu et al. 2005). The ordered porous structure of the templated carbons is expected to provide more adsorption sites within the carbon network resulting in improvement of gas-solid interaction. It was reported that by tailoring the pore structure of carbon based storage materials towards lower pore size, particularly micropores, the hydrogen uptake capacity can be enhanced significantly for carbon based material in moderate adsorption conditions (Yang et al. 2007).

2.2.3 Templated carbon

Kyotani and his co-workers (1997) had first reported the ordered templated carbons with high surface area. Thereafter, different research groups have been exploring the potentials of templated carbons for hydrogen storage application. The synthesis of highly porous templated carbons using different forms of zeolite or silica as template has been reported. In recent studies, different organics precursors such as propylene, butylenes, acrylonitrile, furfuryl alcohol, pyrene, vinyl acetate, sucrose, etc. were used as carbon source for synthesis of templated carbons. Both chemical vapor deposition and carbonization methods were used to synthesize templated carbons (Chen et al. 2007, Yang et al. 2007, Johnson et al. 1997, Meyers et al. 2001, Kruk et al. 2005, Armandi et al. 2008, Nishihara et al. 2009, Kyotani et al. 1997 and Cai et al. 2014). Ma and his co-workers (2002) have reported a two step process consisting of filling of zeolite pores by carbon precursors in liquid phase followed by chemical vapor deposition of hydrocarbons such as propylene or butylenes. Kyotani and his co-workers (2003) reported zeolite templated carbons with surface area in the range of 1040-2470 m^2/g synthesized by chemical vapor deposition method. Chen and co-workers (2007) studied the effect of different counter cations of zeolites (Ca, K, H and Na) on hydrogen storage. The template pore structures were reported to be reflected in the surface properties of carbons. A hydrogen uptake capacity of 0.8 to 2 wt.% was reported at liquid nitrogen temperature and 1 bar pressure.

Templated carbon with a very high surface area of 3189 m^2/g was reported by Yang and his co-workers (2007) synthesized from deposition of acetonitrile vapor on zeolite template. The hydrogen uptake capacity was reported to be 6.9 wt.% at liquid nitrogen temperature and pressure of 20 bar. A linear dependency between hydrogen adsorption capacity and microporosity of prepared carbons was experimentally demonstrated by Armandi et al. (2008). Room temperature hydrogen uptake capacity of 0.41 wt.% for surface area of 1610 m^2/g and 0.87 wt.% for surface area of 3800 m^2/g were reported by Yang et al.(2007) and Nishihara et al. (2009), respectively at 98 bar pressure for zeolite templated carbons. Most of the reported templated carbons were prepared by chemical vapor deposition technique using different forms of zeolite as template.

Silica based mesoporous templates were also used to synthesize the templated carbons using various carbon precursors. The well-ordered MCM48 and SBA15 are two mostly reported silica based templates (Lee et al. 1999, Ryoo et al. 1999, Kruk et al. 2000, Jun et al. 2000 and Fuertes 2004). Ordered mesoporous carbons synthesized from MCM48 template using phenol formaldehyde resin with surface area of 1257 m^2/g was reported by Lee et al. (1999). Using the same template, Ryoo et al. (1999) reported surface area of 1380 m^2/g using sucrose as carbon precursor. Similar results were obtained by Jun and co-workers (2000) using SBA15 as template. Fuertes (2004) reported ordered mesoporous carbon with high surface area using furfuryl alcohol and ordered silica based template by tuning the pore wall thickness. Further, Armandi et al. (2008) studied the effect of synthesis temperature on carbons synthesized from various ordered silica based templates and observed that at higher synthesis temperature graphitic carbon content increased, whereas surface area and pore volume drastically decreased. In another study, Kruk et al. (2005) investigated the effect of infiltration rate of polyacrylonitrile precursor on the surface properties and pore structure of silica templated carbon. The reported Brunauer-Emmet-Teller (BET) surface area was in the range of 700-1790 m^2/g for the carbon synthesized using SBA15 as template and different carbon precursors. Li et al. (2001) reported synthesis of mesoporous carbon having pores in the range of 7-10 nm using amorphous silica gel template and acrylonitrile precursor. The effect of intermediate steps during synthesis was investigated by Bohme et al. (2005) for

amorphous silica gel templated carbon using sucrose as carbon precursor in presence of sulfuric acid. The reported surface area was in the range of 680-1843 m^2/g for the silica gel templated carbons synthesized from different carbon precursors. Most of the silica gel templated carbons were synthesized by carbonization method. The silica based templates were generally preferred for synthesis of mesoporous carbon whereas zeolite based templates were reported to be more suitable for the preparation of microporous carbon (Kruk et al. 2000 and Chen et al. 2007). However, Jimenez et al. (2012) reported that the ordered carbon materials adsorbed less hydrogen than the amorphous carbon.

2.2.4 Doped carbon

The hydrogen uptake capacity of carbon based materials mainly depends on physical properties of the carbons. The physisorption based hydrogen storage capacities at moderate temperature and pressure as reported till date are not adequate for practical mobile applications. In order to enhance the hydrogen uptake capacity under moderate conditions, the interaction between the hydrogen and carbon surface must be improved or modified. The increased interactions can be achieved by enhancing the number of active sites on carbon surface. One of the ways of enhancing the number of active sites is chemical modification of the surface by incorporation of heteroatoms.

Schwarz (1988) established the concept of spillover mechanism in order to explain the increased hydrogen storage capacity by addition of small amount of transition metals to carbon network. The dopant metal is expected to act as additional adsorption site as well as catalyze the dissociation of hydrogen molecules (Conner et al.1995). Chen and his co-workers (1999) reported the enhancement of hydrogen uptake at 200-400 ^oC under ambient pressure for lithium and potassium doped carbon nanotubes. The observed enhancement was greater than that of metal hydride based systems. Lueking and Yang (2004) also reported enhanced hydrogen storage capacity for the metal doped carbons and attributed it to hydrogen spillover.

Various non-metals were also reported as dopant for enhancement of hydrogen uptake capacity. The non-metals are lighter compared to that of metals. The non-metals such as

boron, nitrogen and sulfur have been incorporated in carbon matrix for hydrogen storage application. These non-metals can activate the hydrogen in carbon network (Viswanathan et al. 2003 and Sankaran et al. 2006). Theoretical calculations showed that the presence of different non-metals such as phosphorus, sulphur, boron and nitrogen in the carbon based adsorbents can activate the hydrogen (Viswanathan et al. 2003 and Sankaran et al. 2006). Zhu and co-workers (2006) had investigated the role of boron in graphene sheet for enhancement of hydrogen uptake by using the density functional theory method. They established that the boron substitution destabilized the graphene structure concentrating the electrons around the substituted boron. Later on the enhancement of hydrogen uptake by non-metal doped carbon was experimentally demonstrated. Sankaran et al. (2007) and Chung et al. (2008) reported enhanced hydrogen uptake capacity for boron substituted carbon nanotubes and microporous carbons respectively. Xia et al. (2012) and Sevilla et al. (2011) reported potential of sulfur doped microporous carbon as hydrogen storage material. The phosphorous substituted carbons were studied by Viswanathan et al. (2013). Hydrogen uptake capacity of 1wt.% was reported at room temperature and 40 bar pressure. In the following subsections, the hydrogen storage by different metal and non-metal doped carbons are discussed in details.

2.2.4.1 Doped activated carbon

The highly porous activated carbon with high surface area has gained considerable attention in hydrogen storage applications. However, the hydrogen uptake capacities of activated carbons are reported to be low due to its wide pore size distribution (Dillon et al. 2001). The enhanced hydrogen uptakes attributed to spillover mechanism in presence of metal have been reported by several authors and comprehensive review has been published by Wang et al. (2008). Various studies are reported on carbons doped with different metals such as cobalt, nickel, copper, platinum and palladium for hydrogen storage (Delia et al. 2009, Zielinski et al. 2007, Giraudet et al. 2011, Chuang et al. 2012, Figueroa–Torres et al. 2012 and Park et al. 2008). Nickel doped activated carbons were mostly reported for hydrogen storage at higher pressure and liquid nitrogen temperature. In one of the literature, Zielinski et al. (2007) reported a hydrogen uptake of 0.53 wt.% by nickel doped activated carbon at room temperature and pressure of 30 bars. They studied

the effect of three different nickel loadings, prepared from different nickel precursors, on surface area and pore volume. Figueroa–Torres et al. (2012) reported a hydrogen storage capacity up to 1.6 wt.% at a temperature of 30 ^{o}C and pressure of 50 bar for nickel doped activated carbons prepared by electroless deposition. They observed that the hydrogen uptake capacity of nickel doped activated carbon was two times higher as compared to that of undoped activated carbon.

Further, for nickel and cobalt modified carbons, thermal and acid treatments were reported to modify the textural properties and thereby enhance the hydrogen storage capacity (Delia et al. 2009). The authors observed that the thermal and acid pre-treatments of activated carbons had opposite effects on hydrogen uptakes. Thermal pre-treatment enhanced hydrogen uptake, however, acid pre-treatment did not favor the hydrogen–carbon interactions. Enhanced hydrogen uptake was observed by Park et al. (2008) on copper electroplated activated carbon fiber at a pressure of 30 bar. Fine and uniformly distributed platinum over activated carbon, prepared by vacuum impregnation, showed enhanced hydrogen uptake (Chuang et al. 2012). The transition metals with nearly filled d-shells were observed to be more favorable to initiate the hydrogen spillover (Contescu et al. 2009). Tsao et al. (2009) reported that lattice defects and pore network structure also played important roles in hydrogen adsorption via hydrogen spillover mechanism. The metal doped activated carbons also observed to have a wide range of hydrogen uptake capacity. This is mainly attributed to variation in surface area, metal type and amount as well as on irregular pore structures of activated carbons. Non-metal doped activated carbons were not reported in literature.

2.2.4.1 Doped templated carbon

The high surface area templated carbons have emerged as potential materials due to their ordered pore structure. Limited literatures are available on incorporation of heteroatoms in the templated carbons and are discussed below.

(a) Non metal doped templated carbon

Nitrogen doped carbons have attracted special interest due to their unique electronic, mechanical and adsorption properties among various non-metal modified carbons (Wang et al. 2009). Most of the reported nitrogen doped carbons were synthesized by chemical vapor deposition of acetonitrile on zeolite template (Hou et al. 2005, Yang et al. 2006, Wang et al. 2009, Xia et al. 2009 and Xia et al. 2011). Wide variation in physical properties was reported depending on the synthesis conditions. The surface area variation was reported in the range of 470- 3360 m^2/g and nitrogen loadings in the range of 3.7-8 wt.% . Hou et al. (2005) reported the synthesis of nitrogen doped carbon by vapor phase deposition of aceonitrile-furfuryl alcohol mixture as the feed using zeolite Y as the template. They reported the nitrogen loading and surface area in the range of 4-7 wt.% and 1080-3310 m^2/g respectively at different vapor deposition conditions. However, they did not report any hydrogen uptake. Yang et al. (2006) and Wang et al. (2009) later on reported hydrogen uptakes in the range of 0.5-4.3 wt.% for nitrogen doped carbon synthesized using different zeolite templates such as zeolite Y and zeolite13X. Depending on the synthesis conditions, ~5-8 wt.% nitrogen loading and 22- 1918 m^2/g surface area were reported. Xia et al. (2009 and 2011) reported synthesis of microporous nitrogen doped zeolite templated carbons using acetonitrile precursor by chemical vapor deposition method. Acetonitrile acted both as carbon and nitrogen precursors. A maximum nitrogen loading of 7.6 wt.% and maximum BET surface area of 3360 m^2/g were reported. The hydrogen uptake was observed to be about 6.4 wt.% for nitrogen doped carbon (BET surface area 3360 m^2/g and nitrogen loading 4.7 wt.%) at adsorption temperature of -196 ^oC and 20 bars .

Silica based templates were also reported for synthesis of nitrogen doped carbon by both carbonization and chemical vapor deposition methods. The silica based SBA12, MCM48, SBA15 and TUD1 templates were reported for the synthesis of nitrogen doped carbon using different precursors such as acetonitrile, polyacrylonitrile etc. (Xia et al. 2005, Lu et al. 2004 and Wang et al. 2012). The carbons synthesized using silica based templates were mesoporous in nature with maximum surface area of 1034 m^2/g (Xia et al. 2005). The nitrogen loadings were observed in the range of 0.6-8.8 wt.% (Lu et al. 2004, Xia et

al. 2005 and Wang et al. 2012). Hydrogen storage has not been reported for the nitrogen doped templated carbon synthesized using different silica based templates.

(b) Metal doped templated carbon

The literature on metal doped templated carbon is more scarce as compared to that of non-metal doped carbons. Recently, Giraudet et al. (2011) reported the synthesis of nitrogen enriched nickel doped ordered mesoporous carbon using silica based template. They reported the hydrogen uptake in the range of 0.04 to 2.3 wt.% at adsorption pressure of 30 bar and at different temperatures (100 to -196 ^{o}C). They attributed low uptake capacity to the low surface area. The enhancement of the binding energy between hydrogen and carbon was observed by Yang et al. (2011) in platinum incorporated high surface area zeolite templated carbons synthesized using chemical vapor deposition technique. The reported surface area was 912-2087 m^2/g of platinum doped carbon depending on the platinum loading. The maximum hydrogen uptake capacity of 2 wt.% was reported for 1 wt.% platinum loaded carbon at liquid nitrogen temperature and 1 bar pressure. Alam et al. (2011) reported higher surface area in the range of 1400–2200 m^2/g for platinum doped zeolite templated carbons. They reported 3.5-5.4 wt.% hydrogen uptake capacity at –196^{o}C and 20 bar with highest isosteric heat of adsorption (9 kJ/mol). Masika and his co-workers (2013) very recently reported palladium doped zeolite templated carbons where supercritical carbon dioxide was used as solvent for deposition of palladium nanoparticles. They observed decrease in surface area and pore volume of the templated carbons due to incorporation of palladium. However, they did not observe any change in the pore size and pore size distribution of the carbons due to palladium loading. Enhancement of hydrogen uptake was observed with higher isosteric heat of adsorption of 6.7 kJ/mol for palladium doped carbons as compared to undoped templated carbon (5.3 kJ/mol).

From the extensive literature review, as discussed above, it was observed that various metals and non metals were used as dopant to enhanced hydrogen storage. Among non metals nitrogen was selected for incorporation in templated carbons as it was reported to activate hydrogen and facilitate its adsorption. Among metals nickel, which is used

extensively as hydrogenation and dehydrogenation catalyst (Zielinski et al. 2007), was selected for incorporation in templated carbon to study the effect on hydrogen storage. Lower cost of nickel precursor was an additional advantage.

Chapter 3

Experimental

3.1 Preparation procedure

3.1.1 Materials used

The templated carbons were synthesized by carbonization using various templates such as ammonium zeolite Y (Sigma–Aldrich, Product No. 334413) and silica gel (Sigma–Aldrich, Product No. 403563). The furfuryl alcohol (Spectrochem Pvt. Ltd, 98%) and sucrose (Merck, GR) were used as carbon precursors. Acetonitrile (Merck, 99.9%) and aniline (Merck, 99.5%) were used as nitrogen precursors. The nickel acetate tetrahydrate (Sigma–Aldrich, 98%) and nickel nitrate hexahydrate (Merck, >97 %) were used as the precursors for nickel. Toluene (Merck, > 99 %), sulfuric acid (Merck, 98% GR) and hydrofluoric acid (Merck, 48%, HF) were used at different stages of preparation of templated carbon. The activated carbon used was procured from Sigma-Aldrich. All the chemicals were used in as-received condition.

3.1.2 Templated carbon from furfuryl alcohol

Templated carbons were prepared using zeolite Y and silica gel as the templates. The preparation steps of templated carbon using zeolite and furfuryl alcohol as carbon precursor are shown in Figure 3.1. The zeolite was first pretreated at 200 ^{o}C for 4h. Furfuryl alcohol (16 ml) was added to pretreated zeolite (4g) and stirred at room temperature for 72h. After the zeolite was filled with furfuryl alcohol, the sample was filtered and washed with toluene to remove excess furfuryl alcohol from external surface. The sample was dried at room temperature for 12h. Carbonization of zeolite filled with furfuryl alcohol was done in a stainless steel down flow fixed bed reactor in nitrogen flow. The flow rate of the nitrogen during carbonization was maintained at 100 ml/min. The carbonization was carried out at different temperatures (650, 750 and 850 ^{o}C) for different dwelling times (1, 2, 3 and 4h). Two different heating profiles were used; continuous and stepwise heating. In continuous heating method, sample was heated at constant rate of 10 ^{o}C/min up to desired carbonization temperature. In the stepwise method, the temperature was increased at same rate of 10 ^{o}C/min but a dwelling time of 30 minute was maintained after each increment of 100 ^{o}C. The templated carbons were

synthesized at different flow rates of nitrogen (100 and 50 ml/min) to observe the effect of flow rate, if any, on development of porous structure. After completion of carbonization at desired temperature and dwelling time, the zeolite–carbon composite was cooled down to room temperature under same nitrogen environment. Then the composite was treated in excess amount of 48% aqueous HF solution at room temperature for removal of zeolite. The treatment with aqueous HF was carried out for 24h. The zeolite was dissolved in HF. The black templated carbon was filtered and washed with deionised water several times for complete removal of HF-zeolite solution from the sample. The carbon sample was dried at 150 ^{o}C for overnight.

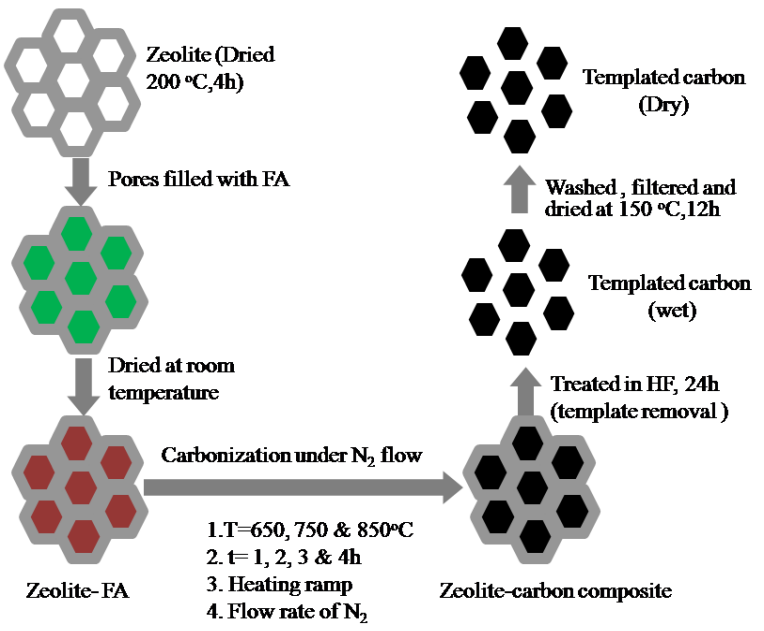

Figure 3.1. Preparation steps for zeolite templated carbon using furfuryl alcohol as carbon precursor.

The removal of zeolite was confirmed by EDX and XRD analysis. In XRD, no peaks due to zeolite were observed in final templated carbons. Al and Si were not detected in EDX. These are discussed in details in section 4.2. In text the zeolite– carbon composites are abbreviated as ZCT-t and final templated carbons are abbreviated as C_f-Z-T-t, where C,

Z, T and t represents carbon, zeolite, carbonization temperature and dwelling time in hour respectively. The subscript 'f' is used to denote the sample that was prepared using furfuryl alcohol.

The silica gel templated carbons were prepared from silica gel and furfuryl alcohol using similar method. The flow rate of the nitrogen during carbonization was kept at 100 ml/min and the stepwise heating profile was maintained for all samples. The silica gel templated carbon samples were abbreviated as C_f-SG-T-t, where SG represents silica gel template. The rest of the symbols are already defined in previous section. Removal of silica gel was confirmed by EDX analysis (Appendix A). No peak due to Si was observed. The complete removal of silica gel was also confirmed by TGA analysis of the templated carbons in oxygen environment. The TGA profile for C_f-SG-650-3 sample is included in Appendix B. The carbon was completely burned out in the temperature range of 400-750 ^oC in oxygen environment. No residual weight was observed after 750 ^oC confirming absence of any silica template.

3.1. 3 Templated carbon from sucrose

Sucrose was used as another carbon precursor for the synthesis of zeolite or silica gel templated carbons. The steps for preparation of zeolite templated carbon using sucrose are shown in Figure 3.2. The required amount of sucrose solution (5 g in 25 ml water) was added to zeolite (5g pretreated at 200 ^oC for 4h) in presence of sulfuric acid (0.05ml) and stirred at room temperature for 4h. The zeolite filled with sucrose solution was dried at 100 ^oC for 12h. The dried sucrose filled zeolite was allowed to undergo mild polymerization at 160 ^oC for 6h to give zeolite-sucrose composite. The added sulfuric acid acted as catalyst for polymerization of sucrose. The carbonization of the zeolite–sucrose composite was carried out at three different temperatures 650, 750 and 850 ^oC. The dwelling time was maintained for 2, 3 and 4h at each carbonization temperature. As discussed earlier, carbonization was carried out in the stainless steel down flow fixed bed reactor in flow of nitrogen (100 ml/min) with the stepwise heating profile. After carbonization, the zeolite-carbon composite was treated with aqueous HF, followed by the filtration and washing as discussed in the previous section. The templated carbons are

referred as C_s-Z-T-t, where the subscript 's' represents the sucrose and other symbols are same as defined in section 3.1.2.

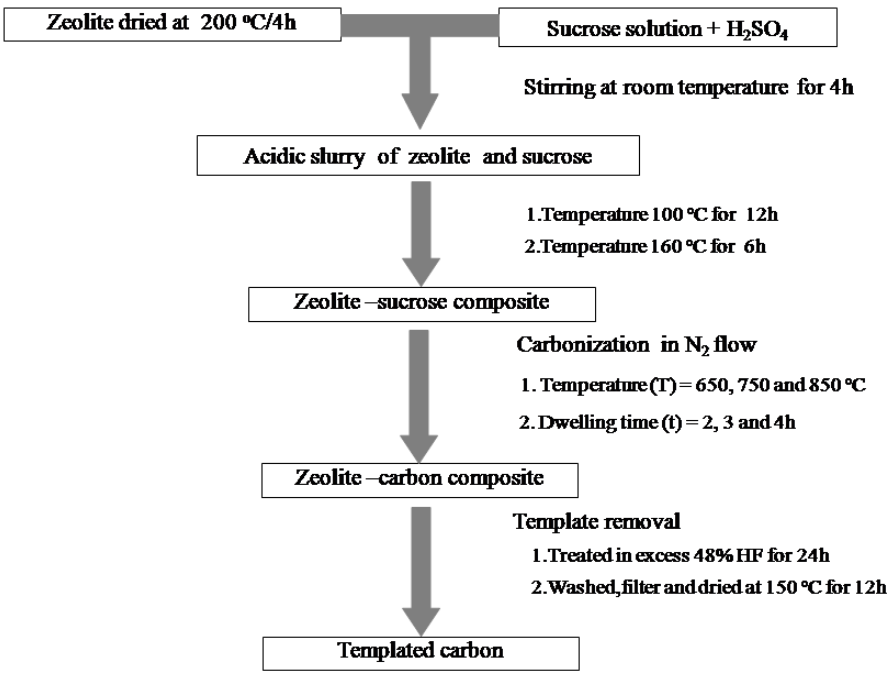

Figure 3.2. Preparation steps for zeolite templated carbon using sucrose as carbon precursor.

The silica gel templated carbon from sucrose was prepared in similar procedure as described above. In this case the carbonization temperature was fixed at 650 ^{o}C with a dwelling time of 3h. The silica gel templated carbon from sucrose is referred as C_s-SG-650-3 in text.

3.1.4 Doped carbon

The nitrogen doped templated carbons were synthesized using zeolite and silica gel templates and furfuryl alcohol as carbon precursor. Both acetonitrile and aniline were used as nitrogen precursors. The synthesis of nitrogen doped carbon was carried out by adding

required amount of nitrogen and carbon precursor to the template. The subsequent steps were similar to the synthesis of undoped templated carbons as described in section 3.1.2 The ratio of the template and precursors were as follows; for silica gel templated doped carbons equal amount of carbon and nitrogen precursors (20 ml each) were added to 5g template, while for zeolite templated doped carbons 10 ml of each of the precursors was added to 5g of zeolite template. The carbonization was carried out at 650 ^{o}C for 3h. The preparation steps for nitrogen doped templated carbon are shown in Figure 3.3. In the text, the doped templated carbon samples are referred as C–(SG or Z) – (Acn or Ani) as applicable, where SG, Z, Acn and Ani represents silica gel, zeolite, acetonitrile and aniline respectively.

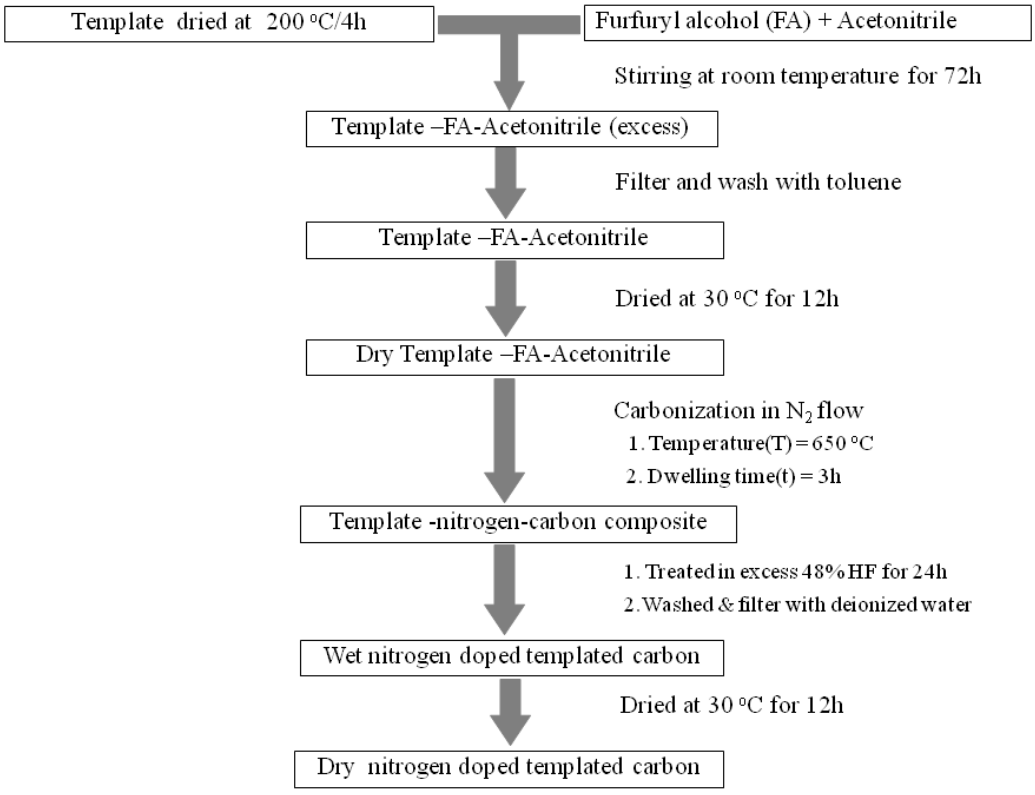

Figure 3.3. Preparation steps for nitrogen doped templated carbon.

The nickel doped templated carbons were synthesized using furfuryl alcohol (10 ml) and sucrose (5g) as carbon precursors and nickel acetate (1.8g) as the precursor for nickel. All nickel doped carbons were prepared by adding carbon and nickel precursor solutions to 5 g of zeolite or silica gel template. The synthesis procedure was similar to respective undoped templated carbon synthesized from furfuryl alcohol and sucrose precursors as described in section 3.1.2 and 3.1.3 respectively. The carbonization temperature and dwelling time were maintained at 650 ^{o}C and 3h respectively for preparation of all nickel doped templated carbons. The nickel doped templated carbons are referred in text as Ni-C_s-Z, Ni-C_s-SG, Ni-C_f-Z and Ni-C_f-SG, where Ni, C, Z, SG, s and f represent nickel, carbon, zeolite, silica gel, sucrose and furfuryl alcohol respectively.

The effect of agitation techniques, during the filling of the pores of the templates by carbon and nitrogen precursors, on final pore structure of templated carbon was studied. For this the mixture of template-furfuryl alcohol-acetonitrile was subjected to two different agitation techniques. The mixture was stirred using conventional magnetic stirrer or treated in ultra-sonicator. The remaining preparation steps were same as discussed in sections 3.1.2.

The nickel doped activated carbons were prepared by the impregnation method. The as–received activated carbon was impregnated by aqueous solution containing required amount of nickel nitrate hexahydrate. The sample was dried overnight at 110 ^{o}C followed by calcination at 300 ^{o}C for 2h to obtain the NiO doped activated carbon. The deposited NiO was reduced at 300 ^{o}C for 1h in hydrogen flow (30cc/min). This reduction temperature was selected based on TPR studies in which the samples were heated at a rate of 10^{o}C/min in the flow of 10 % H_2/Ar (30 cc/min). The steps of synthesis procedure of nickel doped activated carbon are shown in Appendix C.The undoped activated carbon is referred as AC in the thesis. The doped calcined samples are abbreviated as xNiO–AC (x=0, 5, 10, 15, 20, 25 and 30 wt. % of NiO) and corresponding reduced samples are designated as xNi –AC.

3.2 Characterization techniques

Characterizations of templates, templated carbons and doped carbons were carried out by various techniques such as TGA, XRD, surface area and pore analysis, SEM, FESEM, EDX, TEM, TPR and carbon monoxide pulse chemisorption to determine the physicochemical properties and understand their role in hydrogen storage.

3.2.1 Thermo gravimetric analysis

The TGA was carried out to evaluate the decomposition characteristics and thermal stability of the samples. The TGA of the powder sample was carried out in nitrogen environment in the temperature range of 25–900 ^{o}C using Mettler Toledo (TGA/SDTA 851^{e}) thermal analyzer. Heating rate was maintained at 10 ^{o}C/min. To test the completeness of removal of template, TGA of the templated carbons was also carried out in oxygen environment in same temperature range and heating rate as discussed above.

3.2.2 Surface area and pore analysis

The BET surface area and pore size analysis of the samples were determined by using a surface area analyzer (Beckman–Coulter; Model: SA3100) from nitrogen adsorption-desorption isotherm at –196 ^{o}C. The samples were degassed at 200 ^{o}C in vacuum (0.00 - 0.01mmHg) for 60 minutes prior to nitrogen adsorption–desorption measurement. In the instrument the nitrogen adsorption and desorption data were recorded in the relative pressure (Ps/Po) range of 0–0.99 and 0.99–0.43 respectively. The micropore area and micropore volume were calculated by t-plot method. The Barrett–Joyner–Halenda (BJH) method was used for determination of pore size distribution in meso and macropores. Average pore size was calculated based on BJH pore size analysis and hence represented average pore size of macro and mesopores.

3.2.3 X-ray diffraction analysis

The powder X-ray diffraction analysis was carried out for structural studies The X–ray diffractograms of samples were recorded in the 2θ range of 5–80^{o} using a Bucker X–ray D8 advance diffractrometer. The Cu–K_{α} radiation at 45 kV and 40 mA was used. The scan rate was maintained at 0.5 sec/step with an increment of 0.05^{o}. Analysis of the diffraction profiles was done using ICDD-JCPDS database. The crystallite size of sample was calculated using Scherer's formula;

$$D = (0.9\,\lambda / \beta \cos\theta) \qquad (3.1)$$

Where D is the crystallite size in nm and λ is the wavelength of radiation (λ= 0.154 nm). The β and θ are the peak width at half-maximum and peak position respectively. The peak with highest intensity was used for crystallite size calculations.

3.2.4 Scanning electron microscopy

SEM and FESEM were used to study the microstructure and surface morphology of the samples. The SEM analysis of samples was done using ZEOL (JSM 6390LV), whereas FESEM analysis was carried out by ZEISS (Model: 1430VP). For analysis, the samples were dispersed in a solvent and deposited on an aluminum foil which was mounted on a sample holder for gold coating to make the sample conducting. The gold sputtering was done approximately for 3 minute on all the samples.

3.2. 5 Energy-dispersive X-ray spectroscopy

The EDX technique was used to determine the elemental analysis of the samples. The EDX facility available with SEM (LEO, 1430vp) and FESEM (ZEISS, 1430VP) were used to record and analyze the EDX spectra.

3.2.6 Transmission electron microscopy

The TEM images were recorded by JEM 2100 (Make: JEOL). The sample preparation was done by first dispersing the sample in a solvent using ultrasonication, followed by deposition on a copper grid. The grid was further dried to evaporate the solvent and then mounted on the sample holder for TEM analysis.

3.2.7 Temperature programmed reduction

The reduction temperature of metals in metal doped carbon was determined by TPR using Chemisorb 2720 (Make: Micromeritics). The powder sample was outgassed at 150 ^{o}C in helium atmosphere. For each test typically about 30 mg of sample was used. TPR of the sample was carried out in the temperature range of 25–800 ^{o}C in flow of 10 % H_2/Ar. The flow rate of gas was maintained at 30 cc/min and the samples were heated at a rate of 10 ^{o}C/min.

3.2.8 Chemisorption

The dispersion and active metal area of metal doped carbon was determined by carbon monoxide pulse chemisorption at room temperature (30 ^{o}C) and atmospheric pressure. The Chemisorb 2720 (Make: Micromeritics) was used for chemisorption studies. Prior to chemisorption the metal oxide doped carbon sample was outgassed at 150 ^{o}C in helium flow (30 cc/min) followed by reduction of the metal oxide at the predetermined temperature. The reduced samples were flushed with helium (30 cc/min) at 200 ^{o}C for 1h to remove any adsorbed hydrogen. Helium was used as the carrier gas and the 10.6%CO/He gas mixture was used as the active gas. The active gas was injected in equal small volumes (0.5 cc) repeatedly until the sample was saturated. The amount of carbon monoxide adsorbed was calculated based on decrease in peak areas due to adsorption. Initially the calibration for carbon monoxide was done. The calculations for dispersion and active metal area were based on the assumption of linear adsorption of carbon monoxide on metal without any dissociation.

3.2.9 Raman spectroscopy

The graphitic nature of the templated carbons was characterized by Horiba Jobin Vyon, (LabRam HR) using laser of 514 nm. The data were collected in the range of 500 to 2000 cm^{-1} for exposure time of 30 sec.

3.2.10 Fourier Transform Infrared spectroscopy

FTIR was used to detect the functional groups present in the templated carbons. Shimadzu IR Affinity-1 was used. The spectra were recorded in the range of 400 to 4000 cm^{-1} using KBr technique at maximum resolution of 0.5cm^{-1}.

3.3 Hydrogen storage measurement

(a) Atmospheric pressure storage

The hydrogen uptakes at atmospheric pressure and different temperatures were measured by the temperature programmed desorption method (H_2-TPD) using Chemisorb 2720 (Micromeritics). In this method, hydrogen was allowed to adsorb on templated carbon samples at two adsorption temperatures of -100 ^oC and -50 ^oC. The pre-adsorbed hydrogen was analyzed by the TPD method in an inert gas environment. The sample was initially outgassed in flow of inert gas at 150 ^oC for 30 minute. Then the sample was cooled to adsorption temperature and the H_2/Ar gas mixture was passed through the sample for complete saturation. The saturated sample was then flushed with argon at same temperature, followed by gradual increase in temperature in same carrier gas. The desorbed hydrogen was recorded as function of temperature and time. The total area under the peak corresponded to the hydrogen uptake of the sample at the adsorption temperature. The system was initially calibrated with hydrogen gas. Calibration was done using argon as the carrier gas. The same flow rates were maintained for both calibration and analysis. For calibration, known amount of H_2/Ar mixture gas was injected into argon carrier gas and corresponding area under the peak was recorded. The peak areas for different known volume of H_2/Ar mixture gas were recorded. The peak area was plotted as function of hydrogen volume giving the calibration graph. Each point was repeated for

3-4 times and average values were used for minimizing any error. Using the calibration graph the amount of hydrogen desorbed was calculated. For nickel doped activated carbon the hydrogen adsorption was also measured at the higher adsorption temperature of 150 ^{o}C and 200 ^{o}C. For this analysis the hydrogen uptake by the sample was evaluated from the total area under the adsorption peak.

(b) High pressure storage

The hydrogen uptakes at moderate pressures and temperatures were measured using volumetric adsorption instrument iSorb-HP (Make: Quantachrome). The hydrogen adsorption-desorption isotherms were measured at the following conditions: (1) at –196 ^{o}C upto 8 bar, (2) at 0 ^{o}C upto 15 bar and (3) at 20 ^{o}C upto 15 bar.

Chapter 4

Templated carbon

4.1 Analysis of templates

Ammonium zeolite Y and silica gel were used as templates to synthesize the templated carbons at different carbonization temperatures and dwelling times. The physical properties of the templates were determined by surface area, XRD and FESEM analysis. The stability of the templates was evaluated using TGA analysis. To determine the effects of carbonization temperature and dwelling time on the structure of the templates, if any, the templates were characterized after treatment at different temperatures (650, 750 and 850 ^{o}C) for 3h. In the following sub-sections the detailed characterization studies of zeolite and silica gel have been discussed.

4.1.1 TGA analysis

The TGA profile of as-received ammonium zeolite Y is shown in Figure 4.1(a). A weight loss of ~10% was observed at 100 ^{o}C, which can be attributed to the evaporation of trapped water in the sample. The second weight loss of ~20% at higher temperature corresponded to the decomposition of the ammonium counter ions present in the zeolite framework. The decomposition of ammonium ions is not expected to have any adverse effect on the basic zeolite structure apart from increase in the effective aperture size. The ammonium ions decomposed at 240 ^{o}C as can be observed from the respective dm/dT curve. Finally, at 675 ^{o}C the observed weight loss of about 3–5% may be attributed to the loss of constitutive (chemical) water due to dehydration of zeolite structure (Su et al. 2004). No more weight loss was observed up to 900 ^{o}C. Hence, as per TGA analysis zeolite structure was mostly stable up to 900 ^{o}C apart from minor changes due to dehydration at 675 ^{o}C.

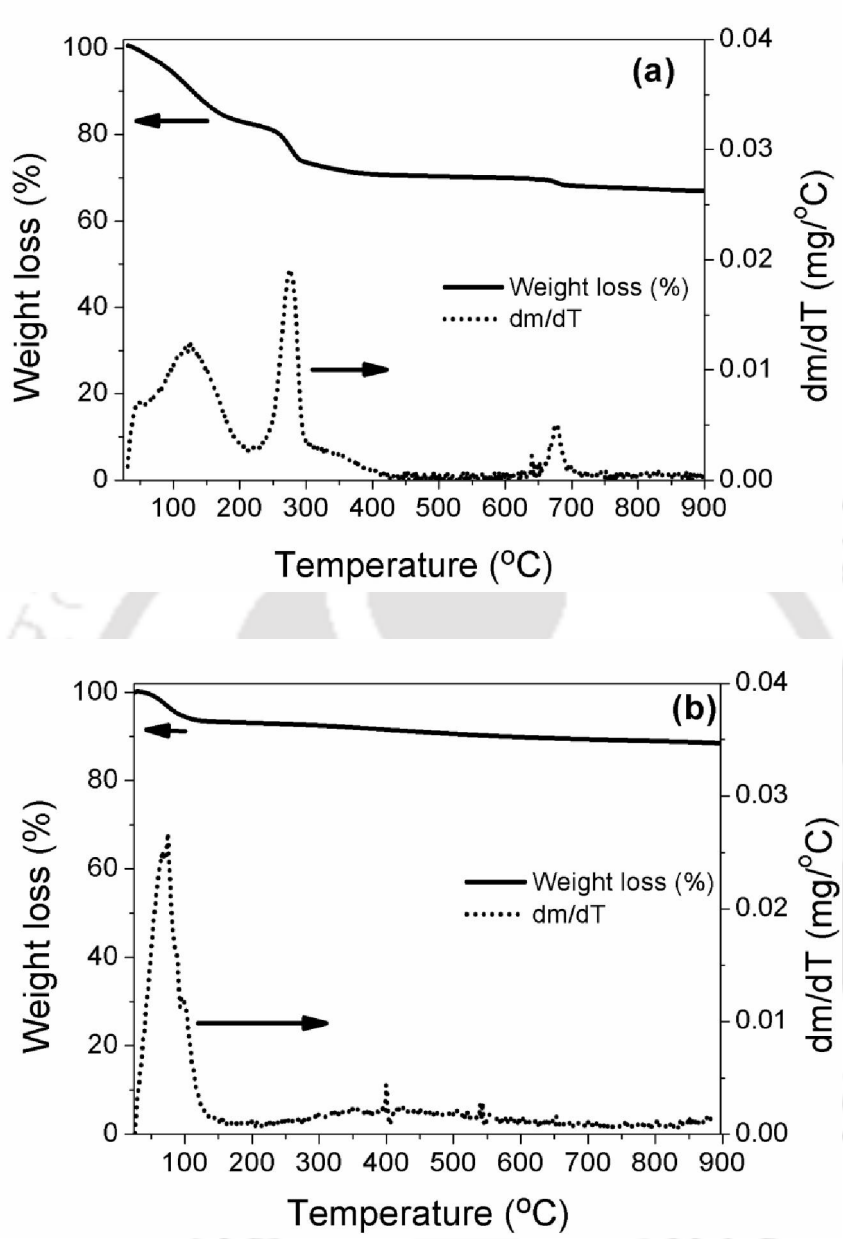

Figure 4.1. TGA profiles of as-received (a) NH_4 zeolite Y and (b) silica gel.

The TGA profile of as-received silica gel is shown in Figure 4.1(b). Weight loss of ~6% was observed at 100 ^oC, which corresponded to evaporation of trapped water. There was a very broad and low intense peak in the range of 300-550 ^oC which may be attributed to gradual loss in structural water. No further significant weight loss was observed up to 900 ^oC. Hence the silica gel was also mostly stable up to 900 ^oC. The effect of temperature on

porous structure and surface area of templates was studied by analyzing templates calcined at different temperatures.

4.1.2 Surface area and pore analysis

The nitrogen adsorption–desorption isotherms of the as–received zeolite and calcined zeolites at 650, 750 and 850 ^{o}C for 3h are shown in Figure 4.2. The nitrogen adsorption-desorption isotherms were of type I corresponding to microporous material (Sing et al. 1985). The volume of nitrogen adsorption decreased with increase in calcination temperature for calcined zeolites compared to as–received zeolite. The surface area, micropore area, pore volume and micropore volume of as–received zeolite and calcined zeolites are tabulated in Table 4.1. The surface area and pore volume decreased to some extent on calcination at higher temperature. The decrease in surface area and pore volume of zeolite was most significant at 850 ^{o}C. The micropore area and micropore volume drastically dropped from 678 m^2/g and 0.31 ml/g of as–received zeolite to 397 m^2/g and 0.18 ml/g respectively for zeolite calcined at 850 ^{o}C. The decrease of surface area and pore volume with calcination temperature may be attributed to partial collapse of the walls of finer pores of zeolite structure due to sintering as well as because of dehydration as observed during TGA analysis.

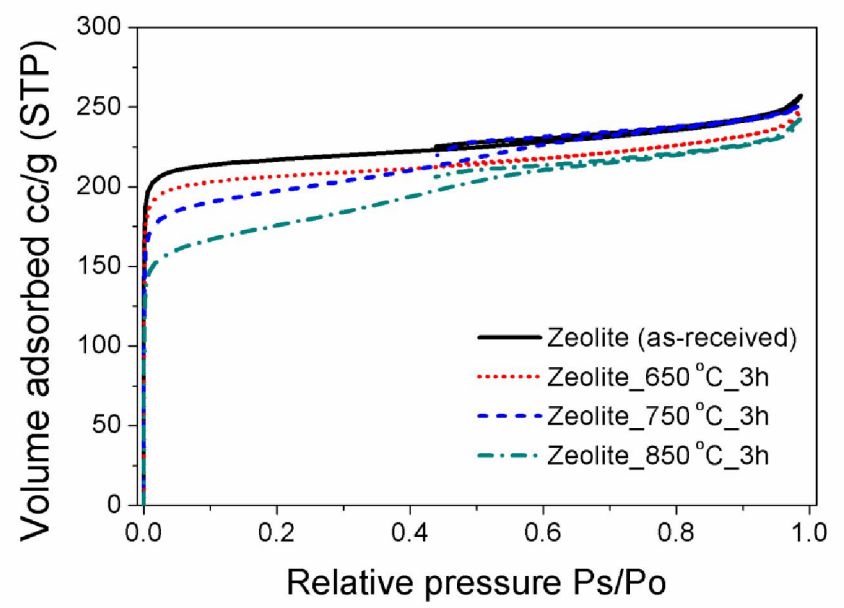

Figure 4.2. **Nitrogen adsorption-desorption isotherms of as-received and calcined zeolites at different temperatures.**

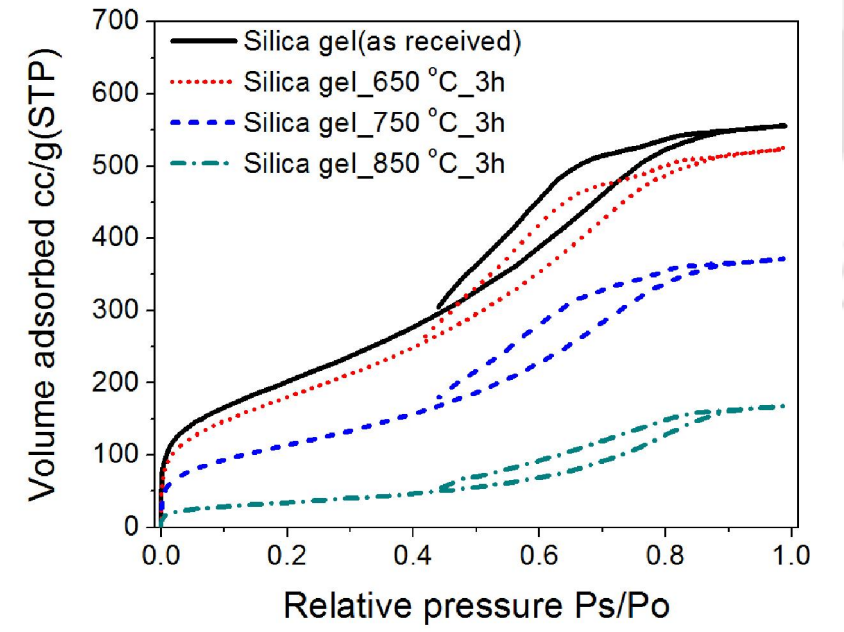

Figure 4.3. **Nitrogen adsorption-desorption isotherms of as-received and calcined silica gels at different temperatures.**

Table 4.1. Physical properties of as-received and calcined templates.

Sample	Calcination temperature (^oC)	Dwel -ling time (h)	BET surface area (m^2/g)	Microp ore surface area (m^2/g)	Total pore volume (ml/g)	Micro pore volume (ml/g)	Meso/ macro pore volume (ml/g)
Zeolite Y	As- received	-	758	678	0.39	0.31	0.08
Zeolite Y	650	3	702	641	0.38	0.29	0.09
Zeolite Y	750	3	668	538	0.39	0.24	0.15
Zeolite Y	850	3	602	397	0.37	0.18	0.19
Silica gel	As-received	-	740	–	0.86	–	0.86
Silica gel	650	3	665	–	0.81	–	0.81
Silica gel	750	3	421	–	0.57	–	0.57
Silica gel	850	3	127	–	0.26	–	0.26

a: based on meso and macropores

Figure 4.3 shows the nitrogen adsorption–desorption isotherms of the as–received silica gel and calcined silica gel samples. All the nitrogen isotherms were of type IV. The observed hysteresis loops were H2 type suggesting the presence of interconnected pores (Sing et al. 1985). Nitrogen adsorption slightly decreased for silica gel calcined at 650 ^oC compared to that of as–received silica gel. With increase in calcination temperature to 750 and 850 ^oC, the nitrogen adsorption further decreased. The surface area, pore volume and average pore size of as–received silica gel and calcined silica gels are included in Table 4.1. It was observed that the BET surface area decreased with increase in calcination temperature. On calcination at 650 ^oC with 3h dwelling time, the BET surface area dropped to 665 m^2/g from 740 m^2/g for as–received silica gel. On calcination of silica gel at 850 ^oC the BET surface area drastically decreased to 127 m^2/g. The total pore volume also decreased with increase in calcination temperature. The total pore volume of 0.86 ml/g of as–received silica gel dropped to 0.26 ml/g for sample calcined at 850 ^oC. The comparison of results for two templates shows that pore structure of silica gel

collapsed to greater extent compared to that of zeolite at higher calcination temperatures. The higher stability of the zeolite may be attributed to its rigid crystalline framework.

The BJH pore size distributions of the as–received zeolite and calcined zeolite samples are shown in Figure 4.4. The corresponding line figures are included in Appendix D. As can be observed from Table 4.1, the zeolite was a microporous material. According to the IUPAC classification; pores with diameter less than 2nm, 2-50nm and greater than 50 nm are considered as micropores, mesopore and macropore respectively. The pore size distributions shown in Figure 4.4 are the distributions of mesopores and macropores. The distribution of mesopores for as-received and calcined zeolite at 650 ^{o}C was more or less similar. Hence, the average pore sizes were also in the same range. For as–received zeolite it was 31.4 nm, and for calcined (at 650 ^{o}C) zeolite it slightly increased to 32.8 nm (Table 4.1). The volume percentage of lower mesopores having pore diameter less than 6 nm was maximum for zeolite when calcined at 750 ^{o}C. This percentage increase in lower mesopore volumes was a consequence of decrease in larger pores having diameter more than 20 nm. As a result, the average mesopore size decreased to 17.2 nm as observed in Table 4.1. At calcination temperature of 850 ^{o}C the pores having diameter less than 6 nm slightly increased due to the decrease in larger pores.

The pore size distributions of the as–received silica gel and calcined silica gel samples are shown in Figure 4.5. The corresponding line figures are included in Appendix D. For the as–received silica gel, about 80% of the pores were observed to have diameter in the range of 2–6 nm with an average pore diameter of 6.2 nm. With increase in calcination temperature, pores in the range of 2–6 nm decreased and pores in the range of 6–16 nm gradually increased. Consequently, the average pore size of calcined silica gels increased to 7.1 nm at 650 ^{o}C, 6.7 at 750 ^{o}C and 8.4 nm at 850 ^{o}C. The shift to higher pore size can be attributed to partial collapse of walls of finer pores. The effect was maximum for sample calcined at 850 ^{o}C resulting in highest average pore size. For all the silica gel samples the mesopores contributed to about 99% of the total pore volume with remaining contribution being from macropores as can be observed from Table 4.1. Micropores were not observed for any silica gel samples.

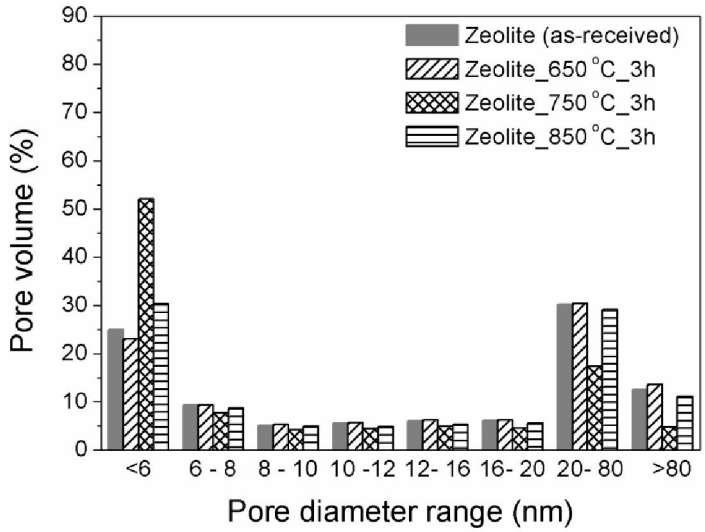

Figure 4.4. Pore size distributions of as-received and calcined zeolites at different temperatures.

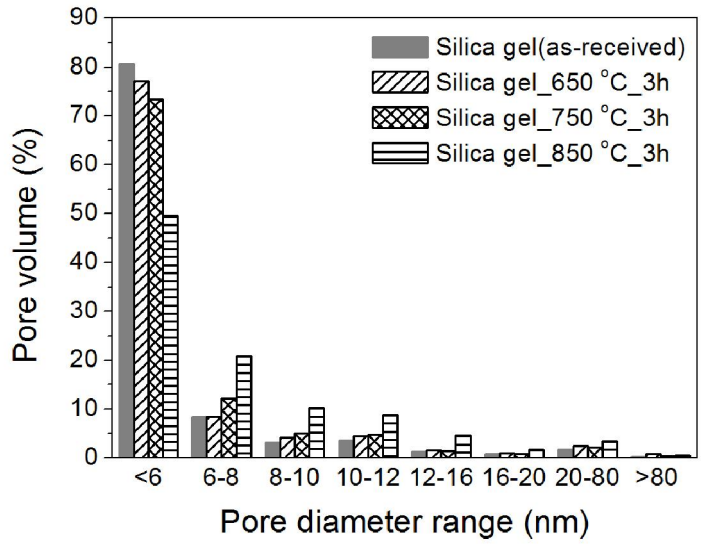

Figure 4.5. Pore size distributions of as-received and calcined silica gels at different temperatures.

4.1.3 XRD analysis

The XRD profiles of as-received zeolite and calcined zeolites (650, 750 and 850 ^{o}C with 3h dwelling time) were recorded to study the effect of temperature on the zeolite framework. The XRD profiles are shown in Figure 4.6. The crystalline nature of as-received zeolite was characterized by several sharp peaks. The strong peak at $2\theta = 6.3^{o}$ corresponded to (111) planes (Su et al. 2004). The intensity of XRD peaks was not affected significantly for zeolites calcined at 650 ^{o}C suggesting structural stability of zeolite. This can also be observed in Table 4.1 which showed only slight decrease in surface area and pore volume for zeolite calcined upto 650 ^{o}C. The TGA study also showed reasonable structural stability of zeolite upto 650 ^{o}C. However, on calcination at highest temperature of 850 ^{o}C noticeable decrease in XRD peak intensities was observed. It was reflected in significant decrease in surface area and pore volume as well (Table 4.1). This can be attributed to partial collapse of zeolite structure as discussed earlier.

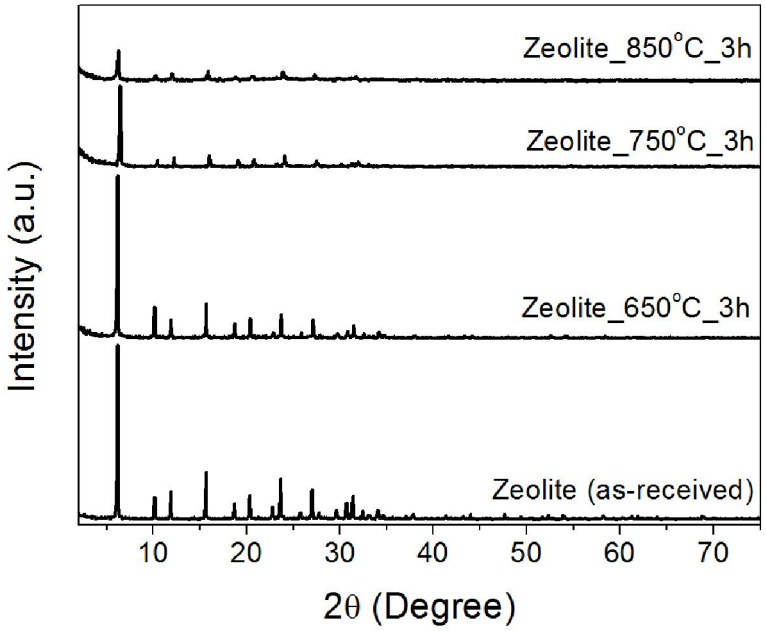

Figure 4.6. XRD profiles of as-received and calcined zeolites at different temperatures.

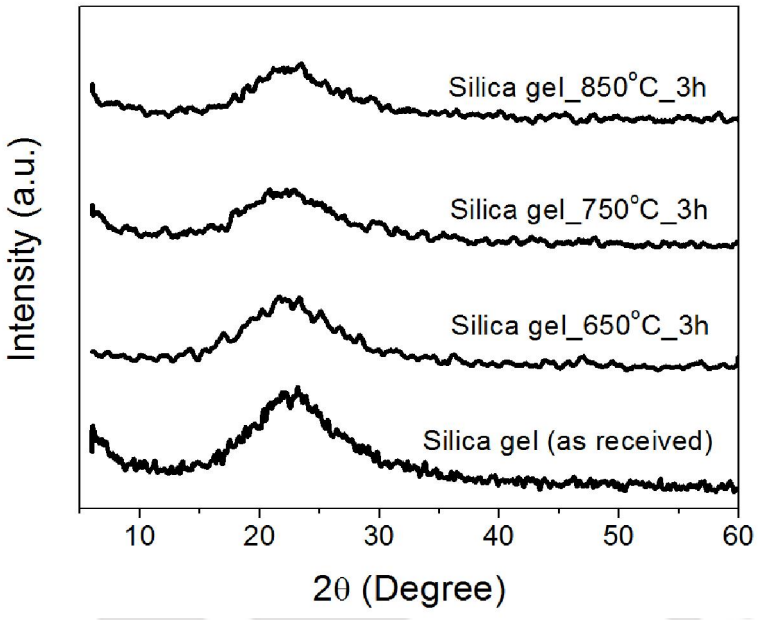

Figure 4.7. XRD profiles of as-received and calcined silica gels at different temperatures.

The XRD profiles of as-received and calcined silica gel at different temperatures are shown in Figure 4.7. The amorphous nature of the as–received silica gel was confirmed by the broad XRD peak which can be assigned to amorphous framework of SiO_2 (Powder diffraction file No. 00–029–0085). The XRD profiles of the calcined silica gel samples also corresponded to amorphous nature. Marginal decrease in peak intensity was observed for calcined silica gel samples.

4.1.4 FESEM analysis

The FESEM images of the as-received zeolite and silica gel are shown in Figure 4.8. Hexagonal and uniform plate shaped particles were observed for zeolite. For silica gel, plate shaped non uniform particles were visible. The images showed that average size of the agglomerated particles were higher for silica gel.

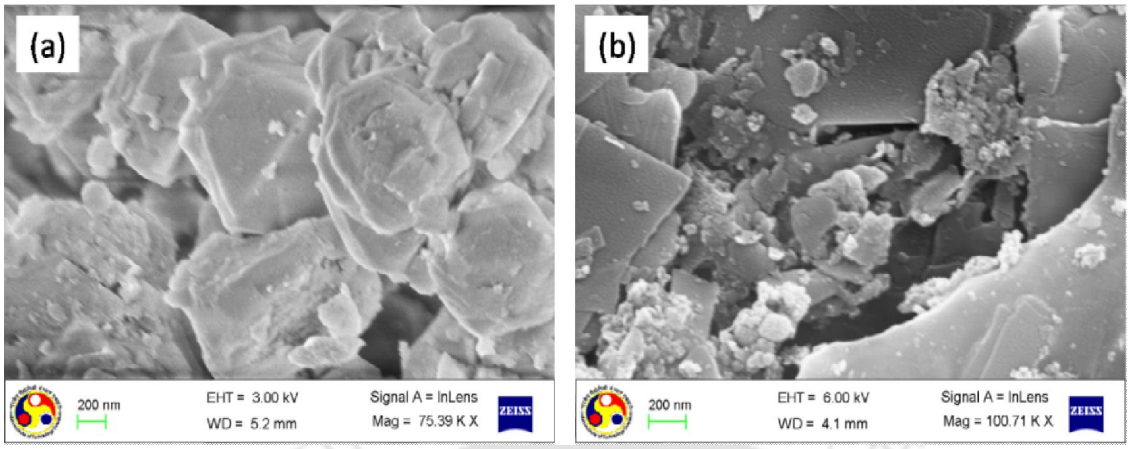

Figure 4.8. FESEM images of as -received (a) zeolite and (b) silica gel.

4.1.5 Summary

The characterizations studies of as-received and calcined templates showed that templates can be used upto 750 ^{o}C without any major effect on template structure. The marginal change in structure at higher temperature may have some effects on the final structure of the templated carbon. However, the effect may be minimized in presence of carbon precursors. The total surface area and morphology of both templates were similar but pore structure was different. For zeolite about 80% pores were below 2 nm while for silica gel the mesopores contributed about 99% of the total pore volume. Hence, zeolite and silica gel respectively may be considered mainly microporous and mesoporous in nature. The crystalline zeolite template was observed to be more stable compared to amorphous silica gel template at higher temperatures.

4.2 Zeolite templated carbon from furfuryl alcohol

Templated carbon was first prepared using zeolite as the inorganic template and furfuryl alcohol as the carbon precursor. The effects of synthesis parameters, such as carbonization temperature, dwelling time, heating profile and flow rate of carrier gas, on the structural development of the carbon materials were investigated in details. This was essential to understand how the synthesis parameters regulated the development of pore structure and to determine the optimum conditions for synthesis of carbon with higher surface area and desired pore sizes. The properties of the zeolite-carbon composites were studied by TGA, XRD and SEM to understand the stability and change in overall crystalline structure, if any, compared to the template itself. The properties of the final templated carbons were studied by surface area and pore analysis, XRD and FESEM. The hydrogen storage capacity was studied at atmospheric pressure at different temperatures.

4.2.1 Characterization of zeolite–carbon composites

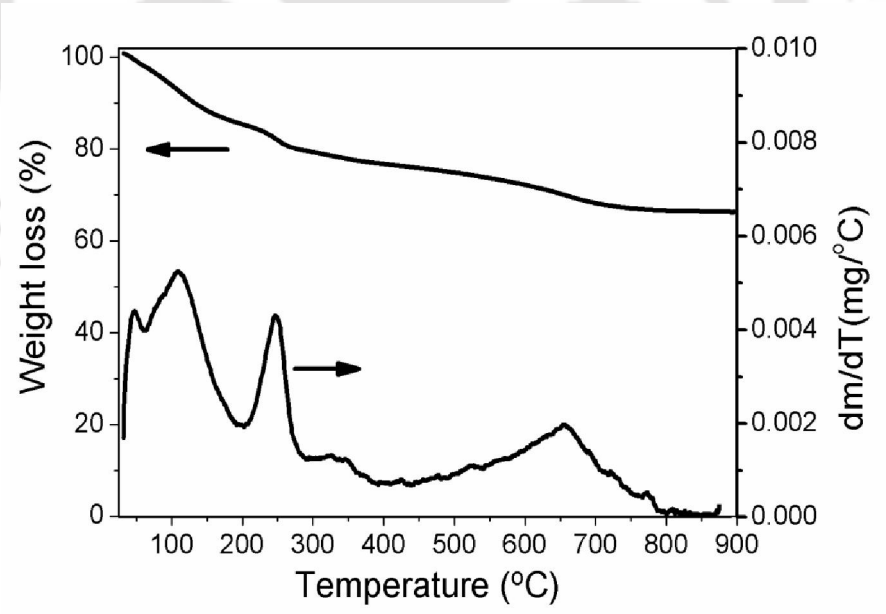

Figure 4.9. TGA profile of zeolite filled with furfuryl alcohol.

The TGA profile of zeolite filled with furfuryl alcohol is shown in Figure 4.9. The peak at 100 ^{o}C may be due to residual moisture in room temperature dried sample after deposition of carbon precursor. Since the zeolite was calcined at 200 ^{o}C for 4h before deposition of furfuryl alcohol, most of the ammonium ions were expected to be removed from the zeolite-furfuryl alcohol sample. Consequently the peak intensity was much reduced compared to that for as-received zeolite as shown in Figure 4.1(a). The furfuryl alcohol gradually decomposed upto 500 ^{o}C corresponding to the broad low intense peak. Similar decomposition of furfuryl alcohol was also observed for silica gel filled furfuryl alcohol sample as discussed in later section of 4.4.1. The observed weight loss in the temperature range of 200-500 ^{o}C was less than 21 %.

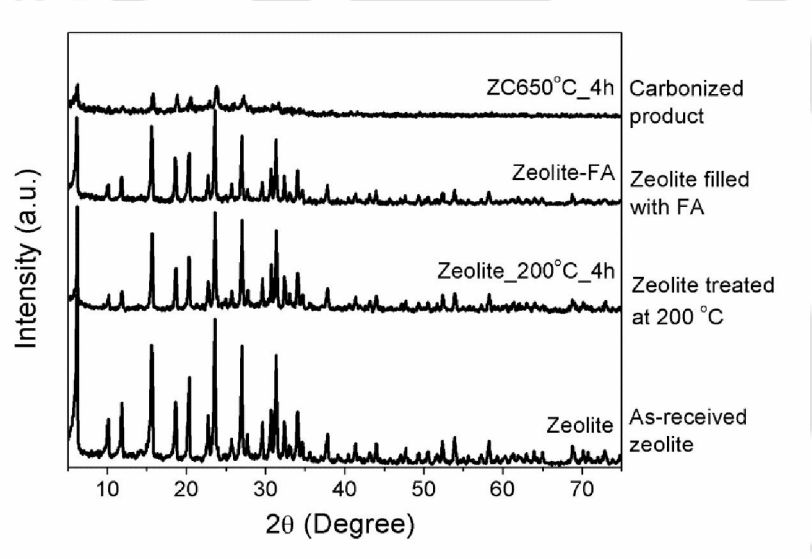

Figure 4.10. XRD profiles of zeolites at different stages of carbonization.

Figure 4.10 shows the XRD profiles of zeolites at each stage of carbonization process. For pretreated zeolite at 200 ^{o}C for 4h, the peak intensities were reduced slightly as compared to as-received. However, addition of furfuryl alcohol did not have much effect on the zeolite structure. Prominent reduction in peak intensities was observed in the XRD pattern of zeolite-carbon composite carbonized at 650 ^{o}C with 4h dwelling time. As was observed from Figure 4.6 the structure of pure zeolite was not affected significantly when calcined at same process temperature of 650 ^{o}C for 4h. The reduction of intensity of

zeolite peaks, as observed in Figure 4.10, may be attributed to presence of significant amount of amorphous carbon in the analyzed sample.

.

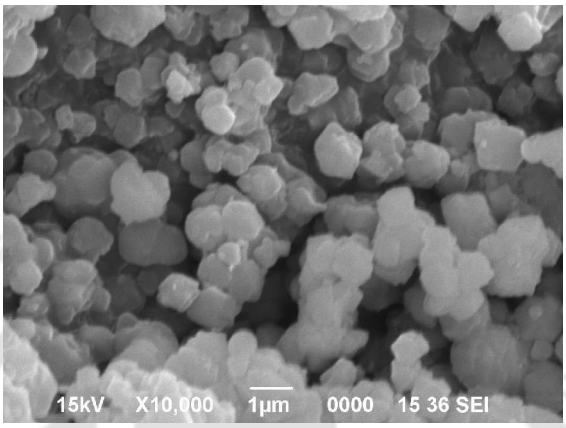

Figure 4.11. SEM image of as-received zeolite.

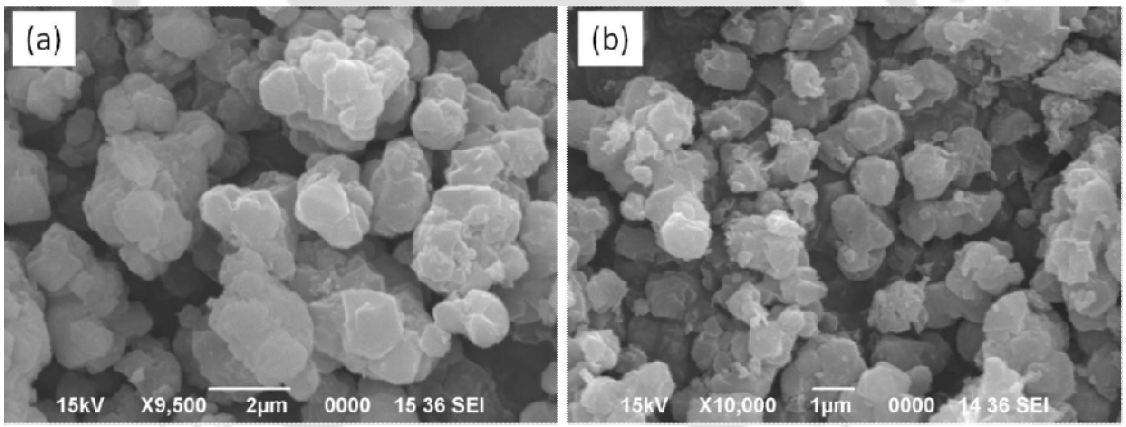

Figure 4.12. SEM images of (a) zeolite filled with furfuryl alcohol (b) zeolite-carbon composite carbonized at 650 ^{o}C.

The SEM image of as-received zeolite is shown in Figure 4.11, while that of furfuryl alcohol filled zeolite and zeolite-carbon composite (carbonized at 650 ^{o}C) are shown in Figure 4.12 (a-b). It was observed that the morphology of as-received zeolite (Figure 4.11) and zeolite-furfuryl alcohol particles possessed the same uniformity indicating that zeolite structure remained unchanged by deposition of furfuryl alcohol. The XRD patterns also agreed with this analysis. However, the particle size seems to be larger for

zeolite- furfuryl alcohol, which may be attributed to higher agglomeration in presence of furfuryl alcohol. The SEM image of zeolite-carbon composite after carbonization at 650 ^{o}C also possessed the same uniform microstructure of particles (Figure 4.12b).

4.2.2 Effect of carbonization temperature and dwelling time

The nitrogen adsorption-desorption isotherms of the templated carbons synthesized at different carbonization temperatures and dwelling times are shown in Figure 4.13 (a–c). The nature of nitrogen adsorption-desorption isotherms was same for templated carbons synthesized at different carbonization temperatures and dwelling times. All the isotherms were of type II according to the IUPAC classification (Sing et al. 1985). The hysteresis loops of H4 type were observed for all the isotherms indicating the presence of narrow slit-shaped pores. The volume of adsorbed nitrogen increased with increase in dwelling time up to 3h thereafter decreased at all carbonization temperatures. Nitrogen adsorption also decreased with increase in carbonization temperature.

Figure 4.14 depicts the BET and micropore areas of templated carbons prepared at various carbonization temperatures and dwelling times. It was observed that for all carbonization temperatures, with increasing dwelling time the BET and micropore areas increased upto 3h and then decreased at higher dwelling time of 4h. Highest BET surface area of 1000 m^2/g was achieved for templated carbon synthesized at 750 ^{o}C for 3h dwelling time. For 2h dwelling time there was not much effect on micropore surface areas as temperature increased from 650 to 750 ^{o}C. For 3h dwelling time, slight decrease in micropore area was observed with increase in temperature. A micropore surface area of 519 m^2/g was observed at 650 ^{o}C which decreased to 500 m^2/g at 750 ^{o}C for 3h dwelling time. Further, for 4h dwelling time micropore area decreased significantly with increase in temperature. Hence for maximum micropore area, 3h dwelling time and carbonization temperature in range of 650-750 ^{o}C were observed to be optimum.

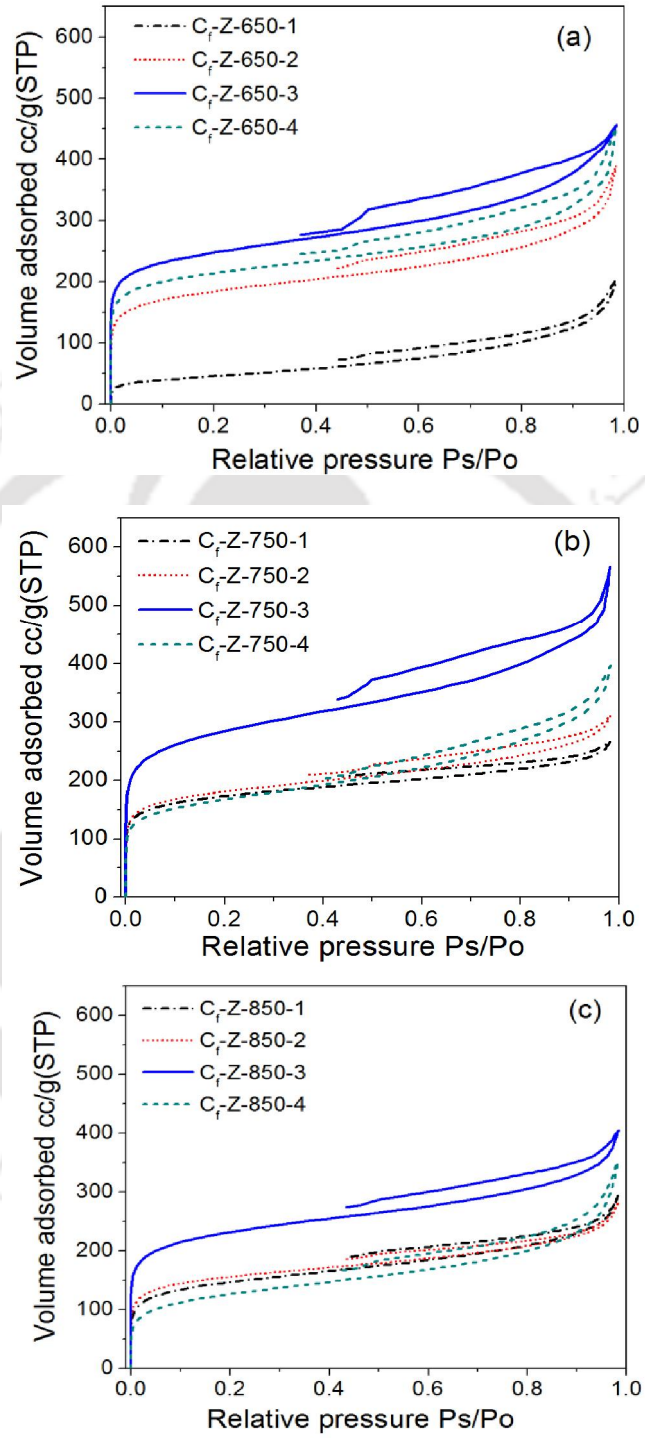

Figure 4.13. Nitrogen adsorption-desorption isotherms of zeolite templated carbons synthesized from furfuryl alcohol at different carbonization temperatures and dwelling times (a) 650 (b) 750 and (c) 850 ^{o}C.

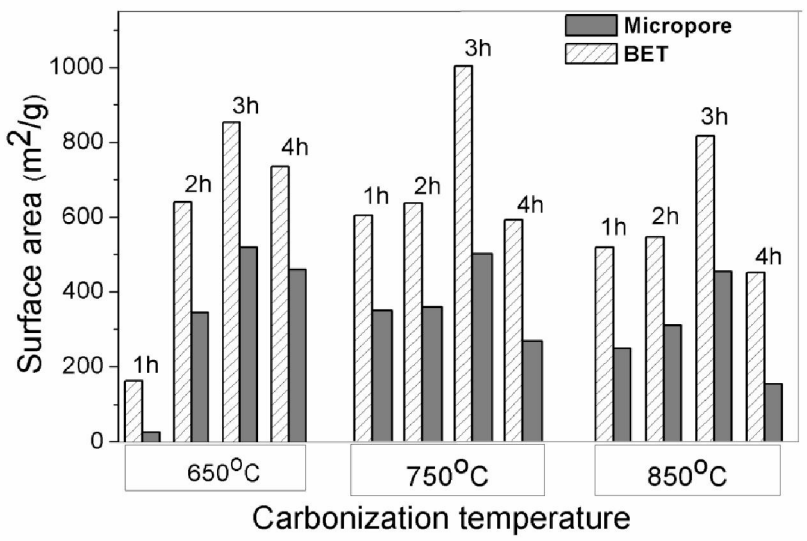

Figure 4.14. BET and micropore areas of zeolite templated carbons synthesized from furfuryl alcohol at various carbonization temperatures and dwelling times.

The pore size distributions of templated carbons are shown in Figure 4.15 (a-c). The volume percentage of pores having pore diameter less than 6 nm was maximum for templated carbon synthesized at 650 ^{o}C with 3h dwelling time. The generation of pores having diameter less than 6 nm was also significant for templated carbons synthesized at 750 ^{o}C with 2 and 3h dwelling times. All the samples consisted of pores mainly in the range of 2-6 nm and 20-80 nm. At all dwelling times, larger pores (20-80 nm) decreased and pores less than 6 nm increased as temperature increased from 650 to 750 ^{o}C. However at 850 ^{o}C, it was observed that larger pores again increased and less than 6 nm pores decreased. The effect was more severe at higher dwelling time of 4h. This observation can be attributed to the partial collapse of template structure at higher temperature and dwelling time thereby increasing larger pores. The volume percent of pores in the mesoporous range of 6-20 nm were not affected by temperature or dwelling time and were similar for all samples. Hence, in terms of maximizing pores of lower size, carbonization temperature of 650 ^{o}C was optimum.

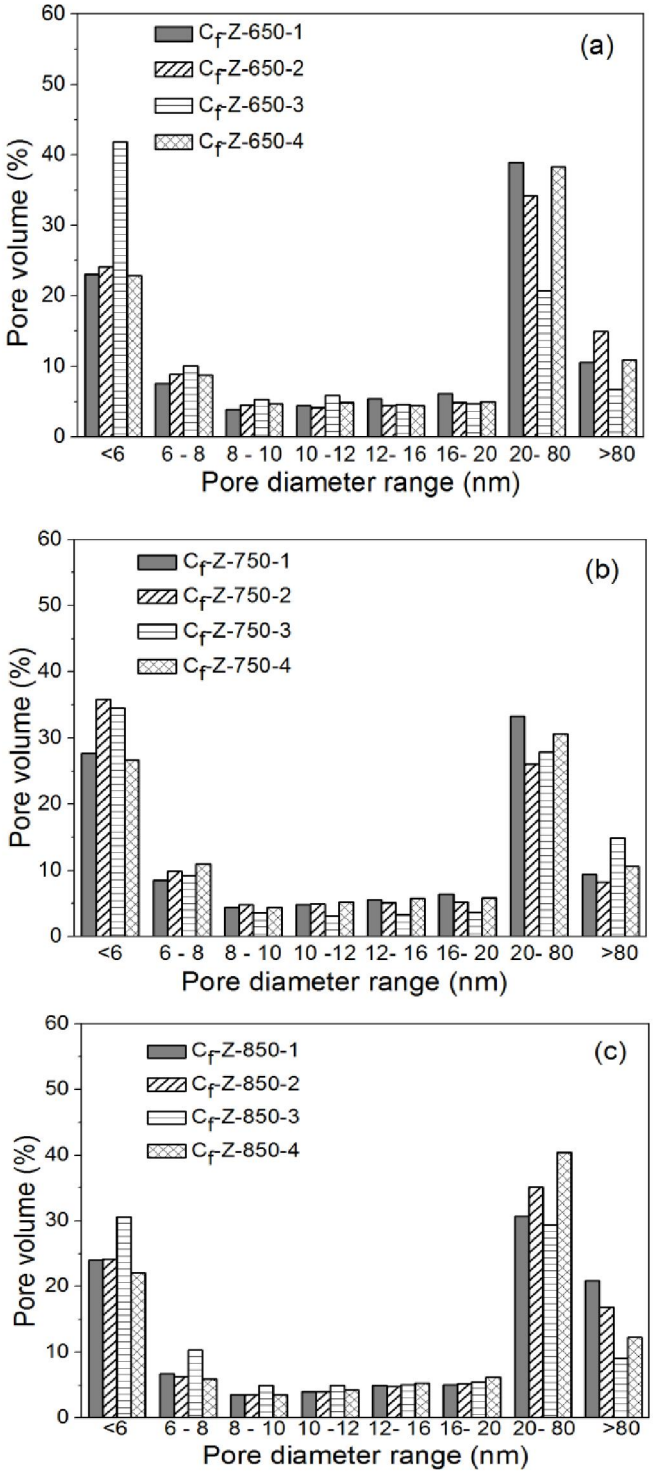

Figure 4.15. Pore size distributions of zeolite templated carbons synthesized from furfuryl alcohol at different carbonization temperatures and dwelling times (a) 650 (b) 750 and (c) 850 ºC.

Table 4.2. Total and micropore volumes of zeolite templated carbons synthesized from furfuryl alcohol at different carbonization temperatures and dwelling times.

Sample ID	Carbonization Temperature (^oC)	Dwelling time (h)	Total pore volume (ml/g)	Micropore volume (ml/g)
C_f-Z-650-1	650	1	0.30	0.01
C_f-Z-650-2	650	2	0.59	0.16
C_f-Z-650-3	650	3	0.70	0.23
C_f-Z-650-4	650	4	0.68	0.20
C_f-Z-750-1	750	1	0.41	0.16
C_f-Z-750-2	750	2	0.48	0.16
C_f-Z-750-3	750	3	0.87	0.22
C_f-Z-750-4	750	4	0.60	0.12
C_f-Z-850-1	850	1	0.45	0.11
C_f-Z-850-2	850	2	0.43	0.14
C_f-Z-850-3	850	3	0.62	0.20
C_f-Z-850-4	850	4	0.53	0.06
C_f-Z-750-3 (Stepwise)	750	3	1.31	0.51
C_f-Z-750-3 (50ml/min)	750	3	0.57	0.14

The total and micropore volumes of the templated carbons, as observed from Table 4.2, increased up to 3h and then decreased at higher dwelling time of 4h for all carbonization temperatures. The effect of carbonization temperature on total and micropore volumes was observed to be dependent on dwelling time. At lower dwelling time of 1h, the total pore volume increased with temperature and micropore volume showed a maximum at 750 ^oC. However, at higher dwelling time, the total and micropore volumes decreased with temperature. At 3h dwelling time highest total pore volume was observed at 750 ^oC.

From these observations, it can be concluded that at all carbonization temperatures, at least 3 h dwelling time was needed for pore formation. At lower dwelling time, pore formation was incomplete and at higher dwelling time sintering resulted in collapse of

pore structure, thereby decreasing total and micropore volumes. The sintering effect was more severe for micropores. Similarly at low carbonization temperature, higher dwelling time was required for pore formation. However, for higher dwelling time of 4h, high temperature of 850 ^{o}C resulted in severe sintering and large decrease in micropore volume.

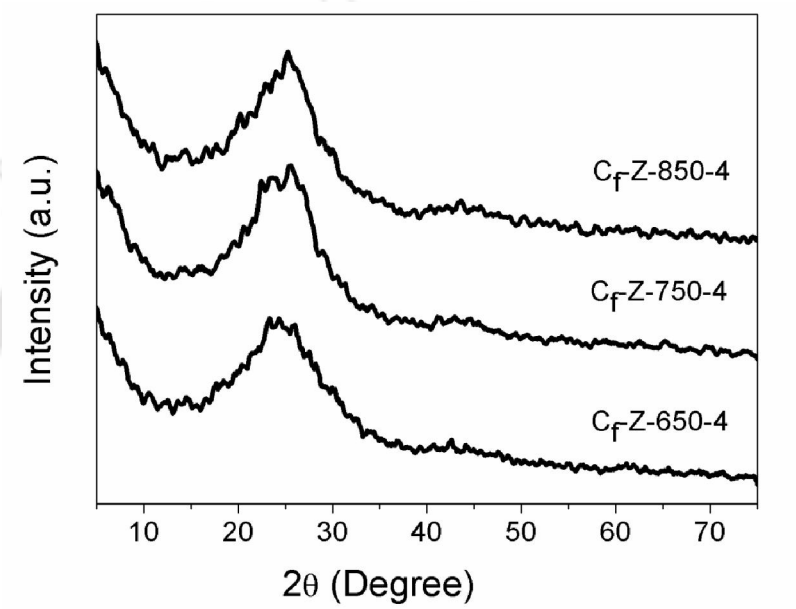

Figure 4.16. XRD profiles of zeolite templated carbons synthesized from furfuryl alcohol at different carbonization temperatures with dwelling time of 4h.

The XRD profiles of templated carbons synthesized at different carbonization temperatures at dwelling time of 4h are shown in Figure 4.16. The XRD patterns of templated carbons exhibited a broad XRD peak at 2θ =25.4^{o} which corresponded to the (002) plane of graphitic carbon. The intensity of the graphitic carbon peak was slightly higher for carbon synthesized at 750 ^{o}C. Absence of any peak due to zeolite in the carbon sample suggested complete removal of the template during HF treatment. This was also confirmed by EDX analysis as shown in Figure 4.17.

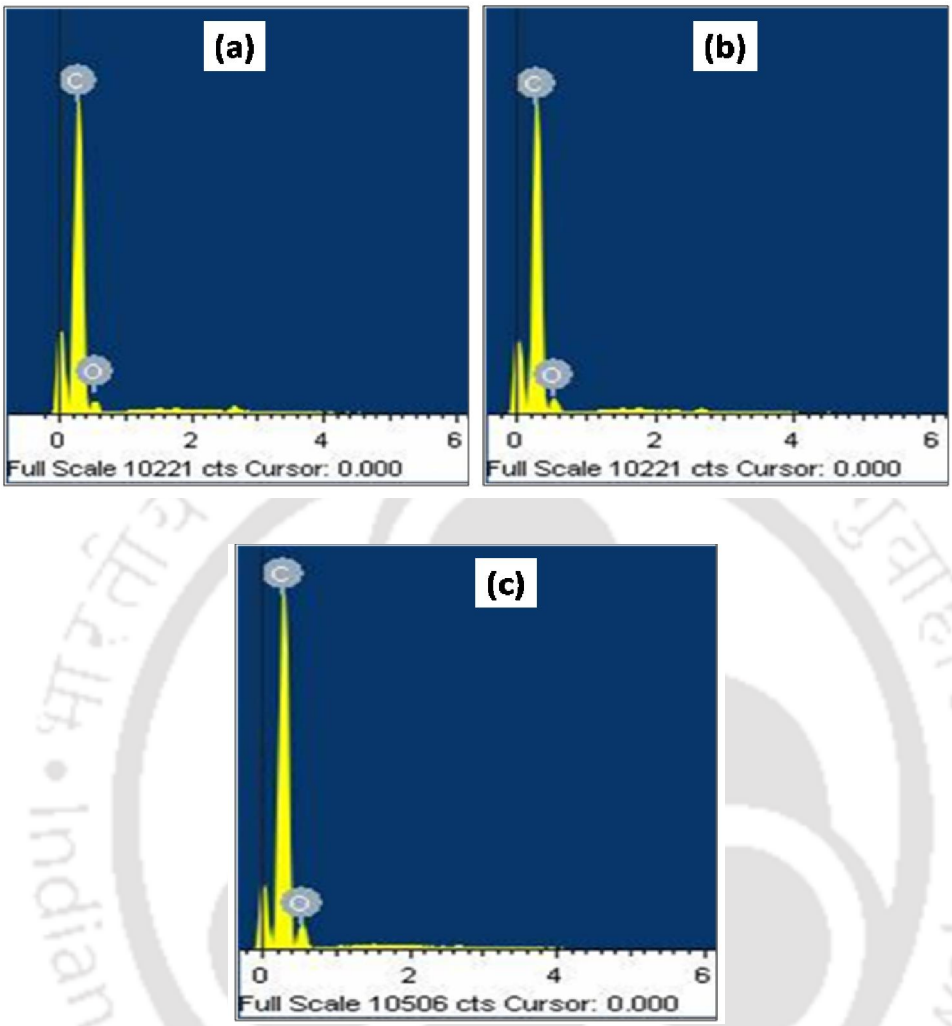

Figure 4.17. EDX spectra of zeolite templated carbons synthesized from furfuryl alcohol at different carbonization temperatures at dwelling time of 3h.

The FESEM images of templated carbons synthesized at different temperatures are shown in Figure 4.18. Flowery kind of structure was observed for all the samples.

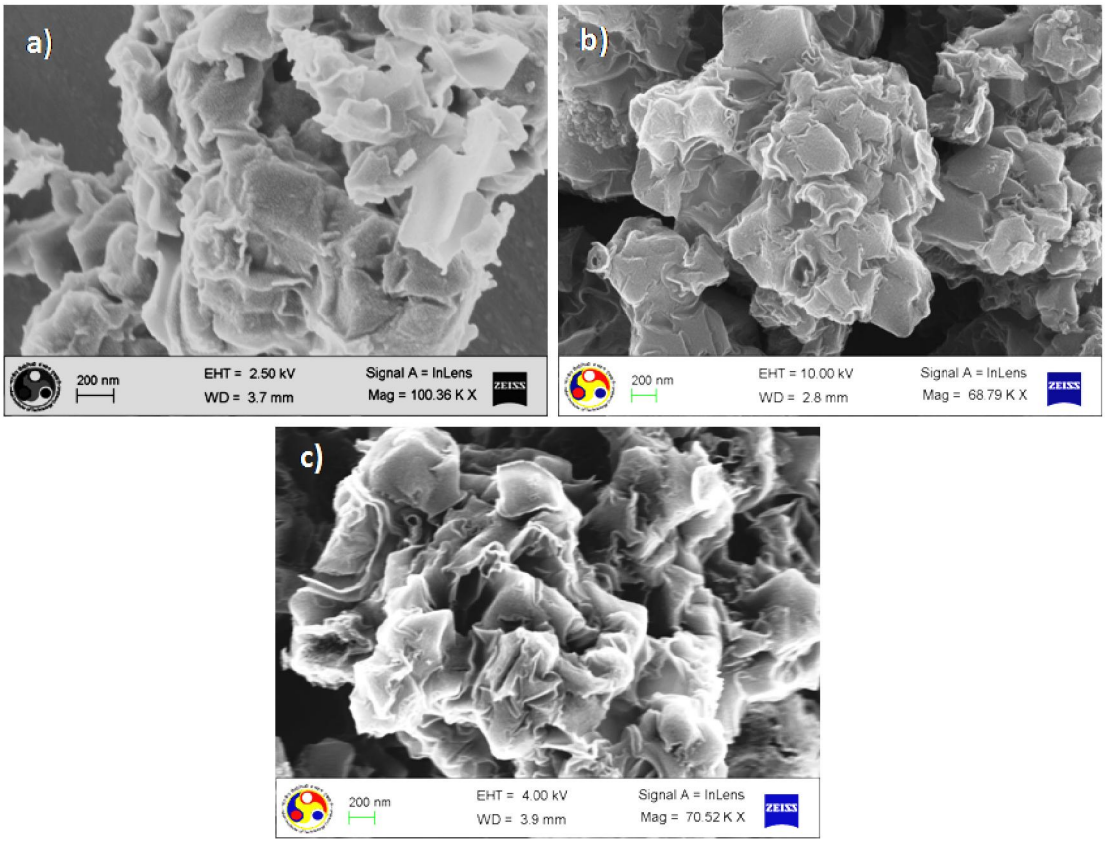

Figure 4.18. FESEM images of zeolite templated carbons synthesized from furfuryl alcohol at dwelling time of 3h and different temperatures of (a) 650 (b) 750 and (c) 850 ^{o}C.

4.2.3 Effect of heating profiles

To study the effect of heating profiles, carbonization was carried out at two conditions; (1) continuous heating at a rate of 10 ^{o}C/min and (2) step wise heating in which temperature was increased at a rate of 10 ^{o}C/min with 30 minute dwelling time at each 100 ^{o}C interval upto the predefined carbonization temperature. Figure 4.19 illustrates the nitrogen adsorption-desorption isotherms of templated carbons synthesized at 750 ^{o}C with 3h dwelling time with and without stepwise rise in temperature. The nature of the isotherms were same for both samples, type II with H4 hysteresis loop, as discussed earlier. It was observed that for stepwise heated samples, nitrogen adsorption was higher.

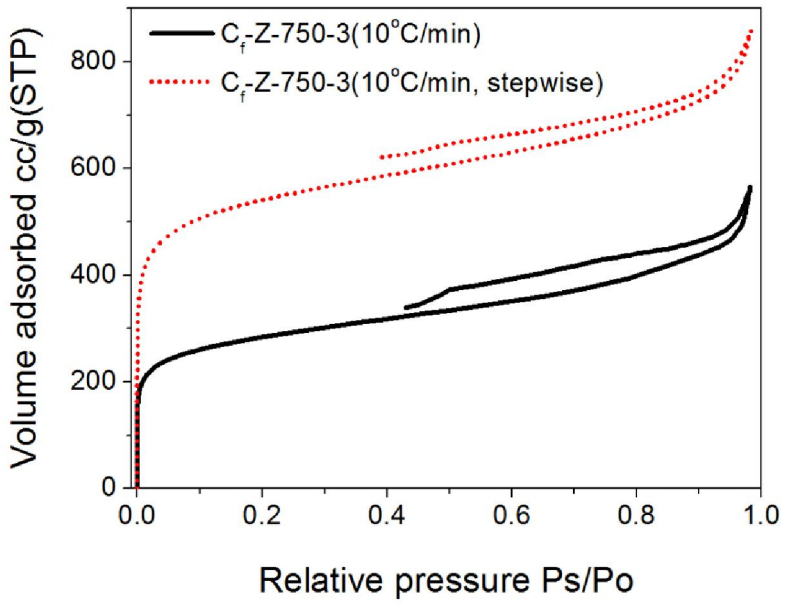

Figure 4.19. **Nitrogen adsorption-desorption isotherms of zeolite templated carbons synthesized from furfuryl alcohol with different heating profiles (carbonization temperature 750 °C with 3h dwelling time).**

Figure 4.20 depicts the corresponding BET and micropore surface areas. The maximum BET surface area of 1886 m^2/g and micropore area of 1136 m^2/g were observed for templated carbon with stepwise heating profile. In stepwise heating, the initiation of carbonization process was expected to be slower than continuous heating process and seemed to have favored formation of pore structure that resulted in higher surface area and micropore area. Thus observed increased in total and micropore volume for stepwise heated sample (Table 4.2) can be attributed to better development of porous structure. However as the final temperature approached, higher residence time in higher temperature may also have resulted in some additional sintering compared to continuous heating profile. This can be observed from the pore size distributions in Figure 4.21 which clearly shows that stepwise heating increased the pores in the range of 20-80 nm.

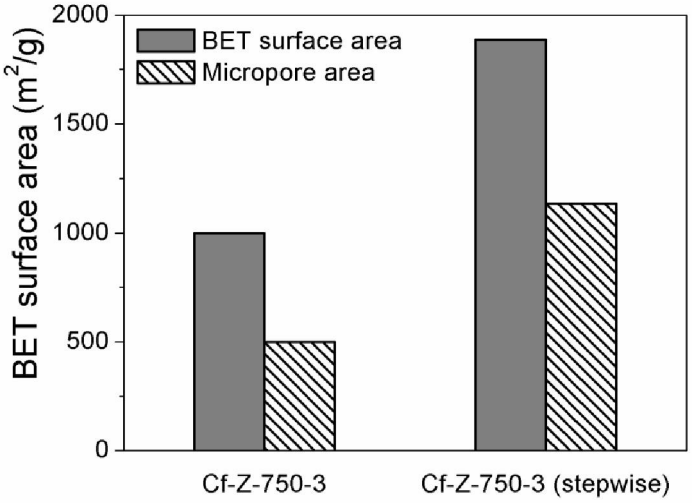

Figure 4.20. BET and micropore areas of zeolite templated carbons synthesized from furfuryl alcohol with different heating profiles (carbonization temperature 750 °C with 3h dwelling time).

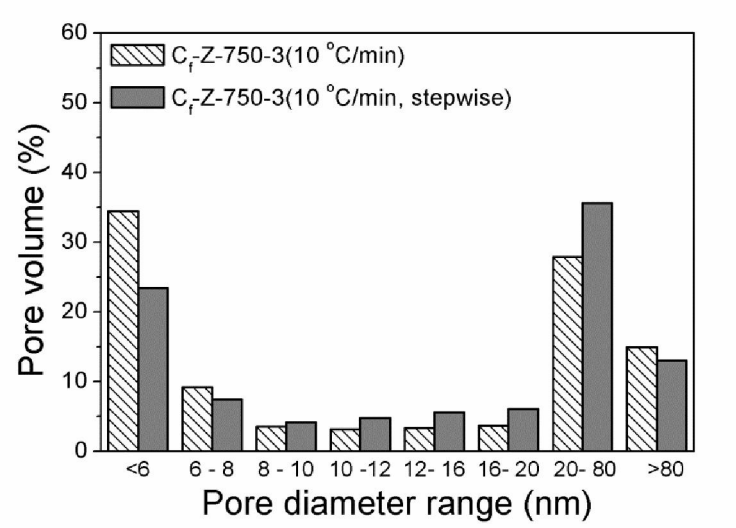

Figure 4.21. Pore size distributions of zeolite templated carbons synthesized from furfuryl alcohol with different heating profiles (carbonization temperature 750 °C with 3h dwelling time).

The XRD patterns of templated carbon samples synthesized with and without stepwise heating profiles are shown in Figure 4.22. A broad peak at $2\theta = 25.4^{o}$ corresponding to

the graphitic carbon was observed in both samples. The intensity of the peak was significantly higher for carbon prepared by stepwise heating (C_f-Z-750-3, stepwise) compared to that prepared by continuous heating (C_f-Z-750-3) implying formation of greater proportion of graphitic carbon in former.

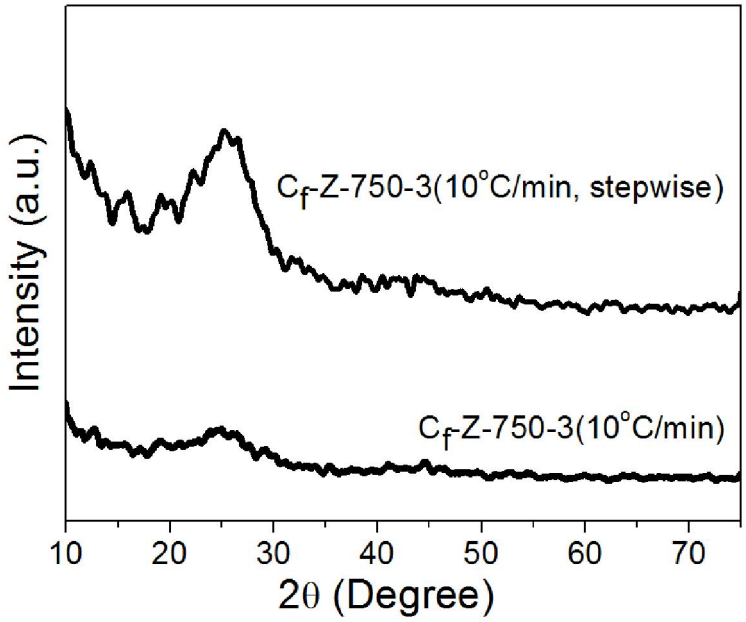

Figure 4.22. XRD profiles of zeolite templated carbons synthesized from furfuryl alcohol with different heating profiles (carbonization temperature 750 °C with 3h dwelling time).

4.2.4 Effect of flow rate of carrier gas

The effect of flow rate of carrier gas on properties of templated carbon was studied at two flow rates of 100 and 50 ml/min at carbonization temperature of 750 °C with 3h dwelling time. The nitrogen adsorption-desorption isotherms of carbons synthesized at the two flow rates are shown in Figure 4.23. The nature of the isotherms was type II with H4 hysteresis loop. Low nitrogen adsorption was observed at lower nitrogen flow rate.

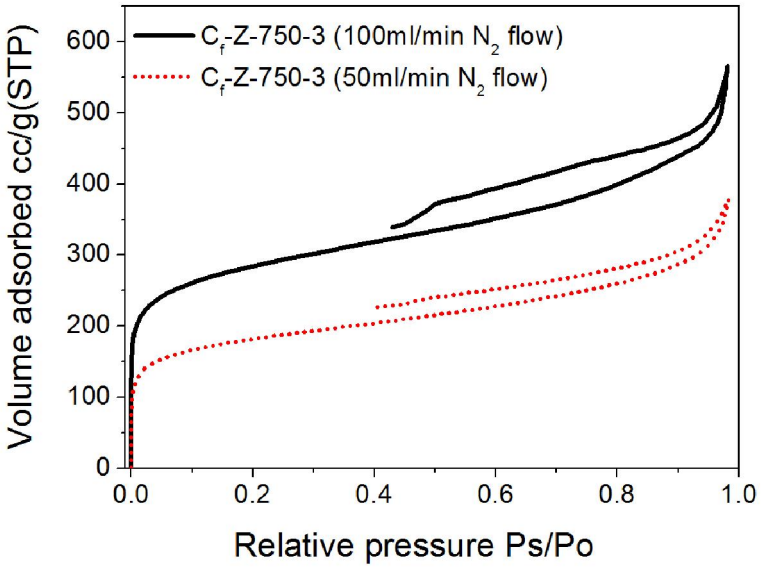

Figure 4.23. Nitrogen adsorption-desorption isotherms of zeolite templated carbons synthesized from furfuryl alcohol with different nitrogen flow rates (carbonization temperature 750 ^{o}C with 3h dwelling time).

The BET and micropore surface areas of templated carbons synthesized at 750^{o}C for 3h dwelling time with different nitrogen flow rates are shown in Figure 4.24. On decreasing the nitrogen flow rate from 100 to 50 ml/min, the BET surface area of 1000 m^2/g decreased to 632 m^2/g, whereas the micropore surface area of 500 m^2/g decreased to 306 m^2/g respectively. The results may be explained as follows. The flow of inert gas helped to remove the product gases of the carbonization and also avoided development of any hotspots. At low flow of nitrogen, slower removal of product gases may have affected the forward reactions, thereby resulting in incomplete pore structure formation giving lower surface area and pore volume. Increased probability of formation of hotspots at lower flow rate may have also resulted in higher sintering and formation of large pores as can be seen in the pore size distribution in Figure 4.25. At lower flow rate pores in 20-80 nm range increased. The XRD profiles (Figure 4.26) showed graphitic peak at 2θ =25.4^{o} for both the carbon samples.

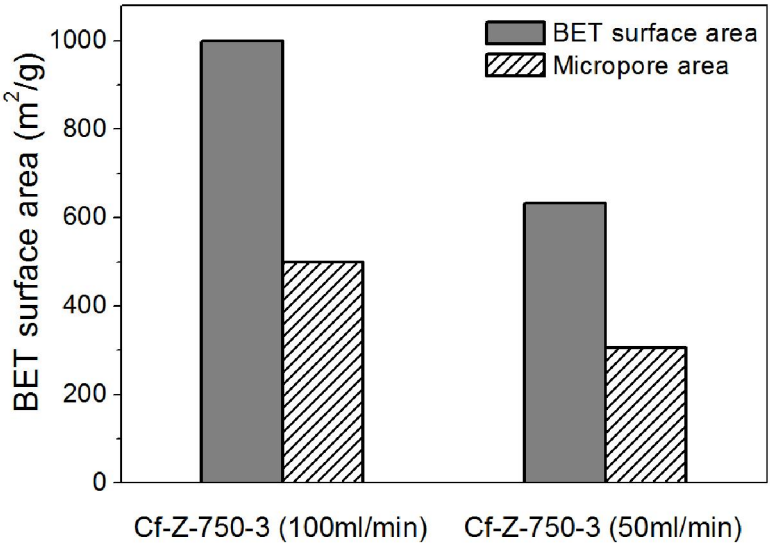

Figure 4.24. BET and micropore areas of zeolite templated carbons synthesized from furfuryl alcohol with different nitrogen flow rates (carbonization temperature 750 °C with 3h dwelling time).

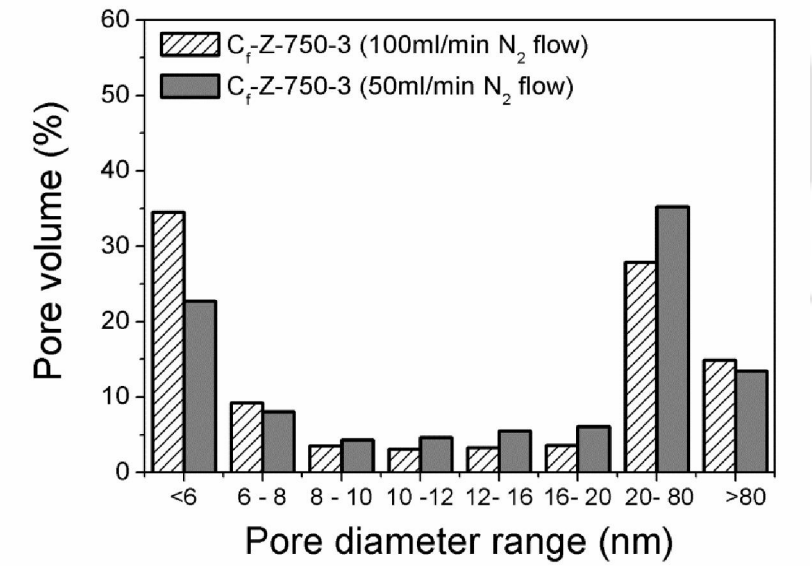

Figure 4.25. Pore size distributions of zeolite templated carbons synthesized from furfuryl alcohol with different nitrogen flow rates (carbonization temperature 750 °C with 3h dwelling time).

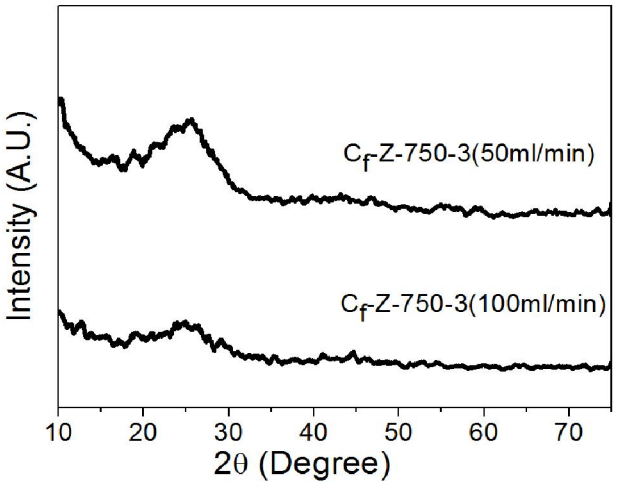

Figure 4.26. XRD profiles of zeolite templated carbons synthesized from furfuryl alcohol with different nitrogen flow rates (carbonization temperature 750 ^{o}C with 3h dwelling time).

4.2.5 Hydrogen storage

The templated carbons, synthesized at 650, 750 and 850 ^{o}C and 3h dwelling time, having higher BET and micropore areas were studied for hydrogen storage measurement. The hydrogen uptake of the samples measured at -100 and -50 ^{o}C and atmospheric pressure are shown in Figure 4.27. Highest hydrogen uptake was observed for sample prepared at 650 ^{o}C with 3h dwelling time (C_f-Z-650-3). About 0.15 wt.% of hydrogen was adsorbed at -100 ^{o}C and atmospheric pressure. The physical adsorption mechanism is expected to be responsible for the hydrogen uptakes for these templated carbons at different subzero temperatures. Hence the hydrogen storage is favored by lower pore size and higher surface area. It was observed that the C_f-Z-650-3 samples though having higher hydrogen uptake had lower BET surface area compared to that of C_f-Z-750-3 sample but contained higher amount of micropores and lower mesopores (less than 6 nm). This agreed with the general observation that in narrower pores, the interaction between pore walls and hydrogen molecule is higher and thereby adsorption is favored.

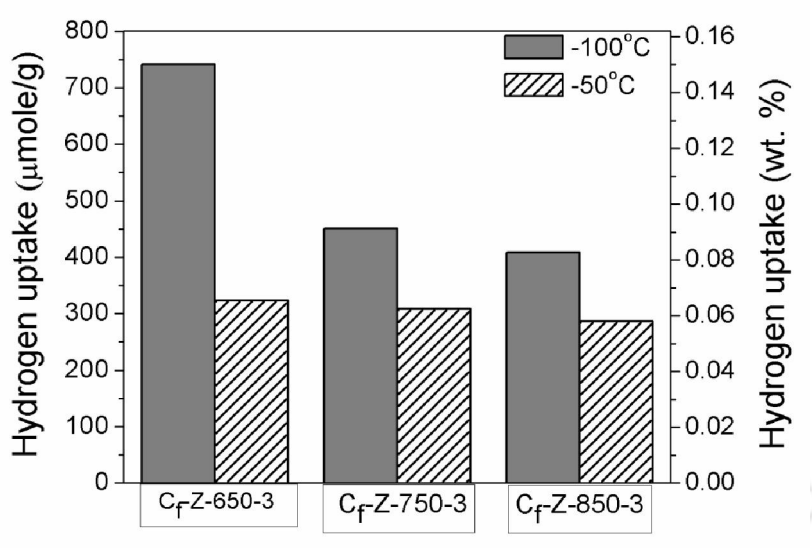

Figure 4.27. Hydrogen uptakes of zeolite templated carbons synthesized from furfuryl alcohol at atmospheric pressure and different adsorption temperatures.

The hydrogen uptake capacities of the zeolite templated carbons with respect to BET and micropore areas are shown in Figure 4.28 (a-b). The uptake capacity of C_f-Z-650-3 sample was observed to be maximum at both the adsorption temperatures even though the sample possessed lower BET surface area compared to C_f-Z-750-3 (Figure 4.28a). As observed from Figure 4.28(b) the hydrogen uptake also increased with increase in micropore area of the samples. The highest hydrogen uptake of 0.15 wt.% was observed at –100 ^oC for C_f-Z-650-3 having highest micropore surface area of 519 m^2/g.

The hydrogen desorption profile of templated carbon prepared at 750 ^oC with 3h dwelling time as function of temperature and time are shown in Figure 4.29 (a-b). Faster desorption kinetics was observed and desorption was completed within 30 minute and below 110 ^oC temperature. The weaker binding energy of physically adsorbed hydrogen on the surface may have resulted in faster desorption kinetics.

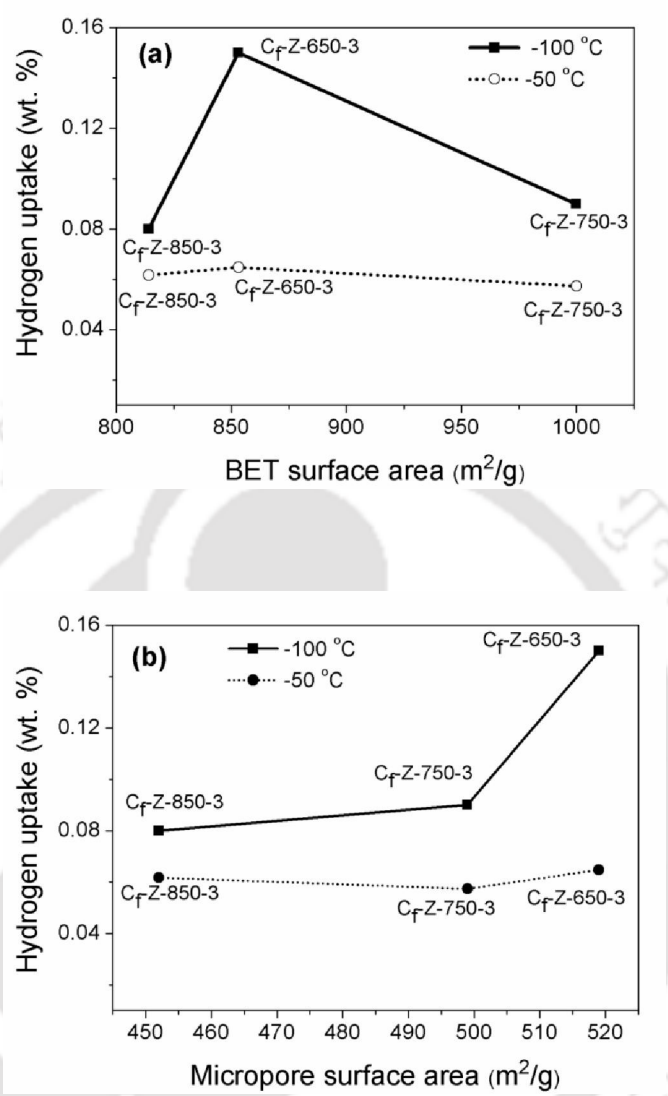

Figure 4.28. Hydrogen uptakes of zeolite templated carbons as function of (a) BET surface area (b) micropore area.

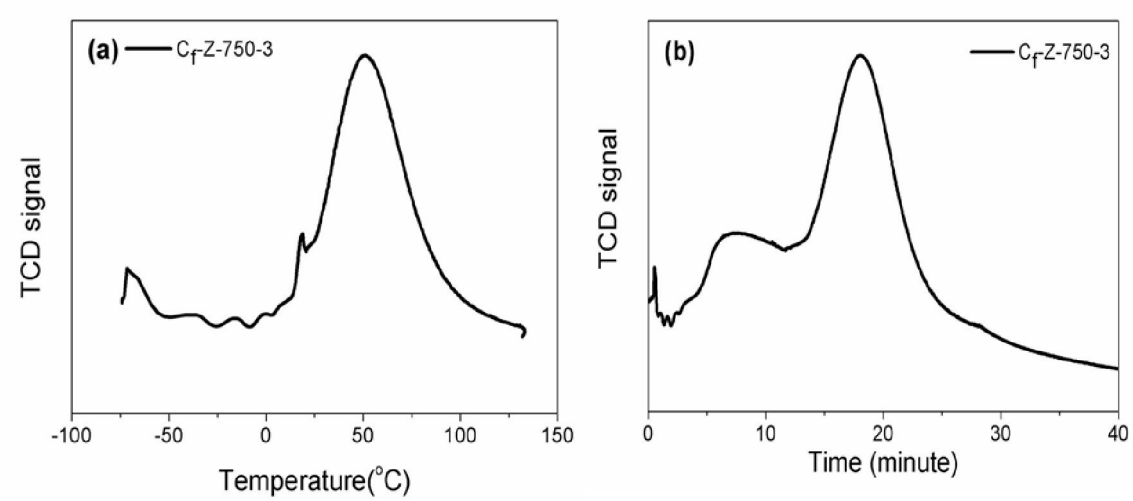

Figure 4.29. Hydrogen desorption profiles of zeolite templated carbon synthesized from furfuryl alcohol as function of (a) temperature and (b) time (adsorption at -100 °C and atmospheric pressure).

The hydrogen uptakes at -100 °C and atmospheric pressure for samples, prepared at different heating profiles, are compared in Figure 4.30. It shows that the uptake capacity of 0.29 wt.% for stepwise heated sample. The higher hydrogen uptake for stepwise heated sample may be attributed to significant enhancement in micropores. Very few studies have reported hydrogen uptake at atmospheric pressure and among few reported studies mostly were carried out at liquid nitrogen temperature. Hence, direct comparison of the present study with the reported values is difficult. For zeolite templated carbons at atmospheric pressure and liquid nitrogen temperature few hydrogen uptake values have been reported. Chen et al. (2007) reported 0.8 wt.% for 1040 m^2/g, Sevilla et al.(2010, 2011) reported 0.8 and 1.1 wt.% for BET surface areas of 1338 and 1626 m^2/g respectively. For present study, slightly lower hydrogen uptake value for comparable surface area (0.29 wt.% for 1886 m^2/g) can be attributed to the higher adsorption temperature.

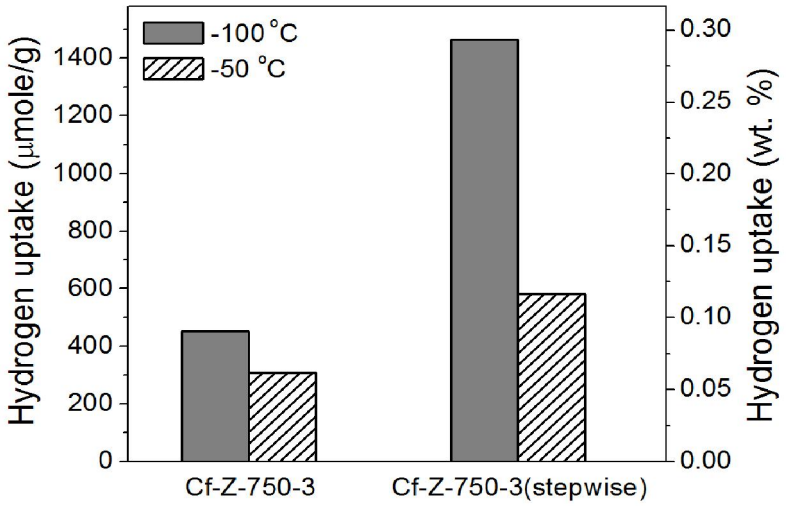

Figure 4.30. Hydrogen uptakes of zeolite templated carbons synthesized from furfuryl alcohol with different heating profiles.

4.2.6 Summary

The study showed that lower carbonization temperature with 3h dwelling time and stepwise heating profile resulted in higher surface and micropore area for templated carbon. The presence of large mesopores and macropores in the templated carbon samples may have resulted from the shrinkage of zeolite-carbon composites during carbonization processes and/or due to the incomplete filling of zeolite channels and cavities by furfuryl alcohol. The degree of the shrinkage and collapse of zeolite framework was observed to be dependent on the carbonization temperature and dwelling time. Higher carbonization temperature and dwelling time resulted in greater shrinkage and collapse of zeolite framework. Further, lower flow of nitrogen also enhanced formation of larger pores resulting in lower surface area and pore volume. The XRD patterns of the all carbon samples exhibited a broad peak corresponding to graphitic carbon. The highest hydrogen uptake of 0.29 wt.% was observed for templated carbon, synthesized at 750 ^{o}C with 3h dwelling time and stepwise heating profile, corresponding to BET area of 1886 m^2/g and micropore area of 1136 m^2/g. The storage capacity was observed to be higher for samples having higher amount of micropores and mesopores less than 6 nm.

4.3 Zeolite templated carbon from sucrose

Templated carbon was also prepared using sucrose as the carbon precursor with ammonium zeolite as the inorganic template. The carbonization of zeolite-sucrose composite was carried out at optimized heating profile and flow rate of carrier gas as discussed in sections 4.2.3 and 4.2.4. The effects of carbonization temperature and dwelling time on structural development of the templated carbons, prepared using sucrose, were investigated. The sucrose with higher carbon number and higher number of hydroxyl groups compared to that of furfuryl alcohol was expected to have different effect on structural development during carbonization process. The physicochemical properties of the sucrose derived zeolite-carbon composites and the product templated carbons were characterized by similar techniques as referred in section 4.2. The hydrogen storage capacity of the templated carbons was measured at atmospheric pressure and different adsorption temperatures.

4.3.1 Characterization of zeolite–carbon composites

The TGA profile of zeolite deposited with sucrose in presence of acid is shown in Figure 4.31. The zeolite-sucrose composite was dried at 100 ^{o}C for 12h prior to TGA analysis. Two broad decomposition peaks at 190 and 250 ^{o}C were observed for zeolite-sucrose composite. No prominent peak around 100 ^{o}C, corresponding to the moisture removal, was observed for the dried sample. The first peak in the temperature range of 130–210 ^{o}C can be assigned to polymerization of sucrose in presence of acid catalyst (Bohme et al. 2005) and the corresponding weight loss was about 12%. The second broad peak showed maximum at 250 ^{o}C. As discussed in section 4.2.1, the ammonium ions were mostly removed in calcined zeolite sample and hence, the second broad peak can be mainly attributed to decomposition of sucrose. A continuous weight loss (~25%) was observed till 500 ^{o}C that suggested gradual decomposition of sucrose.

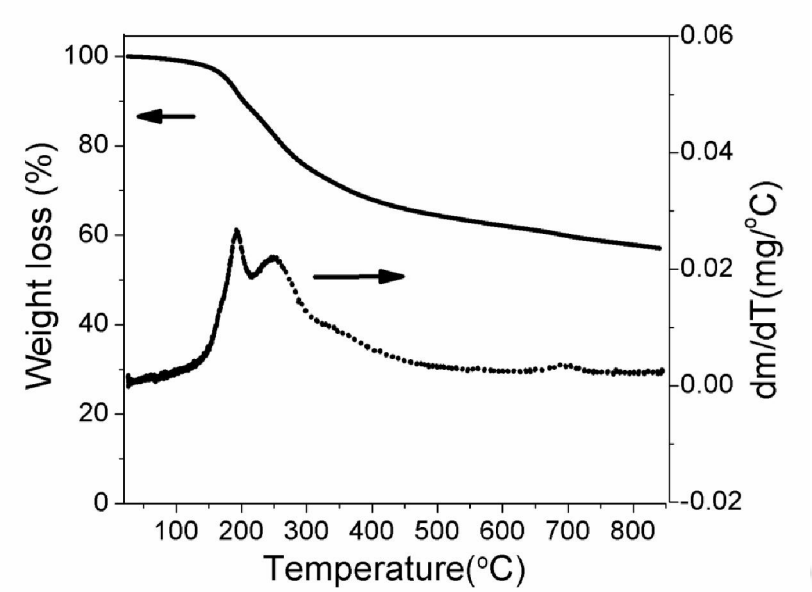

Figure 4.31. TGA profile of zeolite deposited with sucrose.

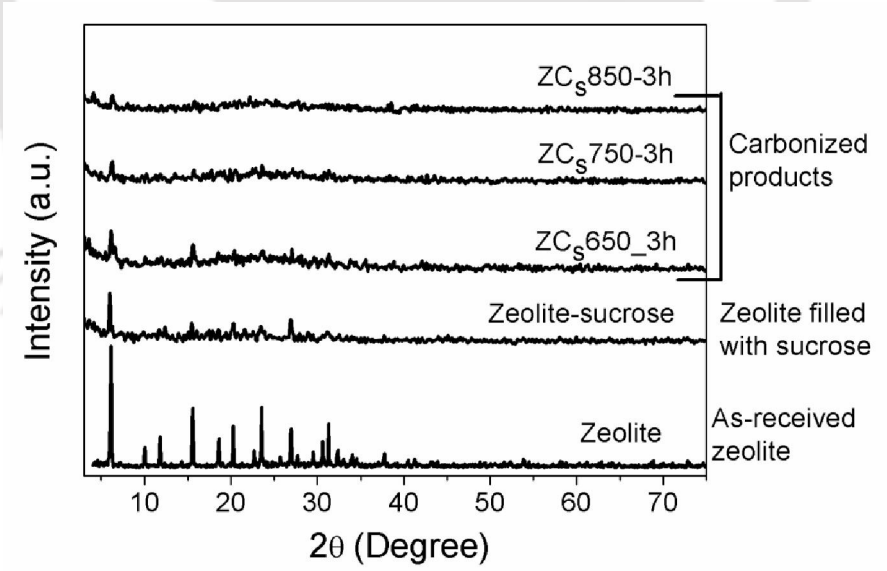

Figure 4.32. XRD profiles of zeolites-sucrose composites at different stages of carbonization.

The XRD profiles of zeolite–sucrose composite at different stages of carbonization are shown in Figure 4.32. Compared to as–received zeolite, the peak intensities of zeolite–sucrose composite were reduced significantly. The significant decrease in intensities cannot be attributed to collapse of zeolite structure, at least up to temperature of 750 ^{o}C, because the zeolites structures were relatively stable up to this temperature (Figure 4.6). Further, the significant decrease in peak intensities was observed for the zeolite–sucrose composite even without the carbonization step. Hence, the decrease in XRD peak intensities for zeolite–sucrose composites as well as for carbonized products compared to as–received zeolite can be attributed mainly to the coverage of zeolite by carbon precursor or carbon respectively. Similar observations were recorded for zeolite –furfuryl alcohol composites as discussed in section 4.2. At 850 ^{o}C the significant decrease in intensity may be attributed to both carbon coverage and partial collapse of zeolite structure.

4.3.2 Effect of carbonization temperature and dwelling time

The nitrogen adsorption-desorption isotherms of templated carbons synthesized at different carbonization temperatures and dwelling times are shown in Figure 4.33 (a–c). The isotherms were similar in nature for all the templated carbons irrespective of carbonization temperature and dwelling time. All isotherms were of type II with H4 type hysteresis loops (Sing et al. 1985). The volume of nitrogen adsorbed on synthesized carbons increased with increase in dwelling time from 2 to 3h and thereafter decreased for 4h dwelling time, at all carbonization temperatures. Similarly, volume of nitrogen adsorbed increased with carbonization temperature from 650 to 750 ^{o}C and thereafter decreased at higher temperature of 850 ^{o}C, for all dwelling times.

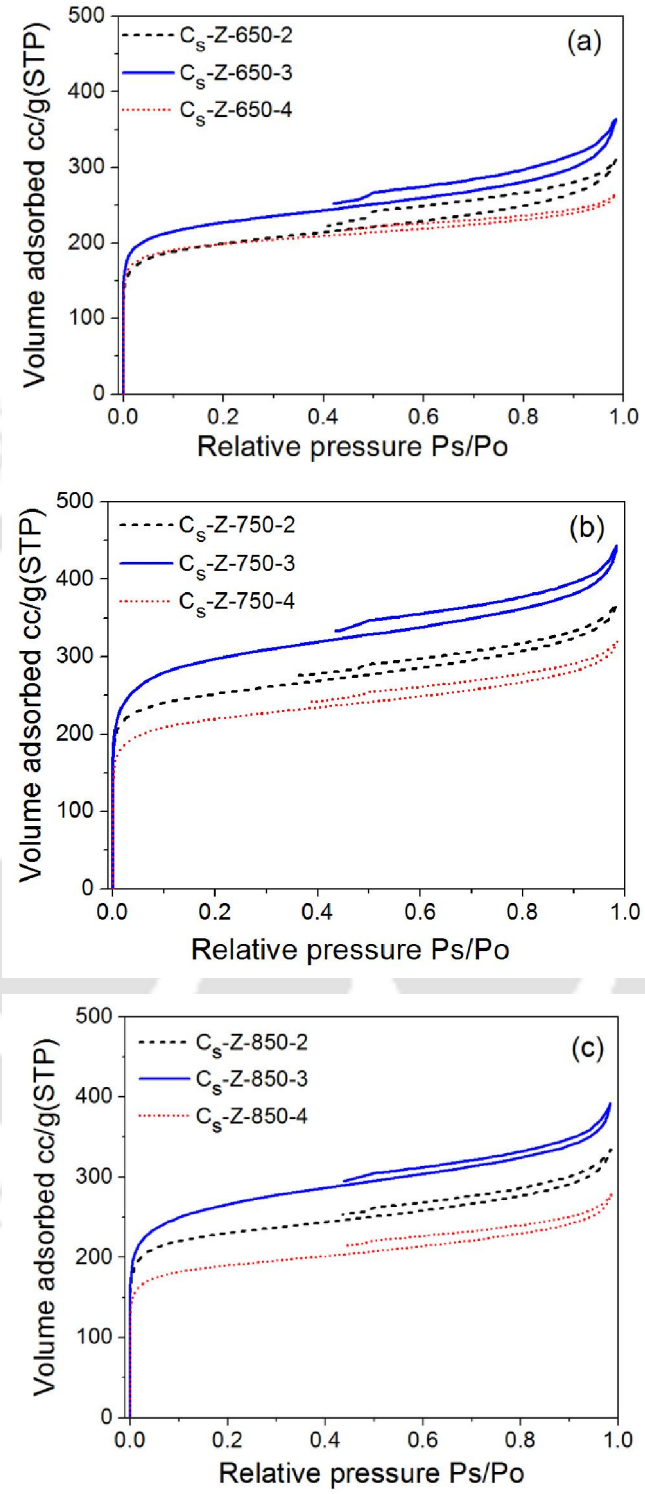

Figure 4.33. Nitrogen adsorption-desorption isotherms of zeolite templated carbons synthesized from sucrose at (a) 650 (b) 750 and (c) 850 ^{o}C with different dwelling times.

Accordingly, at all carbonization temperatures, the BET surface area of carbon increased with increase in dwelling time from 2 to 3h and thereafter decreased at higher dwelling time of 4h as shown in Figure 4.34. The BET surface area increased from 781 to 1033 m^2/g with increase in carbonization temperature from 650 to 750 ^oC. Thereafter, at higher carbonization temperature of 850 ^oC the surface area decreased to 921 m^2/g. The formation of micropores was observed to pass through a maximum at 750 ^oC when carbonization temperature was increased from 650 to 850 ^oC, for all dwelling times. However, the effect of dwelling time on micropore formation was observed to depend on carbonization temperature. The micropore area of the templated carbons increased with increasing dwelling time from 2 to 4h at carbonization temperature of 650 ^oC. At 750 ^oC, the generation of micropore was similar for 2 and 3h dwelling time but decreased at higher dwelling time of 4h. However, at higher carbonization temperature (850 ^oC) the micropore area significantly decreased from 601 to 497 m^2/g with increasing dwelling time (2 to 4h). For templated carbon synthesized at 750 ^oC and 3h dwelling time, the highest BET area of 1033 m^2/g was achieved with micropore area of 647 m^2/g. Though, total BET area and micropore area were lower at 650 ^oC compared to that at 750 ^oC, but percentage micropore area with respect to BET surface area was higher at the former temperature. The percentage micropore area was in the range of 67–80% at 650 ^oC and 63-75% at 750 ^oC. The decrease in micropore area at higher carbonization temperature (850 ^oC) and dwelling time may be attributed to the collapse of template structure and shrinkage of carbon particles. Hence, for the development of templated carbon with higher microporosity carbonization temperature of 650 ^oC was more favorable. However, the absolute value of micropore area was highest for the templated carbon synthesized at 750 ^oC with 3h dwelling time corresponding to 63% micropore area.

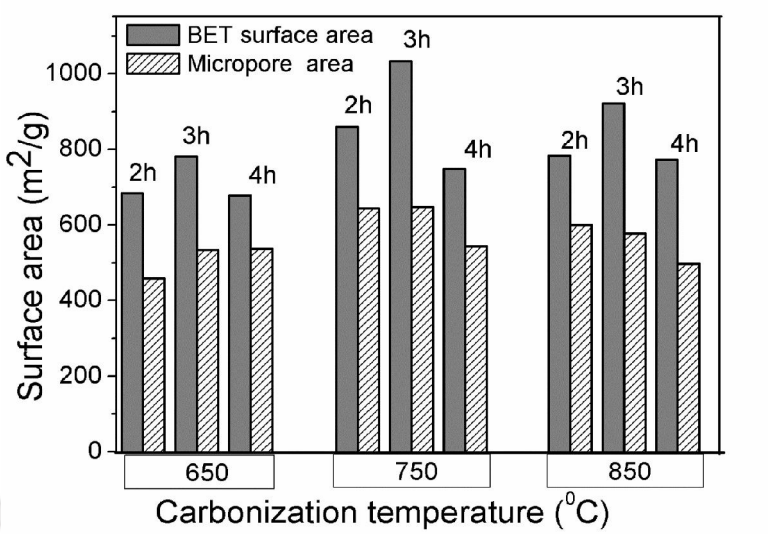

Figure 4.34. BET and micropore areas of zeolite templated carbons synthesized from sucrose at different carbonization temperatures and dwelling times.

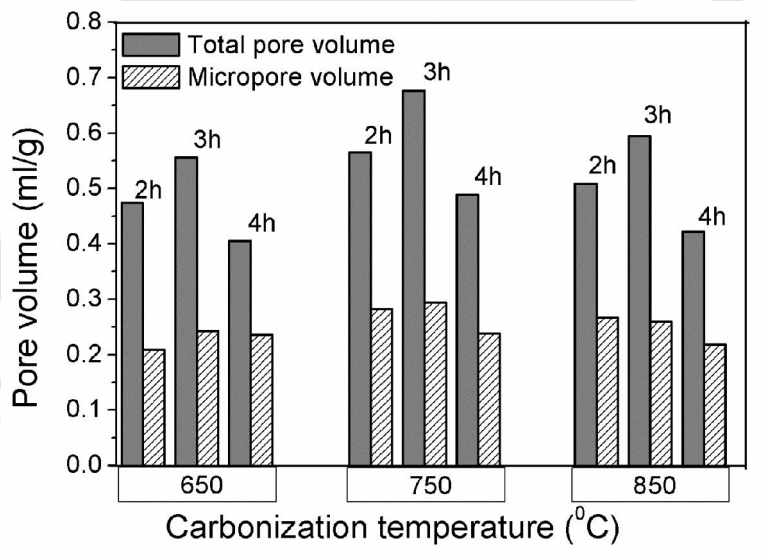

Figure 4.35. Total and micropore volumes of zeolite templated carbons synthesized from sucrose at different carbonization temperatures and dwelling times.

Figure 4.35 shows the total and micropore volumes of templated carbons synthesized at different carbonization temperatures and dwelling times. The increase or decrease in total and micropore volumes with carbonization temperature and dwelling time followed the

same pattern as BET and micropore areas. The highest total pore volume of 0.68 ml/g and micropore volume of 0.29 ml/g were observed for the templated carbon synthesized at 750 ^{o}C and dwelling time of 3h. Depending on the synthesis conditions the micropore volume varied in the range of 40 to 60% of total pore volume.

At given dwelling time, with increase in temperature the surface area and pore volume increased up to 750 ^{o}C and then decreased. On the other hand, at given temperature, with increase in dwelling time, the surface area and pore volume increased up to 3h and then decreased at higher dwelling time of 4h. Therefore, the optimal temperature and dwelling time for obtaining highest surface area and pore volume corresponded to 750 ^{o}C and 3h respectively. For a given dwelling time, at lower temperature the carbonization within the zeolite template may have been incomplete resulting in lower surface area and pore volume as observed. Higher carbonization temperature on other hand, may have caused extensive sintering thereby resulting in decrease in surface area and pore volume. At given temperature, if enough dwelling time was not given for carbonization to occur, then lower surface area and pore volume might be expected. However, at higher dwelling time, increased exposure to temperature may have caused sintering and consequently lower surface area and pore volume.

The pore size distribution of the templated carbon samples synthesized at different carbonization temperatures and dwelling times are shown in Figure 4.36 (a-c). As can be observed from the figures, for all the templated carbons 27-38% of the pores were below 6 nm and 23-31% pores were observed in the range of 20-80 nm. The percentage of pores having diameter less than 6 nm was maximum for carbon synthesized at carbonization temperature of 650 ^{o}C with a dwelling time of 2h. It was observed that there was no significant effect of carbonization temperature or dwelling time on the pore distribution in the range of 6–20 nm and was similar for all samples. About 60 to 70 vol.% of mesopores were in the range of 2–20 nm. In the present study formation of mesopores and macropores in the range of 20-80 nm may be attributed to partial collapse of pore walls due to high carbonization temperature or longer dwelling time.

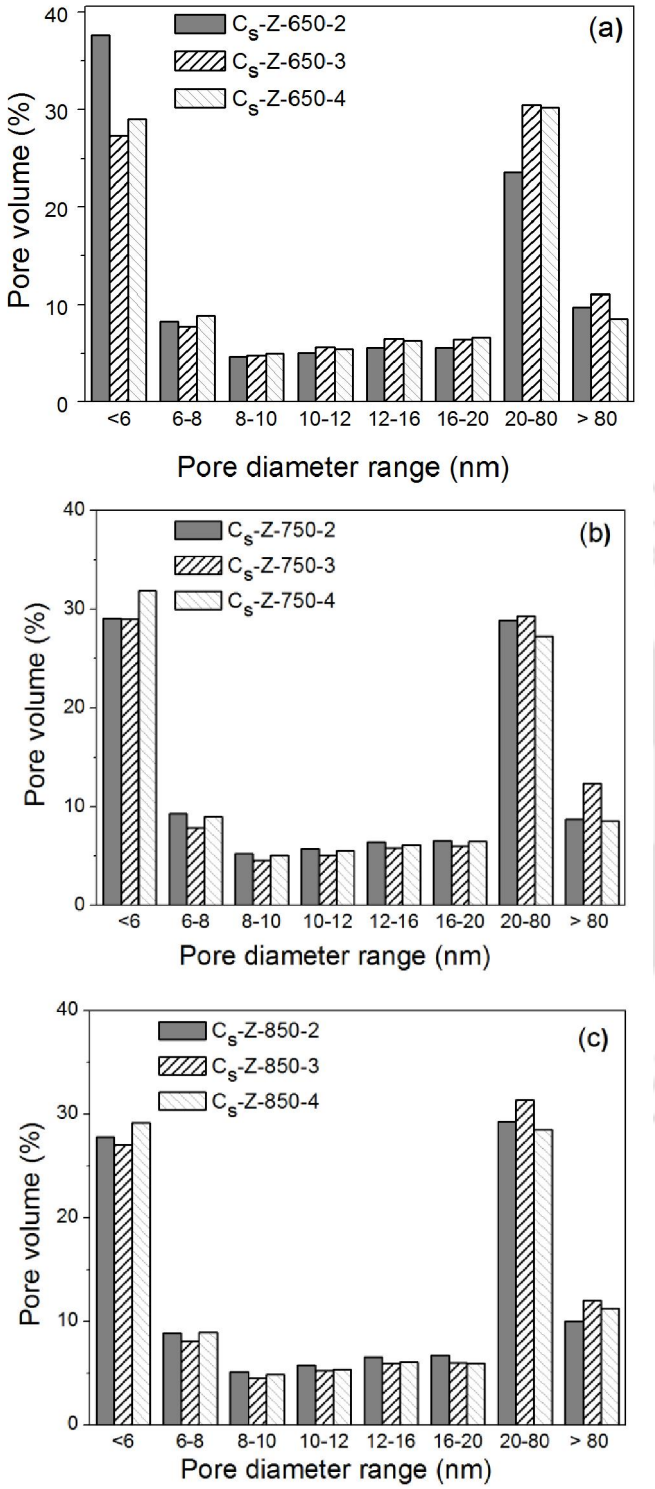

Figure 4.36. Pore size distributions of zeolite templated carbons synthesized from sucrose at different carbonization temperatures and dwelling times.

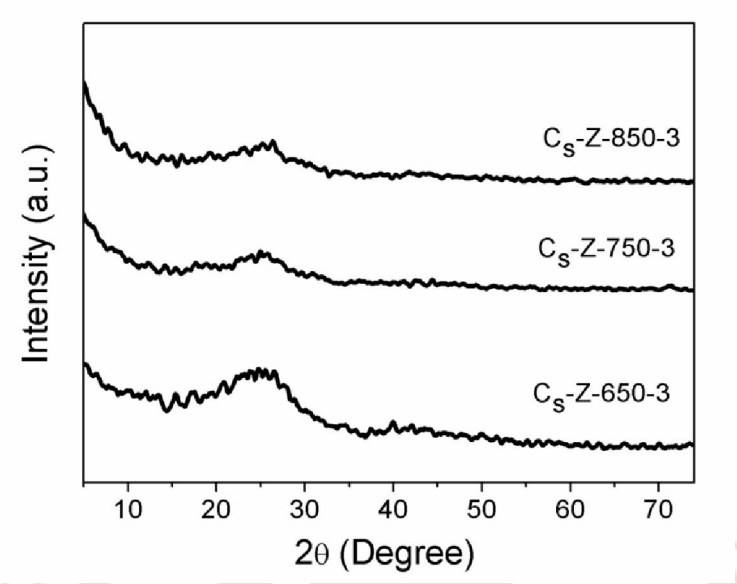

Figure 4.37. XRD profiles of zeolite templated carbons synthesized from sucrose at 650, 750 and 850 °C with 3h dwelling time.

Figure 4.37 depicts the XRD patterns of carbons synthesized at 650, 750 and 850 °C with dwelling time of 3h. The broad peaks of low intensity due to graphitic carbon were observed at 25° for all the samples. The peak intensity was lowest for carbon prepared at 850 °C carbonization temperature.

The FESEM images of templated carbons synthesized at different carbonization temperatures for dwelling time of 3h are shown in Figure 4.38 (a–c). The development of microstructure of the templated carbons varied with the synthesis conditions. Though, all the synthesized carbons possessed porous structure with well-connected pores, the extent of porosity was dependent on synthesis conditions. The porous structure was more uniform for carbon synthesized at 750 °C as can be observed in Figure 4.38(b) and may be attributed to more complete carbonization of sucrose with minimum sintering. The more agglomerated structure for carbon synthesized at 650 °C (Figure 4.38a) might have been caused by incomplete carbonization. With increase in carbonization temperature to 850 °C, larger pores appeared in the porous network of carbon, as shown by Figure 4.38(c). The large pores might have been the result of partial collapse of the pore walls at

severe conditions. The surface area and pore volume for both the carbons prepared at 650 and 850 ^{o}C were lower compared to that prepared at 750 ^{o}C and thus was consistent with the observed microstructure.

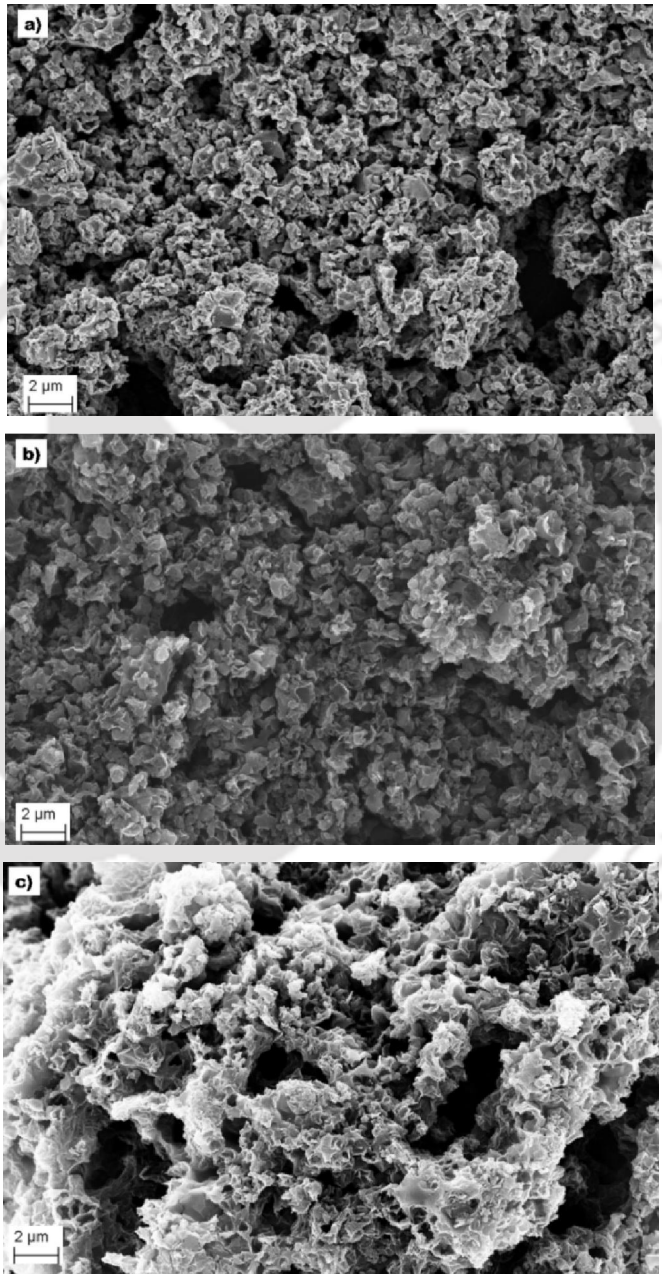

Figure 4.38. FESEM images of zeolite templated carbons synthesized from sucrose with 3h dwelling time at (a) 650 (b) 750 and (c) 850 ^{o}C.

4.3.3 Hydrogen storage

The hydrogen uptake was measured at atmospheric pressure and different subzero temperatures for templated carbons synthesized at 650, 750, and 850 °C. The dwelling time was 3h for all the samples. The hydrogen uptakes at –100 and –50 °C are shown in Figure 4.39. For all the three samples, hydrogen adsorption was higher at lower temperature of –100 °C as compared to that at –50 °C. Physisorption being responsible for hydrogen uptake on carbon based materials, hydrogen adsorption was favored at lower temperature of –100 °C for all the three samples. The hydrogen uptakes as function of BET and micropore areas are shown in Figure 4.40 (a-b). The hydrogen uptake linearly increased with increase in the BET surface area and micropore areas of the samples. The highest hydrogen uptake of 0.30 wt.% was observed at –100 °C for C_s-Z-750-3 having highest surface area of 1033 m^2/g.

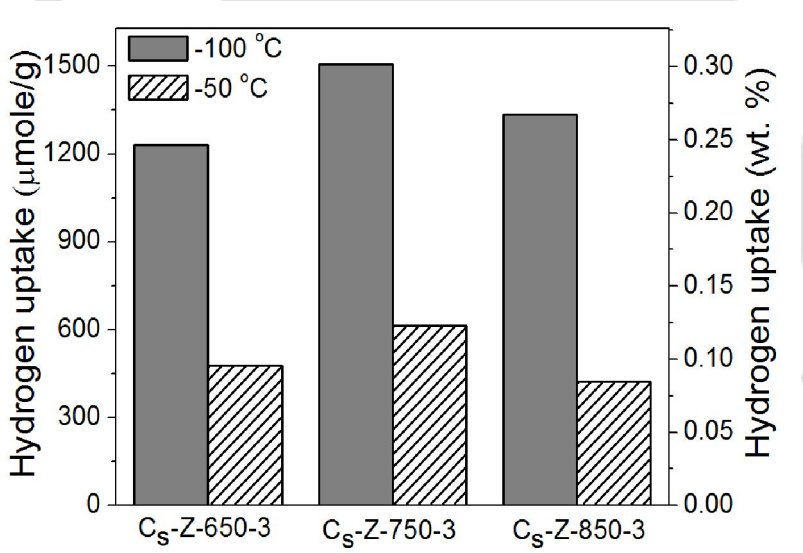

Figure 4.39. Hydrogen uptakes of zeolite templated carbons synthesized from sucrose at atmospheric pressure and different adsorption temperatures.

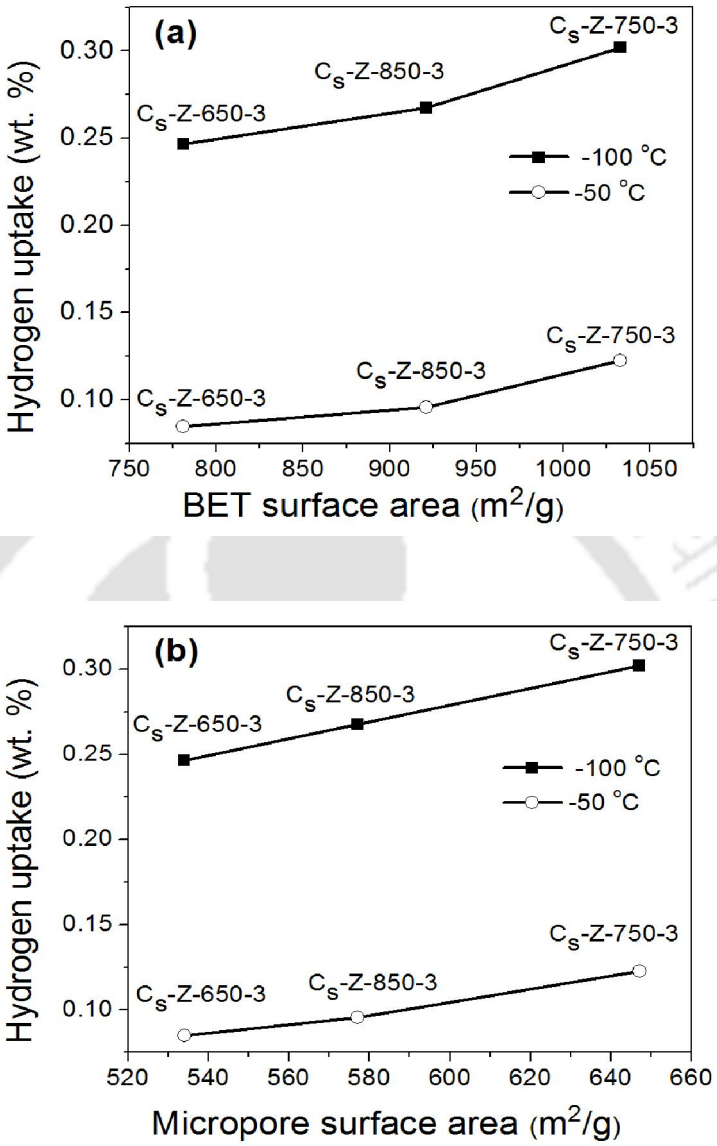

Figure 4.40. Hydrogen uptakes of templated carbons as function of (a) BET surface area (b) micropore area.

As discussed in section 4.2.5 direct comparison of the hydrogen uptake capacities for this study with the reported values in literature is difficult because of different adsorption temperatures. For sucrose derived zeolite templated carbon, Cai et al. (2014) reported uptake capacity of 1.1 wt.% for surface area of 1042 m^2/g at liquid nitrogen temperature and atmospheric pressure. Higher adsorption temperature used in present study may have

resulted in slightly lower hydrogen uptake value for comparable surface area (0.3 wt.% for 1033 m^2/g).

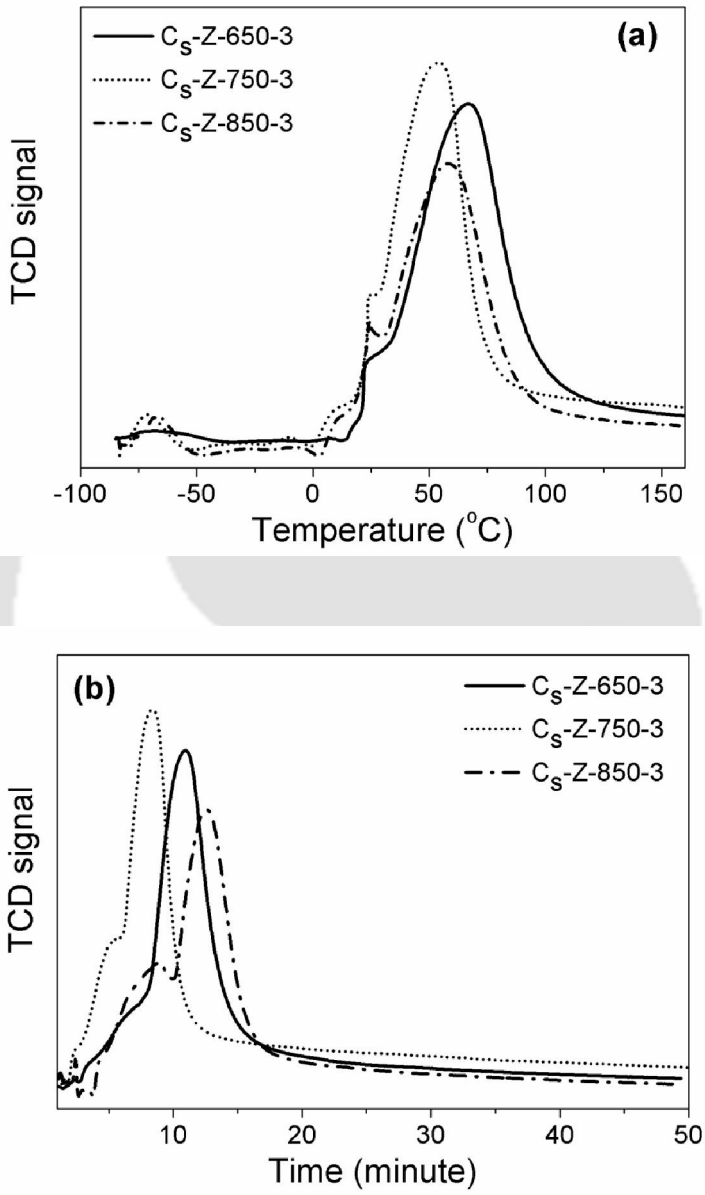

Figure 4.41. Hydrogen desorption profiles of templated carbons as function of (a) temperature and (b) time (Adsorption at -100 °C and atmospheric pressure).

The hydrogen desorption profiles of templated carbons as function of temperature and time are shown in Figure 4.41 (a-b). The desorption kinetics were observed to be fast for

all the samples. The hydrogen desorption for the studied samples was completed within 12-17 minutes and below 90 ^{o}C temperature.

4.3.4 Summary

The present study illustrated that carbonization was effective for preparation of zeolite templated carbon having high surface area and significant micropore area using sucrose as carbon precursor. The templated carbons were obtained with BET surface areas in the range of 684–1033 m^2/g with 63–80% micropore area depending on the synthesis conditions. This study showed that temperature in the range of 650–750 ^{o}C with 3h dwelling time was required for better carbonization of sucrose to generate higher BET and micropore surface areas. At lower temperature and dwelling time, templated carbons with lower surface area and pore volume were obtained due to incomplete carbonization. On the other hand, at higher carbonization temperature and longer dwelling time severe sintering of zeolite or carbon structure resulted in lower area and pore volume. The templated carbon synthesized at 750 ^{o}C with dwelling time of 3h showed hydrogen uptake of 0.30 wt.% at –100 ^{o}C corresponding to highest total surface area of 1033 m^2/g and micropore area of 647 m^2/g.

4.4 Silica gel templated carbon from furfuryl alcohol

The templated carbon was also prepared by using silica gel as template to study the effect of amorphous and mesoporous template on the development of porous structure of the carbon. Furfuryl alcohol was used as the carbon precursors. The templated carbons were prepared at different carbonization temperatures and dwelling times at optimized flow of carrier gas and heating profile. Further the synthesized carbons were characterized by different techniques to correlate their hydrogen uptake capacity with physicochemical properties.

4.4.1 TGA of silica gel-furfuryl alcohol composite

The TGA profile of silica gel filled with furfuryl alcohol is shown in Figure 4.42. A weight loss of ~4% was observed at 100 ^{o}C, which corresponded to evaporation of trapped water present in the sample. The observed weight loss of ~30% in the range of 180 to 500 ^{o}C can be attributed to the degradation of the furfuryl alcohol.

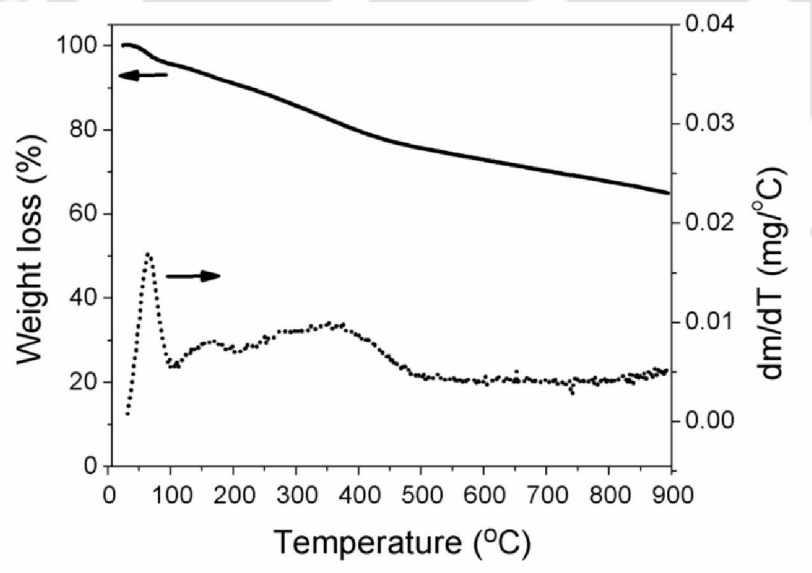

Figure 4.42. TGA profile of silica gel–furfuryl alcohol.

As discussed in section 4.2.1, the observed weight loss was less than 21% in the same temperature range for zeolite filled furfuryl alcohol. The pore volume of silica gel template was higher than zeolite template (Table 4.1). Hence, higher amount of furfuryl alcohol precursor can be incorporated in silica gel template compared to zeolite. The observed higher amount of degradation (~30%) for silica gel filled furfuryl alcohol sample may be attributed to its higher furfuryl alcohol content.

4.4.2 Effect of carbonization temperature and dwelling time

The nitrogen adsorption–desorption isotherms of the templated carbons synthesized at 650 ^{o}C and different dwelling times (1, 2, 3 and 4h) are shown in Figure 4.43.

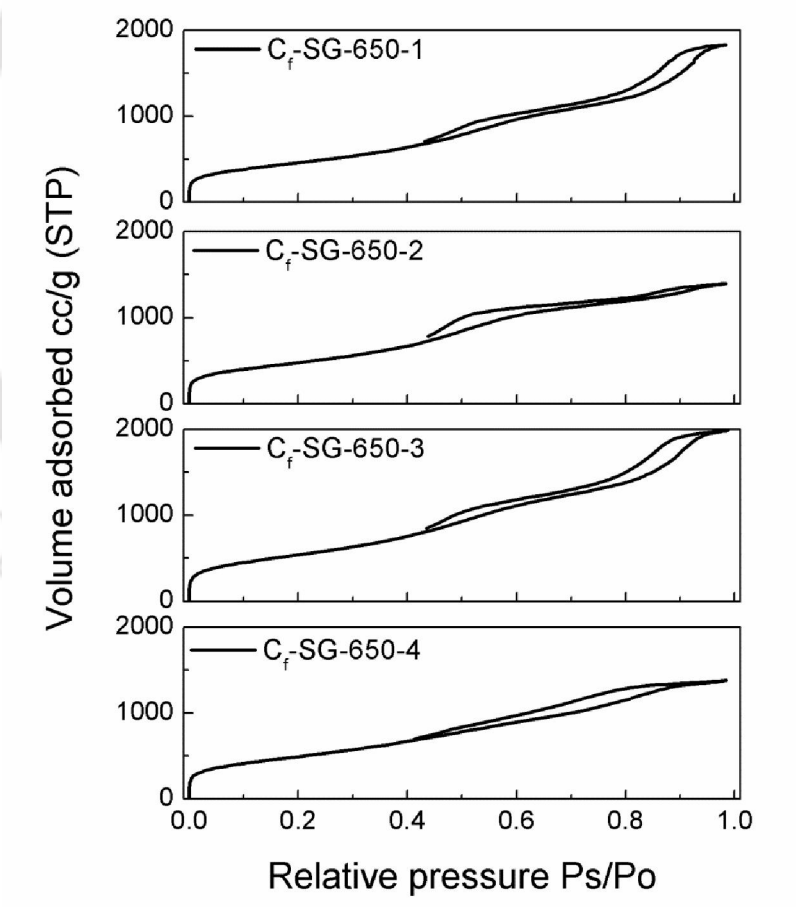

Figure 4.43. Nitrogen adsorption–desorption isotherms of silica gel templated carbons synthesized from furfuryl alcohol at 650 ^{o}C and different dwelling times (1, 2, 3 and 4h).

All the nitrogen isotherms were of type IV but the nature of hysteresis loops was not well defined. The nature was more similar to H2 type suggesting interconnected pores (Sing et al. 1985). The amount of adsorbed nitrogen increased as dwelling time was raised from 1 to 3h and then decreased at higher dwelling time of 4h. The nitrogen adsorption was highest for carbon synthesized at 3h dwelling time.

Table 4.3. Physical properties of silica gel templated carbons synthesized from furfuryl alcohol at different carbonization temperatures and dwelling times.

Sample	Carbonization temperature (^oC)	Dwelling time (h)	BET surface area (m^2/g)	Total pore volume (ml/g)	Mesopore volume (ml/g)	Macropore volume (ml/g)	Average pore size (nm)
C_f-SG-650-1	650	1	1678	2.16	2.14	0.02	8.1
C_f-SG-650-2	650	2	1727	2.83	2.7	0.13	8.9
C_f-SG-650-3	650	3	1975	3.07	3.04	0.03	10.5
C_f-SG-650-4	650	4	1789	2.13	2.10	0.03	8.5
C_f-SG-750-3	750	3	1826	2.96	2.9	0.06	11.7
C_f-SG-850-3	850	3	1725	2.19	2.16	0.03	9.3
C_s-SG-850-3[a]	650	3	1029	1.70			

a: sample contain 58 m^2/g micropore area with micropore volume 0.016 ml/g

The surface area, pore volume and average pore size of silica gel templated carbons synthesized at different carbonization temperatures and dwelling times, are summarized in Table 4.3. The BET surface area increased as dwelling time increased from 1 to 3h and then decreased at higher dwelling time of 4h for carbonization temperature of 650 ^oC as shown in Table 4.3. The highest BET surface area of 1975 m^2/g was observed for the sample synthesized at dwelling time of 3h. Therefore 3h was selected as the optimum dwelling time to study the effect of carbonization temperature on templated carbon structure.

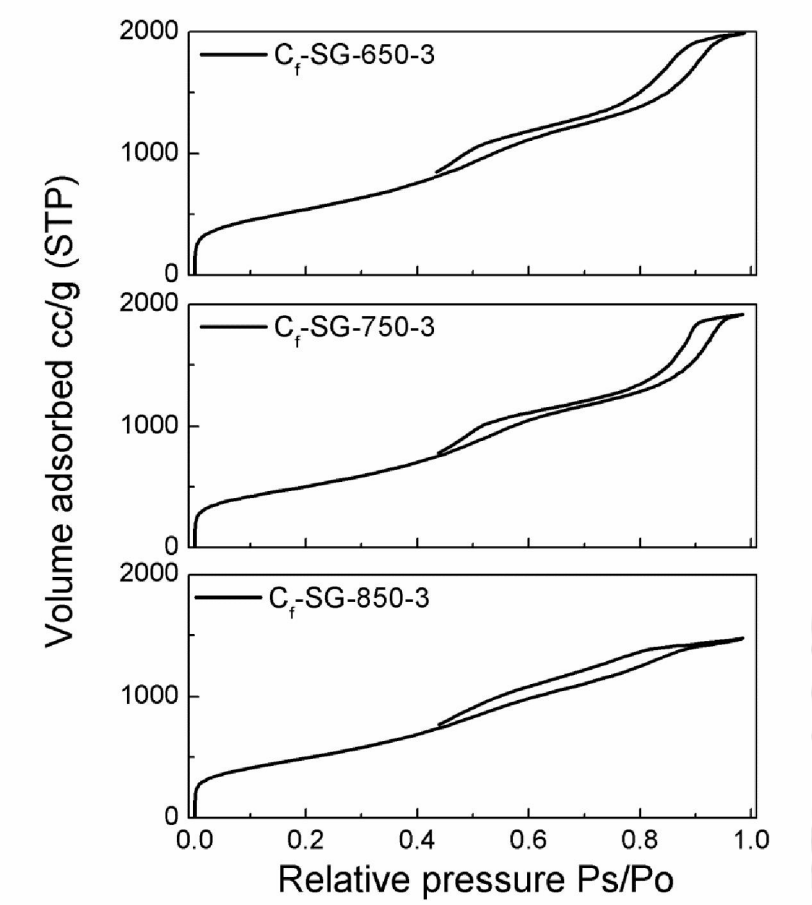

Figure 4.44. Nitrogen adsorption–desorption isotherms of silica gel templated carbons from furfuryl alcohol synthesized at 650, 750 and 850 ^{o}C with 3h dwelling time.

Isotherms of the templated carbons synthesized at different temperatures (650, 750 and 850 ^{o}C) are shown in Figure 4.44. The nature of all the nitrogen adsorption–desorption isotherms was of type IV with H2 type hysteresis loop corresponding to interconnected pores. The effect of temperature on the isotherms was less prominent than that of dwelling time. The amount of adsorbed nitrogen on carbon decreased slightly with increase in the synthesis temperature. From Table 4.3, it was observed that the surface area decreased from 1975 to 1725 m^2/g with increase in temperature from 650 to 850 ^{o}C. The obtained BET surface area of 1975 m^2/g was higher than the surface area values

reported for silica based templated carbons in literature. Moreover, high surface area was obtained at comparatively lower carbonization temperature than reported.

The total pore volume increased with dwelling time and maximum pore volume of 3.07 ml/g was observed at 3h for the carbon synthesized at 650 ^{o}C. Thereafter, pore volume decreased at higher dwelling time of 4h. The pore volume decreased significantly at higher temperature of 850 ^{o}C. For all the templated carbons mesopores contributed about 99% of total pore volume with remaining being macropores (Table 4.3). No micropores were observed in any of the sample.

The results showed that an optimum time of 3h was required for carbonization of furfuryl alcohol to carbon. It was observed that for dwelling time less than 3h, carbonization was incomplete and templated carbon with lower surface area was obtained. At higher dwelling time of 4h, the walls of the fine pores collapsed and the surface area as well as pore volume of carbon decreased significantly. Higher carbonization temperature also resulted in partial collapse of porous structure. Consequently lower surface area and pore volume was observed for samples synthesized at 750 and 850 ^{o}C as compared to that synthesized at 650 ^{o}C. The effect was most severe at 850 ^{o}C as can be observed from Table 4.3.

The pore size distributions of silica gel templated carbons, synthesized at different dwelling times and temperatures, are shown in Figure 4.45 (a-b). For all the samples 90–95 % pores were in the range of 2–20 nm diameters. The mesopores in the range of 2–6 nm contributed about 38–67% of the total pore volume. At 650 ^{o}C, with increase in dwelling time from 1 to 2h, pores in the range of 2–6 nm increased which may be attributed to better carbonization. Further increase in the dwelling time shifted the pore distribution to larger size. As a result the average pore size in the mesopore region increased from 8.1 nm for 1h to 10.5 nm for 3h dwelling time (Table 4.3). This increase may be explained by partial collapse of the pore walls of zeolite-carbon structure as dwelling time increased from 1 to 3h.

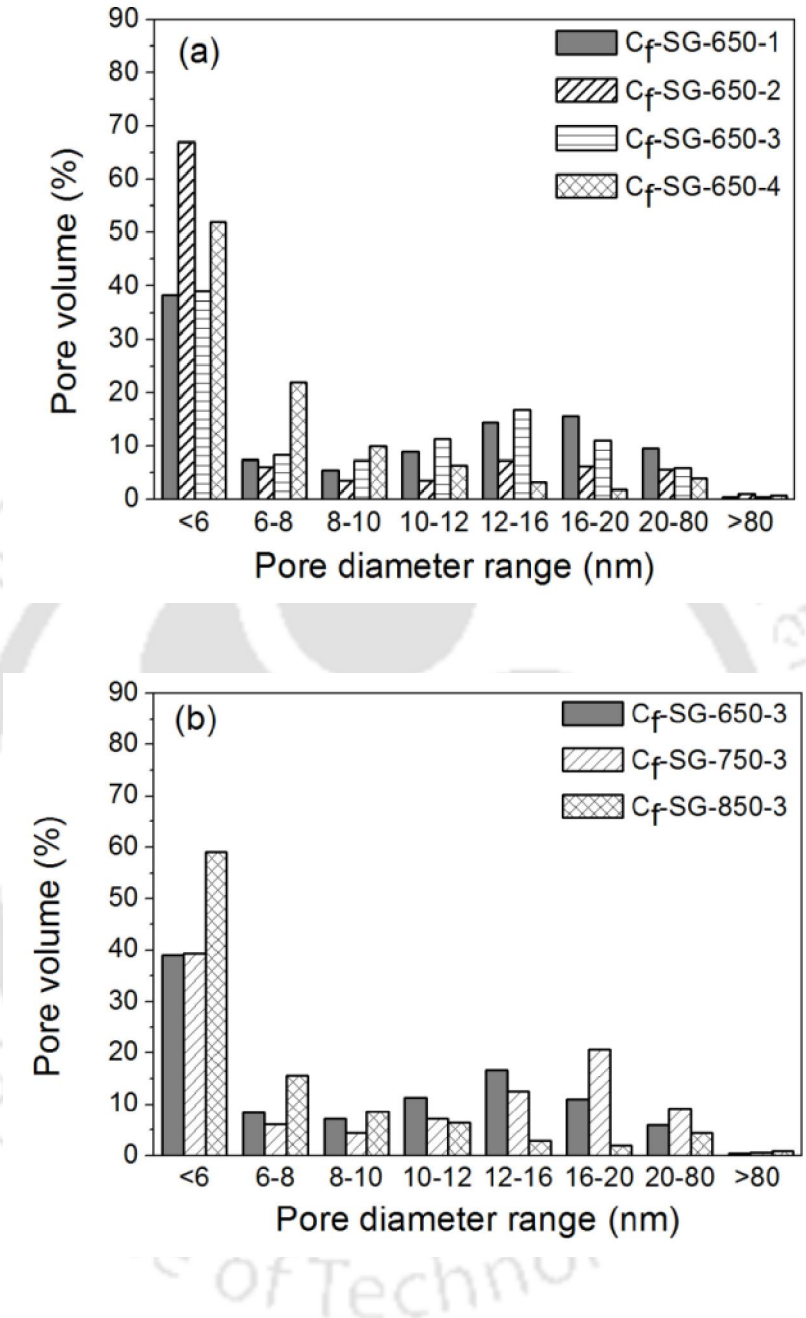

Figure 4.45. Pore size of distributions of silica gel templated carbons synthesized from furfuryl alcohol at (a) different dwelling times at 650 °C and (b) different temperatures with 3h dwelling time.

At the highest dwelling time of 4h, increased exposure to high temperature may have resulted in more severe collapse of the template structure. Consequently carbonization occurred in larger pores of the template resulting in significant decrease in total pore

volume as can be observed from Table 4.3. However, on removal of template, the fine separations between carbons entities of large diameter may have contributed to increased percentage of pores in the range of 2–8 nm, consequently the average pore size decreased to 8.5 nm. Similar phenomenon was also observed when silica-furfuryl alcohol was exposed at high temperature of 850 ^{o}C. The total pore volume and surface area was drastically reduced at 850 ^{o}C but percentage of pores in the range of 2–6 nm was significantly increased as compared to that of samples carbonized at 650 and 750 ^{o}C. Accordingly the average pore size for C_f-SG-850-3 decreased to 9.3 nm as compared to C_f-SG-650-3 (10.5 nm) and C_f-SG-750-3 (11.7 nm) as can be observed from Table 4.3. The carbon synthesized at 850 ^{o}C with dwelling time of 3h contained 60% pores in the diameter range of 2–6 nm as shown in Figure 4.45(b). This can also be attributed to collapse of template structure at higher temperature followed by carbonization in larger pores. It was observed that with increase in carbonization temperature from 650 to 750 ^{o}C there was a small increase in amount of pores with larger diameter which can be attributed to partial collapse of the walls of fine pores.

The FESEM images of the templated carbons synthesized at different temperatures and 3h of dwelling time are shown in Figure 4.46. It was observed that all the templated carbon samples possessed uniform porous structure with well-connected pores. The templated carbon synthesized at higher temperature was more agglomerated in nature which may be attributed to higher extent of sintering. Extensive sintering resulted in lowest surface area and pore volume for C_f-SG-850-3 sample synthesized at 850 ^{o}C with 3h dwelling time. The TEM image of C_f-SG-650-3 sample prepared at 650 ^{o}C with 3h dwelling time is shown in Figure 4.47. Well interconnected but disordered pores were observed in the TEM image.

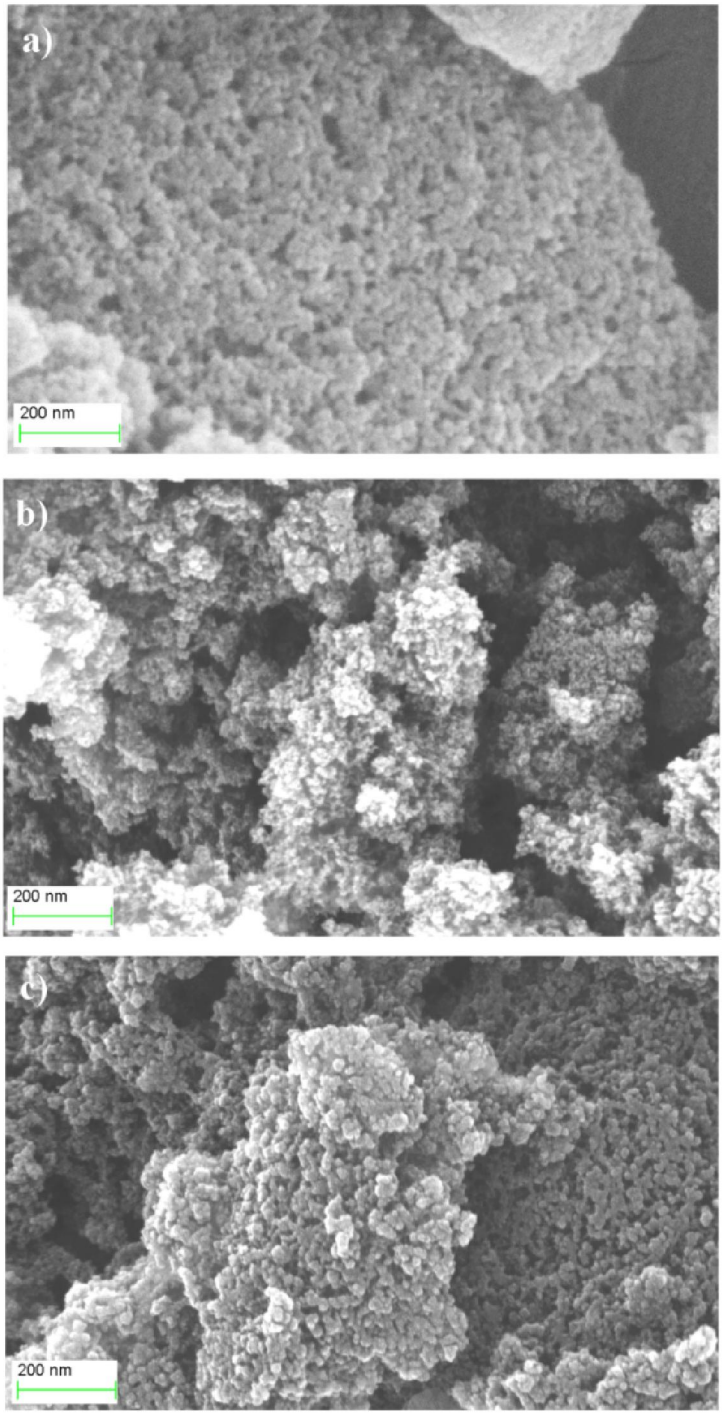

Figure 4.46. FESEM images of silica gel templated carbons synthesized from furfuryl alcohol at different carbonization temperatures (a) 650 (b) 750 and (c) 850 ^{o}C with 3h of dwelling time.

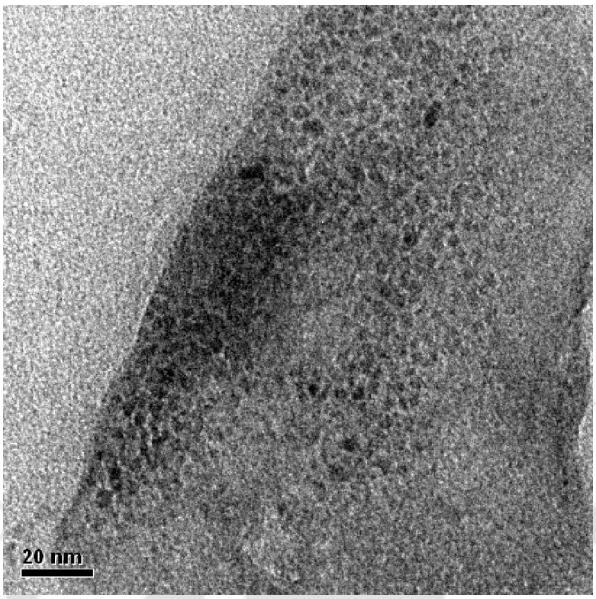

Figure 4.47. TEM image of silica gel templated carbon synthesized from furfuryl alcohol at 650 ºC with dwelling time of 3h.

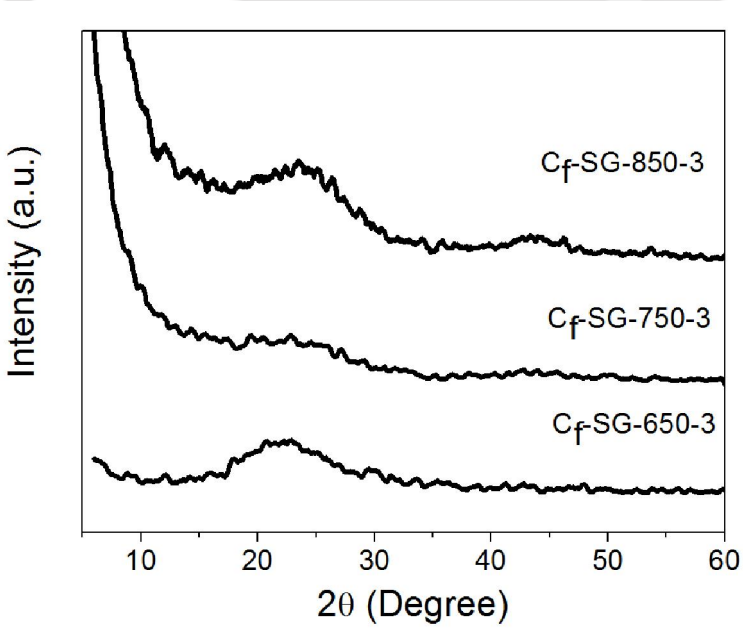

Figure 4.48. XRD profiles of silica gel templated carbons synthesized from furfuryl alcohol at different carbonization temperatures.

The XRD patterns of templated carbon samples synthesized at 650, 750 and 850 ^{o}C are shown in Figure 4.48. The peak corresponding to graphitic plane was observed at 23.5^{o} for carbon samples synthesized at 650 and 750 ^{o}C. For the carbon synthesized at 850 ^{o}C the diffraction peak of graphitic carbon shifted to 24.4^{o} and peak intensity was slightly higher. These changes may be attributed to the higher order of graphitic carbon formed at higher carbonization temperature (Dandekar et al. 1998).

4.4.3 Hydrogen storage

The synthesized templated carbon samples were tested for the hydrogen uptake at atmospheric pressure. Figure 4.49 depicts the hydrogen uptake at –100 and –50 ^{o}C. For all carbon samples hydrogen uptake was higher at –100 ^{o}C than that at –50 ^{o}C corresponding to hydrogen uptake by physisorption. Higher surface area was also expected to result in higher hydrogen adsorption. The hydrogen uptake with respect to BET surface area of the templated carbons is shown in Figure 4.50. The hydrogen uptake linearly increased with increase in the BET surface area at both the adsorption temperatures. The highest hydrogen uptake for C_f-SG-650-3 (1975 m^2/g), synthesized at 650 ^{o}C with 3h dwelling time, was ~0.16 wt.% at adsorption temperature of –100 ^{o}C.

Hydrogen uptake for C_f-SG-650-2 (1727 m^2/g), prepared at 650 ^{o}C with 2h dwelling time, was about 0.15 wt.% at –100 ^{o}C. Similar hydrogen uptake values for C_f-SG-650-2 and C_f-SG-650-3, in spite of lower surface area of the former, may be attributed to the presence of higher percentage of pores in the range of 2–6 nm in C_f-SG-650-2 as compared to that in C_f-SG-650-3.

For mesoporous templated carbon the hydrogen uptake of 0.59 wt.% was reported by Saha et al. (2009) at –3 ^{o}C and 163 bar for BET surface area of 798 m^2/g. Pang and co-workers (2004) reported 1.78 wt.% at –196 ^{o}C and ambient pressure for the sample having BET surface area of 2314 m^2/g. The difference in hydrogen uptake values with present study (0.16 wt.%) can be attributed to difference in surface area and pore size as well as adsorption temperature and pressure.

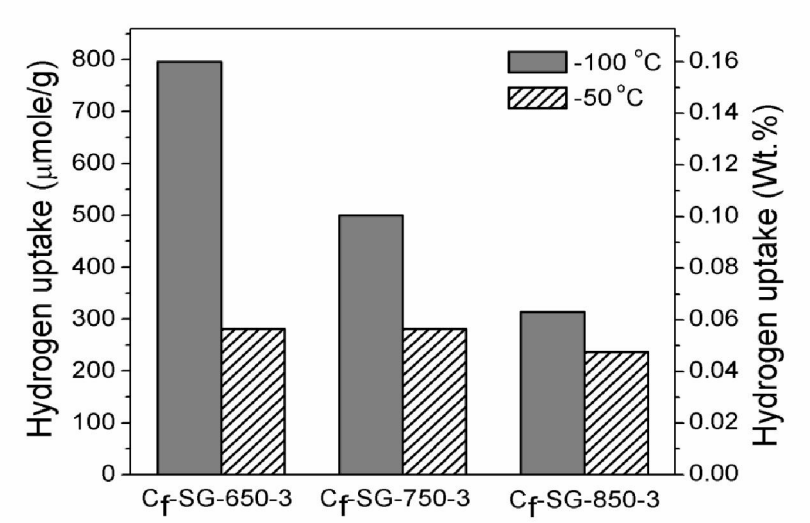

Figure 4.49. Hydrogen uptakes of silica gel templated carbons synthesized from furfuryl alcohol at different adsorption temperatures at atmospheric pressure.

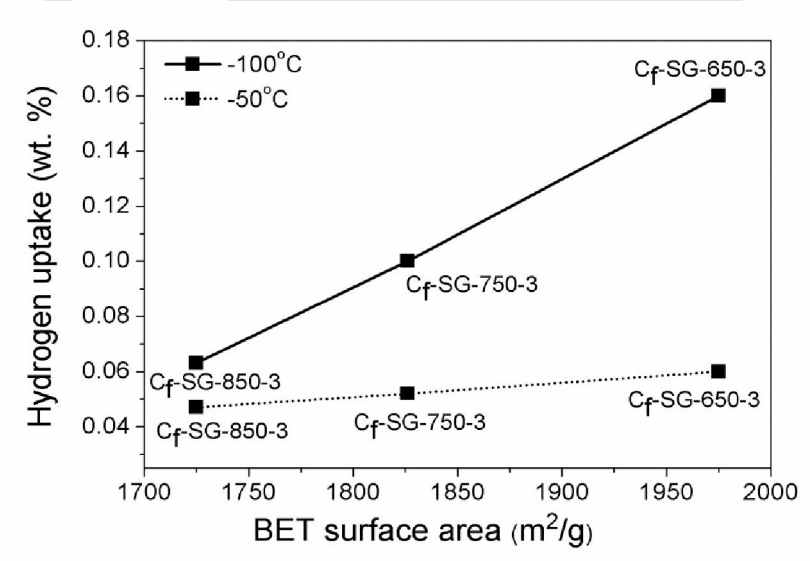

Figure 4.50. Hydrogen uptakes of silica gel templated carbons synthesized from furfuryl alcohol as function of BET surface area.

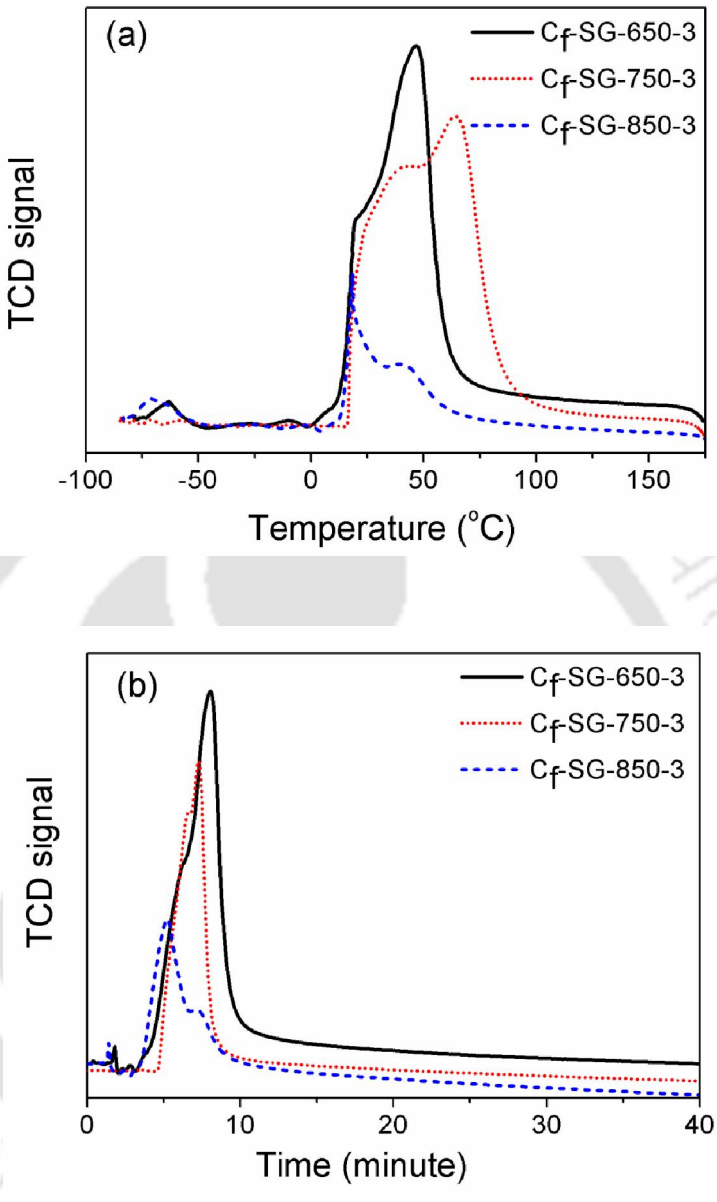

Figure 4.51. Hydrogen desorption profiles of silica gel templated carbons synthesized from furfuryl alcohol as function of (a) temperature and (b) time (adsorption temperature -100 °C at atmospheric pressure).

The hydrogen desorption profiles of templated carbons are shown as functions of temperature and time in Figure 4.51 (a-b). It was observed that the hydrogen desorption started at 5–10 °C and completed below 100 °C for all samples. Area under the curves

decreased corresponding to decrease in hydrogen uptake as the carbonization temperature increased. From Figure 4.51 (b) it can be observed that desorption kinetics was fast for all the samples. The hydrogen desorption was completed within 10 minute for all templated carbons.

4.4.4 Summary

This study explored the potential of inexpensive and commercially available silica gel as template for synthesis of templated carbon for hydrogen storage. Templated carbons with high surface area and pore volume were prepared by carbonization of furfuryl alcohol using silica gel template. BET surface area values were obtained in the range of 1678–1975 m^2/g and total pore volumes were in the range of 2.1–3.1 ml/g depending on the temperature and dwelling time. The highest surface area and pore volume were obtained at temperature of 650 ^oC and dwelling time of 3h. At temperature higher than 650 ^oC, the decrease in surface area and the pore volume can be attributed to collapse of pore structure. Lower surface area and pore volume observed for dwelling time, lower or higher than 3h, can be attributed to incomplete carbonization and collapse of walls of finer pores respectively. The silica gel templated carbons were mainly mesoporous. For all synthesized carbons, 90–95% of the pores were in the range of 2–20 nm and 38 to 67% of the pores were in the range of 2–6 nm depending on the synthesis conditions. FESEM images showed uniform pore structures for all the templated carbons. The hydrogen uptake capacity at atmospheric pressure was maximum (0.16 wt.% at –100 ^oC) for carbon prepared at 650 ^oC and 3h dwelling time and may be attributed to its highest surface area.

4.5 Comparison of templated carbons

4.5.1 Effect of template and carbon precursor

The nitrogen adsorption–desorption isotherms of templated carbons synthesized using different templates and carbon precursors are shown in Figure 4.52. The nature of the isotherms of silica gel templated carbons was of type IV for both the carbon precursors. The hysteresis loops approached H2 type suggesting presence of interconnected pores (Sing et al. 1985). The nature of the isotherm changed when zeolite was used as the template. The change can be attributed to different pore structures of the templates. The isotherms of both the zeolite templated carbons were of type II with H4 hysteresis loop corresponding to narrow slit-shaped pores. For both the templates, lower nitrogen adsorption was observed for the carbons synthesized from sucrose as compared to that prepared from furfuryl alcohol. The volume of nitrogen adsorption for zeolite templated carbons was significantly lower compared to that of silica gel templated carbons.

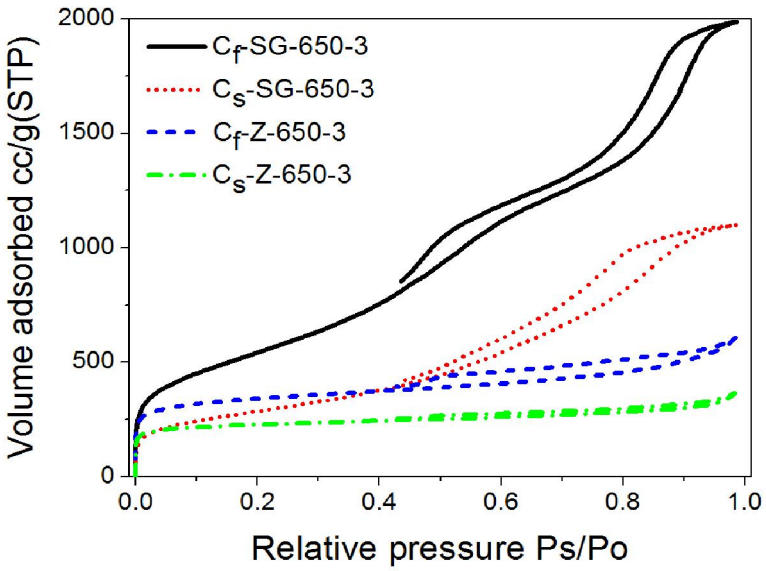

Figure 4.52. Nitrogen adsorption-desorption isotherms of templated carbons synthesized using various carbon precursors and templates.

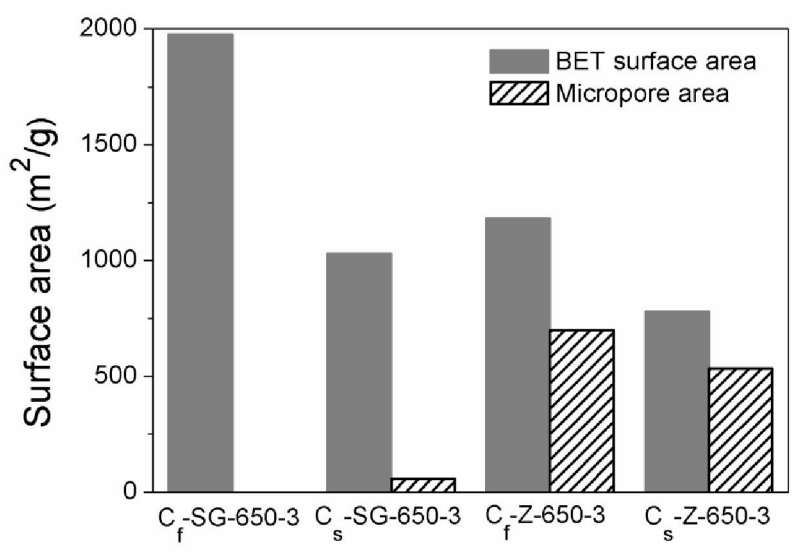

Figure 4.53. BET and micropore surface areas of templated carbons synthesized using various carbon precursors and templates.

The BET and micropore areas of templated carbons synthesized using different templates and carbon precursors are shown in Figure 4.53. The surface area of the carbons derived from silica gel template or furfuryl alcohol was higher than that observed for carbons prepared from zeolite template or sucrose precursor. For silica gel templated carbons, the BET surface area of 1975 m^2/g was observed for furfuryl alcohol precursor, which significantly decreased to 1029 m^2/g for carbon prepared from sucrose. No micropores were observed for silica gel templated carbons synthesized from furfuryl alcohol. However, micropore area of 58 m^2/g was observed for the carbon synthesized from sucrose.

Significant micropore area was observed for zeolite templated carbon derived from both the carbon precursors. The BET surface area of 1183 m^2/g and micropore area of 699 m^2/g were observed for zeolite templated furfuryl alcohol derived carbon. The BET surface area decreased to 781 m^2/g for carbon derived from sucrose. Therefore the BET surface area significantly decreased when sucrose was used as the carbon precursor compared to furfuryl alcohol irrespective of template. The significantly higher surface area for silica gel templated carbons compared to that of zeolite templated samples suggested that larger pore size of silica gel template facilitated incorporation of carbon

precursor within the template pore network. Consequently more extensive pore network was formed for silica gel templated carbon resulting in higher surface area and pore volume.

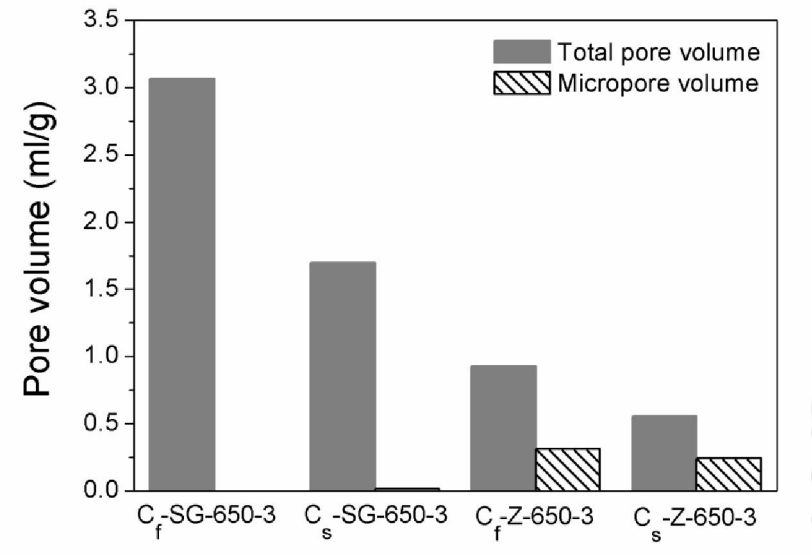

Figure 4.54. Total and micropore volumes of templated carbons synthesized using various carbon precursors and templates.

The total and micropore volumes of templated carbons synthesized using different templates and carbon precursors are shown in Figure 4.54. It was observed that the generation of pore volume followed similar pattern as surface area for the templated carbons. Total pore volume of 3.07 ml/g observed for C_f-SG-650-3 synthesized at 650 ^oC with 3h which further decreased to 1.70 ml/g when dwelling time decreased to 2h for C_s-SG-650-3. The total pore volume for zeolite templated carbons was significantly lower compared to that of silica gel templated carbons for both the carbon precursors, which can be attributed to the inhibition of development of carbon matrix with zeolite template. No micropore volume was observed for furfuryl alcohol derived C_f-SG-650-3, while a micropore volume of 0.02 ml/g was observed for the silica gel templated sucrose derived carbons. These micropores cannot be explained from the template structure. One possible explanation is that on using oxygen rich sucrose, that have comparatively higher carbon

number, more gaseous species such as CO, CO_2, and H_2O were evolved during carbonization and this may have contributed to generation of some micropores (Cai et al. 2014). The percentage microporosity of zeolite templated carbons synthesized from sucrose was also higher than that from furfuryl alcohol. Significant micropore volume was observed for zeolite templated carbons, for both the carbon precursors. For C_s-Z-650-3 sample micropore volume was about 42% of total pore volume.

The results suggested that the development of the porous structure of templated carbons depended both on the structure of the templates and nature of the precursors used. The use of highly crystalline microporous zeolite resulted in templated carbon with significant amount of micropores. On contrary, carbons with mainly mesopores with negligible micropores were produced when mesoporous silica gel was used as the template. The properties of carbon precursors such as size and presence of functional groups seemed to have an effect on the final structure of the templated carbons. Incorporation of precursors into template structure may experience resistance depending on size of the precursors. Higher resistance was expected as the size of the precursor molecules increased. Hence with increase in size incorporation of precursor within the template matrix will be reduced resulting in lower development of porous structure. Accordingly, surface area and pore volume of carbons prepared from sucrose, having larger molecular size, was lower compared to that synthesized from furfuryl alcohol for both the templates. For zeolite, presence of large fraction of micropores and crystalline structure may have offered further resistance to the incorporation of precursors. Hence incorporation of precursors was less in zeolite template resulting in significant decrease in total surface area and pore volume of the zeolite templated carbons compared to that of silica gel templated carbon as observed. The effect was more severe for sucrose precursor.

The pore size distribution was also affected by nature of template and precursor. The pore size distributions of templated carbons synthesized using different templates and carbon precursors are compared in Figure 4.55**.** The contribution of pores, having diameter in the range of 2-6 nm, was about 39% for the silica gel templated carbons, irrespective of the precursor used. The remaining pores were mainly distributed in the mesopore region of 6-20 nm. For C_f-SG-650-3 about 39% pores were in the range of 10-20 nm while 15%

pores were in the range of 6-10 nm diameter. The pores in the range of 10-20 nm decreased to 20%, while pores in the range of 6-10 nm increased to 36% of the total pore volume when sucrose was used as the carbon precursor. Macropores were also present along with mesopores and micropores in zeolite templated carbon. Significant numbers of pores were obtained in the regions of 2-6 nm and 20-80 nm for both the carbon precursors. About 59–73% pores were in the range of 2–20 nm diameter. The generation of larger mesopores (> 20 nm) and macropores were higher for zeolite templated carbons and were observed to be more significant for sucrose precursor. As discussed earlier, larger the size of precursor higher was the resistance to incorporation within the template matrix. The less developed carbon matrix for sucrose derived carbon resulted in higher fraction of larger pores.

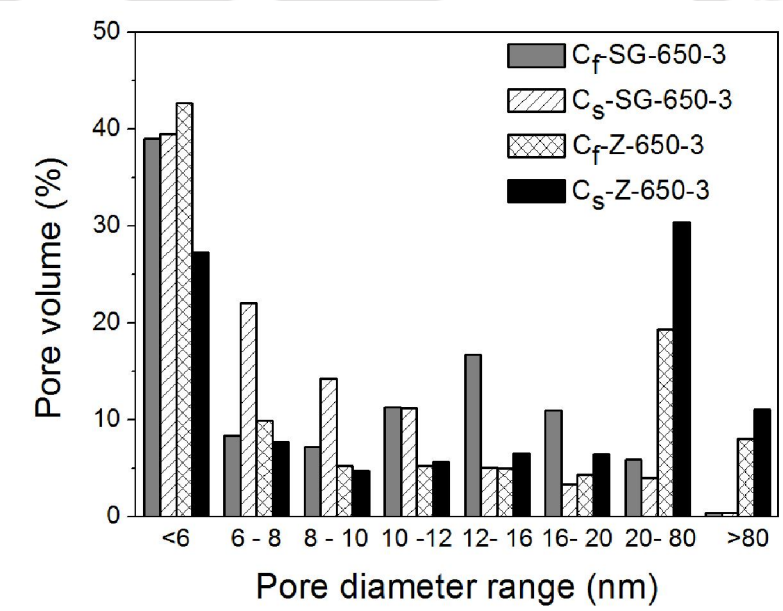

Figure 4.55. Pore size distributions of templated carbons synthesized using various carbon precursors and templates.

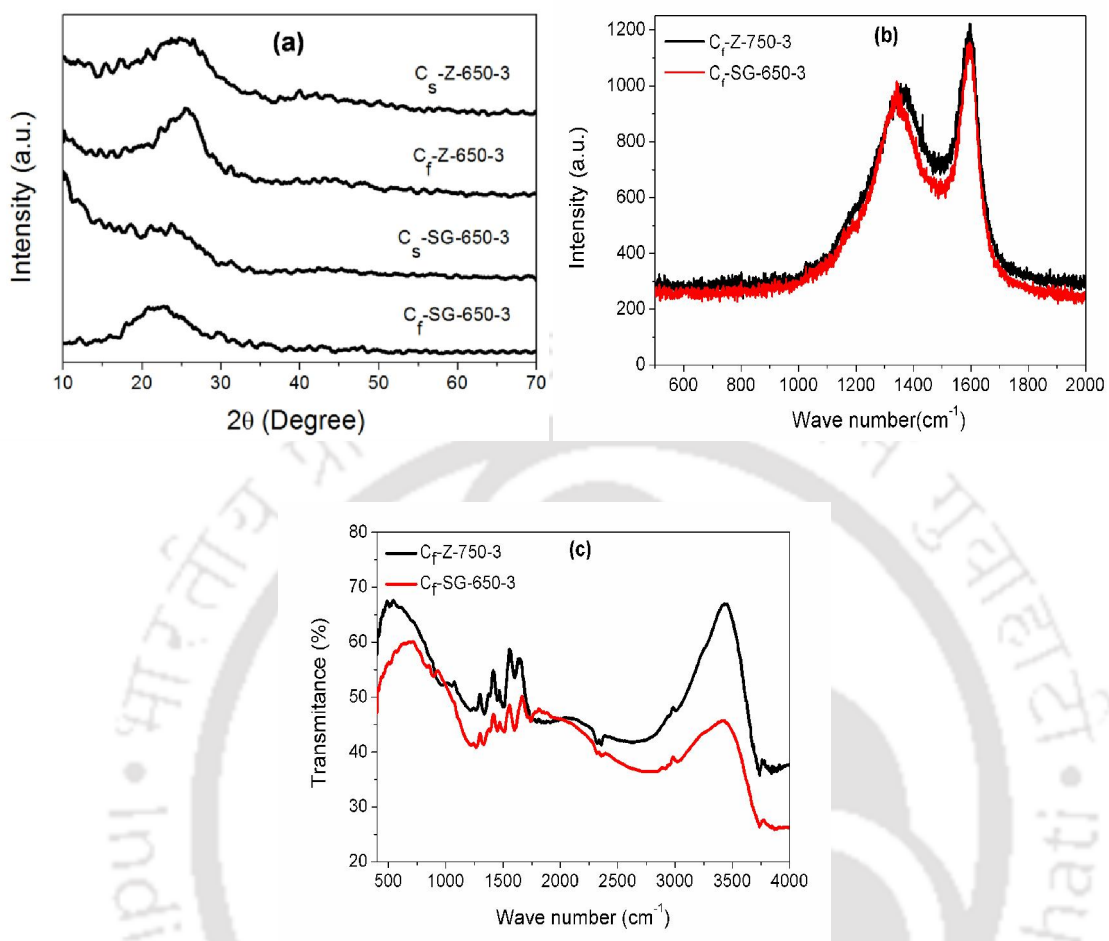

Figure 4.56. (a) XRD profiles of templated carbons synthesized using various carbon precursors and templates, (b) Raman and (c) FTIR spectra of templated carbons synthesized from furfuryl alcohol using different templates.

The XRD profiles of templated carbons synthesized using different templates and carbon precursors are shown in Figure 4.56 (a). A broad XRD peak was observed in the range of 18-30 ^{o} which corresponded to graphitic plane (002) (Dandekar et al. 1998). The intensity of the diffraction peak due to graphitic carbon was comparatively higher when furfuryl alcohol or zeolite was used as carbon precursor or template respectively. This suggested that the higher amount of graphitic carbon was formed when highly crystalline zeolite or furfuryl alcohol were used.

The Raman spectra for templated carbons synthesized using different templates are shown in Figure 4.56 (b). The D and G bands were obtained at wave number 1342-1370

cm^{-1} and 1593-1596 cm^{-1} respectively for both the samples. The intense G band indicated presence of graphitic structure in the templated carbons. Lower intensity ratios of D to G bands (I_D/I_G) signify higher amount of graphitic carbon (Yang et al. 2006). The I_D/I_G ratios were 0.82 and 0.87 respectively for the carbons synthesized using zeolite and silica gel templates. Comparatively lower I_D/I_G ratio for C_f-Z-750-3 sample confirmed the presence of higher amount of graphitic carbon compared to C_f-SG-650-3. This agrees well with the XRD analysis that crystalline structured zeolite template resulted in more amount of graphitic carbon compared to amorphous silica gel template.

The FTIR spectra for undoped templated carbons synthesized using different templates are shown in 4.56 (c). In all cases bands at around 523, 660, 754, 905, 1206, 1266, 1350, 1448, 1500, 1611, 1697, 1742, 2354, 2946, 3050, and 3730 cm^{-1} were observed. The bands in between 523-905 and 1448-1500 cm^{-1} can be assigned to out of plane C-H bending and C-C stretch of aromatic functional group respectively. The band around 1206, 1266, 1611, 1350 cm^{-1}can be assigned to C-O stretching where as 1742 cm^{-1} can be assigned to C=O group respectively. The band in between 2946-3050 cm^{-1} assigned to the presence of C-H aromatic group. The band at 2354 cm^{-1} can correspond to the adsorbed CO_2 on the carbon surface. The band at 3730 cm^{-1} assigned to the presence of –OH group for all the samples (Tipson 1968).

4.5.2 Hydrogen storage

The atmospheric pressure hydrogen uptakes at -100 ^oC for templated carbons synthesized from different templates and carbon precursors are compared in Figure 4.57. Hydrogen uptake of 0.16 wt.% was observed for silica gel templated carbon synthesized from furfuryl alcohol, which dropped to 0.10 wt.% when sucrose was used as the carbon precursor. For sucrose derived carbon the lower hydrogen uptake capacity may be attributed to its lower surface area. The BET surface areas were 1975 and 1029 m^2/g for silica gel templated carbons synthesized from furfuryl alcohol and sucrose respectively.

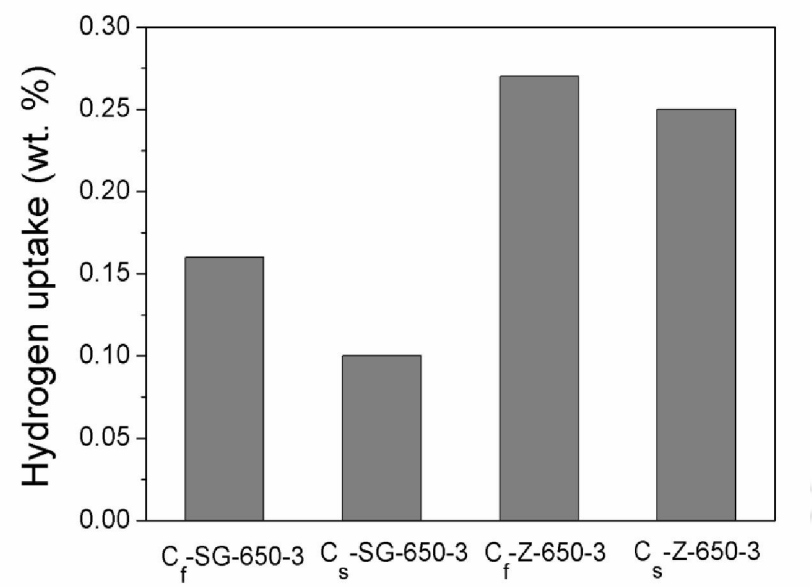

Figure 4.57. Hydrogen uptakes at atmospheric pressure and -100 °C for templated carbons synthesized using various carbon precursors and templates.

As observed from Figure 4.57 hydrogen uptake was comparatively higher for zeolite templated carbons. Hydrogen uptake capacity of 0.27 wt.% was observed for zeolite templated carbon synthesized from furfuryl alcohol, which was considerably higher than silica gel and furfuryl alcohol derived carbon, inspite of lower BET surface area. Higher hydrogen uptake capacity for all the zeolite templated carbons compared to that obtained from silica gel derived carbons inspite of lower surface area may be attributed to presence of significance amount lower size pores particularly micropores in the former. The uptake capacity dropped to 0.25 wt.% for zeolite templated carbon synthesized from sucrose. This may be due to considerably lower BET surface area (781 m^2/g) of sucrose derived C_s-Z-650-3 as compared to 1183 m^2/g of furfuryl alcohol derived C_f-Z-650-3 sample.

4.5.3 Summary

The comparative results showed that the templated carbons with better or similar characteristics can be synthesized using amorphous mesoporous silica gel as template compared to that of crystalline microporous zeolite. The surface area and pore volume of

the silica gel or furfuryl alcohol derived carbons were higher than that observed for zeolite or sucrose derived carbons. The significantly higher surface area for silica gel templated carbons suggested that in presence of larger pores for silica gel, incorporation of carbon precursors within the template matrix was facilitated favoring formation of extensive porous network. The silica gel templated carbons were mainly mesoporous and zeolite templated carbons were microporous in nature irrespective of carbon precursors used. Sucrose favored formation of micropores. Higher amount of graphitic carbon was formed when highly crystalline zeolite or furfuryl alcohol were used as template and carbon precursor respectively. The hydrogen uptake capacities mainly depended on BET and micropore surface areas of the synthesized carbons.

Chapter 5

Doped carbon

Chemically modified carbons were prepared by incorporation of heteroatoms during carbonization. Nitrogen and nickel were selected as nonmetal and metal heteroatoms respectively for incorporation in carbon matrix. Effects of templates and precursors of heteroatoms on carbon structure and corresponding hydrogen uptakes were investigated. Effect of nickel modification was initially studied using activated carbon. Furfuryl alcohol was used as carbon precursor for nitrogen doped templated carbon, whereas both furfuryl alcohol and sucrose were used as carbon precursors for nickel doped templated carbon.

5.1 Nitrogen doped templated carbon

5.1.1 Effect of template and nitrogen precursor

The nitrogen adsorption-desorption isotherms of undoped and doped templated carbons, synthesized using different templates and nitrogen precursors, are shown in Figure 5.1. Types of template as well as nitrogen precursor determined the nature of isotherm and hysteresis loop of doped carbons. The nature of isotherm for silica gel templated doped carbon prepared from acetonitrile precursor was of type IV having H2 loop as also observed for the corresponding undoped carbon. But for doped carbon prepared from aniline precursor it was more similar to type II with H4 hysteresis loop. Hence ink-bottle type interconnected pores were dominant in acetonitrile derived doped carbon while narrow slit shape pores were observed for aniline derived carbon. For zeolite templated doped carbons, isotherms were similar in nature for both the samples derived from acetonitrile and aniline precursors. The isotherms were of type II with H4 hysteresis loop. This was same as observed for undoped zeolite templated carbons.

The volume of adsorbed nitrogen on templated carbons was significantly lower when prepared from zeolite template compared to that prepared from silica gel template. For all the doped carbons the volume of adsorbed nitrogen was lower compared to corresponding undoped carbons. However, the extent of decrease depended on type of template and precursor. For silica gel templated carbon the drop in volume was more significant when aniline was used as precursor compared to when acetonitrile was used.

For zeolite templated doped carbon significant drop in adsorbed nitrogen volume was observed for both nitrogen precursors.

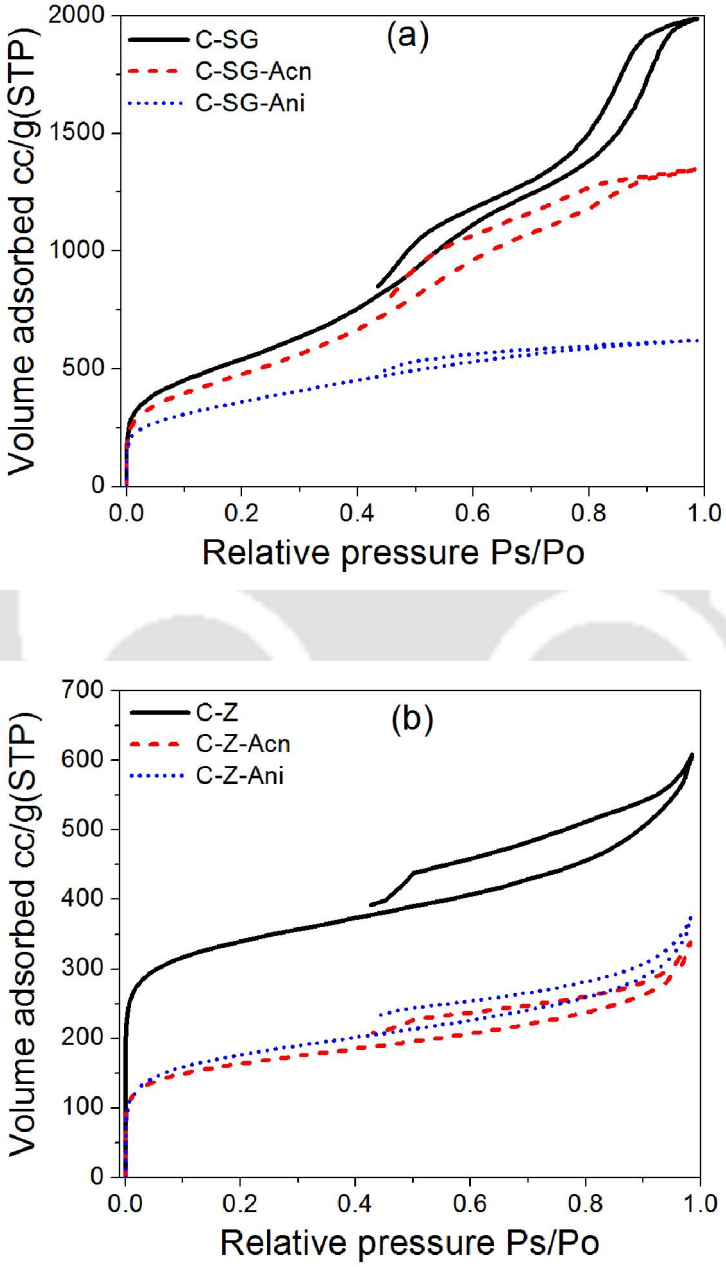

Figure 5.1. Nitrogen adsorption-desorption isotherms of undoped and nitrogen doped templated carbons synthesized using (a) silica gel and (b) zeolite as templates.

Table 5.1. Physical properties and nitrogen contents of doped templated carbons synthesized using different nitrogen precursors.

Sample ID	Template	Nitrogen precursor	BET surface area (m^2/g)	Micropore area (m^2/g)	Total pore volume (ml/g)	Micropore volume (ml/g)	Nitrogen content (Wt.%)
C-SG-Acn	Silica gel	Acetonitrile	1745	-	2.08	-	4.0
C-SG-Ani	Silica gel	Aniline	1296	124	0.96	0.05	6.7
C-Z-Acn	Zeolite	Acetonitrile	573	277	0.52	0.12	8.5
C-Z-Ani	Zeolite	Aniline	624	248	0.57	0.11	7.8

BET surface area, micropore area, total pore volume and micropore volume of the nitrogen doped templated carbons are included in Table 5.1. All the nitrogen doped templated carbons showed drop in surface area and pore volume and the extent of decrease depended both on type of the template and nitrogen precursors. For nitrogen doped silica gel templated carbons, the decrease in surface area was observed to be higher for aniline derived carbon compared to that prepared using acetonitrile. For C-SG-Acn and C-SG-Ani the surface are dropped to 1744 and 1295 m^2/g respectively, compared to surface area of 1975 m^2/g for undoped templated carbon (Table 4.3). The total pore volume of C-SG-Acn and C-SG-Ani sample decreased to 2.08 ml/g and 0.96 ml/g, respectively on nitrogen doping from 3.07 ml/g of undoped carbon. For C-SG-Ani micropore area of 123 m^2/g and micropore volume of 0.05 ml/g was observed. For zeolite templated nitrogen doped carbons, the surface area decreased to 573 and 624 m^2/g for acetonitrile and aniline derived carbons respectively from 1183 m^2/g for undoped carbon (Figure 4.50). The decrease in micropore area for doped carbons was also significant for both nitrogen precursors. The micropore are of a 699 m^2/g of undoped zeolite templated carbon dropped to 277 and 248 m^2/g respectively for acetonitrile and aniline derived carbons. The corresponding decrease in total pore volume was 0.52 and 0.57 ml/g respectively for C-Z-can and C-Z-Ani compared to 0.93 ml/g for undoped zeolite templated carbon. The micropore volume of zeolite templated carbon also dropped on addition of nitrogen. However, no significant difference was observed in total pore

volume and micropore volume (0.12 and 0.11ml/g) of carbons prepared using two different nitrogen precursors.

The above discussion shows that the decrease in surface area for doped silica gel templated carbons was in the range of 10-35 %, while that for doped zeolite templated carbons was about 47-51% compared to undoped templated carbons. The decrease can be attributed to two reasons; the difficulty in incorporation of nitrogen precursor in template and partial blockage of the pores in presence of nitrogen heteroatom. Since the average pore size of silica gel template was higher than that of zeolite template, the nitrogen precursors were able to penetrate more easily in the porous network of the former. Consequently, on removal of the template comparatively more porous network was obtained for silica gel templated carbon giving higher surface area and pore volume. For silica gel template the higher drop in surface area for aniline precursor may be attributed to its larger size. However, for zeolite template since the average pore size was much lower, both the nitrogen precursors underwent resistance during template filling. Hence, the resulting surface areas of templated carbons, prepared using the two precursors, were reduced significantly and almost to same extent.

The nitrogen content was determined by EDX and shown in Table 5.1. The EDX spectra are included in Appendix G. Nitrogen content varied in the range of 4-8.5 wt.%. Higher amount of nitrogen was detected for doped carbon prepared from zeolite template compared to that prepared from silica gel template. This may be explained as follows. Since the resistance faced by precursors during filling was more in microporous zeolite template than that in mesoporous silica gel, as discussed above, then it is probable that the nitrogen will be less dispersed within zeolite. However, for silica gel the nitrogen precursors were able to disperse more uniformly within the interior of porous structure. Consequently, by EDX, a surface analysis technique, higher amount of nitrogen was detected for zeolite templated carbons inspite of lower amount of nitrogen precursor used. For silica gel template using different nitrogen precursors, similar phenomenon was observed. Higher nitrogen content was observed for aniline and silica gel derived carbon compared to that derived from acetonitrile and silica gel. Higher resistance to incorporation of aniline in template matrix due to higher size may have resulted in

agglomeration of nitrogen at pore mouth showing higher nitrogen content in EDX. The minimal difference in nitrogen amount for the two zeolite templated doped carbons prepared from different nitrogen precursors may be attributed to resistance in incorporation of both precursors in zeolite as discussed earlier. The slight higher nitrogen loading for acetonitrile may be attributed to higher molar content of nitrogen in acetonitrile compared to aniline for same volume of precursors.

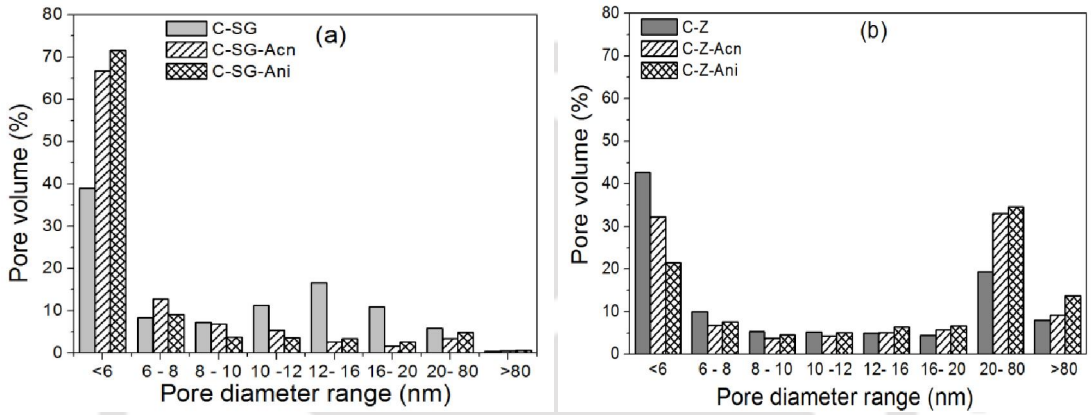

Figure 5. 2. Pore size of distributions of undoped and nitrogen doped templated carbons synthesized using (a) silica gel and (b) zeolite as templates.

The mesopore size distributions of templated carbons synthesized using different templates are shown in Figure 5.2 (a-b). The rearrangement of the pores due to incorporation of nitrogen was clearly observed. For silica gel templated doped carbons the volume percentage of pores having diameter in the range of 2-6nm increased to ~70% for both acetonitrile and aniline derived carbons compared to 39 % for undoped templated carbon (Figure 5.2.a). A significant drop in volume percent of mesopores in the range of 8-20 nm suggested incorporation of nitrogen in these pores. This incorporation of nitrogen precursor in the larger mesopores may have contributed to the increase in the pores in range of 2-6 nm for silica gel templated doped carbon by partial blockages. However, the volume percentage of lower mesopores (2-6nm) decreased from 43 % for undoped carbon to 32 and 21% respectively for acetonitrile and aniline derived zeolite templated doped carbons. The drop was more significant for aniline precursors (Figure

5.2 b). For undoped C-Z the contribution of larger pores (>20nm) was only 27%, while that for C-Z-Acn and C-Z-Ani the values increased to 42 and 48% respectively. As also discussed earlier, due to presence of extensive micropores in zeolites, nitrogen and carbon precursors may have been unable to incorporate deep within the framework of the zeolite template and corresponding development of porous network was poor. This may have resulted in formation of more of larger pores and less of smaller pores (micropores and lower mesopores) (Table 5.1 and Figure 5.2) in zeolite templated doped carbon.

The X-ray profiles of doped templated carbons synthesized using different templates are shown in Figure 5.3 (a-b). The peak maxima for silica gel templated undoped and doped carbons were observed at ~23.5 and 24.5^{o} respectively corresponding to graphitic plane. The slight shift of the peak to higher angle for doped carbons with respect to undoped carbon suggested slight decrease in interplanar spacing of the graphitic planes in the latter (Dhall et al. 2014). This may have resulted from the presence of nitrogen atoms within the carbon matrix for doped carbon. For both undoped and doped zeolite templated carbons the peak maxima were observed at ~ 25.7^{o}. The slight difference in peak position for silica gel and zeolite derived templated carbons may have been due to the difference in graphitic structure prepared from the different templates.

For zeolite sample no significant shift in peak positions for undoped and doped carbons suggested lower presence of nitrogen atoms within the carbon matrix. The absence of any peak due to the templates in the carbon samples suggested that the templates were completely removed during hydrofluoric acid treatment. This was further confirmed by the EDX analysis (Appendix G). No peaks due to Al or Si were observed.

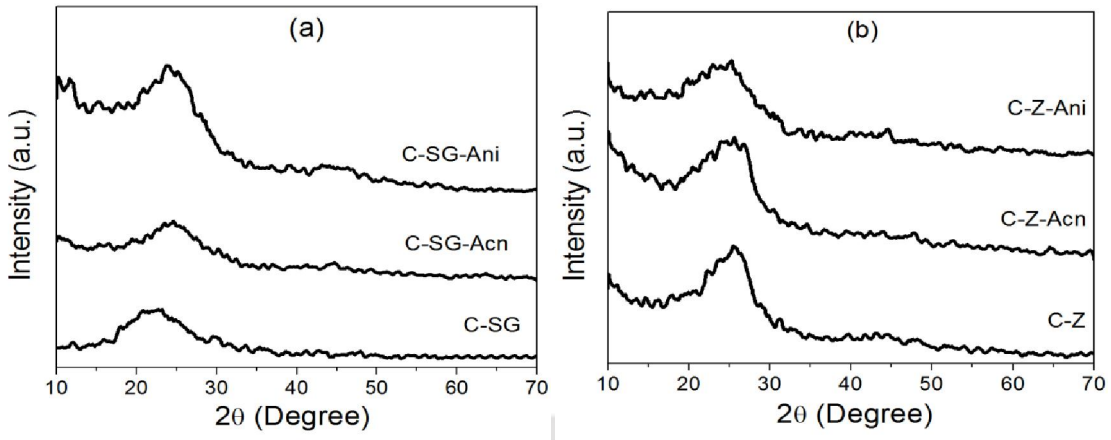

Figure 5.3. XRD profiles of undoped and nitrogen doped templated carbons synthesized using (a) silica gel and (b) zeolite as templates.

The Raman spectra of nitrogen doped templated carbons synthesized using various templates are shown in Figure 5.4(a). The D band was obtained at wave numbers of 1352 and 1374 cm^{-1} for the doped carbons synthesized using silica gel and zeolite template respectively. However, the G band was obtained at a wave number of 1603 cm^{-1} for both the doped carbons. For silica gel templated nitrogen doped carbon, the I_D/I_G =0.81 was comparatively lower than the respective undoped carbon (I_D/I_G = 0.87, section 4.5.1), indicating presence of higher amount of graphitic carbon in the doped sample. However, the observation was not similar to that obtained from XRD analysis. For zeolite templated nitrogen doped carbon, the observed I_D/I_G ratio did not significantly differ from the undoped one suggesting minimal change in structure. As discussed earlier, for zeolite template, the difficulty in incorporation of nitrogen precursors within the template may have resulted in less structural affect on the doped carbon compared to undoped one.

The FTIR spectra for nitrogen doped templated carbons synthesized using silica gel template is shown in 5.4 (b). Similar to undoped carbons, the peaks were observed for C-H, C-C, C-O, C=O and OH groups at similar positions as discussed in section 4.5.1. Normally, the peaks are reported at wavenumber of 1020-1220, 1266, 1410 cm^{-1} for the C-N bonds, 1550-1650 cm^{-1} for C=N bonds and 2120-2180, 2215-2230, 2240-2260 cm^{-1} for carbon nitrogen triple bonds (Tipson 1968). Since these peak positions overlap with

the peaks due to C-H and C-O, hence it is difficult to conclude. However, the intensity of these peaks did not change significantly in doped sample compared to undoped one.

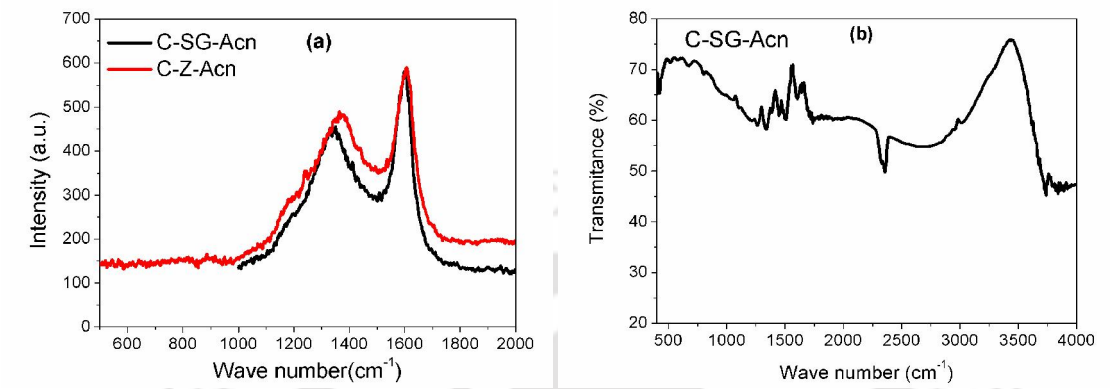

Figure 5.4. Spectral analysis of nitrogen doped templated carbons synthesized using different templates (a) Raman and (b) FTIR spectra.

The FESEM images of nitrogen doped templated carbons synthesized using different templates and acetonitrile precursor are shown in Figure 5.5 (a–b). The development of microstructure of the doped carbons varied in accordance with the structure of used template. Irregular shaped particles with wide particle size distribution were observed when silica gel was used as the template. However, more uniform structure was observed for zeolite templated doped carbons having agglomerated flowery appearance, similar to undoped zeolite templated carbons as can be observed from Figure 4.18. The microstructure of doped silica gel templated carbon was more similar to the template itself (Figure 4.8b) but differed significantly from undoped templated carbon (Figure 4.46). The TEM images of the doped templated carbons, as shown in Figure 5.5 (a–b), also showed the dissimilar morphology of the carbons synthesized using different templates. The well connected pore channels can be observed for both samples.

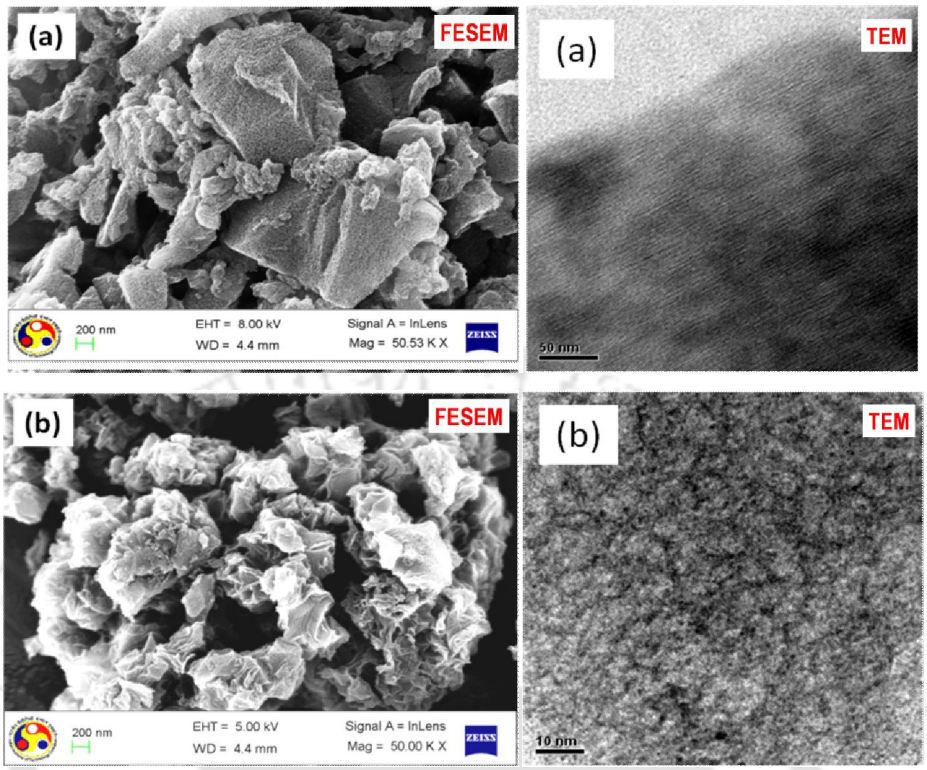

Figure 5.5. Microstructure of nitrogen doped templated carbons synthesized from acetonitrile precursor using (a) silica gel and (b) zeolite.

5.1.2 Effect of agitation

Micropores were observed for silica gel templated nitrogen doped carbon synthesized using aniline. Hence carbon derived using silica gel template and aniline precursor was selected to study the effect of agitation on the surface properties. The nitrogen adsorption-desorption isotherms of nitrogen doped silica gel templated carbons synthesized by stirring and sonication are shown in Figure 5.6 (a). Identical isotherms of type II with H4 hysteresis loop were observed for both samples.

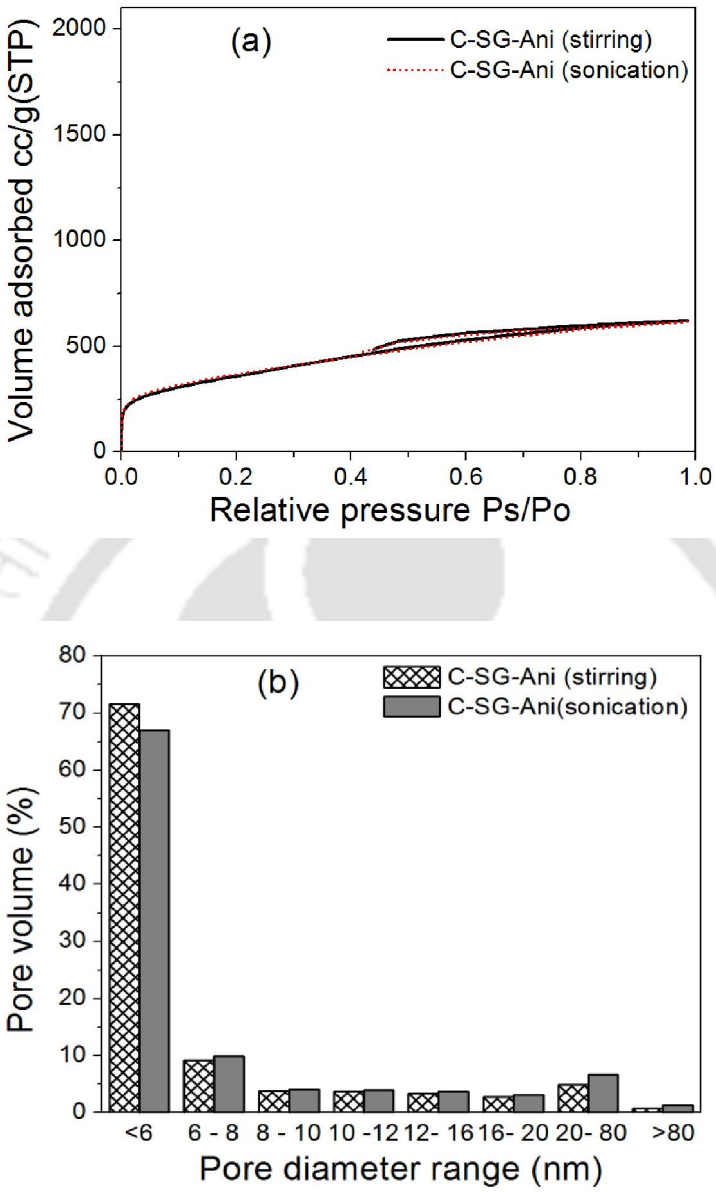

Figure 5.6. **(a) Nitrogen adsorption-desorption isotherms and (b) pore size distributions of nitrogen doped silica gel templated carbons synthesized by stirring and sonication.**

BET surface area of 1295 m^2/g for stirring assisted nitrogen doped carbon slightly increased to 1322 m^2/g for sonication assisted sample (Table 5.1), while the micropore area increased from 123 to 232 m^2/g. It was observed that the total pore volume and

micropore volume followed similar trends as surface area. The pore size distributions of the samples are shown in Figure 5.6(b). No significant difference in pore rearrangement was observed for the two doped carbon samples prepared by stirring and sonication. The pores having diameter in the range of 2-6 nm slightly decreased for sonication assisted sample compared to that of stirring assisted sample.

5.1.3 Hydrogen storage

Hydrogen uptake at atmospheric pressure and -100 ^{o}C for templated carbons synthesized using different nitrogen precursors and templates are shown in Figure 5.7. On nitrogen doping the uptake capacity increased for silica gel templated doped carbons in spite of lower surface area compared to that of undoped carbon. The hydrogen uptake of 0.16 wt.% was observed for silica gel templated undoped carbon as discussed in section 4.4.3. The increase in uptake capacity for doped carbon was more significant when prepared from acetonitrile precursor (0.30 wt.%) than when aniline precursor (0.20 wt.%) was used. This may be due to considerable lower surface area of C-SG-Ani (1295 m^2/g) compared to that of C-SG-Acn (1745 m^2/g).

The observed enhancement of hydrogen uptake for doped carbon in spite of lower surface area can be attributed to the presence of nitrogen. Based on DFT calculation nitrogen was reported to decrease the hydrogen dissociation energy (Viswanathan et al. 2003). The observed increase in hydrogen adsorption for nitrogen doped samples may be attributed to this lowered dissociation energy. Again the reduction potential of nitrogen (0.057V) is higher than that of carbon (-0.132 V) (Viswanathan et al. 2003). Hence, the incorporation of nitrogen in carbon networks may have facilitated the activation of the hydrogen molecules favoring their adsorption compared to that on undoped templated carbons. The hydrogen uptake with respect to BET surface area of the undoped and nitrogen doped templated carbons synthesized using different templates are shown in Figure 5.8. For both the nitrogen doped zeolite templated carbons, C-Z-Acn and C-Z-Ani, significant decrease in uptake capacity was observed compared to that of undoped C-Z, which may be attributed to severe decrease in BET surface area and micropore area for doped carbons as discussed earlier.

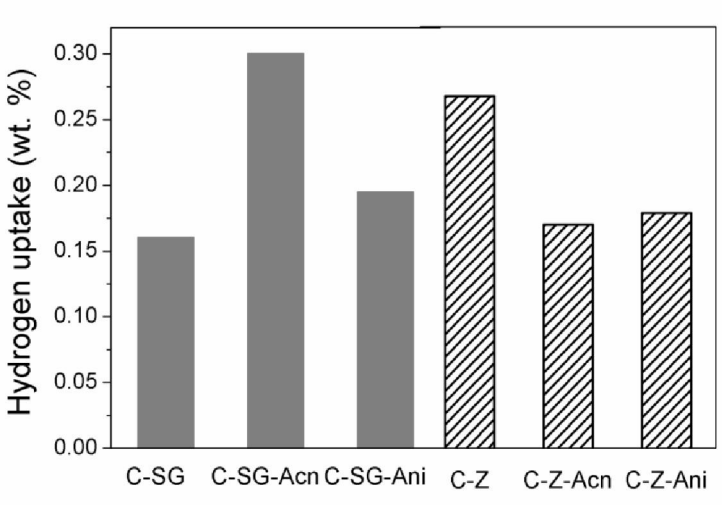

Figure 5.7. Hydrogen uptakes at -100 °C for undoped and nitrogen doped templated carbons synthesized using different templates.

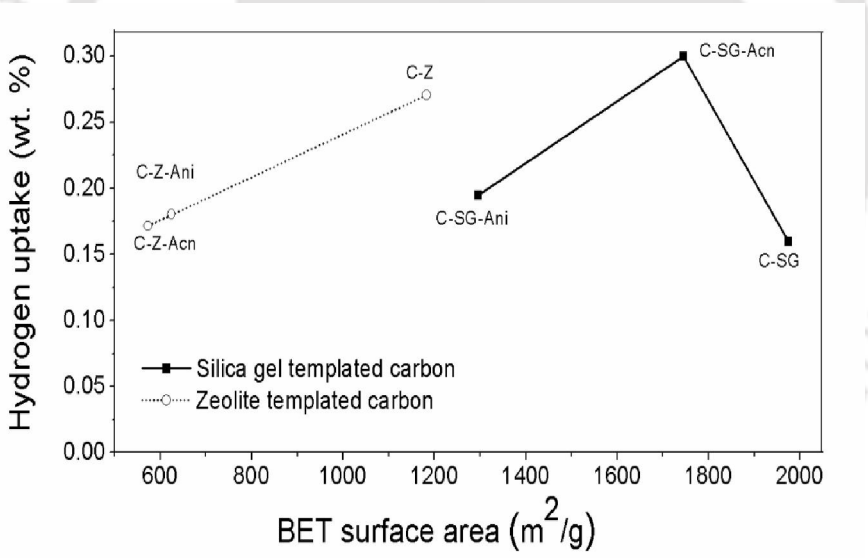

Figure 5.8. Hydrogen uptakes at -100 °C as function of BET surface area for undoped and nitrogen doped templated carbon.

As discussed in section 4.5, the higher hydrogen uptake of undoped zeolite derived carbon (0.27 wt.%) compared to that of undoped silica gel derived carbon can be attributed to higher micropore content in former. Hydrogen uptake of acetonitrile derived

silica gel templated doped carbon, with no micropores, was actually slightly higher than that for undoped zeolite templated carbon. It suggested that heteroatom was able to increase the interaction between hydrogen and carbon surface.

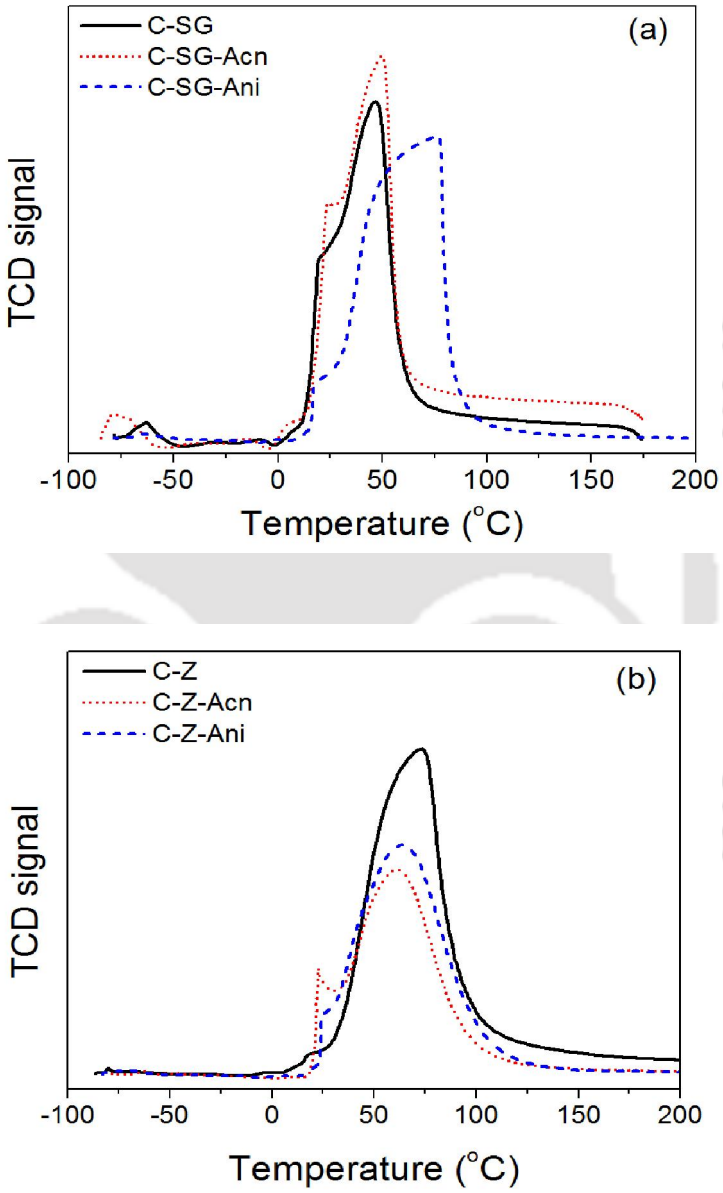

Figure 5.9. Hydrogen desorption profiles as function of temperature for (a) silica gel (b) zeolite templated undoped and nitrogen doped carbons (adsorption at -100°C).

The hydrogen desorption profiles of silica gel and zeolite templated carbons as function of temperature are shown in Figure 5.9 (a-b). Desorption profiles for undoped C-SG and doped C-SG-Acn were initiated at 2 ^{o}C with sharp desorption peak at 47 ^{o}C. The nature of the profiles was similar but area under the curve was higher for doped carbon corresponding to higher hydrogen uptake. However, the desorption profile for doped C-SG-Ani sample shifted towards higher temperature, initiating at 11 ^{o}C with maximum at 73 ^{o}C. The shift of the desorption profile of the doped carbon to higher temperature may have been resulted due to the diffusion resistance offered by micropores present in C-SG-Ani. As discussed earlier, for C-SG and C-SG-Acn samples micropores were not observed.

For all zeolite templated carbons the hydrogen desorption peaks started at 17 ^{o}C and ended at 127 ^{o}C. This shift compared to silica gel templated carbons can be attributed to presence of significant amount of micropores. Hydrogen desorption peak was observed at 73 ^{o}C for undoped C-Z, whereas for both nitrogen doped carbons the peak was observed at 64 ^{o}C. The observed difference in peak position for undoped and nitrogen doped zeolite templated carbons may be attributed to the difference in microporosity of the samples. In undoped sample higher microporosity may have resulted in higher resistance and shift of the peak to higher temperature. The lower area under the curve for doped carbon corresponded to lower hydrogen uptake. Further it can be observed that the nature of the hydrogen desorption profile for silica gel templated C-SG-Ani was similar to that of zeolite templated samples confirming the temperature shift of the desorption pattern of C-SG-Ani sample to presence of micropores. Thus, the desorption kinetics was observed to depend on porous structure. Though the hydrogen uptake was higher in presence of micropores the hydrogen desorption was slower. For C-SG and C-SG-Acn, containing mainly mesopores and no micropores, desorption was completed within in 10 minute, whereas for samples with significant micropores the hydrogen desorption was completed taking higher time of 15 minute (Appendix H). This is in accordance with higher resistance to hydrogen diffusion in presence of micropores.

5.1.4 Summary

Nitrogen doped templated carbons were prepared by simple carbonization method using acetonitrile and aniline as nitrogen precursors. On nitrogen loading the total surface area and pore volumes were reduced as compared to that of undoped carbon. The effect was more significant for the doped carbons synthesized using aniline precursor and zeolite template. The difficulty in incorporation of precursor to the template pores and partial blockage of the carbon pores by nitrogen atom resulted in lower surface area and pore volume for the doped carbons. Wide range of BET surface areas (573 -1745 m^2/g) and pore volumes (0.52–2.08 ml/g) were obtained for the doped carbons depending on the precursors and templates. The zeolite templated carbons were mainly microporous and silica gel templated carbons were mesoporous in nature irrespective of nitrogen precursors used. Significant pore rearrangement occurred for doped carbons due to incorporation of nitrogen. The mesoporous silica gel with higher average pore size was observed to be more suitable template for nitrogen incorporation compared to microporous zeolite. The microstructure of the nitrogen doped carbons varied in accordance with the structure of used templates. Hydrogen storage capacity of silica gel templated doped carbons increased significantly on nitrogen incorporation as compared to undoped carbon. The higher storage capacity of silica gel templated doped carbon in spite of lower surface area was attributed to higher activation of hydrogen by nitrogen present in the carbon network.

5.2 Nickel doped activated carbon

The effect of nickel on carbon structure and hydrogen uptake was studied first using activated carbon followed by templated carbon. The hydrogen capacity and adsorption - desorption kinetics were studied at different temperatures.

5.2.1 Effect of nickel loading

The nickel oxide loading was varied in the range of 5-30 wt.%. To check the effect of calcination temperature on carbon structure, if any, one activated carbon sample without any nickel oxide dopant was calcined at 300 ^{o}C for 2h. The calcined sample was characterized and results are discussed along with that of as-received activated carbon and nickel doped carbon.

The nitrogen adsorption-desorption isotherms of the as-received activated carbon, calcined activated carbon (300 ^{o}C) and nickel doped activated carbons are shown in Figure 5.10. The nitrogen adsorption–desorption isotherms for activated carbon and calcined activated carbon were quite similar in nature, indicating that surface area and pore structure of the as–received activated carbon remained mostly unaffected by the heat treatment at 300 ^{o}C for 2h. The nature of isotherms for activated carbon and calcined activated carbon approached type II, but was associated with a significant plateau suggesting presence of considerable amount of micropores.

For nickel oxide doped activated carbons it was observed that the volume of nitrogen adsorbed at any relative pressure decreased as the loading of NiO increased. The extent of plateau also increased with nickel oxide content, shifting the nature of isotherms towards type I, which suggested increased amount of narrower pores. The desorption curves for all the isotherms were observed to be parallel to the adsorption curves corresponding to H4 type of hysteresis loop attributed to narrow slit–like pores (Sing et al. 1985).

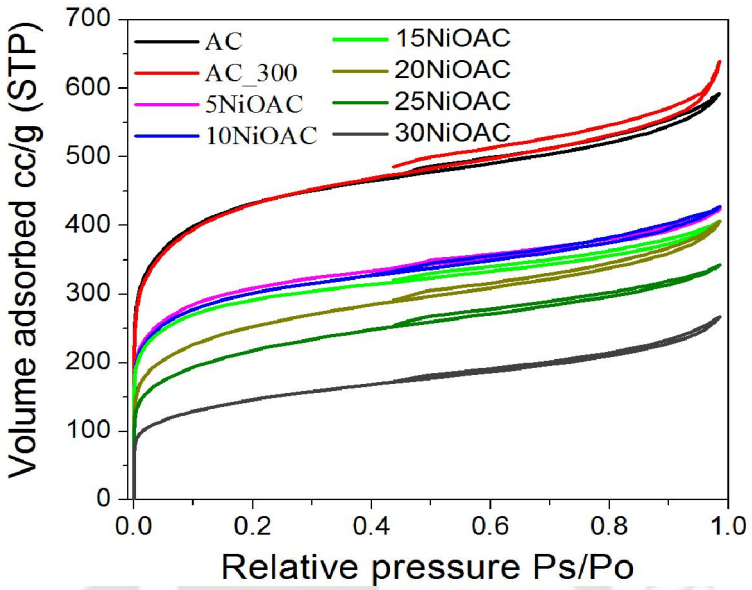

Figure 5.10. Nitrogen adsorption-desorption isotherms of as-received activated carbon, calcined activated carbon and nickel oxide doped carbons.

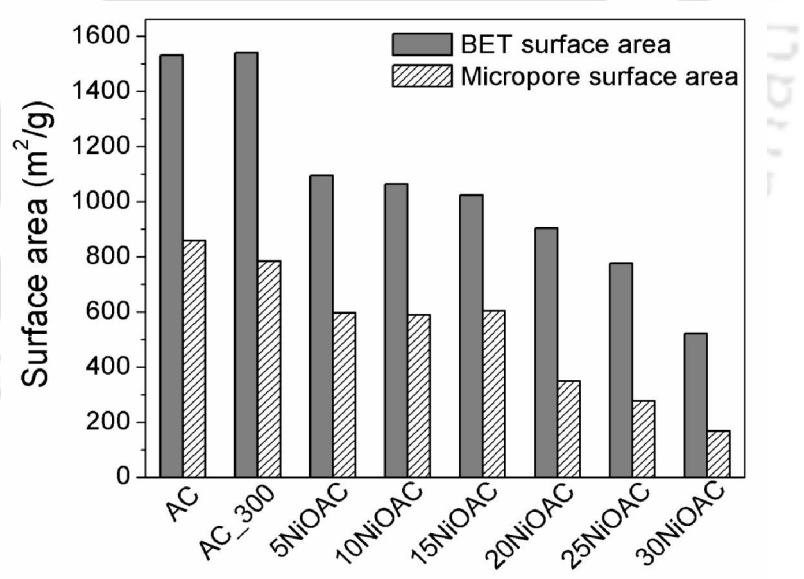

Figure 5.11. BET and micropore surface areas of as– received activated carbon, calcined carbon (AC-300) and nickel doped carbons.

Figure 5.11 shows the BET and micropore surface areas of the as–received activated carbon, calcined activated carbon and nickel doped carbon. The BET and micropore surface areas of as–received activated carbon were observed to be 1530 and 859 m^2/g respectively. After calcination at 300 ^oC for 2h; the BET surface area of the activated carbon was not affected significantly but micropore surface area slightly decreased to 783 m^2/g. At lower nickel oxide loadings of 5–15 wt.%, the BET surface area decreased but micropore area was unaffected. This suggested that nickel oxide mainly occupied the larger mesopores and macropores. This may have resulted in their partial pore blockage and increase in narrower pores as also supported by the change in nature of isotherms with increasing nickel loadings. At higher nickel oxide loadings (20–30 wt.%), the substantial decrease in the BET and the micropore surface area can be attributed to the extensive pore blockage by deposited nickel oxides (Huang et al. 2010).

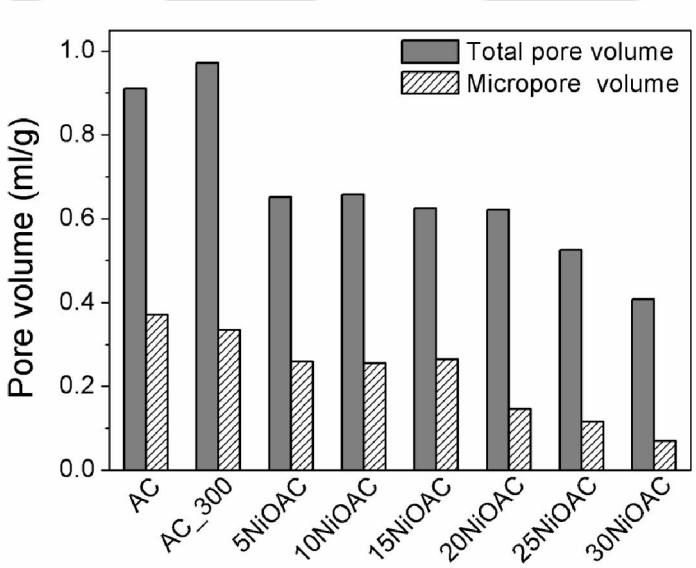

Figure 5.12. Total and micropore volumes of as-received activated carbon, calcined carbon and nickel doped carbons.

The total and micropore volumes of as–received activated carbon, calcined activated carbon and doped carbons are shown in Figure 5.12. The effect of calcination on the pore volumes of the as–received activated carbon was insignificant. At lower NiO loadings

(5–15 wt.%) the micropore volume remained almost unaffected, whereas at higher loadings (20–30 wt.%) both the total and micropore volumes significantly decreased due to blockage of the pores by deposited nickel oxides as discussed earlier.

The pore size distributions of as–received activated carbon and doped carbons are shown in Figure 5.13. On addition of NiO to activated carbon, the decrease in percentage of macropores and larger mesopores confirmed that the nickel initially resided in those pores. In all the doped activated carbon the increase in the pore volumes of size less than 6 nm may be due to the partial blockage of macropores by nickel oxide as also discussed earlier.

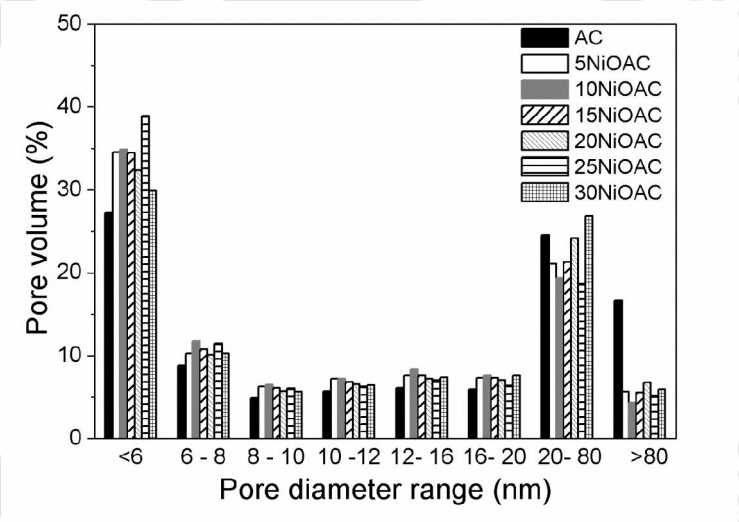

Figure 5.13. Pore size distributions of as-received activated carbon and nickel doped carbons.

The XRD profiles of as–received activated carbon and calcined carbon are shown in Figure 5.14 (a). The two peaks observed at 2θ = 26.6 and 43.4^{o} can be attributed to the (111) and (010) lattice planes, respectively, of graphitic carbon [JCPDS No. 01–075–2078]. The intensity of these peaks increased on calcination of activated carbon sample at 300 ^{o}C for 2h. The increase in intensity may be attributed to the enhancement of graphitic nature of activated carbon on calcination by rearrangement of molecules (Dandekar et al. 1998).

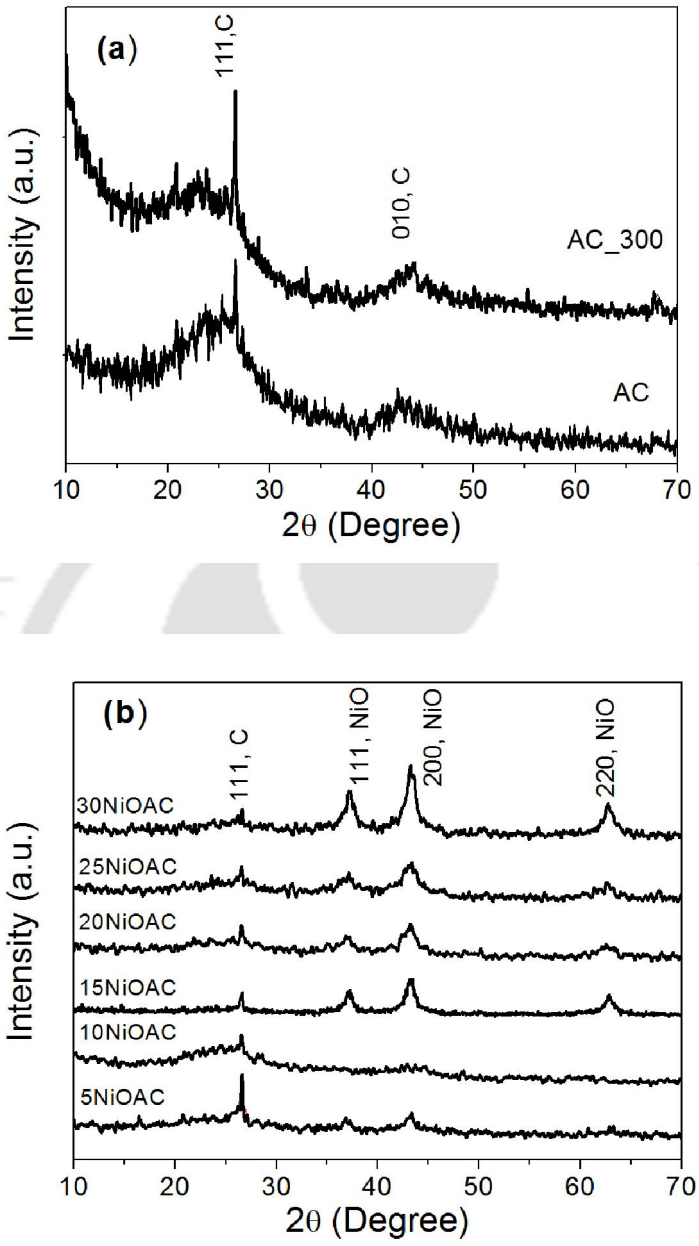

Figure 5.14. XRD profiles of (a) as-received activated carbon and calcined carbon (b) nickel doped carbons.

Figure 5.14(b) depicts the XRD patterns of doped carbons with different wt.% loading of NiO. Peaks were observed at 2θ = 26.6, 37.1, 43.4, and 62.6°. The peak at 26.6° corresponded to graphitic carbon (111) as was also observed for undoped activated

carbons. The intensity of carbon peak (2θ = 26.6°) was gradually reduced with NiO loading. This reduction in peak intensity can be attributed to the coverage of carbon by deposited NiO. The peaks at 2θ = 37.1, 43.4, and 62.6° can be attributed to (111), (200), and (220) planes of NiO respectively [JCPDS No. 01–075–0197]. It was observed that the intensity of NiO peaks increased with NiO loading.

The XRD profiles were also recorded for the reduced form of 15NiO-AC. The sample was reduced in flow of hydrogen and reduction profile is shown in Appendix I. Figure 5.15 compared the XRD profiles of 15NiOAC with the reduced form (15NiAC). In the XRD profile of reduced form, 15NiAC, only peaks corresponding to metallic Ni were obtained at 2θ =44.6 (111) and 52 ° (200) [JCPDS No 00–001–1260]. No peaks of NiO were observed as expected.

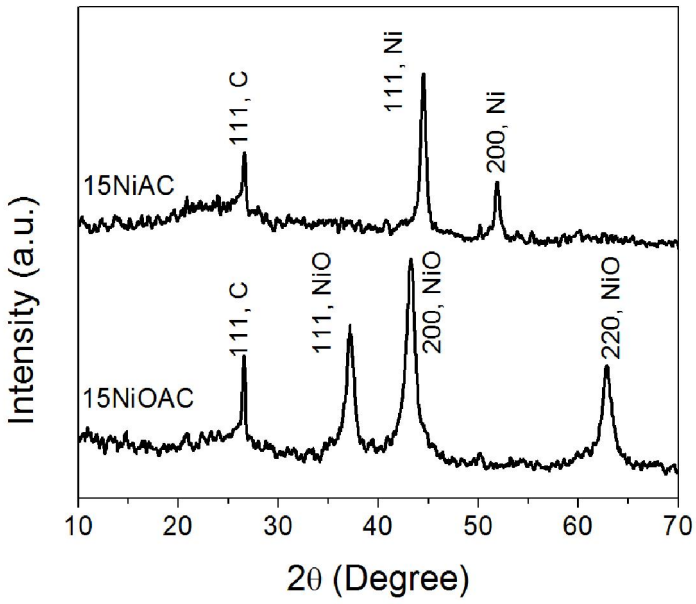

Figure 5.15. XRD profiles of 15 wt.% NiO on activated carbon in oxidized (15NiOAC) and reduced forms (15NiAC).

The dispersion and the metal surface area of nickel for all the doped samples in reduced form were determined by CO–pulse chemisorption. The obtained dispersion values for 5NiAC, 10NiAC, 15NiAC, 20NiAC, 25NiAC and 30NiAC were 0.487, 0.243, 0.176,

0.159, 0.106 and 0.150 % respectively. The reduction in metal dispersion with nickel loadings may be due to the formation of larger nickel clusters. At higher nickel loadings formation of larger cluster lowered the fraction of total nickel exposed for adsorption. The active metal surface areas were calculated to be 0.128, 0.128, 0.138, 0.167, 0.139 and 0.236m^2/g for 5NiAC, 10NiAC, 15NiAC, 20NiAC, 25NiAC and 30NiAC respectively. The increasing trend in metal area with nickel loadings may be attributed to the higher amount of exposed nickel. However, the extent of exposed nickel was not proportional to the total nickel loaded, and hence the dispersion was reduced at higher loadings as observed.

The FESEM images of undoped activated carbon, 15NiOAC, and 30NiOAC are shown in Figure 5.16. Well connected pores with varying pore size were observed for undoped activated carbon in Figure 5.16 (a). For 15NiOAC sample the pores were partially blocked by the doped NiO as observed in the Figure 5.16(b). Significant blockage of the pores was observed for 30NiOAC with highest loading of nickel oxide. As discussed earlier, pore blockage may have been caused by deposition of high amount of NiO. Thus, the FESEM images were in good agreement with the surface area and pore structure results.

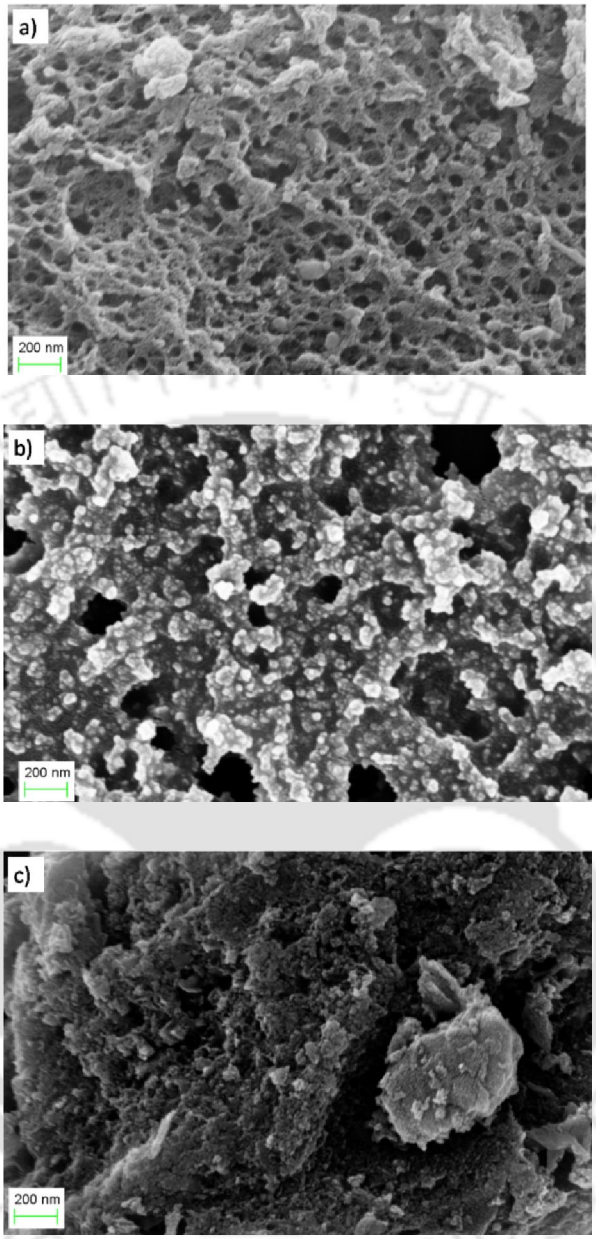

Figure 5.16. FESEM images of (a) as-received activated carbon, (b) 15NiOAC and (c) 30NiOAC.

5.2.2 Hydrogen storage

The hydrogen uptakes of undoped and nickel doped activated carbons are shown in Figure 5.17.

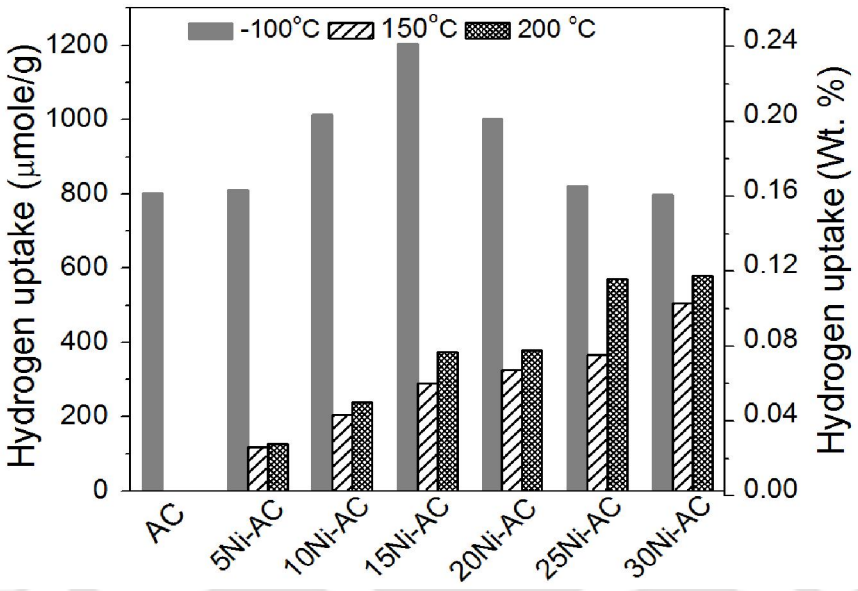

Figure 5.17. Hydrogen uptakes of as-received activated carbon and nickel doped carbons at atmospheric pressure and different adsorption temperatures.

The hydrogen uptake was measured at atmospheric pressure and different temperatures of –100, 150 and 200 °C. For all samples no hydrogen uptake was observed at atmospheric pressure and room temperature. At subzero temperature of –100 °C, the hydrogen uptake was initially enhanced with nickel content up to 15NiAC and thereafter, decreased at higher nickel loadings. For undoped activated carbon, the hydrogen uptake can be attributed mainly to the physisorption of hydrogen, whereas for nickel doped activated carbon the hydrogen adsorption was facilitated by chemisorption on nickel sites. Nickel is also expected to enhance the interaction between hydrogen and carbon surface by catalyzing the dissociation of hydrogen and favoring the spillover mechanism (Lueking et al. 2004). The hydrogen spillover mechanism is schematically shown in Figure 5.18. In this mechanism the hydrogen molecules are catalytically dissociated to hydrogen atoms

at the nickel sites on the activated carbon. Thereafter, the hydrogen atoms diffuse from the metal surface to the carbon surface, followed by diffusion and final adsorption on the carbon surface. At higher loadings (20-30 wt.%) when drop in BET and micropore surface area was significant (Figure 5.13) the hydrogen uptake again decreased. However, in spite of significant drop in surface areas, the hydrogen uptake capacities at the higher nickel loadings (20–30 wt.%) were comparable to uptakes for undoped carbon and carbon with lower nickel loadings of 5 and 10 wt.%. Hence, at lower loadings (5-10 wt.%) though both carbon surface and nickel active sites may have contributed to hydrogen uptake, however at higher loadings (20-30 wt.%) the hydrogen uptake can be attributed mainly to chemisorption and spillover by nickel sites. The results thus suggested that at -100 ^{o}C for nickel doped activated carbon, the mechanism contributing to hydrogen uptake depended on the nickel content.

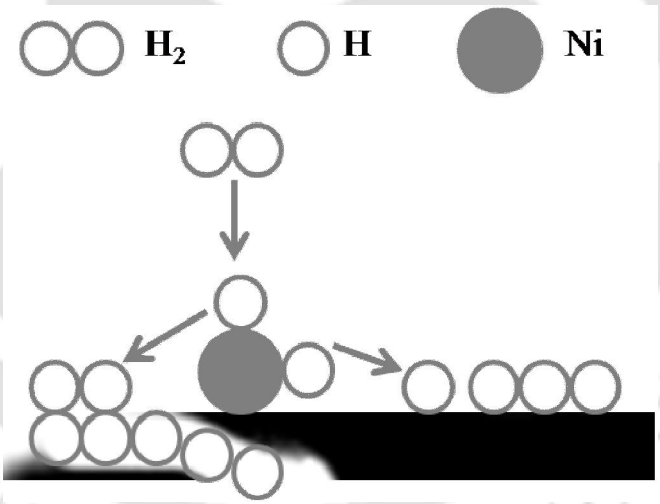

Figure 5.18. Hydrogen spillover mechanism over nickel doped carbon.

At higher temperatures (150 and 200 ^{o}C), the undoped activated carbon did not show any hydrogen uptake. The hydrogen uptake steadily increased with increase in the nickel content from 5 to 30 wt.%. For all nickel doped samples the hydrogen uptake was higher at 200 ^{o}C compared to that at 150 ^{o}C. These observations suggested that the hydrogen adsorption at higher temperature on nickel doped carbon occurred primarily by

chemisorption assisted by the spillover phenomenon. With increase in nickel content the metal dispersion was reduced, but the metal surface area increased and thereby, negated the adverse effect of lower dispersion at higher loadings. In other words, higher dispersion at low nickel loadings and higher metal area at high nickel loadings may have provided the required adsorption sites for hydrogen chemisorption. The optimum amount of nickel was observed to be essential for maximizing the number of exposed adsorption sites and thereby, hydrogen uptake. At the conditions studied the optimum loading was observed to be 15 wt.% of NiO giving the highest hydrogen uptake of 0.24 wt.%.

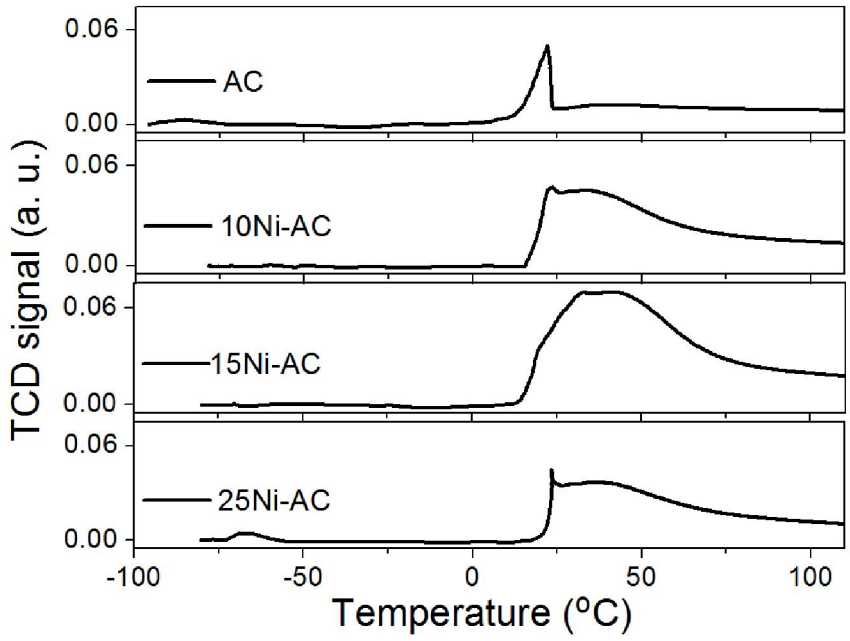

Figure 5.19. Hydrogen desorption profiles of as-received activated carbon and nickel doped carbons as function of temperature (Adsorption temperature -100 °C at atmospheric pressure).

The hydrogen desorption profiles of undoped and nickel doped activated carbons as function of temperature are shown in Figure 5.19. The corresponding adsorption was carried out at -100 °C and atmospheric pressure for all the samples. Hydrogen desorption for all the samples was completed within 20-25 minutes and below 100 °C temperature. Desorption profile for undoped activated carbon was characterized by a sharp desorption

peak at 21 ^{o}C which can be ascribed to desorption of the physisorbed hydrogen on activated carbon. The desorption of hydrogen for undoped activated carbon was completed within 23 ^{o}C. For all nickel doped activated carbons the desorption profiles contained overlapping multiple peaks that resulted in observed broadening. The first desorption peak was observed in the range of 16-26 ^{o}C and can be attributed to physisorbed hydrogen as similar to undoped carbon. For the undoped carbon desorption started around temperature of 12 ^{o}C but for doped activated carbons the desorption profiles started at higher temperature. The starting temperature increased from 16 to 20 ^{o}C with increase in nickel loading. The shift of the first desorption peak (assigned to physisorbed hydrogen) to higher temperature for doped carbons may have resulted due to the diffusion resistance developed by the presence of nickel clusters within the pores. With increase in nickel loading the extent of temperature shift was higher. The subsequent peaks of the profiles at higher temperatures may be assigned to desorption of chemisorbed hydrogen from nickel adsorption sites. The higher desorption temperature suggested stronger binding energy corresponding to chemisorption. Therefore, for doped activated carbon desorption kinetics was slower but hydrogen uptake was higher compared to undoped carbon. The area under the peak was maximum for 15NiAC corresponding to highest hydrogen uptake as discussed earlier at -100 ^{o}C adsorption temperature. The desorption profiles were consistent with the mechanism of hydrogen uptake by physisorption on undoped activated carbon and both by physisorption and chemisorption on nickel doped activated carbon at lower temperature of -100^{o}C.

The high temperature adsorption profiles of nickel doped activated carbons are shown in Figure 5.20 (a). The temperature of the adsorbent was increased from room temperature to 200 ^{o}C in flow of 5% H_2 in argon and maintained at 200 ^{o}C for 30 minute. The adsorption was carried out at atmospheric pressure. For all samples the hydrogen adsorption started at around 100 ^{o}C. The area under the peaks increased with nickel loading corresponding to enhanced hydrogen adsorption. This enhancement of hydrogen uptake can be attributed to the increased chemisorption of hydrogen on nickel sites at high temperature.

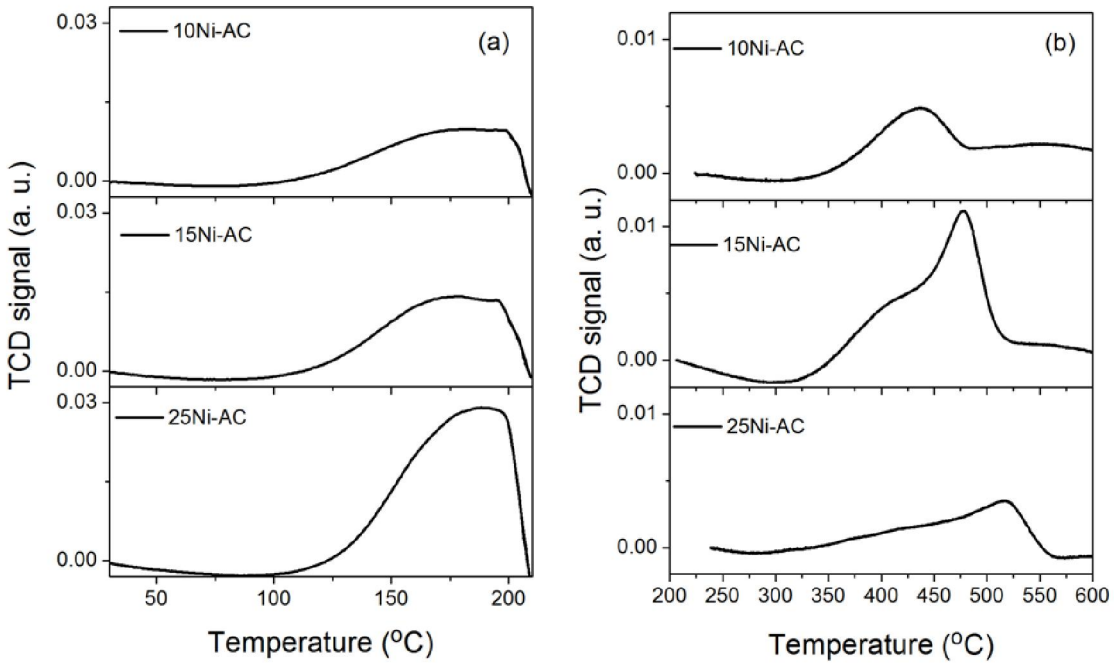

Figure 5.20. For as-received activated carbon and nickel doped carbons (a) adsorption profile at 200 °C and (b) desorption profiles upto 600 °C (at atmospheric pressure).

The corresponding hydrogen desorption profiles, (for adsorption at 200 °C), for nickel doped carbons are shown in Figure 5.20 (b). It was observed that the desorption of hydrogen started at 325°C for all doped carbon samples. For 10NiAC, the hydrogen desorption was completed within 480 °C, whereas for 15NiAC the hydrogen desorption continued till 525 °C. For 25NiAC the desorption of hydrogen was observed till 560 °C. The desorption peak intensities (that is the peak area under the desorption curve) for all nickel doped carbons significantly decreased compared to corresponding adsorption peak intensities as observed from Figure 5.20 (a-b). The lower desorption peak area compared to corresponding adsorption peak area suggested that the chemisorbed hydrogen on the nickel sites was not completely desorbed even at higher temperature. Hence, for high temperature hydrogen adsorption on nickel doped activated carbons, complete reversibility was not observed for all the samples. The desorption peaks also shifted

towards higher temperature with increase in the nickel content. These phenomena may be attributed to stronger interaction of hydrogen at nickel sites.

5.2.3 Summary

The nickel doped activated carbon was prepared by impregnation method and the nickel loading was varied from 5-30 wt.%. On increasing the nickel content, the BET surface area and pore volume decreased significantly due to the partial pore blockage of carbon by nickel oxide. The maximum hydrogen uptake of 0.24 wt.% was observed for optimum loading of 15 wt.% NiO at adsorption temperature of – 100 ^{o}C and atmospheric pressure. Nickel enhanced the carbon–hydrogen interaction and hydrogen uptake by providing additional active sites for chemisorption, catalyzing the hydrogen dissociation and facilitating hydrogen spillover. For carbon with lower nickel loadings both physisorption and chemisorption were responsible for hydrogen uptake, whereas at higher nickel loadings chemisorption was the main contributing factor. Further at subzero temperature both physisorption and chemisorption were responsible for hydrogen uptake. At higher adsorption temperature only chemisorption was observed to be responsible for hydrogen uptake. For doped activated carbon desorption kinetics was slower but hydrogen uptake was higher compared to undoped carbon. Desorption profiles showed that with increase in nickel content the adsorbent-hydrogen interaction became stronger, and consequently desorption kinetics was slow. At higher temperature loss in reversibility of hydrogen uptake was observed.

5.3 Nickel doped templated carbon

5.3.1 Effect of template and carbon precursor

The nitrogen adsorption-desorption isotherms of nickel doped templated carbons, synthesized using different carbon precursors and templates, are compared with undoped carbons in Figure 5.21(a-b). For nickel containing carbons, shape and nature of isotherms were similar to that of the corresponding in undoped one. The nature of isotherm for silica gel templated nickel doped carbons was of type IV, whereas that for zeolite templated doped carbon was type II. The nature of hysteresis loop was also different for doped carbons derived from the two templates corresponding to development of different pore structure. For the silica gel and zeolite templated carbons H2 type loop corresponding to the interconnected pores and H4 hysteresis loop corresponding to slit pores were observed, respectively. The volume of nitrogen adsorption decreased only marginally on addition of nickel for all modified carbons except that for furfuryl alcohol and zeolite derived Ni-C_f-Z, which showed a significant drop. This suggested that simultaneous incorporation of nickel and carbon precursors did not affect the basic structure development of carbon; however, presence of nickel obstructed some of the pores resulting in lower nitrogen adsorption. The volume of adsorbed nitrogen for all zeolite templated carbons was significantly lower compared to that of silica gel templated carbons. For both the templates, lower nitrogen adsorption was observed for the carbons synthesized from sucrose as compared to that prepared from furfuryl alcohol.

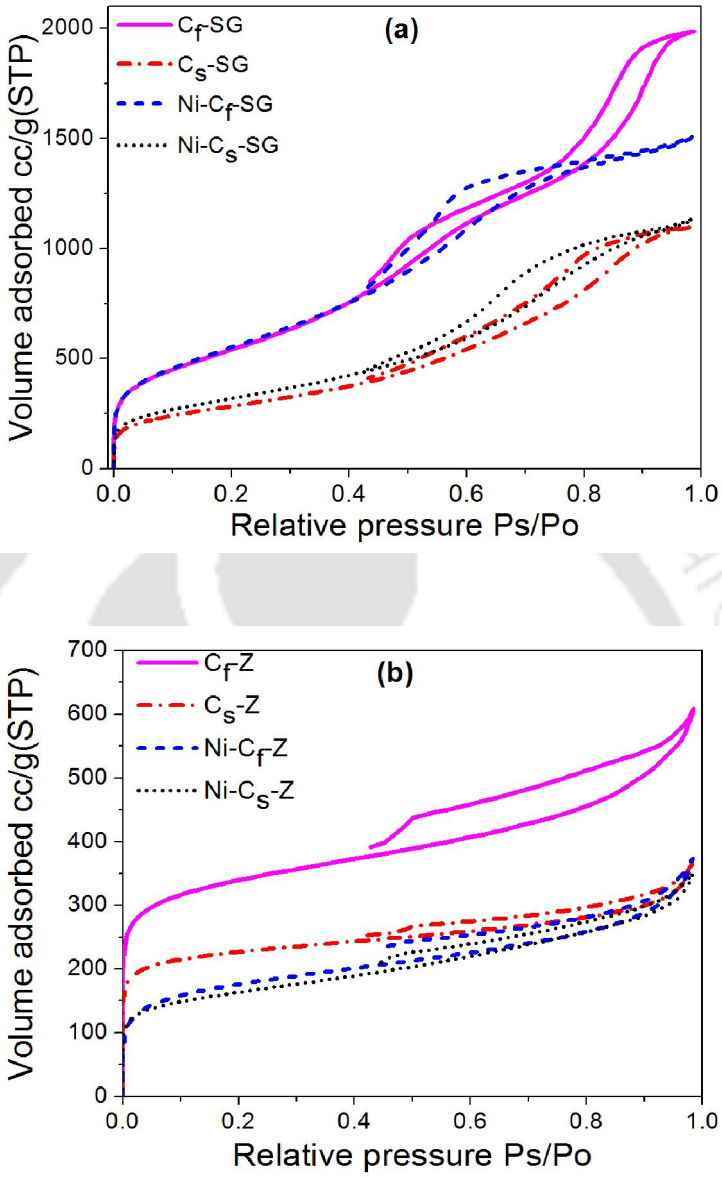

Figure 5.21. Nitrogen adsorption-desorption isotherms of undoped and nickel doped templated carbons synthesized using (a) silica gel and (b) zeolite as templates.

Table 5.2. Physical properties and nickel contents of doped templated carbons synthesized using different carbon precursors and templates.

Sample ID	Template	Carbon precursor	BET surface area (m^2/g)	Micropore area (m^2/g)	Total pore volume (ml/g)	Micropore volume (ml/g)	Nickel content (wt.%)
Ni-C_f-SG	Silica gel	FA	2008	-	2.32	-	-
Ni-C_s-SG	Silica gel	Sucrose	1157	26	1.75	7E-4	3.35
Ni-C_f-Z	Zeolite	FA	625	248	0.57	0.11	0.21
Ni-C_s-Z	Zeolite	Sucrose	571	257	0.53	0.11	6.4

The physical properties for nickel doped templated carbons are included in Table 5.2. The surface areas were 1975 and 1029 m^2/g for undoped silica gel templated carbons derived from furfuryl alcohol and sucrose respectively (Table 4.3 and Figure 4.34). The incorporation of nickel precursor resulted in slight increase of surface area for silica gel templated carbons for both the carbon precursors. The marginal increase in surface area may be attributed to the pore rearrangements due to nickel. Highest surface area of 2008 m^2/g was observed for nickel modified silica gel templated carbon prepared from furfuryl alcohol. The effect was different when zeolite was used as the template. For zeolite templated furfuryl alcohol derived carbon surface area was 1183 m^2/g and that for sucrose derived carbon was 781 m^2/g. The lower surface area and higher percentage of micropore area for zeolite derived carbons have been discussed in section 4.5. The lower surface areas for zeolite derived carbons were attributed to higher resistance to incorporation of precursors, whereas higher percentage of micropore areas had been attributed to microporous nature of zeolites. Incorporation of nickel precursor along with carbon precursor resulted in significant drop in both surface area and pore volume as can be observed from table. This may have been resulted from the higher resistance to incorporation of precursors in microporous zeolite matrix in presence of nickel precursors. The lower surface area for all the sucrose derived carbons may be attributed to higher size of sucrose molecules as discussed in section 4.5. Accordingly the lowest

area was observed for nickel doped zeolite templated carbon derived from sucrose as carbon precursor (571 m^2/g).

The pore volumes were 3.07 and 1.70 ml/g for furfuryl alcohol and sucrose derived undoped silica gel templated carbons, respectively. The pore volume dropped for doped carbons compared to that of undoped one. This may have resulted from the partial blockage of the pores by nickel present in the carbon matrix as mentioned earlier. For silica gel templated carbon, the total pore volume of nickel doped Ni-C_f-SG decreased to 2.32 ml/g compared to 3.07 ml/g for undoped C_f-SG suggesting better incorporation of precursors within the template matrix. For larger carbon precursor, such as sucrose, higher resistance to precursor incorporation resulted in less developed carbon matrix and much lower pore volume of 1.7 ml/g for C_s-SG sample. Addition of nickel precursor, which is actually of lower size compared to sucrose, resulted in slight increase in pore volume for nickel doped silica gel templated carbons form sucrose. The probable reason for presence of micropores in sucrose and silica gel derived templated carbons has been discussed in section 4.5 For zeolite templated furfuryl alcohol derived carbon the total pore volume and micro pore volumes were 0.93 and 0.32 ml/g respectively while that for sucrose derived carbon were 0.56 and 0.24 ml/g respectively. The total pore volumes and micropore volumes decreased for nickel modified zeolite templated carbons prepared from both the carbon precursors compared to that of the respective unmodified carbons. This can be attributed to inhibition of formation of porous structure as well as partial pore blockages due to presence of nickel. However, no significant difference in micropore volumes was observed for Ni-C_f-Z and Ni-C_s-Z.

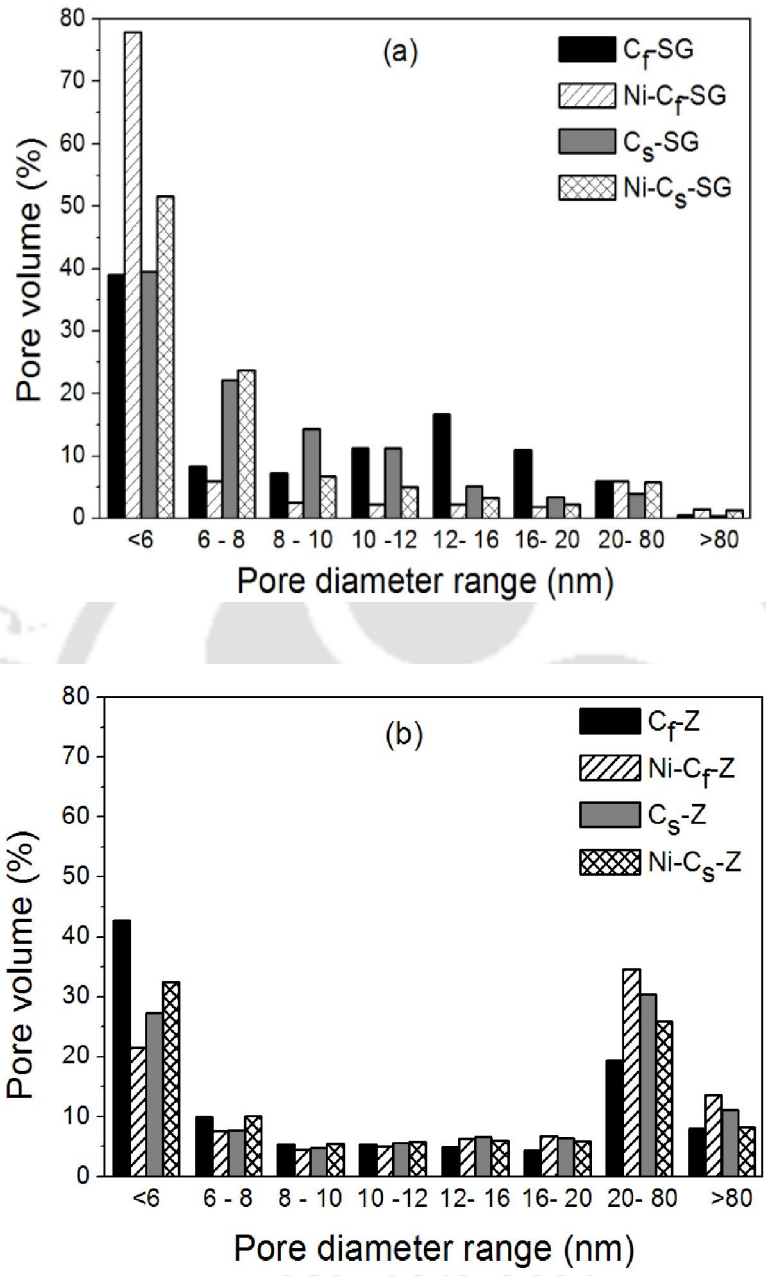

Figure 5. 22. Pore size distributions of undoped and nickel doped templated carbons synthesized using (a) silica gel and (b) zeolite as templates.

The BJH pore size distributions of the templated carbons, synthesized by using different templates and precursors, are shown in Figure 5.22 (a-b). Rearrangement of the pores was observed for doped carbons due to incorporation of nickel. The contribution of pores,

having diameter in the range of 2-6 nm, was about 39% for both the silica gel templated undoped carbons. The remaining pores of the undoped carbon were mainly distributed in the mesopore region of 6-20 nm. When nickel was incorporated to silica gel templated carbons, the volume percentage of pores having diameter in the range of 2-6 nm increased significantly to ~78 and 52 % for furfuryl alcohol and sucrose derived carbons, respectively. A simultaneous decrease in mesopore volume in the range of 6-20 nm was observed. This suggested that the incorporation of nickel in silica gel template may have partially blocked the larger mesopores (6-20 nm) and contributed to the significant increase in the lower mesopores (<6 nm). For zeolite templated carbons, significant number of pores were obtained in the regions of 2-6 nm and 20-80 nm. The relative percentage of these pores was changed on addition of nickel. The volume percentage of lower mesopores (2-6 nm) decreased on incorporation of nickel for furfuryl alcohol and slightly increased for sucrose precursor. This was accompanied with simultaneous increase and decrease in larger pores for doped carbon derived from furfuryl alcohol and sucrose, respectively.

As discussed in section 4.5, larger the size of precursor higher was the resistance to incorporation within the template matrix and effect was more severe for zeolite matrix having significant fraction of micropores. Therefore, higher volume percentage of larger meso and macro pores were observed for zeolite templated carbon prepared from sucrose compared to that prepared from furfuryl alcohol. When nickel precursor was used in addition to carbon precursor, the resistance was expected to increase. Consequently, poor development of porous structure occurred and again resulted in higher fraction of larger pores in all zeolite templated nickel modified carbons. The presence of nickel may have also caused partial blockage of few pores resulting in slight decrease in larger pores and simultaneous increase in volume percentage of lower mesopores (2-6 nm) for sucrose derived carbon. No significant change in pore distribution was observed in the range of 6-20nm for zeolite templated carbons on incorporation of nickel.

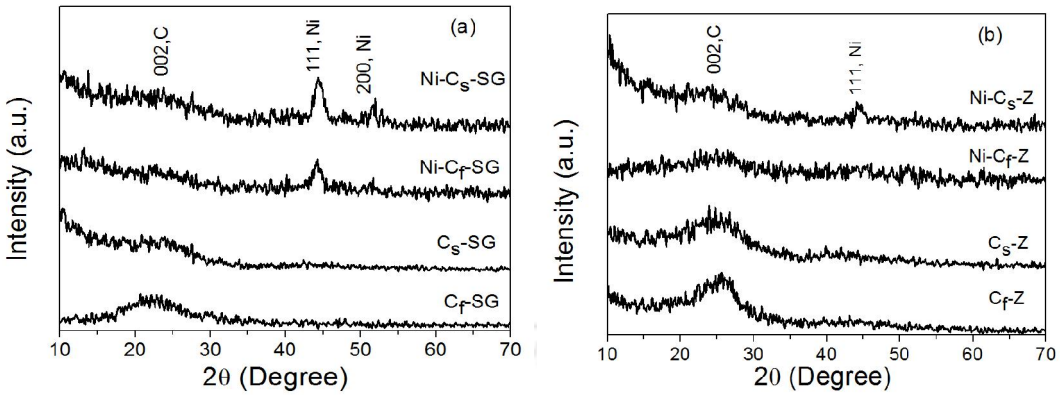

Figure 5. 23. XRD profiles of undoped and nickel doped templated carbons synthesized using (a) silica gel and (b) zeolite as templates.

The X-ray diffraction profiles of templated carbons, prepared from different precursors and templates, are shown in Figure 5.23 (a-b). Very low intense peaks were observed for graphitic carbons in both nickel doped samples. Distinct peaks due to metallic nickel were observed at 44.6 and 52 ^{o} [JCPDS No 00–001–1260]. The intensity of nickel peaks was higher for silica gel derived doped carbons compared to that prepared from zeolite template. This suggested presence of nickel in higher agglomerated state in the silica gel derived carbon matrix. The crystallite size of nickel was 10 and 11.5 nm respectively in silica gel templated carbons derived from sucrose and furfuryl alcohol. The crystallite size of nickel in zeolite and sucrose derived doped carbon was 11.7 nm. The calculations of nickel crystallite sizes are shown in Appendix K. The intensity of nickel peak was very low for zeolite and furfuryl alcohol derived doped carbon. The lower nickel peak intensity for zeolite derived doped carbon may have resulted from either lower incorporation of nickel within the bulk matrix of template or inhibition of agglomeration of nickel particles. The lower incorporation of nickel precursor in the zeolite pores can be attributed to additional resistance in microporous zeolite template as discussed earlier.

The highly structured nature of zeolite template may have also contributed to inhibition of movement and agglomeration of nickel particles resulting in low intensity nickel peak. Mesoporous and amorphous nature of silica gel matrix, on the other hand, may have facilitated incorporation as well as agglomeration of nickel particles resulting in highly

crystalline nickel in silica gel derived doped carbons. For both templates, the intensity of metallic nickel peak was observed to be higher for carbon synthesized using sucrose as carbon precursor compared to that obtained from furfuryl alcohol. This may be possibly explained by higher interaction between sucrose and nickel acetate facilitating incorporation of nickel within the template matrix. The higher interaction of nickel acetate with sucrose may have arisen from the interaction with the hydroxyl groups present in sucrose in larger number.

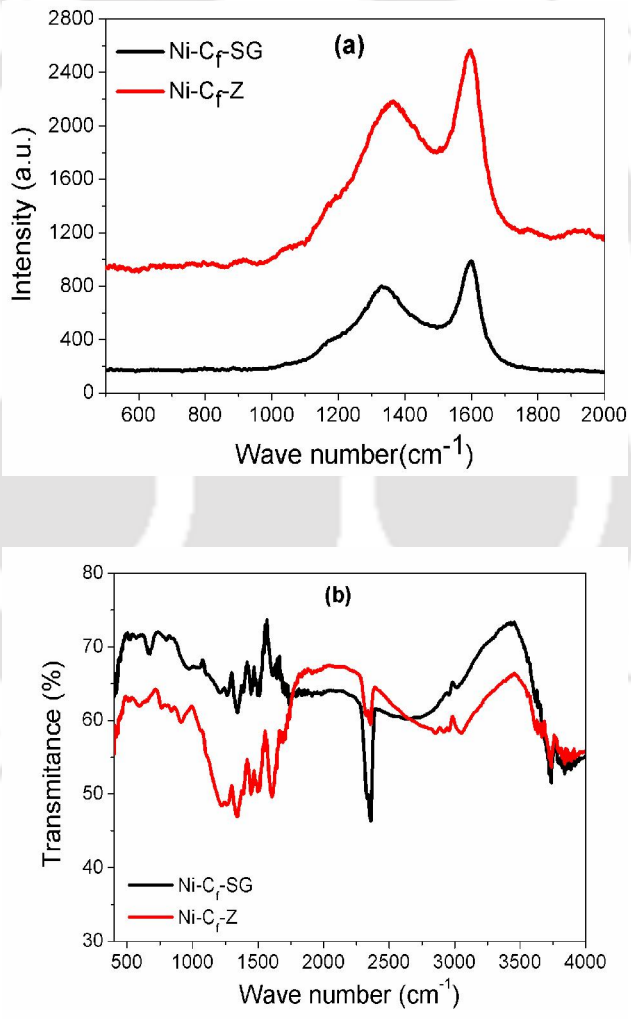

Figure 5.24. Spectral analysis of nickel doped templated carbons synthesized using different templates (a) Raman and (b) FTIR spectra.

The Raman spectra of nickel doped templated carbons synthesized using silica gel and zeolite templates are shown in Figure 5.24(a). Distinct D and G bands were obtained similar to undoped carbons as discussed in section 4.5.1. For silica gel templated nickel doped carbon the lower I_D/I_G ratio (0.82) compared to respective undoped carbon (0.87) indicated formation of higher amount of graphitic carbon for former. However, higher I_D/I_G ratio of 0.85 was observed for zeolite templated nickel doped carbon compared to corresponding undoped one (0.82).

The FTIR spectra for nickel doped templated carbons synthesized using various templates are shown in 5.24 (b). For both the nickel doped templated carbons the peaks due to the C-H, C-C, C-O, C=O and OH group were observed at the similar position with the respective undoped carbons. However, the intensity of the peak observed at 2354 cm^{-1} corresponded to the adsorbed CO_2 on carbon surface was significantly higher for both the nickel doped carbons.

The FESEM images of nickel doped templated carbons synthesized from silica gel and zeolite are shown in Figure 5.25(a-c). Porous spherical agglomerates were observed for furfuryl alcohol and silica gel derived nickel doped carbons. On comparison with FESEM image of corresponding undoped templated carbon (Figure 4.46), higher agglomeration was observed on addition of nickel. The nickel modified carbon derived using sucrose as carbon precursor also showed an agglomerated morphology. A uniform flowery kind of structure was observed for nickel doped zeolite templated carbon as shown in Figure 5.25 (c). This morphology was almost same as undoped zeolite templated carbon (Figure 4.18) discussed in section 4.2.2. A highly developed porous structure for silica gel derived carbon agrees with the discussed proposition that the precursors experienced less resistance in mesoporous template. This resulted in better incorporation of precursors within the matrix giving well developed porous structure with high surface area and pore volume.

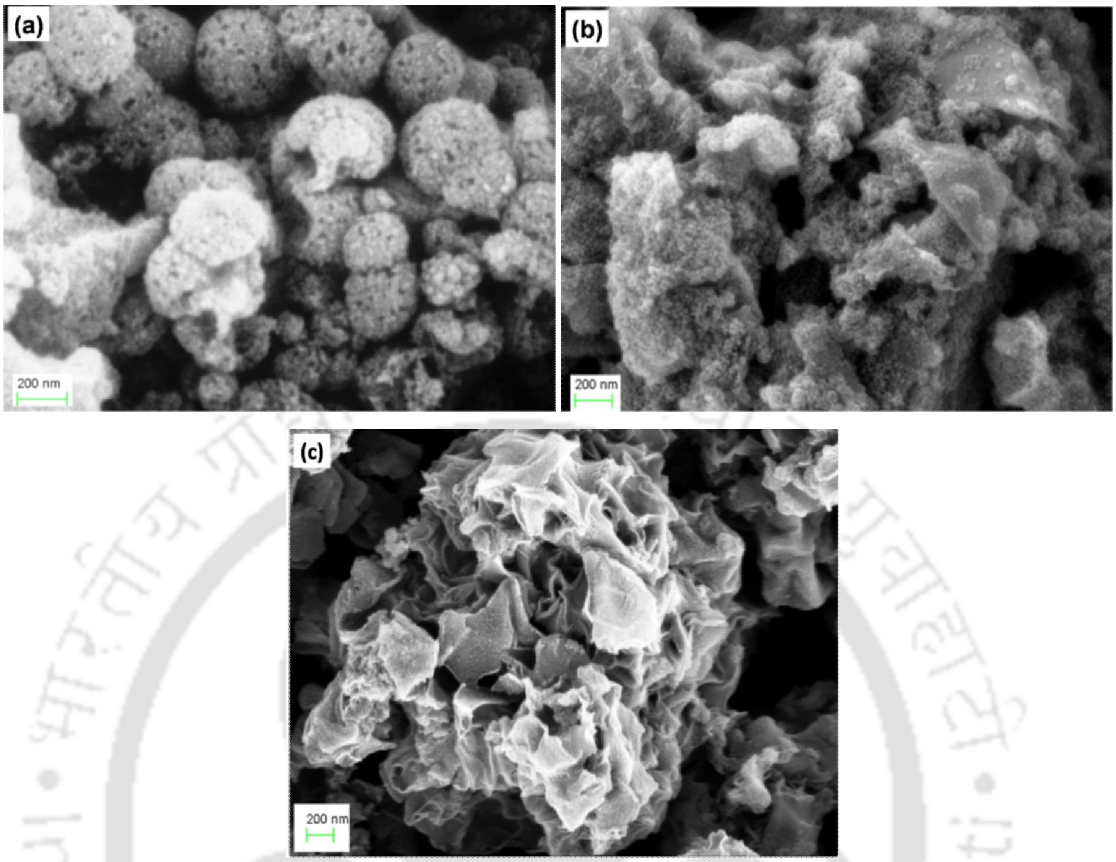

Figure 5.25. FESEM images of nickel doped templated carbon prepared from (a) furfuryl alcohol, (b) sucrose using silica gel template, and (c) furfuryl alcohol using zeolite template.

The EDX analysis confirmed that no other elements were present other than nickel in the synthesized doped templated carbons. Hence, the observed spherical particles in the silica gel templated doped carbon were cluster of nickel. For silica gel templated doped carbon synthesized from sucrose the nickel loading was 3.4 wt.%. For zeolite templated doped carbons the observed nickel loadings were 0.21 and 6.4 wt.% respectively for furfuryl alcohol and sucrose precursors. The EDX spectra of nickel doped templated carbons synthesized using different carbon precursors and templates were included in Appendix L.

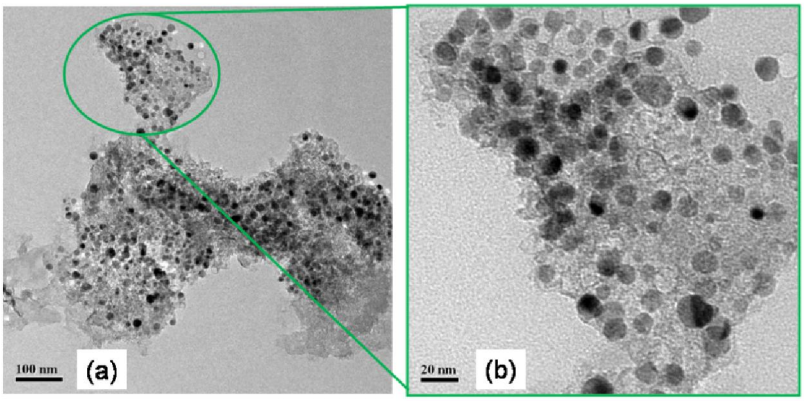

Figure 5.26. TEM images of silica gel templated nickel doped carbons synthesized from furfuryl alcohol.

The TEM images of silica gel templated nickel modified carbon synthesized using furfuryl alcohol are shown in Figure 5.26. It can be observed that nickel was uniformly distributed in the carbon matrix with average particle size of about 10 nm. The result agreed well with the average crystallite size obtained from the XRD studies. The results suggested that the structured templated carbon was able to prevent agglomeration and produce nano nickel particles. The density of nickel particles was about 4500 particles per square micrometer as calculated from TEM image. Calculation for determination of density of the nickel particles is included in Appendix M.

5.3.2 Effect of agitation

The effect of agitation on the surface properties of nickel doped carbon was studied for silica gel, furfuryl alcohol and nickel acetate derived sample showing highest BET surface area. The nitrogen adsorption-desorption isotherms of nickel doped carbons synthesized by stirring and sonication are shown in Figure 5.27.

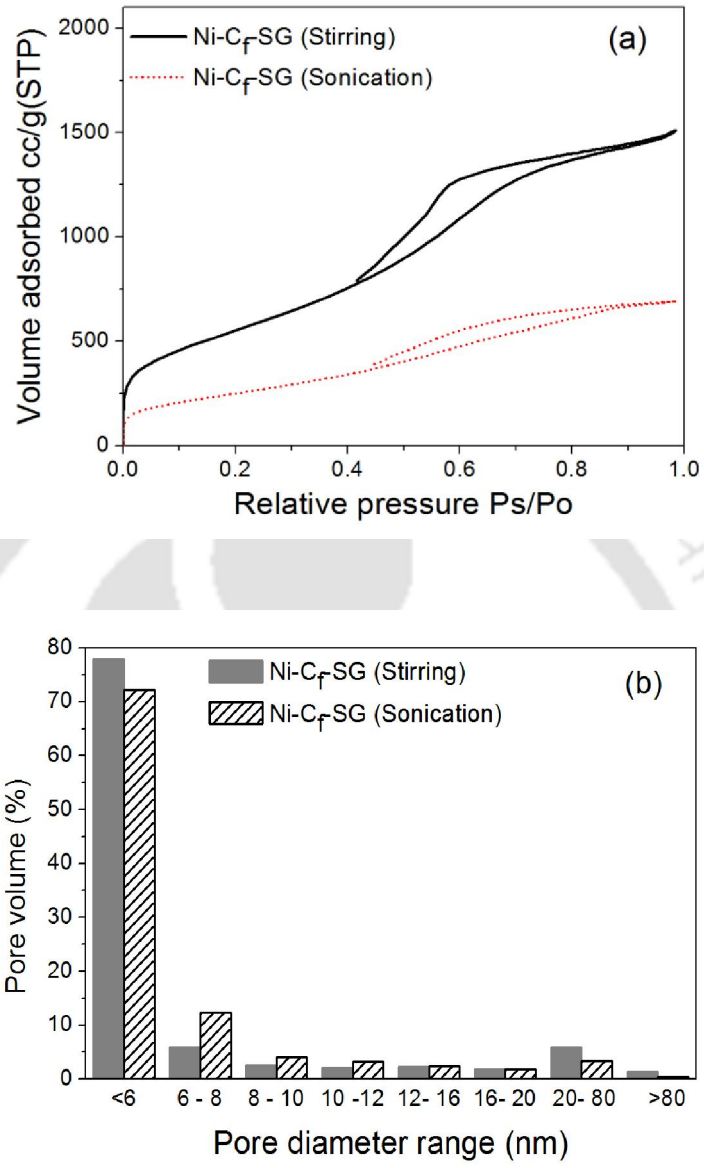

Figure 5.27. (a) Nitrogen adsorption-desorption isotherms and (b) pore size distributions of nickel doped silica gel templated carbons synthesized by stirring and sonication.

Both the isotherms were of type IV with H2 hysteresis loop. However, volume of nitrogen adsorption was significantly dropped in case of sonication assisted sample. The BET surface area of 2007 m^2/g for stirring assisted nickel doped carbon was drastically dropped to 911m^2/g for the sonication assisted sample with no micropores. Similar drop

was observed in case of total pore volume of sonication assisted sample compared to that of stirring assisted sample. The pore size distributions of the stirring and sonication assisted samples are shown in Figure 5.27(b). The pores having pore diameter in the range of 2-6nm slightly decreased for sonication assisted sample while that in 6-8 nm range increased compared to that of stirring assisted sample.

5.3.3 Hydrogen storage

Hydrogen uptake at atmospheric pressure and -100 ^{o}C for nickel doped templated carbons are compared with corresponding undoped carbon in Figure 5.28. The hydrogen uptake capacities of 0.16 and 0.10 wt.% were observed for silica gel templated undoped carbons prepared from furfuryl alcohol and sucrose, respectively. The lower uptake capacity for the sucrose derived carbon can be attributed to its lower surface area as discussed in section 4.5. On nickel doping the uptake capacity increased to 0.21 and 0.14 wt.% for silica gel derived Ni-C_f-SG and Ni-C_s-SG samples synthesized using furfuryl alcohol and sucrose respectively. The hydrogen uptake with respect to BET surface area of the undoped and nickel doped templated carbons synthesized using different templates are shown in Figure 5.29. Since the total surface areas for silica gel templated undoped and nickel doped carbons were in the similar range, the observed increase in hydrogen uptake capacity can be attributed mainly to the presence of nickel in the carbon matrix. The presence of nickel facilitated chemisorptions as well as the hydrogen spillover phenomenon within the carbon network and enhanced the hydrogen uptake capacity.

The hydrogen uptakes were 0.27 and 0.25 wt.% for zeolite templated undoped carbons synthesized using furfuryl alcohol and sucrose, respectively. The higher uptake of zeolite derived carbons may be attributed to the presence of significant amount of micropores. This has been discussed in section 4.3.3. The hydrogen uptake capacity decreased to 0.18 and 0.16 wt.% for nickel doped samples Ni-C_f-Z and Ni-C_s-Z, respectively. This decrease in hydrogen uptake capacity may have been caused by the significant decrease in total and micropore surface areas for nickel doped zeolite templated samples (Figure 5.29). The significant drop in surface area is attributed to the poor development of pore

structure due to inhibition of precursor incorporation as well as partial blockage of pores by nickel.

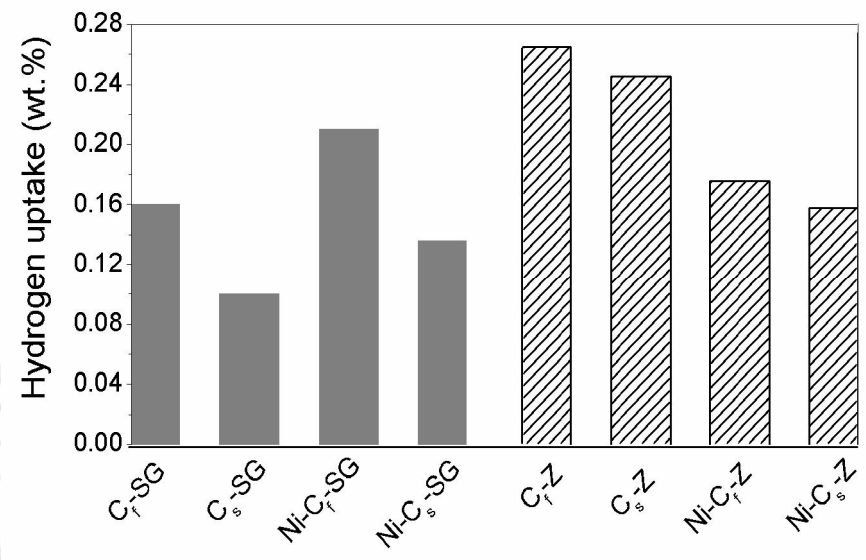

Figure 5.28. Hydrogen uptakes at atmospheric pressure and -100 °C temperature for undoped and nickel doped templated carbons synthesized using different templates and carbon precursors.

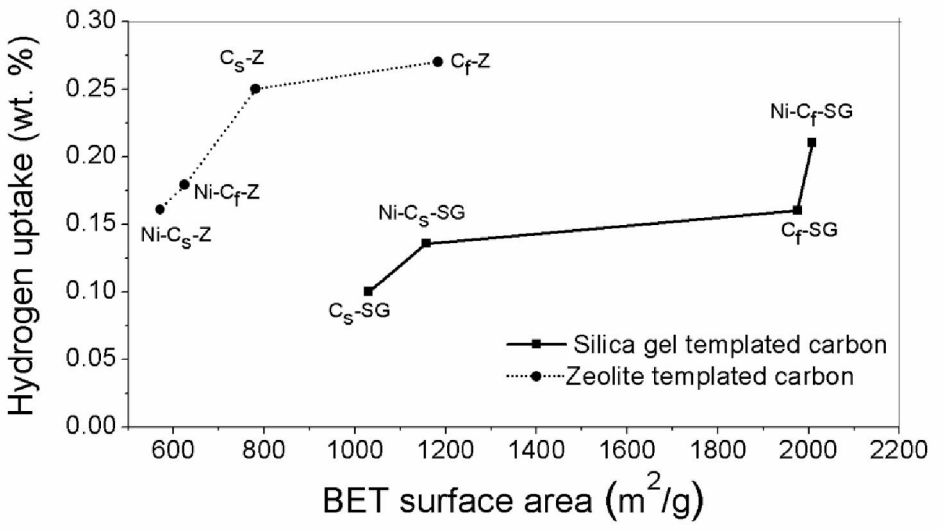

Figure 5.29. Hydrogen uptakes for undoped and nickel doped templated carbons as function of BET surface area.

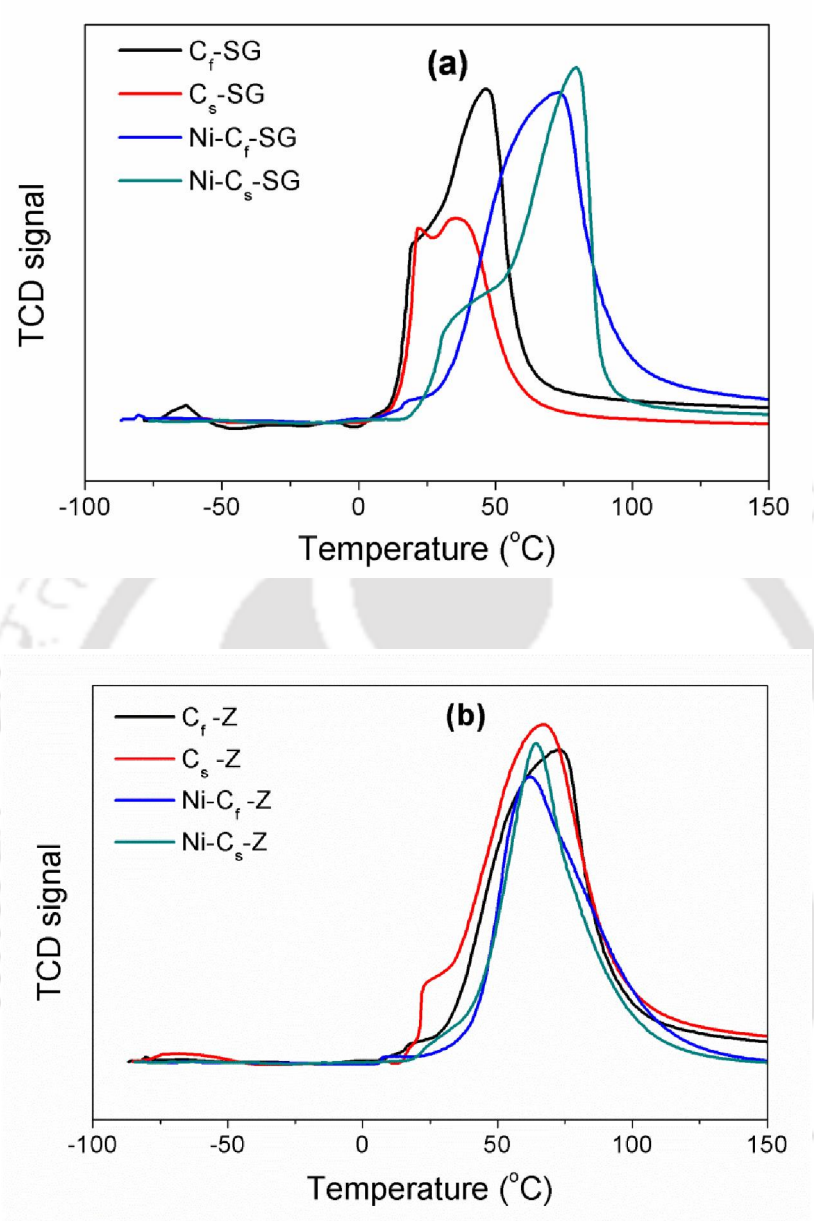

Figure 5.30. Hydrogen desorption profiles as function of temperature for (a) silica gel (b) zeolite templated undoped and nickel doped carbons (adsorption at -100 °C).

The hydrogen desorption profiles of undoped and nickel doped silica gel and zeolite templated carbons as function of temperature are shown in Figure 5.30 (a-b). As discussed in section 5.1.3, the desorption profiles for both the undoped silica gel templated carbons were characterized by sharp desorption peak at 47 °C. The nature of

the profiles was similar but area under the curve was lower for the carbon synthesized using sucrose precursor, corresponding to lower hydrogen uptake compared to furfuryl alcohol precursor. However, the desorption profiles for both nickel doped Ni-C_f-SG and Ni-C_s-SG samples shifted towards higher temperature, with maximum at 74 and 79 ^oC, respectively. On incorporation of nickel, significant pore rearrangement occurred for the doped carbons and pores less than 6 nm significantly increased as discussed in section 5.3.1. The shift of the desorption profiles to higher temperature may have resulted due to the diffusion resistance offered by lower mesopores present in significant amount in nickel doped carbons.

For all zeolite templated undoped and doped carbons the hydrogen desorption peaks started at 15^oC and ended at 120 ^oC. The peak maxima were observed at more or less similar temperature. The area under the curve for nickel doped templated carbons was less compared to the respective undoped carbons corresponding to lower hydrogen uptake for the doped carbons. The doped and undoped zeolite templated carbons were mainly microporous in nature. Hence, almost equal diffusion resistance to hydrogen desorption resulted in more or less similar desorption profiles for the zeolite templated carbons.

5.3.4 Summary

Nickel doped templated carbons were prepared by carbonization method using different carbon precursors and templates. At carbonization temperature of 650 ^oC the development of surface area, porous structure and nickel dispersion were investigated as function of carbon precursor and inorganic template. The microporous zeolite was observed to offer more resistance to incorporation of carbon and nickel precursors resulting in less developed porous carbon matrix compared to that obtained from silica gel template. Consequently nickel doped templated carbons with higher surface area were derived from silica gel template. The highest surface area of 2008 m^2/g was observed for nickel doped silica gel templated carbon derived from furfuryl alcohol, whereas nickel doped zeolite and sucrose derived carbon showed the lowest surface area of 571 m^2/g. Further the use of zeolite template resulted in mainly microporous carbon while silica gel

template resulted in mesoporous carbon. The incorporation of nickel to the carbon networks resulted in rearrangement of pores. The incorporation of nickel and its final morphology within the carbon matrix was defined by template and carbon precursor used. Mesoporous and amorphous silica gel was observed to facilitate the incorporation as well as agglomeration of nickel particles. The incorporation of nickel in template matrix was also facilitated in presence of sucrose. Porous and spherical shaped structure was observed for silica gel derived nickel doped carbon, whereas uniform flowery kind of structure was observed for nickel doped zeolite templated carbon using furfuryl alcohol. The hydrogen uptake capacity increased on addition of nickel for silica gel templated nickel doped carbons irrespective of carbon precursors. However, for zeolite templated nickel doped carbons hydrogen uptake decreased due to severe decrease in surface areas.

5.4 High pressure hydrogen storage

5.4.1 Effect of adsorption pressures and temperatures

The nitrogen doped silica gel templated carbon synthesized from acetonitrile showed maximum hydrogen uptake at -100 ^{o}C and atmospheric pressure. The same sample was subjected to hydrogen uptake at higher pressure. The hydrogen uptake capacities at different temperatures and pressures are shown in Figure 5.31. At 1 bar adsorption pressure the uptake capacity was 1.01, 0.006 and 0.005 wt.% at -196, 0 and 20 ^{o}C, respectively. As discussed in section 5.1.3 nitrogen assisted physisorption mechanism was mainly responsible for hydrogen adsorption on nitrogen doped carbon and hence, higher adsorption capacity was observed at lower temperature. As pressure was increased to 8 bar the storage capacities increased at all temperatures. The observed uptake capacities were 2.45, 0.09 and 0.07 wt.% at -196, 0 and 20 ^{o}C, respectively.

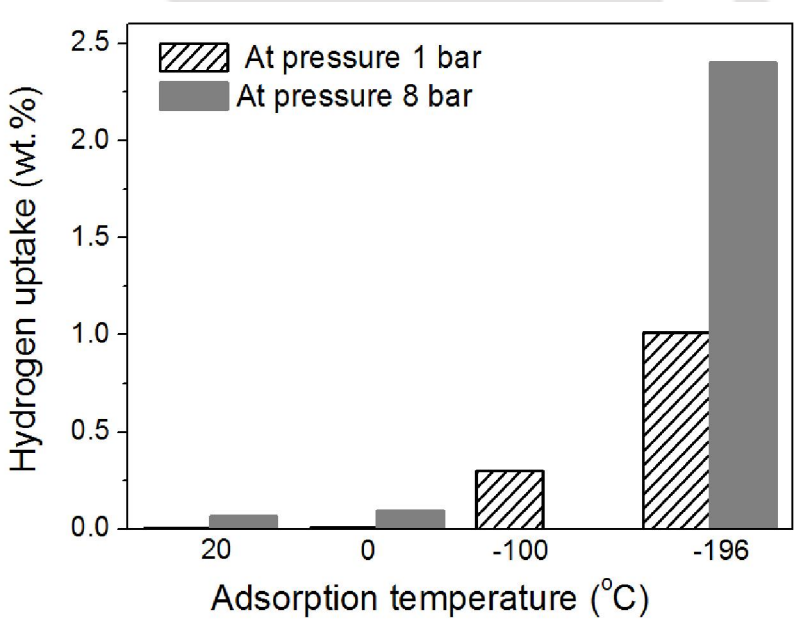

Figure 5.31. Hydrogen uptakes at different adsorption temperatures and pressures for silica gel templated nitrogen doped carbon synthesized from acetonitrile.

Limited literatures have reported hydrogen uptake capacity of nitrogen doped templated carbons. Mokaya et al. (2006) reported 2-4.5 wt.% of hydrogen uptake capacity for zeolite templated carbons at a pressure of 20 bar and liquid nitrogen temperature. The uptake capacities in present studies are comparable. The hydrogen uptake of the same sample was tested for three cycles of adsorption at liquid nitrogen temperature and is shown in Figure 5.32. The hydrogen uptakes for 2nd and 3rd cycles were slightly higher compared to first cycles. The lower value of hydrogen uptake for first cycle may be attributed to less extensive surface cleaning during degassing in instrumental conditions.

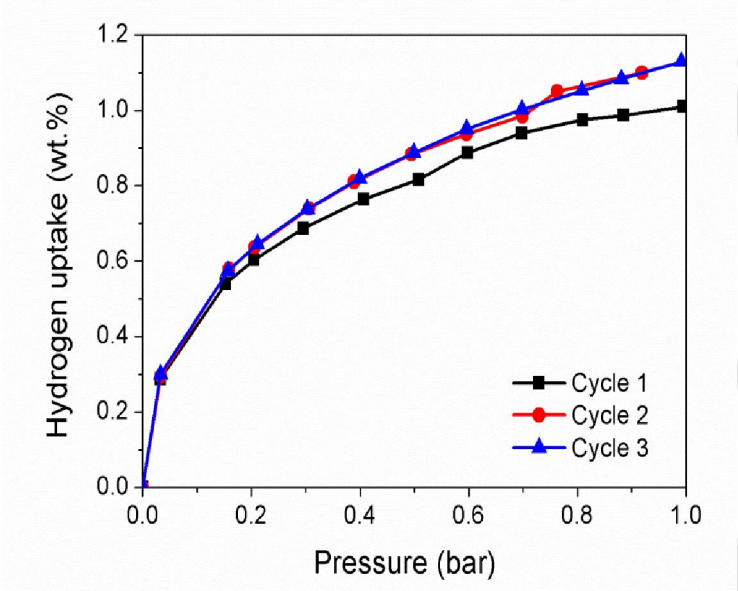

Figure 5.32. Hydrogen uptakes at -196 ºC upto 1 bar for silica gel templated nitrogen doped carbon corresponding to three adsorption cycles.

The hydrogen isotherms of undoped C-SG and nitrogen doped C-SG-Acn samples at different adsorption temperatures and pressures (upto 15 bar) are shown in Figure 5.33. The observed hydrogen isotherms were similar in nature at different adsorption temperatures for both the undoped and doped carbons. The heat of adsorption was calculated by clausius-clapeyron equation and calculation is shown in Appendix N. The heat of adsorption was 6.1 kJ/mol for undoped silica gel templated carbons and 9.5 kJ/mol for nitrogen doped templated carbon. The higher heat of adsorption for doped

carbon corresponded to higher interaction of hydrogen with surface in presence of nitrogen.

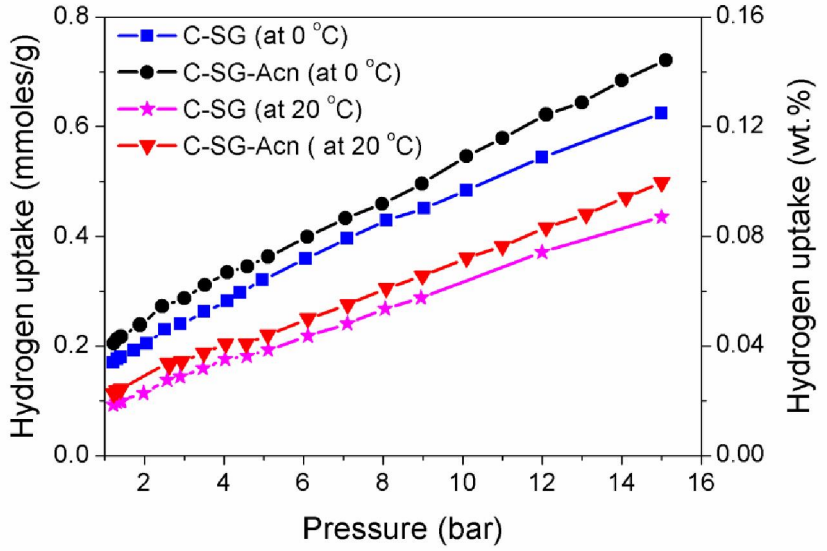

Figure 5.33. Hydrogen uptakes upto pressure of 15 bar at two temperatures (0 and 20°C) for silica gel templated undoped and nitrogen doped carbons.

5.4.2 Summary

The hydrogen storage capacities at moderate pressure were higher compare to that at atmospheric pressure for all carbons at all adsorption temperatures. At all condition of pressure and temperature, the hydrogen uptake was higher for nitrogen doped carbon compared to undoped carbon. For undoped templated carbon hydrogen uptake capacity of 0.13 wt.% was observed at 0 °C and further on nitrogen doping the capacity increased till of 0.15 wt.% at the same adsorption conditions. Highest hydrogen uptake capacity of 2.45 wt.% was obtained for nitrogen doped silica gel templated carbon synthesized from acetonitrile and furfuryl alcohol at pressure of 8 bar and liquid nitrogen temperature. Higher heat of adsorption for nitrogen doped carbon (9.5 kJ/mol) was observed compared to that of undoped carbon (6.1 kJ/mol).

Chapter 6

Conclusions and recommendations

6.1 Conclusions

1. Zeolite and silica gel both were thermally stable in nitrogen environment and can be used as template for carbonization. The total surface area and morphology of both the templates were similar but pore structure was different. Zeolite was crystalline and microporous while silica gel was mostly amorphous and mesoporous. The respective templated carbon acquired similar pore structure. Furfuryl alcohol as carbon precursor favored formation of templated carbon with higher surface area and sucrose as carbon precursor favored the formation of micropores.

2. Carbonization temperature, dwelling time and heating profile affected the development of surface area and pore volume significantly. For zeolite templated carbons carbonization temperature of 750 ^{o}C with 3h dwelling time and stepwise heating profile resulted in high surface area and pore volume irrespective of carbon precursors. BET surface area and total pore volume were obtained in the range of 163-1886 m^2/g and 0.30-1.31 ml/g, respectively, when furfuryl alcohol was used as the carbon precursor. For sucrose derived carbons the BET surface area was in the range of 684-1033 m^2/g. Incomplete carbonization at lower temperature and dwelling time may had caused templated carbons with lower surface area and pore volume. At higher carbonization temperature and longer dwelling time severe sintering of zeolite or carbon structure resulted in lower area and pore volume. The highest hydrogen uptake of 0.29 wt.% was observed for the templated carbon having BET and micropore areas of 1886 and 1136 m^2/g respectively. The hydrogen storage capacity was observed to be higher for samples having higher BET surface area, micropores and mesopores less than 6 nm.

3. BET surface area in the range of 1678–1975 m^2/g and total pore volume in the range of 2.10–3.07 ml/g were obtained for furfuryl alcohol derived silica gel templated carbon. The carbonization temperature of 650 ^{o}C with 3h dwelling time was optimum, giving highest surface area of 1975 m^2/g and pore volume of 3.07 ml/g. The use of sucrose as carbon precursors lowered the surface area but favoured

the formation of micropores in spite of use of mesoporous template. No micropores were obtained for furfuryl alcohol derived silica gel templated carbon. Hydrogen uptake of 0.16 wt.% at –100 ^{o}C and atmospheric pressure was obtained for carbon prepared at 650 ^{o}C and 3h dwelling time and may be attributed to its highest BET surface area.

4. Nitrogen doped templated carbons were prepared using acetonitrile and aniline as nitrogen precursors and furfuryl alcohol as carbon precursor. On nitrogen loading the total surface area and pore volumes were reduced as compared to that of undoped carbon. This may be attributed to partial blockage of the carbon pores by nitrogen atom as well as to the lower development of carbon matrix due to the difficulty in incorporation of precursors to the template matrix. The effect was more significant when aniline was used as the precursor and zeolite as the template which can be attributed to the relative size of the precursor and the template pores. The surface area was 1745 and 1296 m^2/g for acetonitrile and aniline derived silica gel templated doped carbon. For zeolite templated doped carbon surface area values were 573 and 624 m^2/g respectively for acetonitrile and aniline derived carbons. Significant pore rearrangement occurred for the doped carbons depending on the precursors and templates. The mesoporous silica gel with higher average pore size was observed to be more suitable template for nitrogen incorporation compared to microporous zeolite. Hydrogen storage capacity of silica gel templated doped carbons (0.30 wt.%) increased significantly on nitrogen incorporation as compared to undoped carbon (0.16 wt.%) in spite of lower surface area and can be attributed to higher activation of hydrogen by nitrogen present in the carbon network. For zeolite templated doped carbon significant drop in hydrogen uptake compared to corresponding undoped carbon may have been caused by severe lowering of surface areas.
5. The mesoporous silica gel template was more suitable for the preparation of nickel doped templated carbons. Highest surface area of 2008 m^2/g was observed for nickel doped silica gel templated carbon derived from furfuryl alcohol, whereas nickel doped zeolite templated sucrose derived carbon showed the lowest surface

area of 571 m^2/g. The final morphology of the carbon matrix was defined by the type of template and carbon precursors. The hydrogen uptake capacity increased on addition of nickel for silica gel templated doped carbons irrespective of carbon precursors. The presence of nickel facilitated chemisorptions as well as the hydrogen spillover phenomenon enhancing the hydrogen uptake capacity. However, for zeolite templated nickel doped carbon hydrogen uptake decreased due to severe decrease in surface areas. For carbon with lower nickel loadings both physisorption and chemisorption were responsible for hydrogen uptake, whereas at higher nickel loadings chemisorption was the main contributing factor.

6. All the undoped templated carbons exhibited broad XRD peak around $2\theta = 25°$ which corresponded to the diffraction of (002) graphitic carbon. Higher amount of graphitic carbon was formed at higher carbonization temperature when crystalline zeolite or furfuryl alcohol was used. For nitrogen doped carbons presence of different amount of nitrogen resulted in difference in graphitic structure prepared from different templates. The nickel was present in higher agglomerated state in the silica gel derived carbon matrix.
7. All the templated carbons possessed uniform porous structure with well-connected pores. The development of microstructure and the extent of porosity depended on synthesis conditions and the structure of used template. Irregular shaped particles with wide size distributions were observed for silica gel templated undoped and nitrogen doped carbons. For nickel doped silica gel derived carbons, porous spherical agglomerates were observed for both the carbon precursors. More uniform microstructure was observed for all the zeolite templated doped and undoped carbons having flowery kind of appearances.
8. The nitrogen doped silica gel templated carbon synthesized from acetonitrile and furfuryl alcohol showed maximum hydrogen uptake among all the prepared templated carbons at -100 ^oC and atmospheric pressure. The same sample was subjected to hydrogen uptake at higher pressure and the observed highest hydrogen uptake capacity was of 2.45 wt.% at liquid nitrogen temperature and pressure of 8 bar. The heat of adsorption increased for nitrogen doped carbon (9.5 kJ/mol) compared to that of undoped carbon (6.1 kJ/mol).

6.2 Recommendations

In continuation to present studies the following areas can be explored further.

1. Modification of the templated carbons by other heteroatoms such as Pt, Pd, B etc.

2. Detailed studies on effect of concentration of heteroatoms on porous structure of the templated carbons and further characterization of the doped carbons.

3. Hydrogen uptake studies at additional pressures and temperatures for the developed templated carbons.

4. Investigation on type of adsorption-desorption model suitable for the developed templated carbons.

5. Application of developed undoped and doped templated carbons in other catalytic and adsorption processes.

References

References

Aardahl CL, Rassat SD. Overview of systems considerations for on-board chemical hydrogen storage. International Journal of Hydrogen Energy (**2009**) 34, 6676-6683.

Alam N, Mokaya R. Characterisation and hydrogen storage of Pt-doped carbons templated by Pt-exchanged zeolite Y. Microporous and Mesoporous Materials (**2011**) 142(2-3), 716-724.

Anton D, Semelsberger T, Siegel D, Brooks K, Hardy B. Hydrogen storage materials requirements to meet the 2017 on board hydrogen storage technical targets. Materials Requirements Webinar. **(2013)** http://www.energy.gov/eere/fuelcells .

Armandi M, Bonelli B, Arean CO, Garrone E. Role of microporosity in hydrogen adsorption on templated nanoporous carbons. Microporous and Mesoporous Materials (**2008**) 112(1-3), 411-418.

Attia NF, Lee SM, Kim HJ, Geckeler KE. Nanoporous polypyrrole: preparation and hydrogen storage properties. International Journal of Energy Research (**2013**) doi:10.1002/er.3095.

Barghi SH, Tsotsis TT, Sahimi M. Chemisorption, physisorption and hysteresis during hydrogen storage in carbon nanotubes, International Journal of Hydrogen Energy (**2014**), 1390-1397.

Beebe RA, Taylor HS. A rapid method for the determination of heats of adsorption and some values for hydrogen on nickel and copper. Journal of American chemical Society (**1924**) 46, 43-52.

Benard P, Chahine R. Storage of hydrogen by physisorption on carbon and nanostructured materials. Scripta Materialia (**2007**) 56, 803-808.

Berube V, Radtke G, Dresselhaus M, Chen G. Size effects on the hydrogen storage properties of nanostructured metal hydrides: A review. International Journal of Energy Research (**2007**) 31, 637-663.

Biniwale RB, Rayalu S, Devotta S, Ichikaw M. Chemical hydrides: Asolution to high capacity hydrogen storage and supply. International Journal of Hydrogen Energy (**2008**) 33, 360 -365.

Bohme K, Einicke WD, Klepel O. Templated synthesis of mesoporous carbon from sucrose-the way from the silica pore filling to the carbon material. Carbon (**2005**) 43, 1918-1925.

Broom DP. Hydrogen storage materials, the characterisation of their storage properties. Springer (**2011**).

Budd PM, Butler A, Selbie J, Mahmood K, McKeown NB, Ghanem B, Msayib K, Book D, Walton A. The potential of organic polymer-based hydrogen storage materials. Physical Chemistry Chemical Physics (**2007**) 9, 1802-1808.

Cai JJ, Yang M, Xing Y, Zhao X. Large surface area sucrose-based carbons via template-assisted routes: Preparation, microstructure, and hydrogen adsorption properties. Colloids and Surfaces A: Physicochemical and Engineering Aspects (**2014**) 444, 240- 245.

Cejka J, Corma A, Zones S. Zeolites and catalysis synthesis, reactions and applications. Edited, Wiley-VCH (**2010**).

Chahine R, Bose TK. Low-pressure adsorption storage of hydrogen. International Journal of Hydrogen Energy (**1994**) 19(2), 161-164.

Chen P, Wu X, Lin J, Tan KL. High H_2 uptake by alkali-doped carbon nanotubes under ambient pressure and moderate temperatures. Science (**1999**) 91, 285.

Chen L, Singh RK, Webley P. Synthesis, characterization and hydrogen storage properties of microporous carbons templated by cation exchanged forms of zeolite Y with propylene and butylene as carbon precursors. Microporous and Mesoporous Materials (**2007**) 102(1-3), 159-170.

Cheng H-M, Yang Q-H, Liu C. Hydrogen storage in carbon nanotubes. Carbon (**2001**) 39(10), 1447-454.

Chuang H-Y, Yu M-S, Chen C-H, Chung T-Y. Preparation of platinum impregnated activated carbon via vacuum treatment and effect on hydrogen storage rate. Journal of the Taiwan Institute of Chemical Engineers (**2012**) 43,585-590.

Chung K-H. High-pressure hydrogen storage on microporous zeolites with varying pore properties. Energy (**2010**) 35, 2235-2241.

Chung TCM, Jeong Y, Chen Q, Kleinhammes A, Wu Y. Synthesis of microporous boron-substituted carbon (B/C) materials using polymeric precursors for hydrogen physisorption. Journal of American chemical Society (**2008**) 130, 6668-6669.

Conner WC, Falconer JL. Spillover in heterogeneous catalysis. Chemical Reviews (**1995**) 95 (3), 759-788.

Contescu CI, Brown CM, Liu Y, Bhat VV, Gallego NC. Detection of hydrogen spillover in palladium-modified activated carbon fibers during hydrogen adsorption. Journal of Physical Chemistry C (**2009**) 113(14), 5886-5890.

Dandekar A, Baker RTK, Vannice MA. Characterization of activated carbon, graphitized carbon fibers and synthetic diamond powder using TPD and drifts. Carbon (**1998**) 36(12), 1821-1831.

Darkrim F, Aoufi A, Malbrunot P, Levesque D. Hydrogen adsorption in the NaA zeolite: A comparison between numerical simulations and experiments. Journal of Chemical Physics (**2000**) 112 (13), 5991-5999.

Darkrim FL, Malbrunot P, Tartaglia GP. Review of hydrogen storage by adsorption in carbon nanotubes. International Journal of Hydrogen Energy (**2002**) 27, 193–202.

Dehouche Z, Klassen T, Oelerich W, Goyette J, Bose TK, Schulz R. Cycling and thermal stability of nanostructured MgH_2-Cr_2O_3 composite for hydrogen storage. Journal of Alloys Compound (**2002**) 347, 319–323

D'Elia LF, Gonzalez I, Saavedra K, Gottberg V. A comparative study of hydrogen uptake features of Co, Ni and Pd modified nanofibres and activated carbon. International Journal of Hydrogen Energy (**2009**) 34, 1958-1964.

Dhall S, Jaggi N. Improvement in structural and electrical properties of cuprous oxide-coated multiwalled carbon nanotubes. Bulletin of Materials Science (**2014**) 37(6) 1427-1431.Dillon AC, Jones KM, Bekkedahl TA, Kiang CH, Bethune DS , Heben MJ. Storage of hydrogen in single-walled carbon nanotubes. Nature (**1997**) 386, 377-379.

Dillon AC, Heben MJ. Hydrogen storage using carbon adsorbents: past, present and future. Applied Physics A -Materials Science & Processing (**2001**) 72(2), 133-142.

Dimitrakakis GK, Tylianakis E, Froudakis G E. Pillared graphene: A new 3-D network nanostructure for enhanced hydrogen storage. Nano Letter (**2008**) 8(10), 3166-3170.

Dundar-Tekkaya E, Karatepe N. Hydrogen adsorption of carbon nanotubes grown on different catalysts. International Journal of Hydrogen Energy (**2014**) http://dx.doi.org/ 10.1016/ j.ijhydene.2014.10.145.

Fakioglu E, Yurum Y, Veziroglu TN. A review of hydrogen storage systems based on boron and its compounds. International Journal of Hydrogen Energy (**2004**) 29, 1371-1376.

Figueroa–Torres MZ, Domrnguez–Rios C, Cabanas–Moreno JG, Vega–Becerra O, Aguilar–Elgue´zabal A. The synthesis of Ni–activated carbon nanocomposites via electroless deposition without a surface pretreatment as potential hydrogen storage materials. International Journal of Hydrogen Energy (**2012**) 37, 10743-10749.

Kulprathipanja S. Zeolites in Industrial Separation and Catalysis. Edited, Wiley-VCH (**2010**).

Fraenkel D, Shabtai J. Encapsulation of hydrogen in molecular sieve zeolites. Journal of American Chemical Society (**1977**) 99, 7074.

Fuertes AB. Synthesis of ordered nanoporous carbons of tunable mesopore size by templating SBA-15 silica materials. Microporous and Mesoporous Materials (**2004**) 67 (2-3), 273-281.

Giasafaki D, Bourlinos A, Charalambopoulou G, Stubos A, Steriotis Th. Synthesis and characterisation of nanoporous carbon–metal composites for hydrogen storage Microporous and Mesoporous Materials (**2012**) 154, 74-81.

Giraudet S, Zhu Z. Hydrogen adsorption in nitrogen enriched ordered mesoporous carbons doped with nickel nanoparticles. Carbon (**2011**) 49, 398-405.

Graetz J, Reilly JJ, Yartys VA, Maehlen JP, Bulychev BM, Antonov VE, Tarasov BP, Gabis IE. Aluminum hydride as a hydrogen and energy storage material: Past, present and future. Journal of Alloys and Compounds (**2011**) 509S, S517– S528.

References

Green econometrics Information (2007) http://greenecon.net/with-choices-like-biodiesel-and-ethanol-what%E2%80%99s-the-best-fuel-foryourvehicle/energyeconomics.html

Grimes CA, Varghese OK, Ranjan S. From hydrocarbons to hydrogen: towards a sustainable future. Light, water, hydrogen, the solar generation of hydrogen by water photoelectrolysis. Springer (**2008**).

Guan C, Wang K, Yang C, Zhao XS. Characterization of a zeolite-templated carbon for H_2 storage application. Microporous and Mesoporous Materials (**2009**) 118, 503-507.

Gupta RB. Hydrogen fuel production, transport and storage. Edited, CRC Press (**2009**).

Hagstrom MT, Lund PD, Vanhanen JP. Metal hydride hydrogen storage for near-ambient temperature and atmospheric pressure applications, a PDSC study. International Journal of Hydrogen Energy (**1995**) 20 (11), 897-909.

He Z, Wang S, Wang X, Iqbal Z. Hydrogen storage in hierarchical nanoporous silicon–carbon nanotube architectures. International Journal of Energy Research (**2013**) 37, 754-760.

Hirscher M. Handbook of hydrogen storage: new materials for future energy storage. Edited, Wiley-VCH (**2010**).

Hirscher M, Becher M, Haluska M, Zeppelin F, Chen X, Dettlaff WU. Are carbon nanostructures an efficient hydrogen storage medium?. Journal of Alloys and Compound (**2003**) 356–357, 433–437.

Hoffman KC, Reilly JJ, Salzano FJ, Waide CH, Wiswall RH, Winsche WE. Metal hydride storage for mobile stationary applications. International Journal of Hydrogen Energy (**1976**) 1, 133-151.

Hou P-X, Orikasa H, Yamazaki T, Matsuoka K, Tomita A, Setoyama N, Fukushima Y, Kyotani T. Synthesis of nitrogen-containing microporous carbon with a highly ordered structure and effect of nitrogen doping on H_2O adsorption. Chemistry of Materials (**2005**) 17, 5187-5193.

Hu Q, Lu Y, Meisner GP. Preparation of nanoporous carbon particles and their cryogenic hydrogen storage capacities. Journal of Physical Chemistry C (**2008**) 112, 1516–1523.

Huang C-C, Chen H-M, Chen C-H, Huang J-C. Effect of surface oxides on hydrogen storage of activated carbon. Separation and Purification Technology (**2010**) 70, 291-295.

Hwang JY, Lee SH, Sim KS, Kim JW. Synthesis and hydrogen storage of carbon nanofibers. Synthetic Metals (**2002**)126(1), 81–85.

Ibrahim F. Microporous organic framework polymers for hydrogen storage applications International Journal of Chemical & Petrochemical Technology (**2013**) 3(3), 17-26.

Imamura H, Takada T, Tsuchiya S. Hydrogen storage in metal hydrides by the use of Methanol: a new way of hydriding by chemical hydrogen carriers. International Journal of Hydrogen Energy (**1988**) 13 (1), 11-13.

Ioannatos GE, Verykios XE. H_2 storage on single- and multi-walled carbon nanotubes. International Journal of Hydrogen Energy (**2010**) 35, 622–628.

Jadhav J, Patange M, Biswas S. Ferromagnetic Ni-doped ZnO nanoparticles synthesized by a chemical precursor method. Carbon -Science and Technology (**2013**) 5(2) 269 - 274.

Jain IP, Jain P, Jain A. Novel hydrogen storage materials: A review of lightweight complex hydrides. Journal of Alloys and Compounds (**2010**) 503, 303–339.

Jain IP, Lal C, Jain A. Hydrogen storage in Mg: A most promising material. International Journal of Hydrogen Energy (**2010**) 35, 5133-5144.

Jena P. Materials for hydrogen storage: past, present, and future, Journal of Physical Chemistry Letters (**2011**) 2, 206–211.

Jimenez V, Ramirez-Lucas A, Snchez P, Valverde J L, Romero A. Improving hydrogen storage in modified carbon materials. International Journal of Hydrogen Energy (**2012**) 37, 4144-4160.

Jin H, Lee YS, Hong I. Hydrogen adsorption characteristics of activated carbon. Catalysis Today (**2007**) 120(3-4), 399-406.

Johnson SA, Brigham ES, Ollivier PJ, Mallouk TE. Effect of micropore topology on the structure and properties of zeolite polymer replicas. Chemistry of Materials (**1997**) 9(11), 2448-2458.

Jun S, Joo SH, Ryoo R, Kruk M, Jaroniec M, Liu Z, Ohsuna T, Terasak O. Synthesis of new, nanoporous carbon with hexagonally ordered meso structure. Journal of American Chemical Society (**2000**) 122(43), 10712-10713.

Kamegawa K, Yoshida H. Preparation and characterization of swelling porous carbon beads. Carbon (**1997**) 35(5), 631-639.

Kharlamov A, Bondarenko M, Kharlamova G, Gubareni N, Fomenko V. A New Method of Synthesis Carbon with Onion-Like Structure with High (10-13%) Content of Nitrogen from Pyridine. Universal Journal of Materials Science (**2013**) 1(2), 78-86.

Klebanoff LE, Keller JO. 5 Years of hydrogen storage research in the U.S. DOE metal hydride center of excellence (MHCoE). International Journal of Hydrogen Energy (**2013**) 38, 4533-4576.

Kojima Y, Kawai Y, Koiwai A, Suzuki N, Haga T, Hioki T, Tange K. Hydrogen adsorption and desorption by carbon materials. Journal of Alloys and Compounds (**2006**) 421, 204-208.

Kruk M, Dufour B, Celer EB, Kowalewski T, Jaroniec M, Matyjaszewski K. Synthesis of mesoporous carbons using ordered and disordered mesoporous silica templates and polyacrylonitrile as carbon precursor. Journal of Physical Chemistry B (**2005**) 109(19), 9216-9225.

Kruk M, Jaroniec M, Ryoo R, Joo SH. Characterization of ordered mesoporous carbons synthesized using MCM-48 silicas as templates. Journal of Physical Chemistry B (**2000**) 104(33), 7960-7968.

Kuc A, Zhechkov L, Patchkovskii S, Seifert G, Heine T. Hydrogen sieving and storage in fullerene intercalated graphite. Nano Letter (**2007**) 7(1), 1-5.

Kyotani T. Control of pore structure in carbon. Carbon (**2000**) 38(2), 269-286.

Kyotani T, Ma Z, Tomita A. Template synthesis of novel porous carbons using various types of zeolites. Carbon (**2003**) 41, 1451–1459.

Kyotani T, Nagai T, Inoue S, Tomita A. Formation of new type of porous carbon by carbonization in zeolite nanochannels. Chemistry of Materials (**1997**) 9, 609-615.

Langmi HW, Book D, Walton A, Johnson SR, Al-Mamouri MM, Speight JD, Edwards PP,Harris IR, Anderson PA. Hydrogen storage in ion-exchanged zeolites. Journal of Alloys Compounds (**2005**) 404, 637-642.

Langmi HW, Walton A, Al-Mamouri MM, Johnson SR, Book D, Speight JD, Edwards PP, Gameson I, Anderson PA, Harris IR. Hydrogen adsorption in zeolites A, X, Y and RHO. Journal of Alloys and Compounds (**2003**) 356-357, 710-715.

Lee J, Yoon S, Hyeon T, Oh SM, Kim KB. Synthesis of a new mesoporous carbon and its application to electrochemical double-layer capacitors. Chemical Communications (**1999**) (21), 2177-2178.

Lee J-Y, Wood CD, Bradshaw D, Rosseinsky MJ, Cooper AI. Hydrogen adsorption in microporous hypercrosslinked polymers. Chemical Communication (**2006**), 2670–2672.

Leon A. Hydrogen storage, hydrogen technology mobile and portable applications. Edited, Springer (**2008**).

Li Z, Jaroniec M. Silica gel-templated mesoporous carbons prepared from mesophase pitch and polyacrylonitrile. Carbon (**2001**) 39(13), 2080-2082.

Liang C, Li Z, Dai S. Mesoporous carbon materials: synthesis and modification. Angewandte Chemie-International Edition (**2008**) 47, 3696-3717.

Lin X, Jia J, Zhao X, Thomas K M, Blake A J, Walker GS, Champness NR, Hubberstey P, Schrder M. High H_2 adsorption by co-ordination framework materials. Angewandte Chemie-International Edition (**2006**) 45, 7358-7364.

Liu F, Zhang X, Cheng J, Tu J, Kong F, Huang W, et al. Preparation of short carbon nanotubes by mechanical ball milling and their hydrogen adsorption behaviour. Carbon (**2003**) 41, 2527–2532.

Lu A, Kiefer A, Schmidt W, Schüth F. Synthesis of polyacrylonitrile-based ordered mesoporous carbon with tunable pore structures. Chemistry of Materials (**2004**) 16(1), 100-103.

Lu J, Fang ZZ, Sohn HY. A dehydrogenation mechanism of metal hydrides based on Interactions between $H^{\delta+}$ and H^{-}. Inorganic Chemistry (**2006**) 45 (21), 8749- 8753.

Lueking AD, Yang RT. Hydrogen spillover to enhance hydrogen storage - study of the effect of carbon physicochemical properties. Applied Catalysis A-General (**2004**) 265(2), 259-268.

Ma Z, Kyotani T, Tomita A. Synthesis methods for preparing microporous carbons with a structural regularity of zeolite Y. Carbon (**2002**) 40(13), 2367-2374.

Makowski P, Thomas A, Kuhn P, Goettmann F. Organic materials for hydrogen storage applications: from physisorption on organic solids to chemisorption in organic molecules. Energy & Environmental Science (**2009**) 2, 480–490

Marsh H, Rodriguez-Reinoso F. Activated carbon. Elsevier (**2006**).

Masika E, Bourne RA, Chamberlain TW, Mokaya R. Supercritical CO_2 mediated incorporation of Pd onto templated carbons: A route to optimizing the Pd particle size and hydrogen uptake density. Applied Materials & Interfaces (**2013**) 5, 5639-5647.

Meyers CJ, Shah SD, Patel SC, Sneeringer RM, Bessel CA, Dollahon NR, Leising RA, Takeuchi ES. Templated synthesis of carbon materials from zeolites (Y, beta, and ZSM-5) and a montmorillonite clay (K10): Physical and electrochemical characterization. Journal of Physical Chemistry B (**2001**) 105(11), 2143-2152.

Milanese C, Girella A, Bruni G, Cofrancesco P, Berbenni V, Matteazzi P, Marini A. Mg–Ni–Cu mixtures for hydrogen storage: A kinetic study. Intermetallics (**2010**) 18, 203–211.

Moussa G, Moury R, Demirci UB, Şener T, Miele P. Boron-based hydrides for chemical hydrogen storage. International Journal of Energy Research (**2013**) 37, 825-842.

Mulder FM, Dingemans TJ, Wagemaker M, Kearley GJ. Modelling of hydrogen adsorption in the metal organic framework MOF5. Chemical Physics (**2005**) 317, 113-118.

Nishihara H, Hou PX, Li LX, Ito M, Uchiyama M, Kaburagi T. High-pressure hydrogen storage in zeolite-templated carbon. Journal of Physical Chemistry C (**2009**) 113(8), 3189-3196.

Nishihara H, Kyotani T. Templated nanocarbons for energy storage. Advanced Materials (**2012**) 24, 4473–4498.

References

Noh JS, Agarwal RK, Schwarz JA. Hydrogen storage systems using activated carbon. International Journal of Hydrogen Energy (**1987**) 12(10), 693-700.

Orinakova R, Orinak A. Recent applications of carbon nanotubes in hydrogen production and storage. Fuel **(2011**) 90 (11), 3123–3140.

Pang J, Hampsey JE, Wu Z, Hu Q, Lu Y. Hydrogen adsorption in mesoporous carbons. Applied physics letters (**2004**) 85(21), 4887-4889.

Park S-J, Kim B-J, Lee Y-S, Cho M-J. Influence of copper electroplating on high pressure hydrogen–storage behaviors of activated carbon fibers. International Journal of Hydrogen Energy (**2008**) 33, 1706-1710.

Parmentier J, Vix-Guterl C, Gibot P, Reda M, Ilescu M, Werckmann J, Patarin J. Study of the structural evolutions of mesoporous MCM-48 silica infiltrated with carbon by different techniques. Microporous and Mesoporous Materials (**2003**) 62, 87-96.

Pinkerton FE, Meisner GP, Meyer MS, Balogh MP, Kundrat MD. Hydrogen desorption exceeding ten weight percent from the new quaternary hydride $Li_3BN_2H_8$. Journal of Physical Chemistry B (**2005)** 109 (1), 6-8.

Poirier E, Chahine R, Benard P, Cossement D, Lafi L, Melançon E, Bose TK, Desilets S. Storage of hydrogen on single-walled carbon nanotubes and other carbon structures. Applied Physics A (**2004**) 78, 961-967.

Pupysheva OV, Farajian AA, Yakobson BI. Fullerene nanocage capacity for hydrogen storage. Nano Letter (**2008**) 8(3), 767-774.

Rallapalli PBS, Raj MC, Patil DV, Prasanth KP, Somani RS, Bajaj HC. Activated carbon @MIL–101 (Cr): a potential metal-organic framework composite material for hydrogen storage. International Journal of Energy Research (**2013**) 37, 746-753.

Rashidi AM, Nouralishahi A, Khodadadi AA, Mortazavi Y, Karimi A, Kashefi K. Modification of single wall carbon nanotubes (SWNT) for hydrogen storage. International Journal of Hydrogen Energy **(2010)** 35 (17), 9489–9495.

Rosi NL, Eckert J, Eddaoudi M, Vodak DT, Kim J, OKeeffe M, Yaghi OM. Hydrogen Storage in Microporous Metal-Organic Frameworks. Science (**2003**) 300 (5622), 1127-1129.

Ross DJ, Halls MD, Nazri AG, Aroca RF. Raman scattering of complex sodium aluminum hydride for hydrogen storage. Chemical Physics Letters (**2004**) 388, 430–435.

Rouquerol F, Rouquerol J, Sing K. Adsorption by powders and porous solids principles, methodology and applications. Academic press (**1999**).

Rowsell JLC, Yaghi OM. Metal–organic frameworks: a new class of porous materials Microporous and Mesoporous Materials (**2004**) 73, 3-14.

Ryoo R, Joo SH, Jun S. Synthesis of highly ordered carbon molecular sieves via template-mediated structural transformation. Journal of Physical Chemistry B (**1999**). 103(37), 7743-7746.

Saha D, Deng SG. Enhanced hydrogen adsorption in ordered mesoporous carbon through clathrate formation. International Journal of Hydrogen Energy (**2009**) 34(20), 8583-8588.

Sakintuna B, Lamari-Darkrim F, Hirscher M. Metal hydride materials for solid hydrogen storage: A review. International Journal of Hydrogen Energy (**2007**) 32, 1121 - 1140.

Sandrock G. A panoramic overview of hydrogen storage alloys from a gas reaction point of view. Journal of Alloy and Compound (**1999)** 293–295, 877–888.

Sankaran M, Viswanathan B. The role of heteroatoms in carbon nanotubes for hydrogen storage. Carbon (**2006**) 44(13), 2816-2821.

Sankaran M, Viswanathan B. Hydrogen storage in boron substituted carbon nanotubes. Carbon (**2007**) 45(8), 1628-1635.

Schlapbach L, Zuttel A. Hydrogen-storage materials for mobile applications. Nature (**2001**) 414, 353-358.

Schwarz JA. Metal assisted carbon cold storage of hydrogen. United StatesPatent (**1988**) 4, 716-736.

Sevilla M, Alam N, Mokaya R. Enhancement of hydrogen storage capacity of zeolite-templated carbons by chemical activation. Journal of Physical Chemistry C (**2010)** 114, 11314–11319.

Sevilla M, Fuertes AB, Mokaya R. Preparation and hydrogen storage capacity of highly porous activated carbon materials derived from polythiophene. International Journal of Hydrogen Energy (**2011**) 36(24), 15658-15663.

Shaijumon MM, Ramaprabhu S. Studies of yield and nature of carbon nanostructures synthesized by pyrolysis of ferrocene and hydrogen adsorption studies of carbon nanotubes. International Journal of Hydrogen Energy (**2005**) 30, 311–317.

Sing KSW, Everett DH, Haul RAW, Moscou L, Pierotti RA, Rouquerol J, et al. Reporting Physisorption Data for Gas Solid Systems with Special Reference to the Determination of Surface-Area and Porosity (Recommendations 1984). Pure and Applied Chemistry (**1985**) 57(4), 603-619.

Strobel R, Garche J, Moseley PT, Jorissen L, Wolf G. Hydrogen storage by carbon materials. Journal of Power Sources (**2006**) 159, 781-801.

Su F, Zeng J, Yu Y, Lv L, Lee JYg, Zhao XS. Template synthesis of microporous carbon for direct methanol fuel cell application, Carbon (**2005**) 43, 2366–2373.

Su FB, Zhao XS, Lv L, Zhou ZC. Synthesis and characterization of microporous carbons templated by ammonium-form zeolite Y. Carbon (**2004**) 42(14), 2821-2831.

Takagi H, Hatori H, Soneda Y, Yoshizawa N, Yamada Y. Adsorptive hydrogen storage in carbon and porous materials. Materials Science and Engineering B (**2004**)108,143-147

Takeichia N, Senoh H, Yokota T, Tsuruta H, Hamada K, Takeshita HT, Tanaka H, Kiyobayashi T, Takano T, Kuriyama N. Hybrid hydrogen storage vessel, a novel high pressure hydrogen storage vessel combined with hydrogen storage material. International Journal of Hydrogen Energy (**2003**) 28, 1121-1129.

Taylor HS. The adsorption of gases by solids. Faraday Society, London, (**1932**) 131.

Thomas JM. The existence of endothermic adsorption. Journal of Chemical Education (**1961**) 38, 138-139.

Thomas JM, Thomas WJ. Principles and Practice of Heterogeneous Catalysis. VCH (**1997**).

Thomas KM. Hydrogen adsorption and storage on porous materials. Catalysis Today (**2007**) 120(3-4), 389-398.

Tipson RS. Infrared spectroscopy of carbohydrates: A review of the literature. National Bureau of Standards Monograph (1968) 110, 5-8.

Tsao CS, Yu M-S, Wang C-Y, Liao P-Y, Chen H-L, Jeng U-S, Tzeng Y-R, Chung T-Y, Wu H-C. Nanostructure and hydrogen spillover of bridged metal-organic frameworks. Journal of American Chemical Society (**2009**) 131 (4), 1404-1406.

United Nations Industrial Development Organization International Centre for Hydrogen Energy Technology, http://www.unido-ichet.org/ICHET-transition.php.

Vasiliev LL, Kanonchik LE. Activated carbonfibres and composites on its base for high performance hydrogen storage system. Chemical Engineering Science (**2010**) 65, 2586-2595.

Viswanathan B, Murugesan S, Ariharan A, Lakhi KS. Hetero atom substituted carbon-potential hydrogen storage materials. Advanced Porous Materials (**2013**) 1, 122-128.

Viswanathan B, Sankaran M, Scibio, MA. Can carbon nanomaterials are they appropriate candidates for hydrogen storage. Bulletin of Catalytic Society of India **(2003)** 2(1), 13–26.

Walker G. Solid-state hydrogen storage Materials and chemistry. Edited, CRC Press (**2008**).

Wang B, Ang TP, Borgna A. A rapid hard template method for the synthesis of N doped mesoporous carbon replicated from TUD-1. Microporous and Mesoporous Materials (**2012**) 158, 99-107.

Wang H, Gao Q, Hu J. High hydrogen storage capacity of porous carbons prepared by using activated carbon. Journal of American Chemical Society (**2009**) 131(20), 7016-7022.

Wang L, Yang FH, Yang RT. Hydrogen storage properties of B- and N-doped microporous carbon. AIChE Journal (**2009**) 55(7), 1823-1833.

Wang L, Yang RT. New sorbents for hydrogen storage by hydrogen spillover – a review. Energy and Environmental Science (**2008**) 1, 268–279.

Wang L, Yang RT. Hydrogen storage properties of N-doped microporous carbon. Journal of Physical Chemistry C (**2009**) 113, 21883-21888.

West RC, CRC Handbook of Chemistry and Physics, 62nd ed. CRC Press, (**1982**).

Xia Y, Mokaya R. Generalized and facile synthesis approach to N-doped highly graphitic mesoporous carbon materials. Chemistry of Materials (**2005**) 17(6), 1553-1560.

Xia Y, Mokaya R, Grant DM, Walker GS. A simplified synthesis of N-doped zeolite-templated carbons, the control of the level of zeolite-like ordering and its effect on hydrogen storage properties. Carbon (**2011**) 49, 844-853.

Xia Y, Walker GS, Grant DM, Mokaya R. Hydrogen storage in high surface area carbons: experimental demonstration of the effects of nitrogen doping. Journal of American Chemical Society (**2009**) 131, 16493-16499.

Xia Y, Zhu Y, Tang Y. Preparation of sulfur-doped microporous carbons for the storage of hydrogen and carbon dioxide. Carbon (**2012**) 50(15), 5543-5553.

Xu W-C, Takahashi K, Matsuo Y, Hattori Y, Kumagai M, Ishiyama S, Kaneko K, Iijima S. Investigation of hydrogen storage capacity of various carbon materials. International Journal of Hydrogen Energy (**2007**) 32, 2504–2512.

Yang J, Sudik A, Wolverton C, Siegel DJ. High capacity hydrogen storage materials: attributes for automotive applications and techniques for materials discovery. Chemical Society Reviews (**2010**) 39, 656–675.

Yang Y, Brown CM., Zhao C, Chaffee AL , Nick B, Zhao D, Webley PA, Schalch J, Simmons JM, Liu Y, Her J-H, Buckley CE, Sheppard DA. Micro-channel development and hydrogen adsorption properties in templated microporous carbons containing platinum nanoparticles. Carbon (**2011**) 49(4), 1305-1317.

Yang Z, Xia Y, Mokaya R. Enhanced hydrogen storage capacity of high surface area zeolite -like carbon materials. Journal of American Chemical Society (**2007**) 129(6), 1673-1679.

Yang Z, Xia Y, Sun X, Mokaya R. Preparation and hydrogen storage properties of zeolite-templated carbon materials nanocast via chemical vapor deposition: Effect of the zeolite template and nitrogen doping. Journal of Physical Chemistry B (**2006**) 110(37), 18424-18431.

Yuan S, White D, Mason A, Liu DJ. Porous organic polymers containing carborane for hydrogen storage. International Journal of Energy Research (**2013**) 37, 732-740.

Yurum Y, Taralp A, Veziroglu TN. Storage of hydrogen in nanostructured carbon materials. International Journal of Hydrogen Energy (**2009**) 34, 3784-3798.

Zhao D, Yuan D. Zhou H-C. The current status of hydrogen storage in metal–organic frameworks. Energy Environmental Science (**2008**) 1, 222–235.

Zhao XB, Villar-Rodil S, Fletcher AJ, Thomas KM, Journal of Physical Chemistry B (**2006**) 110, 9947.

Zhong ZY, Xiong ZT, Sun LF, Luo J, Chen Z, Wu X, Lin J, Tan KL. Nanosized nickel (or cobalt) / graphite composites for hydrogen storage. Journal of Physical Chemistry B (**2002**) 106, 9507-9513.

Zhou Li. Progress and problems in hydrogen storage methods. Renewable and Sustainable Energy Reviews (**2005**) 9, 395–408.

Zhu ZH, Lu GQ, Hatori H. New insights into the interaction of hydrogen atoms with boron-substituted carbon. Journal of Physical Chemistry B (**2006**) 110, 1249-1255.

Zielinski M, Wojcieszak R, Monteverdi S, Mercy M, Bettahar MM. Hydrogen storage in nickel catalysts supported on activated carbon. International Journal of Hydrogen Energy (**2007**) 32, 1024 - 1032.

Zuttel A. Materials for hydrogen storage. Materials today **(2003)** 6(9), 24–33.

Zuttel A, Orimo S. Hydrogen in nanostructured, carbon-related and metallic materials. MRS Bulletin (**2002**) 27(9), 705–711.

Zuttel A, Rentsch S, Fischer P, Wenger P, Sudan Mauron P, Emmenegger C. Hydrogen storage properties of $LiBH_4$. Journal of Alloy Compound (**2003**) 356–357,515–520.

Zuttel A, Sudan P, Mauron Ph, Kiyobayashi T, Emmenegger Ch, Schlapbach L. Hydrogen storage in carbon nanostructures. International Journal of Hydrogen Energy (**2002**) 27, 203–212.

Appendices

Appendix A: EDX spectra of silica gel templated carbon

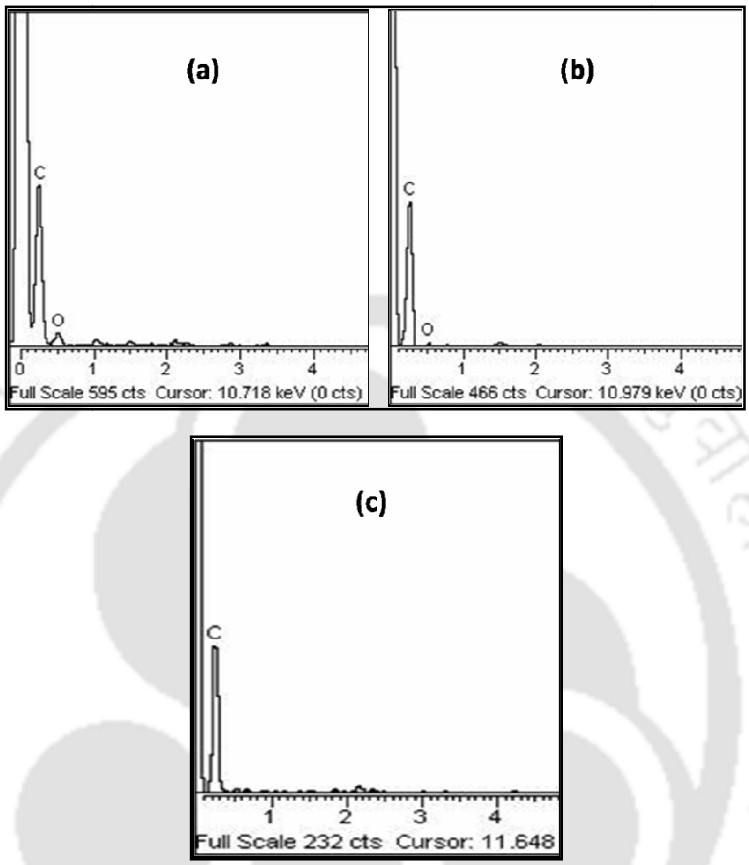

Figure A1. **EDX spectra of silica gel templated carbons synthesized from furfuryl alcohol at (a) 650 (b) 750 and (c) 850 ^{o}C with a dwelling time of 3h.**

Appendix B: TGA profile of templated carbon in oxygen environment

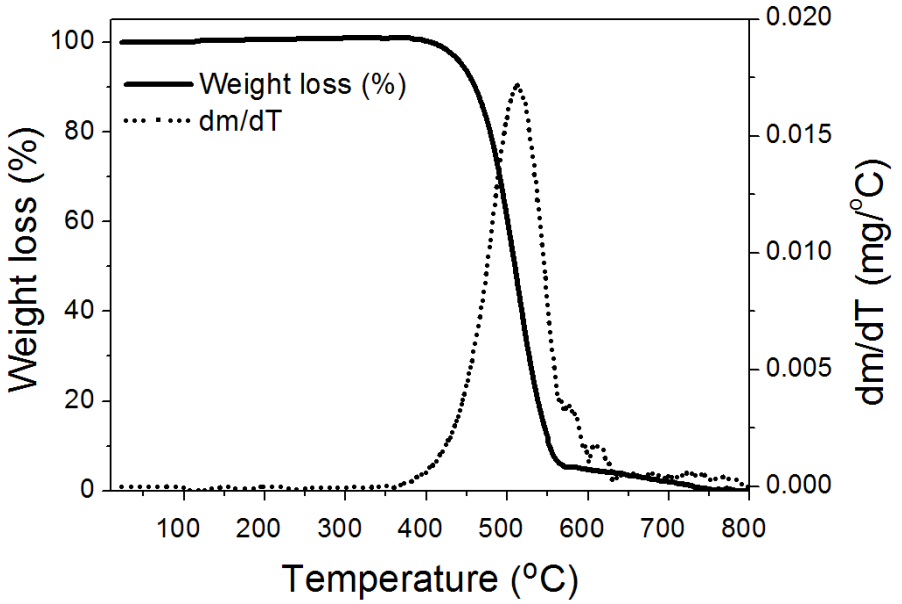

Figure A2. **TGA profile of silica gel templated carbon synthesized at 650 °C with dwelling time of 3h in oxygen environment.**

Appendix C: Preparation of nickel doped activated carbon

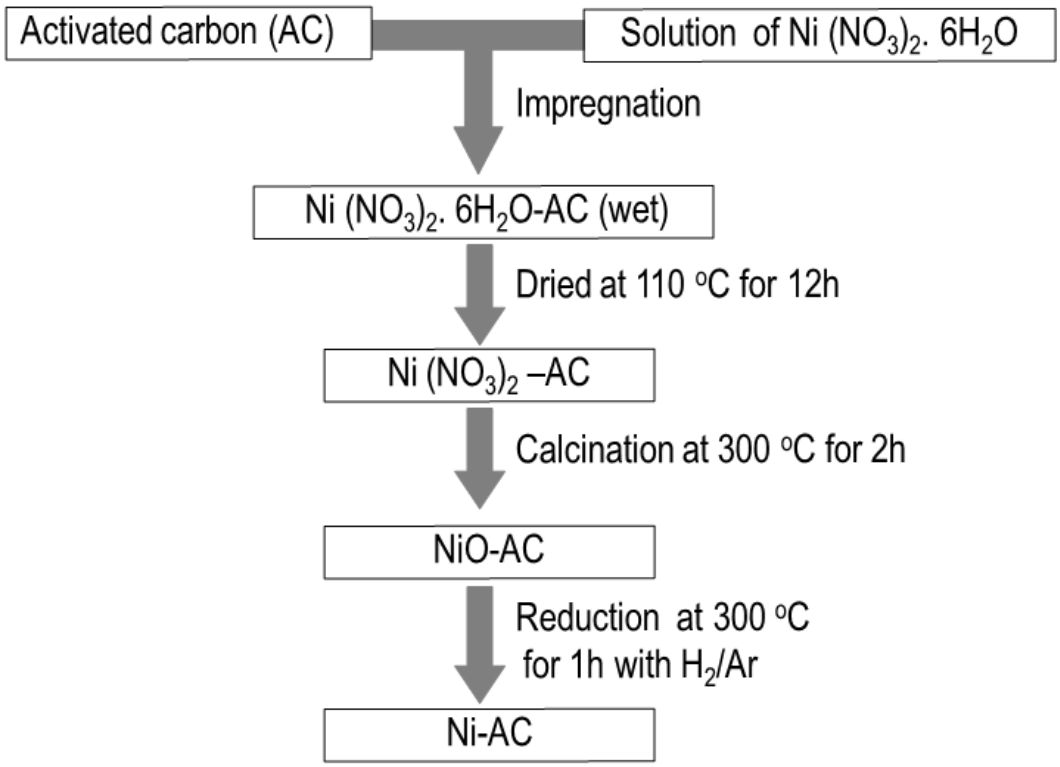

Figure A3. Preparation steps for nickel doped activated carbon.

Appendix D: Line figures for pore size distribution

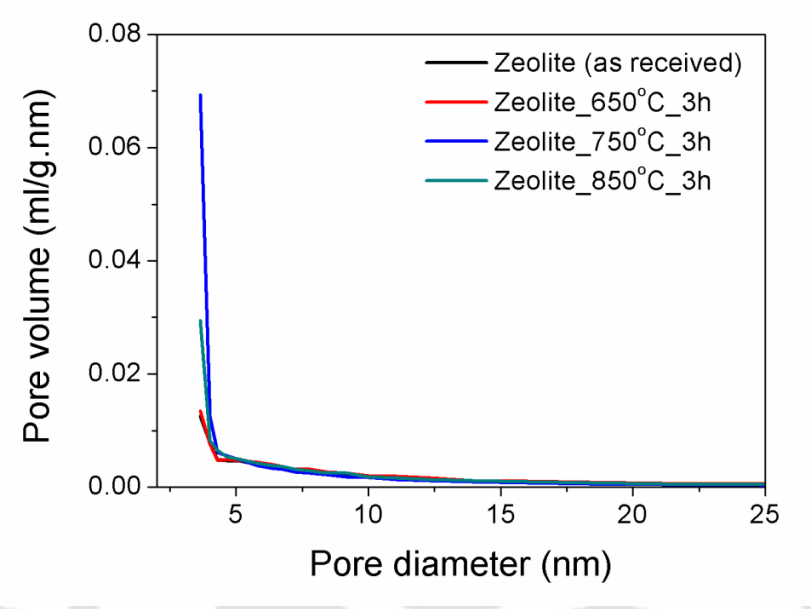

Figure A4. **Pore size distributions of as-received zeolite and calcined zeolites at different temperatures (corresponding to Figure 4.4 in text).**

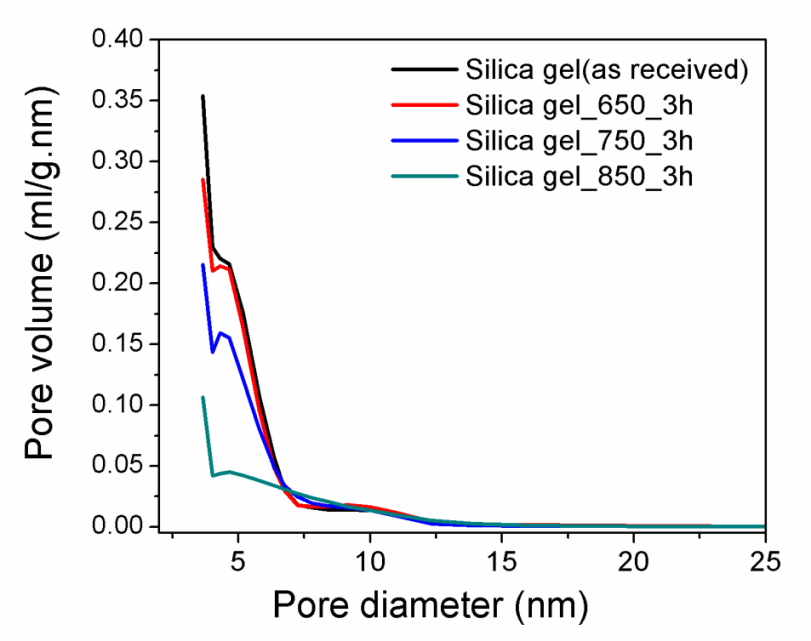

Figure A5. **Pore size distributions of as-received silica gel and calcined silica gels at different temperatures (corresponding to Figure 4.5 in text).**

Appendix E: Calculation for hydrogen uptake

Sample calculation for hydrogen uptake is described with respect to the desorption profile shown in Figure A6. The calibration curve used for hydrogen uptake calculation is shown in Figure A7.

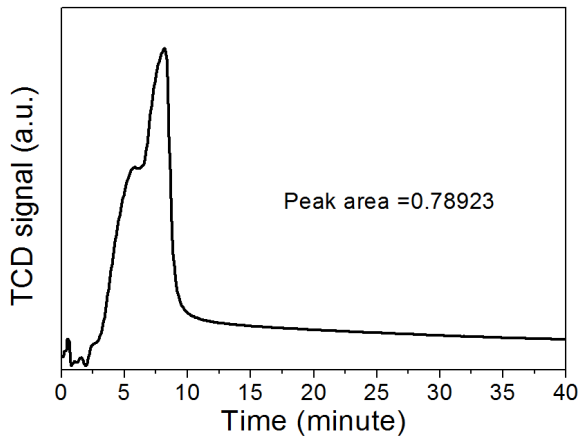

Figure A6. Hydrogen desorption profile as function of time. (Sample amount = 0.0277g)

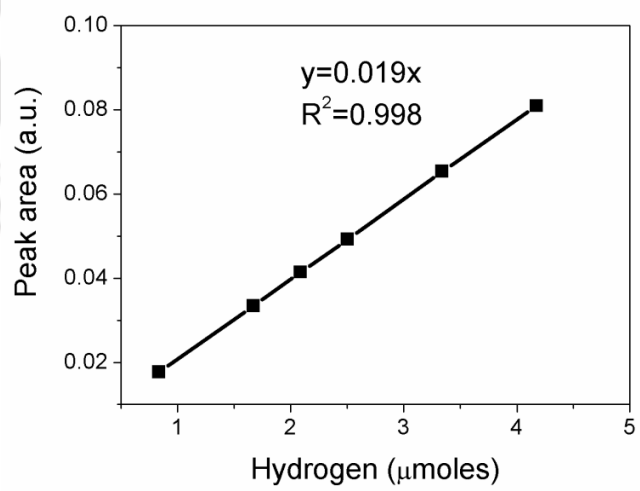

Figure A7. Hydrogen calibration curve (carrier gas: argon, active gas: 9.35 % H_2 in Ar).

From calibration curve (Figure A7)

$$y = mx = 0.019x$$

$$\text{Peak area} = 0.019\ (H_2, \mu\text{moles})$$

$$H_2\ (\mu\text{mol}) = \frac{\text{Peak area}}{0.019}$$

The total peak area corresponding to the desorption profile of hydrogen is 0.78929 (from Figure A6). Hence corresponding µmol of hydrogen is given as

$$H_2\ (\mu\text{mol}) = \frac{0.78923}{0.019} = 41.5\ \mu\text{mol} = 8.308\times10^{-5}\text{g}$$

$$\text{Hydrogen uptake (wt.\%)} = \frac{\text{Desorbed hydrogen}}{\text{Amount of sample}} \times 100$$

$$= \frac{8.308\times10^{-5}\text{g}}{0.0277\text{g}} \times 100 = 0.30\text{wt.\%}$$

Appendix F: EDX spectra of sucrose derived zeolite templated carbon

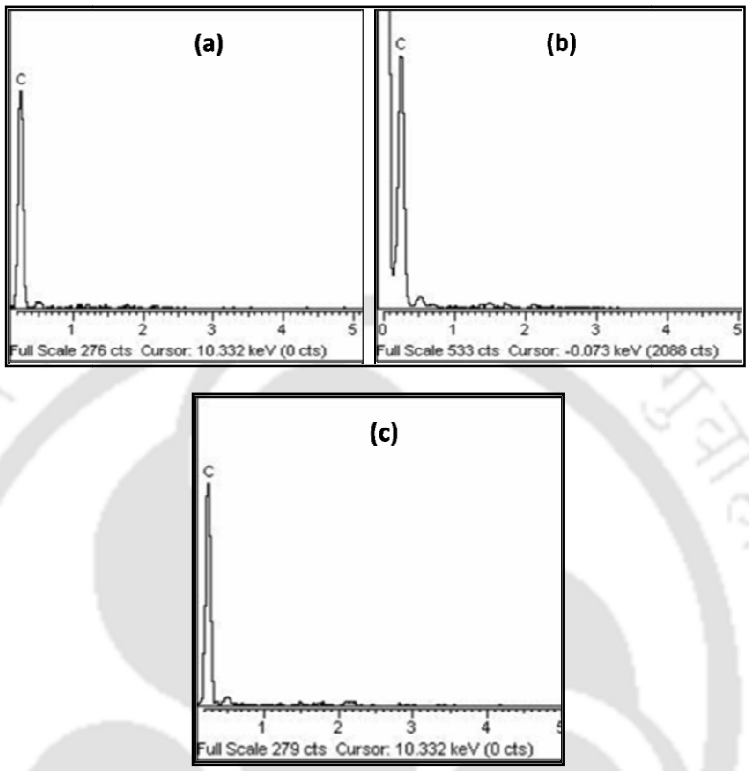

Figure A8. EDX spectra of templated carbons synthesized at (a) 650 (b) 750 and (c) 850 ^{o}C with dwelling time of 3h.

Appendix G: EDX spectra of nitrogen doped templated carbon

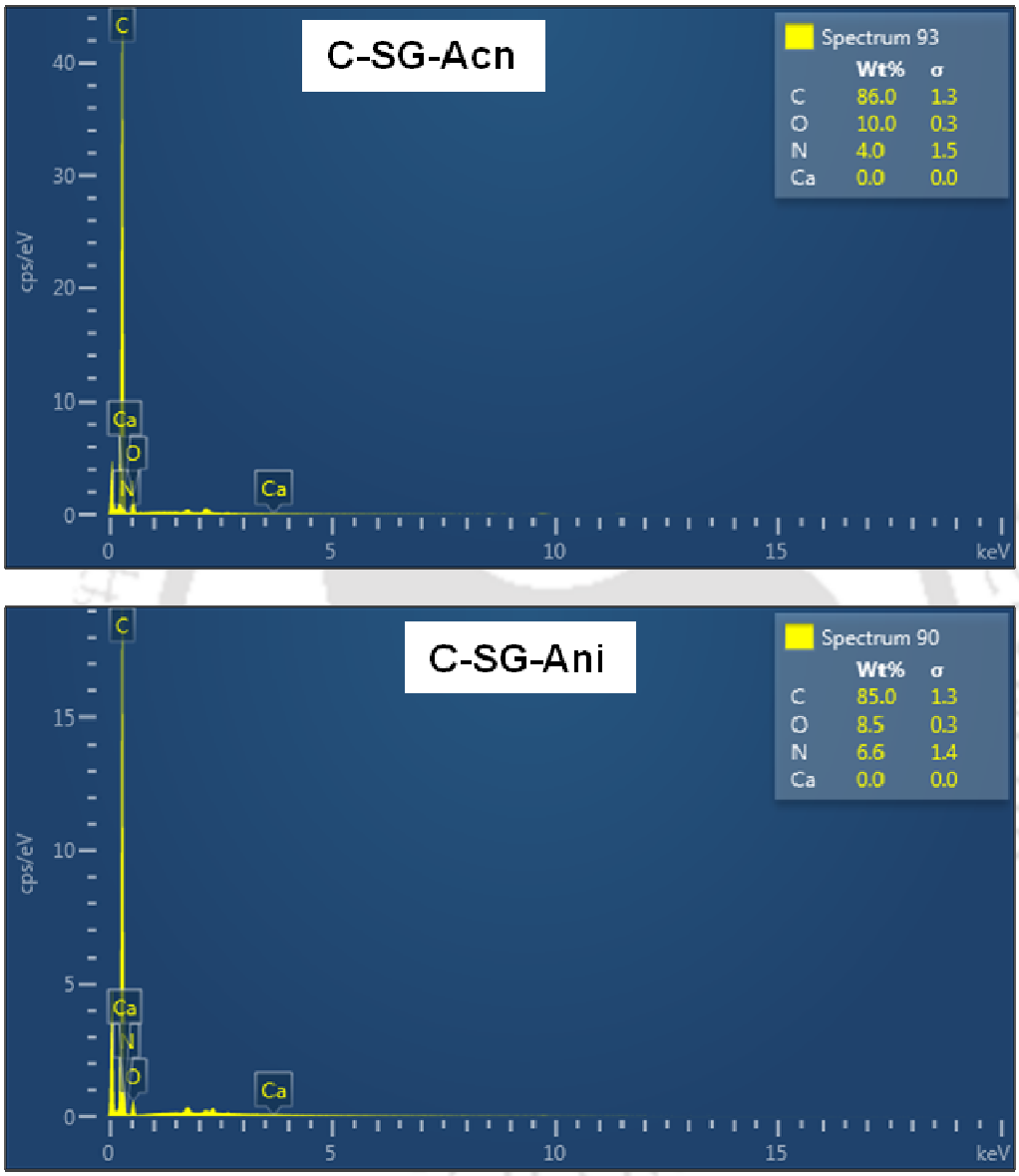

Figure A9. EDX spectra of silica gel templated nitrogen doped carbons.

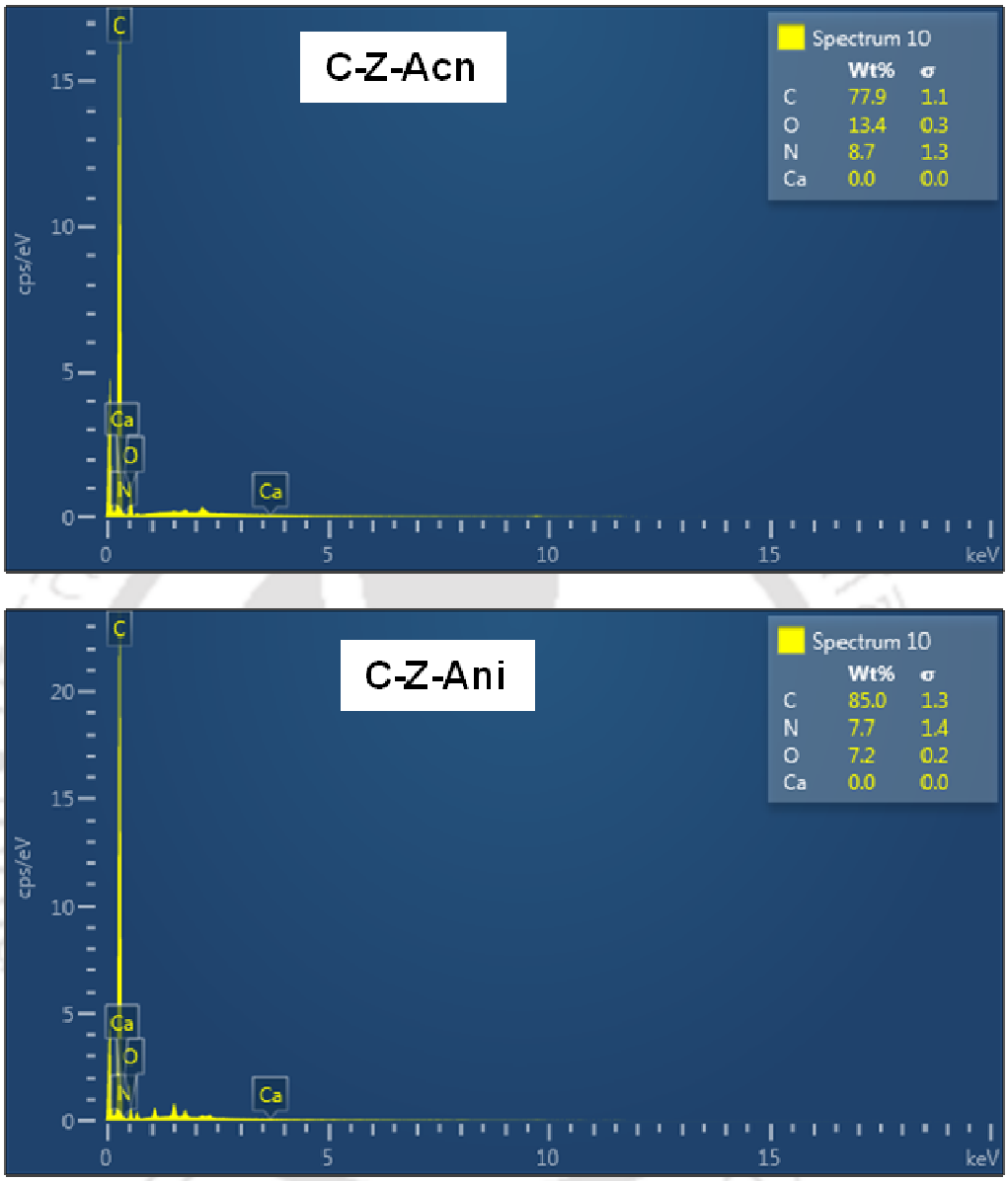

Figure A10. EDX spectra of zeolite templated nitrogen doped carbons.

Appendix H: Hydrogen desorption profiles for nitrogen doped templated carbons

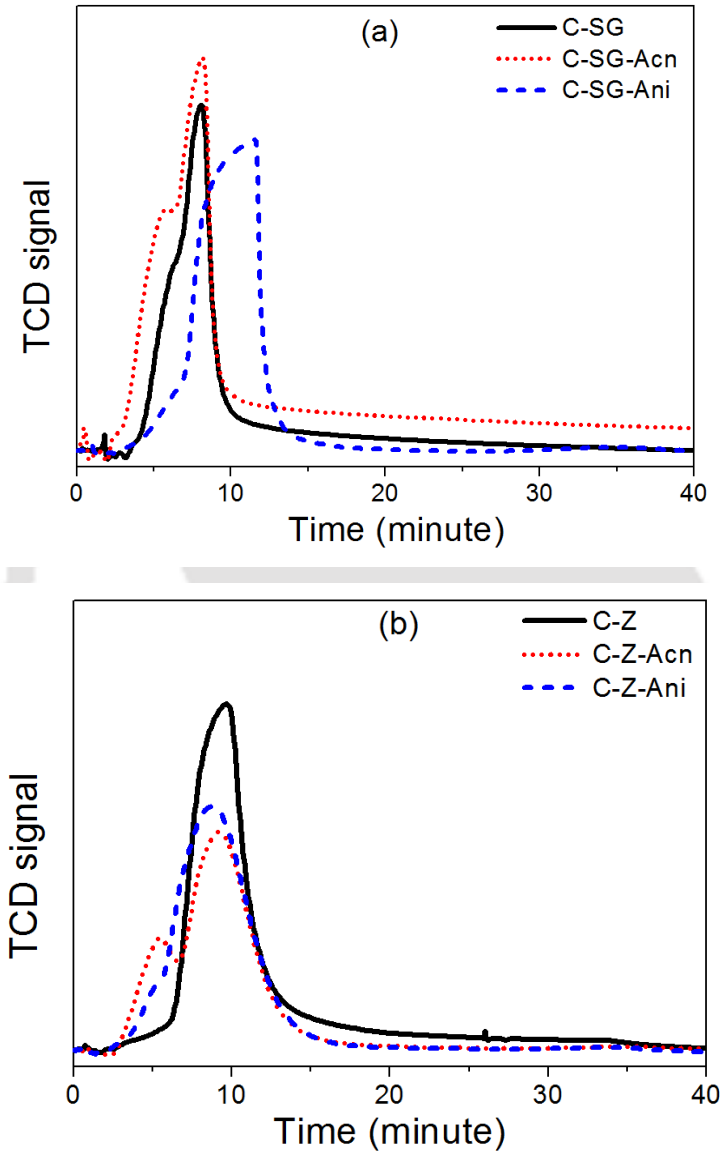

Figure A11. Hydrogen desorption profiles for templated undoped and nitrogen doped carbons as function of time (a) silica gel templated carbon and (b) zeolite templated carbons (adsorption at -100 °C and atmospheric pressure).

Appendix I: TPR profiles of nickel oxide doped activated carbons

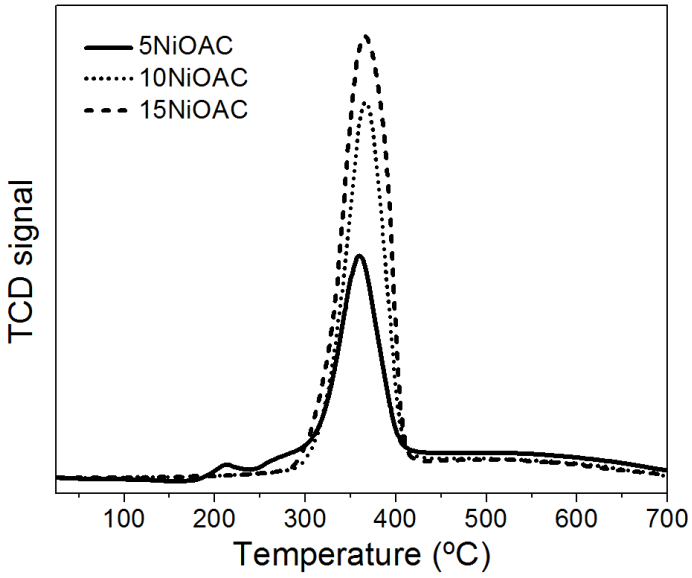

Figure A12. TPR profiles of xNiO–ACs (x= 5, 10, 15 wt.% NiO).

Appendix J: Calculations for metal dispersion and active surface area

(a) Calculation for metal dispersion

The sample calculation for metal dispersion is included for 5NiO-AC sample.

Sample amount: 0.0277g; Active gas: 10% Co/He; Carrier gas: He; Sample temperature: 22 ^{o}C ; Each pulse volume: 0.5cm^3.

The sample was given 5 (five) pulses; each pulse was of 0.5cm^3 volume. Five peaks were obtained and area for each peak is given in Table S1. The area differences corresponded to volume of CO chemisorbed on the metals.

Table A1. Peak areas for five pulses of CO injected to the sample.

Pulse no.	Peak areas	Area difference (Ai-Aj)
1	0.0171258	0.0008042
2	0.01793	0
3	0.01793	0
4	0.01793	0
5	0.01793	0
	Total area	0.0008042

A_j = area under each peak; A_i= area for 0.5 cm^3 peak = 0.01793

At STP, volume of active gas injected = V_{inj}

$$V_{inj} = V_{syr} \times \frac{T_{std}}{T_{amb}} \times \frac{P_{amb}}{P_{std}} \times \frac{A}{100} \qquad [J1]$$

Where,

V_{syr} = injected syringe volume =0.5 cm^3,

T_{std} = standard temperature= 273K ; T_{amb} = ambient temperature =22^{o}C=295 K

P_{amb} = ambient pressure = 743 mmHg; P_{std} = standard pressure = 760 mmHg

A = % active gas = 10%

From Equation [J1]

$$V_{inj} = 0.5 \times \frac{273}{(295)} \times \frac{743}{760} \times \frac{10}{100}$$

$$V_{inj} = 0.045 cm^3$$

Hence, 0.01793 area corresponding to 0.5 cm^3 of mixture actually represented volume of 0.045 cm^3 at STP.

For sample amount of 0.0277g, the total area of adsorption = 0.0008042.

$$\text{Hence adsorbed CO} = \frac{0.045\ cm^3}{0.01793\ (area)} \times 8.04\times10^{-4}\ (area) = 2.02\times10^{-3}\ cm^3/0.0277g$$

$$\text{or Volume of CO adsorbed} = \frac{2.02\times10^{-3}\ cm^3}{0.0277\ g\ of\ sample} = 0.073\ \frac{cm^3}{g} = \frac{0.0730}{22414} = 3.25\times10^{-6}\ \frac{moles}{g}$$

Metal dispersion (D) is defined as

$$D = \frac{\text{Total no.of exposed surface atom } (N_s)}{\text{Total no. of metal atoms present in the sample } (N_T)} \qquad [J2]$$

For 5 wt. % NiO/Carbon on 1g basis,

$$\text{Total moles of nickel oxide present} = \frac{0.05}{74.7} = 6.7\times10^{-4}\ \frac{\text{moles of NiO}}{\text{g of sample}}$$

Where 74.7 is the molecular weight of NiO

$$\text{Hence , total moles of nickel atom present in sample} = N_T = 6.7\times10^{-4}\ \frac{\text{moles of Ni}}{\text{g of sample}}$$

The total number of exposed surface atoms is taken as equivalent to moles of adsorbed CO, assuming stoichiometric factor of one that is one molecule of CO is adsorbed on one atom of Ni. Hence,

$$N_s = 3.25 \times 10^{-6} \ \frac{\text{moles of Ni}}{\text{g of sample}}$$

From equation [J2]

$$\% \text{ D} = \frac{3.25 \times 10^{-6}}{6.7 \times 10^{-4}} \times 100 = 0.48 \ \%$$

(b) Calculation of active metal surface area

The active metal surface area (MSA) per gram of the sample is defined as

$$\text{MSA} = S_f \times \frac{V_{ads}}{V_g} \times N_A \times \delta_m \ m^2 \qquad [J3]$$

Where, S_f = Stoichiometry factor = 1

V_{ads}=Volume adsorbed= $0.073 \ \frac{cm^3}{g}$

V_g=Molar volume of the gas at STP=$22414 \ \frac{cm^3}{mol}$

N_A=Avogadro's number =$6.023 \times 10^{23} \ \frac{\text{molecules}}{\text{mol}}$

δ_m =Cross-sectional area of active metal atom=$0.065 \ nm^2 = 0.065 \times 10^{-18} \ m^2$

From equation [J3]

$$\text{MSA} = 1 \times \frac{0.073}{22414} \times 6.023 \times 10^{23} \times 0.065 \times 10^{-18}$$

Hence, MSA= $0.127 \ \frac{m^2}{\text{g sample}}$

Appendix K: Calculation for crystallite size of nickel

The sample calculation for nickel crystallite size is done for Ni-Cs-SG sample. Maximum intensity peak at 2θ = 44.4 corresponding to Ni (111) plane was selected for crystal size calculation.

The crystallite size was calculated using Scherer's formula:

$$D=\frac{0.9\times\lambda}{\beta\cos\theta} \qquad \text{(K1)}$$

Where,

D= crystallite size in nm,

λ = wavelength of radiation = 0.154056nm

θ = 44.4/2 =22.2

β = Full width of half-maximum intensity = 0.01396

Hence, from equation [K1], crystallite size is given as

$$D=\frac{0.9\times0.154056}{0.01396\times0.92602}=10\text{ nm}$$

Appendix L: EDX spectra of nickel doped templated carbon

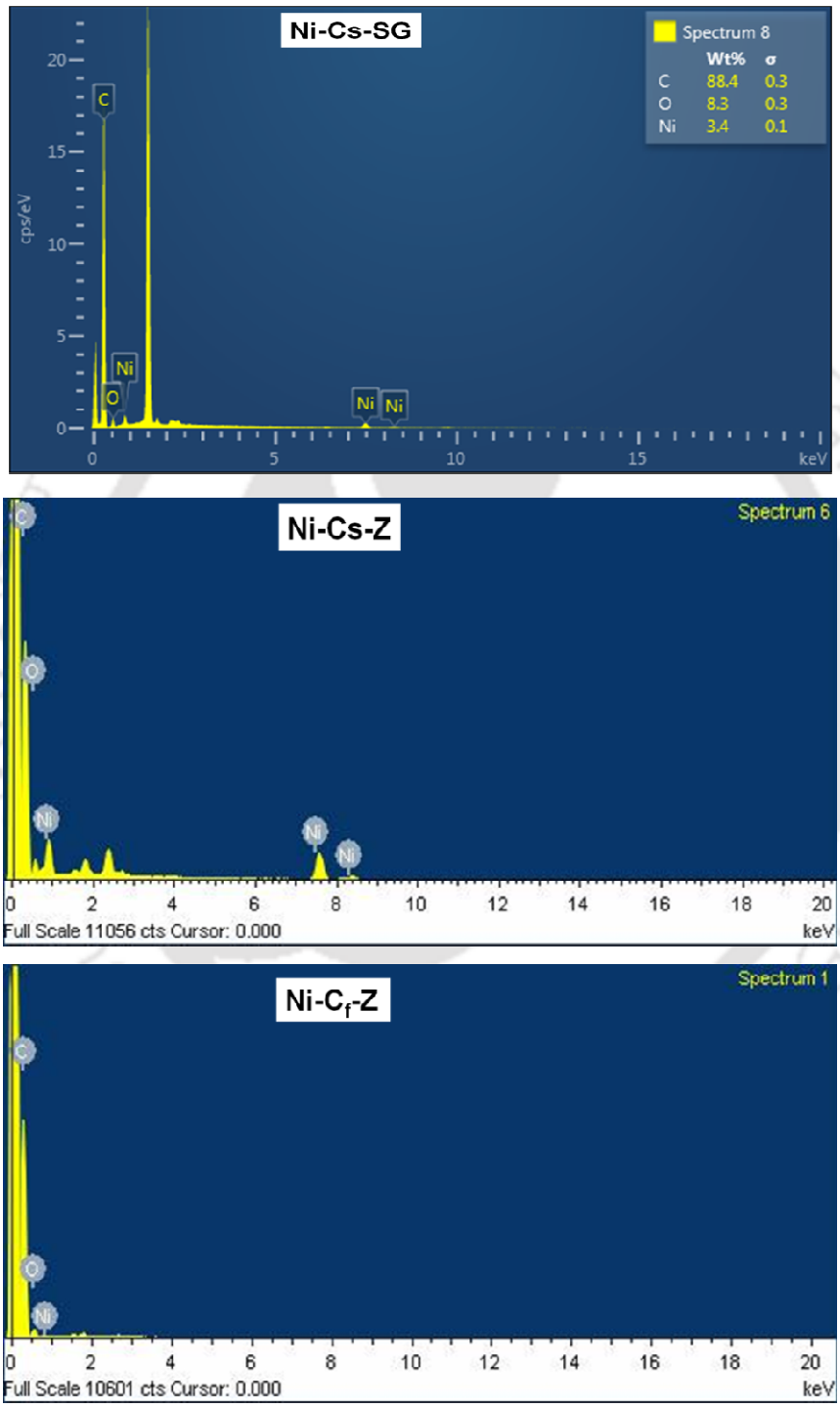

Figure A13. EDX spectra of nickel doped templated carbons.

Appendix M: Calculation for density of nickel particles

The density of nickel particles was calculated from TEM image as shown in Figure A14.

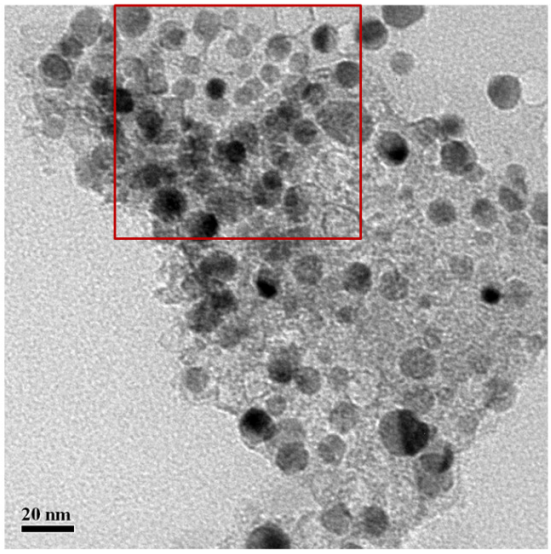

Figure A14. TEM image of nickel doped templated carbon

For calculation of nickel density, an area on the image was selected and numbers of nickel particles were counted.

Selected area $=93\times93\ nm^2=8649\ nm^2$

Total number of nickel particles in selected area =39

Hence Ni particle density$=\frac{39\ \text{Ni particles}}{8649\ nm^2}=4504\ \text{Ni particles}/\mu m^2$

Appendix N: Calculation for heat of adsorption

The heat of adsorption (ΔH) was calculated by using Clausius-Clapeyron equation as given by equation (N1).

$$\ln\left(\frac{P_2}{P_1}\right)=\frac{\Delta H}{R}\left[\frac{1}{T_1}-\frac{1}{T_2}\right] \qquad (N1)$$

The P_1 and P_2 were evaluated from the adsorption isotherms of C-S-Acn at two different temperatures as shown in figure below:

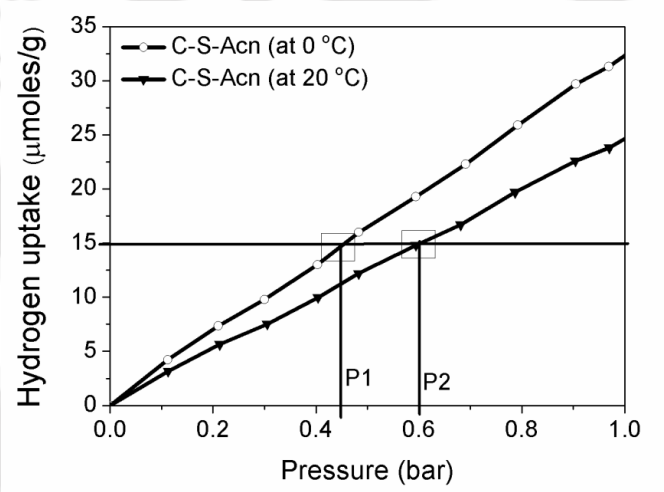

Figure A15. Hydrogen uptakes at different temperatures and pressures for silica gel templated nitrogen doped C-SG-Acn sample.

15 μmoles/g of hydrogen was adsorbed on the carbon sample at temperature 0 ^{o}C and 20 ^{o}C at pressure P_1 = 0.45 bar and P_2= 0.6 bar respectively.

Hence from equation (N1)

$$\ln\left(\frac{0.45\ \text{bar}}{0.6\ \text{bar}}\right)=\frac{\Delta H}{8.3144\ \text{J mol}^{-1}\text{K}^{-1}}\left[\frac{1}{273\text{K}}-\frac{1}{293\text{K}}\right]$$

$$\Delta H = 9.57\ \text{kJmol}^{-1}$$